Heparinized bioactive hybrid scaffolds for promoting and improving bone angiogenesis

Griselda Valeria Nájera Romero BEng, MSc

This dissertation is submitted for the degree of Doctor of Philosophy

June 2021

Engineering Department

To

My parents, because they taught me to be persistent;

My sisters, for their motivation and company when I needed it;

JM, for his immense patience and love;

FM, my baby, for sharing with me his endurance and joy.

“In nature, there is no separation among design, engineering, and fabrication; the bone does it all”

Neri Oxman

Declaration

This thesis has not been submitted in support of an application for another degree at this or any other university. It is the result of my own work and includes nothing that is the outcome of work done in collaboration except where specifically indicated. Many of the ideas in this thesis were the product of discussion with my supervisor Dr Ihtesham ur Rehman.

Excerpts of this thesis have been published in the following conference manuscripts and academic publications.

Presentation of work in:

- Engineering Researcher Symposium. (June 2017, University of Sheffield), poster
- Tissue Engineering and Regenerative Medicine Society World Congress. (September 2018), poster
- Biomaterials Symposium. (February 2019, Lancaster University), poster
- Engineering Postgraduate Research Conference. (July 2019, Lancaster University), presentation

Publication:

- Nájera-Romero, G. V., Yar, M. & Rehman, I. U. Heparinized chitosan/hydroxyapatite scaffolds stimulate angiogenesis. *Functional Composite Mater* **1**, 9 (2020). https//doi.org/10.1186/s42252-020-00012-y

Awards:

- Armourers and Brasiers Travel Grant. (March 2018)
- SMEA, Sheffield Metallurgical and Engineering Association, Travel Grant. (May 2018)

Griselda Valeria Nájera Romero BEng, MSc

Lancaster University, UK

Acknowledgements

I feel very grateful with:

My academic supervisor, Professor Ihtesham ur Rehman, for accepting me as part of his research group. He allowed me to have freedom in work, but always providing me his guidance and support. Dr Muhammad Yar, for his help and assistance during this research.

My Mexican and International friends who offered me their company, help, and with whom I shared very cheerful moments. Specially I would like to thank Ana Isabel, Dr Ricardo Aguilar, Cristina, and Carlos who became my family during this journey.

All members of the research group who helped me with my experiments. Specially to Fatma Zehra for her company in the lab and her constant motivation and help throughout this research project.

To everyone in Kroto Research Institute and Hadfield Building, in the University of Sheffield, and to the staff of Faculty of Science and Technology in Lancaster University, for their assistance and support.

Additionally, my gratitude goes to Armourers and Brasiers, and to Sheffield Metallurgical and Engineering Association for funding me with a travel grant for conferences and presentation of my work.

Finally, I would like to thank the Mexican National Council for Science and Technology (CONACyT) for funding my PhD.

Abstract

Formation of blood vessels at required number and time during bone regeneration represents a major challenge for tissue engineered constructs. Poor revascularization leads to scaffold failure and consequently, the loss of the implant. There are several problems associated with the use of growth factors in clinic such as low stability, controlled delivery to the site, and high price. Heparin is known to bind with angiogenic growth factors influencing the process of new blood vessels formation. The aim of the present study was to explore the potential of heparin to produce pro-angiogenic bone regeneration materials. Heparin was electrostatically loaded onto composite materials from porous chitosan/hydroxyapatite scaffolds. Different concentrations of heparin were successfully loaded onto the scaffolds, and the release performance of the scaffold was analysed by toluidine blue assay showing that the scaffolds loaded with lowest concentration provide a sustained release. The angiogenic activity of the heparin loaded synthesized materials was evaluated by chorioallantoic membrane (CAM) assay. After six day of materials implantation on CAM it was noted that overall low heparin concentrations exhibited a positive effect, with approximately 28µg per scaffold showed a significant increment in blood vessels. The synthesized materials showed no cytotoxic effects when evaluated by using U2OS cell line. Also, as showed by the SEM images the scaffolds exhibited that interconnected porosity and a pore size able to support osteoblasts proliferation.

This research provides information about the pro-angiogenic effect of heparin in potential bone regeneration materials.

Griselda Valeria Nájera Romero – June 2021

Table of contents

List of figures

List of tables

List of histograms

Abbreviations

AGF	Angiogenic Growth Factor
BMP	Bone Morphogenic Protein
CAM	Chorioallantoic Membrane
CS	Chitosan
DD	Deacetylation Degree
DMEM	Dulbecco's Modified Eagle Medium
DNA	Desoxyribonucleic Acid
EC	Endothelial Cell
ECM	Extracellular Matrix
EDTA	Ethylenediaminetetraacetic acid
EDX	Energy Dispersive X-Ray Spectroscopy
ELISA	Enzymed-linked Immunosorbent Assay
EPC	Endothelial Progenitor Cell
FCS	Foetal calf serum
FDA	US Food and Drug Administration
FGF	Fibroblast Growth Factor
FTIR-ATR	Fourier Transformed Infrared Spectroscopy Attenuated Total Reflection
GAG	Glycosaminoglycan
GEA	Gradual Electrostatic Assembling
GF	Growth Factor
GlcA	Glucuronic Acid
Glu	Glutamine
HA	Hydroxyapatite
HIF	Hypoxia-induced Factor
HMWH	High Molecular Weight Heparin
HUVEC	Human Umbilical Vein Endothelial Cell
IMS	Industrial Methylated Spirits
IPN	Interprenetrating Networks
IU	International Units
LMWH	Low Molecular Weight Heparin
MSC	Mesenchymal Stem Cell
MW	Molecular Weight
OPC	Osteoprogenitor Cell
PBS	Phosphate Buffer Solution
PCL	Polycaprolactone
PDGF	Platelet Derived Growth Factor
PGA	Polyglycolic Acid
PLA	Polylactic Acid
PTH	Parathyroid Hormone
PVA	Polyvinyl Acetate
RANK	Receptor Activator of Nuclear Factor κ
RANKL	Receptor Activator of Nuclear Factor κ Lingand
SBF	Simulated Body Fluid

SD	Standard Deviation
SEM	Scanning Electron Microscopy
TB	Toluidine Blue
TGF	Transforming Growth Factor
ULMWH	Ultra-low Molecular Weight Heparin
UV	Ultraviolet
VEGF	Vascular Endothelial Growth Factor
VIx	Vasculogenic Index
Wk	Week
β-TCP	β- Tricalcium Phosphate

1

Introduction

Bone possesses the capacity to repair itself whenever an injury occurs. Successful bone healing depends on several factors that include, age, nutrition and, type of fracture among others [1,2]. However, cases such as tumour removal, traumatic fractures, or injury infection, are highly prone to become critical size defects, where the loss of bone exceeds its self-healing ability. Bone grafting represents the main alternative for bone substitution. However, this technique presents some drawbacks that favour the investigation of more options for bone regeneration [3–6]. Hence, materials research aiming to mimic bone tissue properties constitutes a major subject in tissue engineering. The developed scaffolds should fulfil three fundamental functions: (1) the scaffold must provide an optimal structure for bone formation process; (2) it should promote the regenerative capacity of the tissue; and, (3) it must match the mechanical properties of the implantation site [4,5,7].

One of the challenges of current bone treatment strategies is how to stimulate blood vessel development [8,9]. Revascularization during bone regeneration is key to a proper healing, as blood vessels provide nourishment, excretion pathways, and allow progenitor cells to reach from their niches to the injured site. Angiogenesis is the generation of blood vessels from pre-existing vasculature. Therefore, tissue engineering for bone has investigated a wide range of options to approach the limitation of enhancing angiogenesis during bone repair [9,10].

Currently, delivery of growth factors has been favoured, as they highly influence the course of both processes: angiogenesis and osteogenesis. Vascular endothelial growth

factor (VEGF) and fibroblast growth factor (FGF) families have been preferred for these purposes. However, the direct use of these biomolecules has presented some drawbacks such as: high costs, unknown doses, contradictory results or possible tumour inducement, which have raised doubts concerning their applicability as a completely effective therapy for revascularization during bone regeneration [9–12].

Heparin has been widely studied as an aid for the load and release of the aforementioned growth factors [13,14]. This glycosaminoglycan binds to several angiogenic growth factors, thus, influencing their action [15].

Regardless of the vast information available regarding the use of heparin to bind growth factors to scaffolds, not many studies regarding the angiogenic influence of heparin itself on the bone healing process have been reported. Therefore, the purpose of this study is to evaluate the angiogenic effect of heparin concentration present on bioactive scaffolds fabricated by employing chitosan and hydroxyapatite.

1.1 Project Aim

The aim of this project is to obtain a material capable of improving and promoting the process of angiogenesis during bone regeneration.

1.2 Hypothesis

Our hypothesis is based on the potential of heparin to bind with several angiogenic factors [15]. Therefore, it is assumed that it will interact with the angiogenic growth factors from the surroundings and will induce a pro-angiogenic response. Additionally, the precise amount to achieve the purpose of promoting angiogenesis should be determined.

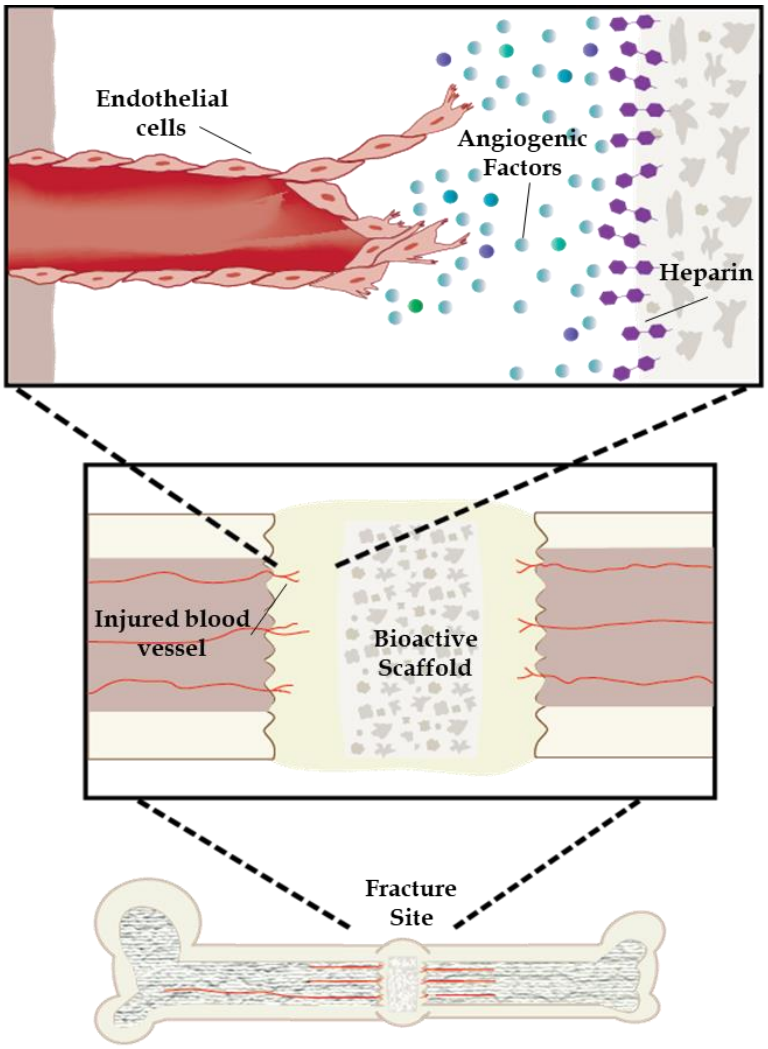

Figure 1.1 Schematic representation of the proposed heparinized scaffold. Ideally, the scaffold is to be inserted on the bone defect zone, heparin then will interact/bind with the angiogenic growth factors from the surrounding bio-environment, inducing an angiogenic response.

1.3 Objectives

- **Production of freeze-gelled scaffolds**

  Fabrication of stable scaffolds from chitosan and hydroxyapatite using freeze-gelation method, suitable to be used as bone regeneration scaffold.

- **Heparin loading onto the scaffolds**

  To obtain a material containing heparin, by forming a chitosan/hydroxyapatite and the heparin composite scaffold.

- **Determine the presence of heparin in the scaffolds**

  Using toluidine blue assay the amount and distribution of the heparin in the scaffold can be estimated.

- **Characterization of the morphology of the obtained scaffolds**

  Determining the surface characteristics of the obtained materials by Scanning Electron Microscopy (SEM). Ideal scaffolds should exhibit an interconnected porous structure.

- **Characterization in simulated body fluid (SBF)**

  Bioactivity is assessed by the observation of apatite formation in the scaffold after immersion in SBF.

- **Evaluation of cytotoxicity**

  Using AlamarBlue® assay viability test in osteosarcoma cell line, to carry an assessment of any possible noxious effects by the combination of these compounds, prior the evaluation on CAM assay.

- **Evaluation of angiogenic potential**

  To observe blood vessel formation and infiltration in the material implanted in the chick-embryonic membrane, by means of a CAM (chorioallantoic membrane) assay.

1.4 Outline

This work has been divided into four major chapters: literature review, materials and methodology, results and discussion, and conclusions.

In general, the literature review includes relevant information regarding bone and bone healing, to present the ideal function of this tissue. Then, the common challenges in bone regeneration and revascularization, as well as the current alternatives for this

problem in tissue engineering are presented. Lastly, the available information regarding the use of heparin for revascularization techniques is also introduced in this chapter.

The materials and methodology chapter describes the main materials used for scaffold preparation: chitosan, hydroxyapatite, and heparin; providing a complete description of their characteristics. Likewise, this chapter contains a stepwise description of the methodology followed to prepare the scaffolds as well as detailed information regarding the characterization methods used. This chapter also contains a full account of the procedure followed to define the final approach to produce the scaffold, justifying the use of our final methodology.

Within the results and discussions chapter a detailed description of the results obtained by the characterization methods is provided. A comprehensive explanation on every result is included, for instance: explaining the reasons why a certain porosity and microstructure were observed on the SEM images.

Finally, the conclusions chapter presents a summary of the findings and the main contributions produced from this work. This chapter also contains suggestions on how to improve this research project and what other perspectives could have been considered to improve the possibilities on bone revascularization.

1.5 Summary

Revascularization of bone has been widely investigated through several techniques and materials. As described in the following chapters, the challenges include the generation of a structure similar to functional bone tissue, as well as to generate the appropriate microenvironment to induce angiogenesis in the zone. Hence, the need for different approaches to achieve a successful revascularization of bone is required.

2

Literature Review

This chapter provides the significant background of the research that has been conducted in this study. Initially, a general description of bone and its composition, necessary information related to the research aim and healing process during bone regeneration is described. Therefore, after describing bone's composition and how its healing process normally occurs, a general overview of abnormal healing and its consequences is mentioned. This leads to the current therapies that are being addressed and reported in literature to tackle this important aspect of bone repair and regeneration. Different approaches have been introduced and discussed in this chapter with the main emphasis on angiogenesis and the agents (i.e., growth factors, etc.) studied to stimulate angiogenesis. A number of agents have been used to encourage angiogenesis and one of them is heparin, which is the main focus point of this study. To understand it fully, finally, the heparin characteristics are outlined with the aim to explore its full potential for promoting bone repair and regeneration.

2.1 Bone Tissue

Bone is a specialized connective tissue that constitutes a main part of the skeletal system. [16–18]. Due to bone's complex composition, it is seen as a composite from the materials point of view [19]. Bone consists of mainly two matrices and water, altogether contributing to this important tissue its complex biomechanical behaviour. [18,19].

Osseous tissue also possesses an extraordinary remodelling capacity, which keeps this tissue fit according to the needs of the bone site and the individual's activity [18,20]. This healing ability allows bone to restore itself when an injury occurs, though this process can be limited by the size of the bone loss [21].

The next sections will describe the most remarkable aspects of bone tissue, focusing on those that are more relevant to its auto-repairing activity and how tissue engineering aims to assist this process.

2.1.1 Bone composition

Bone consists of cells and extracellular matrix (ECM), in the same way like most connective tissues, however, ECM in bone is mineralized [16,17]. From a material point of view, bone is considered an anisotropic composite which is mainly made of two matrices: an organic matrix and an inorganic matrix, as well as a water content [1,18–20,22]. Bone matrices are responsible for the biomechanical properties of this tissue, the inorganic nature allows bone to be resistant, while the organic portion gives bone its characteristic tensile strength and elasticity [23,24].

2.1.1.1. Organic Matrix

During bone formation, osteoblasts secrete a material named *osteoid* which mainly consists of collagen, various proteoglycans, and glycoproteins [16,25]. This material undergoes a mineralization process prompted by the mineralizing sacs, also released by osteoblasts [16,23].

Majority of the organic matrix of bone is comprised of type I collagen (90% of its content) [18,23,25]. The structure of collagen I is described as a triple helix, which is stabilized by hydrogen bonds among them. These triple helical fibres may also incorporate other types of collagen; such as type V in bone tissue [1,26]. The characteristics

of bone collagen are defined by its posttranslational modifications and hydroxylation array. Likewise, bone collagen is affected by its mineralization pattern, which can be intrafibrillar (apatite crystals are deposited within the collagen fibrils) and interfibrillar (apatite crystals are between the collagen fibrils) [22,24,26]. During bone formation, woven bone is formed mainly by haphazard collagen fibrils, which are mineralized subsequently by deposition of inorganic component among and within them. According to Olszta et al (2007), Ferreira et al. (2012) and Wang et al. (2012) collagen is able to activate, spread and orient the mineralization process in woven bone [22,27,28]. Defects in collagen structure, fibre orientation, stability, and mineral distribution have a major impact on the mechanical properties finally achieved by bone tissue [29].

Osteoblasts secrete several macromolecules other than collagen to form bone matrix. Among them: glycoproteins, proteoglycans, fibronectin, osteonectin, bone sialoprotein, osteopontin, and bone morphogenic proteins (BMPs). All of these molecules have important roles on signalling processes that impact mineralization, formation, and remodelling of bone [1,18,30].

2.1.1.2 Inorganic Matrix

Bon is comprised of approximately 70% of inorganic matrix [1,25]. It consists of calcium phosphate crystals distributed orderly in the organic matrix [1,31]. Chemical composition of this calcium phosphate resembles the structure of geological hydroxyapatite (HAp), $Ca_{10}(PO_4)_6(OH)_2$. Thus, it is constantly referred as 'biological apatite'. However, it contains different ions which include magnesium, potassium, strontium, sodium, carbonate, and fluoride among others [1,32].

The process by which bone mineral is formed, is still not well elucidated [16,30]. However, it is known that osteoblasts secrete osteocalcin and mineralizing vesicles. Osteocalcin attracts calcium ions and the matrix vesicles release alkaline phosphatase, among other

enzymes. Therefore, the surrounding media acquires the necessary ion concentration and with the aid of several biomolecules, the formation and deposition of apatite crystals is possible [16,33]. This mineralization process takes place along different sites of the collagen fibrils, thus, the mineral crystals can be considered as fillers on the organic matrix providing rigidity to this tissue [1,32,34]. Due to findings of traces of different amorphous calcium phosphates in biological apatite, it is hypothesised that during mineralization process *in vivo*, the nucleation begins with an amorphous crystal growing. These amorphous crystals act as precursor of a more stable hydroxyapatite found in mineralized tissue such as bone [22,28,33].

The mineral phase grants hardness to bone tissue, but its distribution and amount play a major role, since over-mineralized bone can be very brittle and prone to fracture [32].

2.1.1.3 Bone Cells

Though bone matrix is crucial and endows bone tissue with its main characteristics, bone cells are the organisms directing the how and when all of the decisive processes are going to take place in bone. The following main cells define the pathway to be followed, from formation and maintenance to remodelling of bone.

2.1.1.3.1 Osteoblasts

These marrow-derived cells are responsible for producing the material to build bone both during human growth and maturity [35]. As aforementioned, osteoblasts secrete the osteoid, collagen, glycoproteins and other proteins, as well as the matrix sacs that finally will help to create the appropriate environment for the mineralization of bone [1,18,35]. Likewise, osteoblasts express cytokines and enzymes, like alkaline phosphatase, that influence critical events during bone repair and remodelling, such as bone resorption, mineralization and osteoprogenitor recruiting. Once their life cycle is completed, these cells can turn into osteocytes or die via apoptosis [35].

2.1.1.3.2 Osteocytes

These branched cells distribute throughout the mineralized bone matrix. As mentioned before, osteocytes proceed from osteoblasts that ended up embedded in the bone matrix inside cavities named *lacunae*. While becoming osteocytes, the cell-precursors developed dendrites which form a communication system among them known as *canaliculi*. These channels also allow cell nourishment and substance exchange [16,18,23,35]. The well recognized function of osteocytes is to uphold the state of bone by receiving and transmitting signals. Osteocytes can detect several different hormones and allow bone adaptation to mechanical stimuli through remodelling process, that ultimately define its density and mechanical functionality [18]. Likewise, these cells intervene in bone regeneration detecting the interruption communication when an injury takes place [35].

Osteocyte survival depends on the vascularization of the zone they are allocated and they are able to live for years providing this state is preserved [23].

2.1.1.3.3 Osteoclasts

Osteoclasts are multinucleated cells of large size and are found on bone tissue surface. These cells are in charge of bone resorption by acidic degradation of its matrix [1,36]. This process is triggered and regulated by a series of molecules among them: hormones, proteins and enzymes, such as RANK (receptor activator of nuclear factor κ), RANKL (receptor activator of nuclear factor κ ligand), parathyroid hormone (PTH), cathepsin K and calcitonin [18,23,36,37]. Therefore, bone resorption is a process that helps to regulate calcium availability within the body. However, this process is very active during the first stages of bone remodelling and bone repair, in which old or damaged bone respectively, are removed to give rise to new bone formation [18,36]. Thus, osteoclasts play a very important role in preserving functionality of bone, since a lack of resorption

or an excess of it may lead to serious diseases such as osteopetrosis or osteoporosis, respectively [16,37].

2.1.1.3.4 Other bone cells

Cell precursors, such as pre-osteblasts and pre-osteoclasts, are also found in bone. Likewise, bone lining cells are inactive osteoblasts located in the bone periphery and though their functions remain unclear, it is presumed that they are involved in the regulation of bone resorption [18,23,37].

2.1.2 Bone structure and properties

Bone function within the body can be summarized mainly in three types:

- Metabolic: If necessary, diverse ions can be released from this tissue. Ions such as calcium and phosphate are essential for various biological processes [16,24].
- Protector: Bones form the skeleton structure, which protects the internal organs, i. e. brain, heart, and lungs. Likewise, this tissue shelters bone marrow, which provides hematopoietic cells [16,19,20].
- Mechanical: As important elements of the skeletal system, bones help to provide support and maintain the shape of the body, allowing displacement [16,18–21].

Hierarchical models have been proposed to study bone's architecture and function, while explaining the particular biomechanical properties of this tissue [22,33,38,39]. A variety of models have been suggested, however they all share their focus on the different features exhibited from the nano- to the macro-organization of the bone components [22,33,38]. Weinkamer & Fratzl (2010) explain the hierarchical structure of

bone tissue according to the distribution of its components at different scales: At a nanometric scale, bone is formed by collagen molecules with apatite mineral distributed among them (Figure 2.1 part 1). Mineralised collagen fibrils arrange themselves in patterns named bone *lamellae*, which in time form bone layers of the osteons and an intricate framework called *trabeculae* (Figure 2.1 parts 2 to 5). The micrometric sizes of these structures round between 10^{-6} and 10^{-4}m. The macrometric scale represents the organization and distribution of trabecular and compact bone in a complete bone structure (Figure 2.1 part 6) [40].

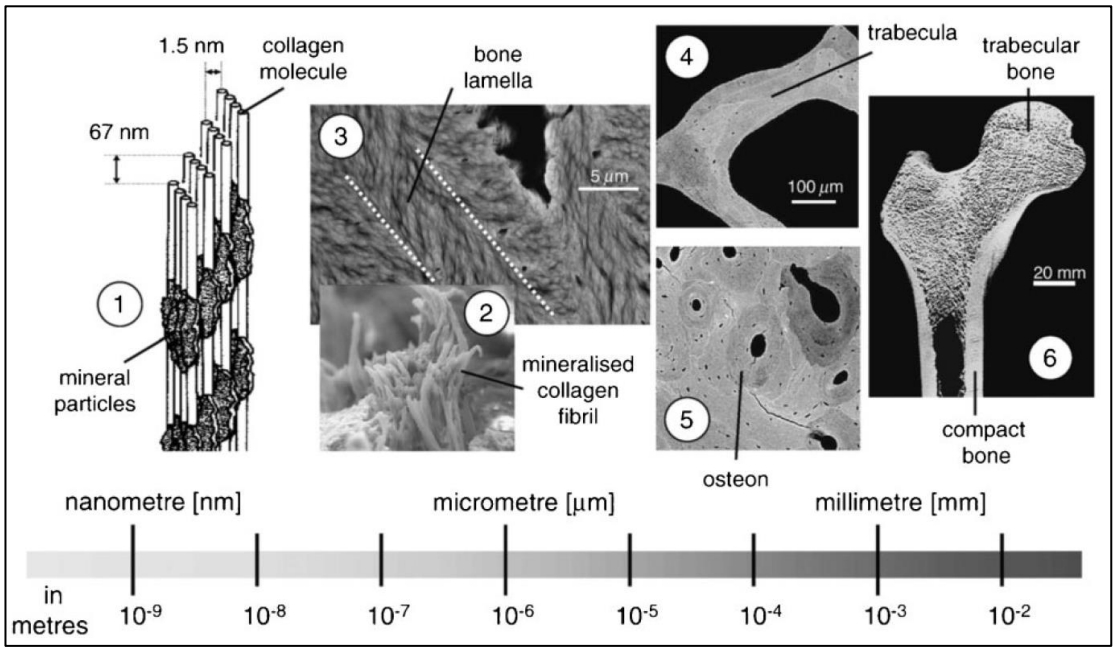

Figure 2.1. Hierarchical structure of bone tissue: (1) Mineralized collagen fibres; (2 and 3) Microarray of mineralized collagen into lamellae; (4 and 5) Flat arrangement (trabecula) and cylindrical arrangement (osteon) of lamellae; (6) Complete bone structure (femur) formed by compact and trabecular bone. Picture taken from Weinkamer & Fratzl (2010) [40].

2.1.2.1 Microstructure of bone tissue

During bone formation, collagen fibres organize into flat layers once its mineralization is achieved. These layers, better known as *lamellae*, take part of the two different stages of bone configuration at a microscale level [38,39]. On one side, ***woven bone*** is mainly

comprised by collagen fibres randomly organized and exhibiting poor mineralization patterns. This type of bone is mostly observed during embryo ossification, infant's growth, and early stages of bone regeneration in adults, which later is replaced with *lamellar bone* [1,23]. On the other side, *lamellar bone* consists on a well-structured array of the mineralized sheets (*lamellae*). Usually the lamellae organize in a cylindrical structure better known as ***osteon***, though parallel arrangement is also found. The channel around which the osteon is built is called Haversian channel, therefore this structure is also identified as Haversian system [16,39]. Figure 2.2 shows the structure of the Haversian system and its relation with the resultant macrostructure of bone [18]. It is important to highlight how blood vessels and nerves travel axially through the Haversian channels and transversely through the Volkmann channels in this system [16]. Rho et al. (2016) emphasize the impact of the osteon's inner arrangement on its biomechanical properties, as lamellae disposition defines the mechanical resistance achieved by the osteon, and ultimately influences the one reached by the tissue itself [39].

2.1.2.2 Macrostructure of bone tissue

On a macroscopic level, bone is classified in two types: *trabecular* and *cortical*. *Trabecular* bone, also known as *cancellous* or *spongy* bone, is mainly formed by a complex porous framework of lamellae. This particular array named *trabeculae*, is not as randomly ordered as it may seem, since it has been proven to be strategically organized to support loads, providing the distribution of its pores and the lamellae orientation [18,39]. On the other hand, *cortical* bone, also called *compact* bone, is mainly formed by mineralized sheets tightly packed and is generally identified to be formed by the Haversian system [18] described in section 2.1.2.1.

Majority of bones within the body are comprised by both types of bone, cortical and trabecular, and this composition is defined depending on their location and consequently their function [30]. Long bones such as femur, humorous or clavicles exhibit a thick cortical component, surrounding the trabeculae portion that wraps the marrow canal [23,30]. Whereas small bones such as vertebrae and those of the craniofacial skeleton, consist on a large section of trabecular bone enclosed by a slight fraction of cortical sheets [23,30]. Figure 2.2 depicts the common disposition of these types within a large bone structure [18].

Mechanical properties exhibited by cancellous and cortical bone depend on the distribution and content of inorganic and organic constituents, as well as on the arrangement of both osteons and trabeculae. Cortical bone possesses an anisotropic elastic modulus, being its mean value higher than that of cancellous bone, this is mainly attributed to the porosity of the latter [41].

2.2 Bone repair

The integrity of bone tissue depends on several factors, such as: the location of the bone, the individual's gender, health, genetics, diet, and activity. Remodelling process deals with most of the damage of the bone structure throughout an individual's life. However, sometimes the rate or efficiency at which the bone is replaced is lower than the loss of tissue and its mechanical properties turn defective, therefore fractures may ensue [1,2,21].

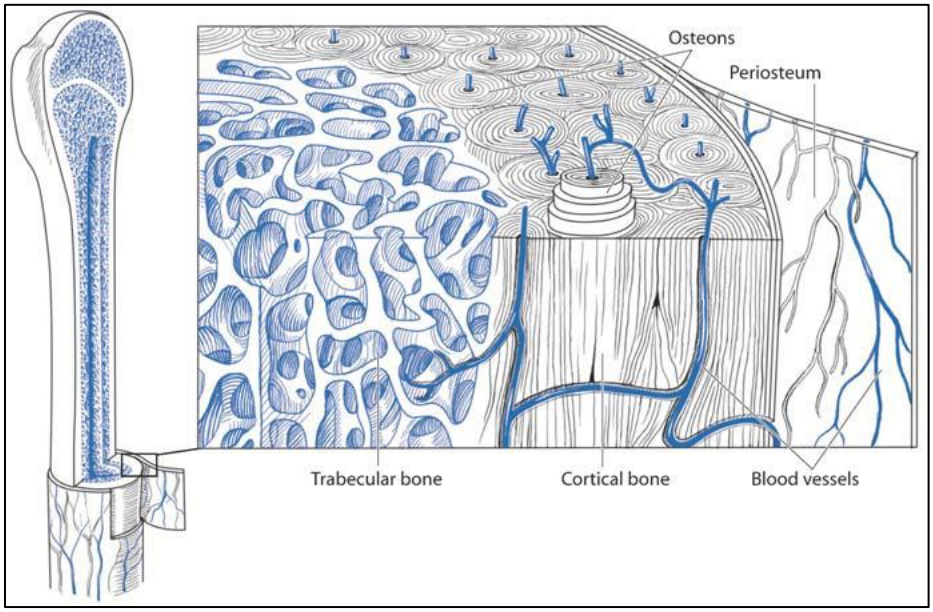

Figure 2.2. Structure of a large bone. Cortical and trabecular bone distribution with the vascular system running through them [18].

Bone possesses the ability of repairing itself without scar formation whenever an injury occurs or an absence is produced, limited, however, by the size of the loss [6,21]. Bone fractures can be produced by two main causes: 1) *Acute damage*, is when the applied load or the direction in which is inflicted to the tissue exceeds its limits. 2) *Fatigue,* if there is an accumulative microdamage on the osseous tissue the cracks are able to propagate, which leads to failure [2,42,43].

Bueno et al. (2011) and Prendergast et al. (2001) coincide on describing bone repair by two main processes: *primary* and *secondary* healing. During primary restoration, ossification takes place through *intramembranous* formation. In this process, osteoclasts resorb the tissue at the edges of the fracture, followed by osteoblasts secreting osteoid. Thus, forming woven bone, which is later replace by lamellae, in a common remodelling pattern. This type of healing is observed if the fracture is perfectly fixed

and requires very stable conditions to occur, therefore, is less observed than secondary healing [1,6].

Secondary repairing is a process of various steps which requires the synchronized interaction of several biological factors and routes to produce a proper bone restoration, achieved ultimately by endochondral ossification [1,6]. When an injury occurs, there is an immediate interruption of communication through that specific part of the bone, as vascularity and tissue continuity are disturbed. As part of the healing process, this disruption causes necrosis and hypoxia at the bony edges. [1,9,10]. This activates the hypoxia-inducible factor (HIF) which attempts to remediate this state by regulating gene activation and stimulating different pathways and growth factors, such as Vascular Endothelial Growth Factor (VEGF) [10,11,44]. Likewise, the blood coagulation cascade responds forming a clot around the injured site, due to the platelet aggregation [10].

From the resulting haematoma, platelet derived growth factor (PDGF) and other signalling carriers are liberated, and the inflammatory response ensues [10,11]. On this stage, the fibrin mesh established by the haematoma allows inflammatory cells to arrive. Neutrophils are the first polymorphonuclear cells to reach the site, followed by the macrophage [11]. Macrophage and osteoclasts deprive the injured site from debris and necrotic osseous tissue. Likewise, inflammatory cells release more signalling molecules to attract mesenchymal stem cells (MSC), fibroblasts and osteoprogenitor cells (OPC) [9–11].

With the aid of the aforementioned growth factors, the transforming growth factor (TGF), the bone morphogenic proteins (BMP), and the fibroblast growth factor (FGF) mediate the differentiation process of the MSC and OPC into chondrocytes and osteoblasts. These cells then produce the extracellular matrix (ECM) [10,45,46]. Thus, endochondral ossification takes place throughout the fracture breach ultimately

joining its edges. This soft callus (cartilage) is only provisional as it subsequently becomes mineralized by the osteoblast population (hard callus formation) [10,11]. At the same time, intramembranous ossification advances from the inner periosteum assisting bone formation towards the fracture breach [1].

During the hard callus formation, blood vessel ingrowth increases due to the coordinated action of various biochemical signals released mainly from the apoptosis of chondrocytes, thus improving blood flow for the healing to continue [11]. Ultimately, once the cartilage becomes completely mineralized, it undergoes the normal remodelling process. This restores the anatomical composition of bone and consequently its mechanical stability and complete functionality [1,9–11].

2.3 Angiogenesis in bone repair

Angiogenesis is the process by which pre-existing blood vessels give rise to new ones [15,47]. Figure 2.2 clearly illustrates the distribution of blood vessels within the bone structure. It is possible to observe how vascularization travels from the surface (periosteum) to the interior of the trabeculae; spreading all over the osteon system throughout the Harversian channels and connecting from osteon to osteon through the Volksman's channels [16]. Therefore, angiogenesis is crucial during repairing and regeneration processes, not only for bone, but for mostly all the body tissues (except for cartilage, as it is not vascularized). The term '*angiogenic-osteogenic coupling*' has been coined to refer to the fact that without a proper vascularization, osteogenesis is compromised. Similarly, key factors and processes during blood vessel formation are also determined and regulated by osteogenesis development [44,48].

In bone, blood vessels provide nourishment, gas exchange, and waste product elimination [9,10]. A vast variety of biomolecules circulate throughout the blood vessels.

Among them we can name growth factors, enzymes, vitamins, ions, proteins, and hormones. These biomolecules play key roles in the development and maintenance of this tissue [9–11,46]. Likewise, blood vessels are the conduits by which OPCs and MSCs are transported from their niches to the fracture site, when they are needed for regeneration processes [44]. Thus, vascularity helps to modify and maintain the metabolic microenvironment of bone, providing the angiogenic and osteogenic elements during its repair [10,44].

In their reviews, Saran et al. (2014) and Hankenson et al. (2011) highlight the relevance of angiogenesis in bone repair. They reference examples of different studies where diminished or complete lack of blood supply in the injury lead to healing problems. Among them: fracture non-union (healing is not achieved) and delayed union (the injury takes a long time to heal). Furthermore, the failure of implanted scaffolds can be also attributed to the deficiency of blood vessel formation within the structures [9,10].

Likewise, Lafage-Proust et al. (2010) emphasize the relationship between bone blood flow and bone mass. It has been observed that blood flow can decrease with the lowering of bone mass; in the same way, bone mineral density lessens in patients with peripheral artery disease. These and other examples point to a close, though non-linear, relation between bone vascularization and bone's maintenance and repair [49].

As reviewed in section 2.2, there are several signalling molecules influencing bone repair. Moreover, many of these have shown an angiogenic effect as well. Table 2.1 presents some of the most relevant of these biomolecules with dual effect.

Important biomolecules in bone repair		
Factor	**Osteogenic or angiogenic effect**	**Function**
HIF	Both	Activation of genes and pathways involved in angiogenesis, erythropoiesis, increase VEGF expr.
VEGF	Both	Recruitment of osteoblasts, MSC and EC. Influence in another GF
TGF-β	Both	MSC recruitment, Differentiation of Osteoblasts
PDGF	Both	Stimulation of osteoblasts
FGF	Angiogenic	Mitogenic factor for EC, MSC and osteoblasts
BMPs	Both (Angiogenic Indirectly)	Differentiation osteoblast-like cells, recruitment for neighbouring EC
RANK & RANKL	Osteogenic	Recruitment of bone cells and osteoclasts

Table 2.1. Important Biomolecules in Bone Repair. Abbreviations: **GF**: Growth factor, **EC**: Endothelial Cells, **MSC**: Mesenchymal Stem Cells. Factors: **HIF**: Hypoxic Inducible Factor/ **VEGF**: Vascular Endothelial Growth Factor/ **TGF-β**: Transforming Growth Factor Beta/ **PDGF**: Platelet Derived Growth Factor/ **FGF**: Fibroblast Growth Factor/ **BMPs**: Bone Morphogenetic Proteins/ **RANK**: Receptor Activator of Nuclear Factor-Kappa B/ **RANKL**: Receptor Activator of Nuclear Factor-Kappa B Ligand. (Adapted from: Loi et al. (2016), Saran et al. (2014) and Maes & Clemens (2014)).

2.4 Current approaches to improve vascularization during bone repair

Bone tissue engineering research has investigated a wide range of strategies to overcome the limitation of enhancing neovascularization during bone repair. The use of one technique, or a combination of them, have been explored as means of improving vascularization during bone regeneration. Nevertheless, the search for the most

optimal combination of techniques and materials to achieve maximum regeneration is still in progress.

The aim of the following subsections is to present general information regarding the current approaches to improve vascularization during bone repair. This, just to provide a general scenario of how tissue engineering is facing this issue, we are not using all these techniques in our research.

2.4.1 Porous synthetic scaffolds

Autografts represent the golden standard when it comes to bone tissue substitution. However, though autografts show exceptional biocompatibility and wound healing properties, their low availability, morbidity of donor site and long-term pain mean serious disadvantages for their use in bone tissue engineering [3,6].

Therefore, the chance of using scaffolds made of biomaterials for bone substitution has been extensively studied. From the bone tissue engineering point of view, a scaffold can be defined as a three-dimensional structure that provides the needed healing environment allowing new bone formation [50]. Ideally the scaffold should allow cells to grow, proliferate and differentiate; provide mechanical stability and strength; promote vascular infiltration and growth; and it should not unchain a cytotoxic response [10,50].

To date, a variety of natural and synthetic polymers have been used in bone tissue engineering studies, for example, collagen, gellatin, fibrin, chitosan, PLA (polylactic acid), PGA (polyglycolic acid), PCL (polycaprolactone), among others. These materials, depending on the fabrication technique, have been able to produce porous scaffolds with interconnected matrices. However, natural polymers exhibit poor mechanical properties or inadequate degradation characteristics. On the other hand, synthetic polymers exhibit low bioactivity or unsatisfactory cell interaction [9,10,50]. Moreover, most of the scaffolds produced are unable to meet the vascularization

requirements once implanted, i. e. vascular infiltration *in situ* is deficient which leads to the failure of the implant [9].

Thus, the use of different materials polymers, ceramics, and their combination, is currently analysed. Furthermore, the combination of scaffolds and the addition of many biomolecules has improved the perspective in the use of biomaterials for improving vascularization in bone tissue engineering.

2.4.2 Growth factor delivery

As described in sections 2.2 and 2.3, bone healing is a series of coordinated events that culminate in the restoration of the bone tissue without leaving a scar. The final outcome of the healing process will be determined by the mechanical stimulus and the biological environment of the injured zone [10,11]. Growth factors are secreted molecules that affect (mediate) various processes of the cells. Depending on the range and receptors present, these biomolecules will finally aid to regulate the local environment in the fracture [50]. It is not surprising that research aiming to understand their functions or to exploit their influence, has been very active. Among the growth factors used with therapeutic purposes in bone tissue engineering we can include: VEGF (Vascular Endothelial Growth Factor), FGF (Fibroblast Growth Factor), TGF-β (Transforming Growth Factor Beta) and PDGF (Platelet Derived Growth Factor), as well as BMPs (Bone Morphogenetic Proteins). These particular growth factors brought attention to research due to their action along the different stages of bone healing [9–11,51,52].

Regarding their improvement of angiogenesis during bone regeneration, Hankenson et al. (2011), Saran et al. (2014) and Hu & Olsen (2016) reference various studies concerning the administration of the aforementioned growth factors (single growth factor or combination of growth factors), the results from the cited publications present contradictory conclusions, no matter the growth factor used. The use of exogenous

growth factor was able to provide positive angiogenic and healing effects, however, in some findings, the quality of the bone was not adequate. Moreover, even when blood vessel formation may be able to be induced, malformed vessels were present [9,10,46]. This is mainly due to the effect of the in vivo environment (extracellular matrix, cell signalling, general health of the test subject) on the action of the growth factor.

Yu et al. (2015) explain how the influence of the growth factors is naturally regulated through the cell secretion if needed, which explains why some of them intervene at different stages of the bone healing process. This undoubtedly represents a challenge for therapeutic growth factor delivery, since not only the carrier should be effective to reach the treated site, but also a maintained release needs to be achieved without exceeding the necessary dosage to its effectiveness, becoming toxic [51]. Another drawback of this therapy is the order of application, since, biologically, the secretion of growth factors is a response of the stimulus sent to the cells during the healing process. However, in a therapeutic delivery, this is not yet adjustable and the outcomes of applying a growth factor when not needed can be unsuitable [9,51,52]. Moreover, most of the information available regarding the effects of growth factors in bone healing resides in analysing the effects of the absence of the growth factors or blocking its receptors, rather than the application of the substance itself [53].

Lastly, the incorporation of growth factors into a scaffold as its delivery system has represented another difficulty, mainly due to the abovementioned reasons: controlled and sustainable release. Inclusion of heparin or heparan sulphates have presented viable alternatives for growth factors such as VEGF and FGF [54–56], which increases the already expensive cost of the growth factor delivery therapy. Nonetheless, the research to improve growth factor delivery is ongoing in bone tissue engineering, aiming to improve delivery systems to achieve accuracy and regulation in growth factor release.

2.4.3 Cell scaffolds

Bone tissue engineering has also focused its attention on the use of cells that can promote osteogenesis as well as angiogenesis. Primary studies show the use of Mesenchymal Stem Cells (MSCs) coming from the bone marrow, under the premise that they would stimulate both bone and vascular growth [9,57,58]. On different *in vitro* studies MSCs have shown the ability to differentiate into osteoblasts or chondrocytes, moreover, MSCs can also be precursor for endothelial cells that ultimately will give rise to vascularity [9,57]. According to García & García's (2016) review *in vivo* experiments, MSCs show a positive effect on both processes when done separately, i. e. MSCs where able to differentiate into osteogenic line or to exhibit an endothelial potential to promote vascularization, the use of growth factors to stimulate the latter effect should be highlighted as the unknown dose and order of application of these give rise to other issues [57].

The use of more than one cell line has also been tested, as some examples of these, we can mention co-cultures of: MSCs and endothelial progenitor cells (EPC), Osteoblasts and endothelial Cells (ECs), osteoblasts and human umbilical vein endothelial cells (HUVECs), among others. Results from most of these co-cultures in vitro show a good capacity of both cell lines to produce osteogenic and angiogenic effects. However, when translating to *in vivo* studies, mixed results are exhibited. Some researches show positive vascular infiltration and bone formation, compared to studies using only one cell type [57]. On the other hand, studies like Koob et al. (2010) and Sharma et al (2018) using HUVECs and Bone Marrow Stromal Cells respectively show that though proper vascularization can be achieved, bone formation was not enhanced or defective [59,60].

One of the main drawbacks for the use of any of the previously mentioned cell lines is their limited availability [10,61]. Recent findings culturing MSCs from different sources,

such as adipose tissue, are ongoing with promising results. However, it has also been observed that the nature of the cell source determines its behaviour for regeneration potential. Moreover, factors such as cell culture protocols, culture media, number of cells used, animal model chosen, among others have been proven to highly influence the outcome of the study [57]. In view of this discrepancy of results among different studies, it seems very obvious that further investigation is required before any definitive conclusions regarding the delivery of osteogenic and vasculogenic cells into bone defects.

2.4.4 Gene therapy

The main purpose of using gene therapy for bone and angiogenic regeneration is to modify the cells in order to have a stable expression of the target growth factor. Thus, having an expression of this molecule in response to the physiological needs, both vasculogenic and osteogenic [51,57,62]. If successful, this would eliminate the use of external doses of growth factors [51].

There are two main forms to deliver genes, using viral vectors or non-viral vectors. The use of viruses as a vehicle to transfer nucleic information to the target cells has presented the most efficient results, but their limitation for feasible clinical trials stems from their potential risks of immune responses in the hosts [10,51,57,62]. On the other hand, non-viral vectors, consisting on a variety of options going from polymers, phosphates to liposomes [51,57]. This type of delivery vehicle presents a low efficiency due to their non-specificity to the cells with which they interact [62].

Regardless of the transfection method the major concern remain for the influence on the cell nucleus may have latent modifications in their DNA, which could lead to uncontrolled protein expression, unwanted effects or atypical tissue healing [10,51,57,62].

Current results from these type of therapy, however, show successful formation and differentiation of basic vascular structures, developing of microvasculature on implantation and improvement of bone healing process [10]. It is important to highlight that most of the work has been performed on rats or mice models, with varied induced defects (calvarial, femoral, or muscular injection). Equally important is to mention that there have been some studies showing irregular cell expression prior re-implantation on the subject. These type of results keep this therapy from being feasible for clinical application yet [10].

2.5 Heparin and revascularization improvement

Heparin possesses an anionic nature due to the presence of sulphate ion groups on its structure (see section 3.1.4). Along with a variety of macromolecules, mainly with growth factor families, heparin influence in neovascularization processes has attracted a lot of attention.

Chiodelli et al. (2015) published an extensive review on heparin and heparan sulphate proteoglycans molecular interactions related to neovascularization. In this review, the authors highlight heparin ability to bind with angiogenic growth factors (AGFs), which include both inhibitors and promoters. The balance between these two is the way heparin aids neovascularization regulation. Likewise, they present available information about the specific heparin sulphate groups that interact with angiogenic regulators [15], a summary is presented in Table 2.2.

Furthermore, Bhakuni et al. (2016) and Rema et al. (2003) address the fact that molecular weight of heparin plays an important role on its angiogenic activity [63,64]. According to Rema et al. (2003) and Collen et al. (2000), low molecular weight heparin (LMWH) has shown to inhibit angiogenesis when compared to high molecular weight

heparin (HMWH) on a chorioallantoic membrane assay (CAM assay) [64,65]. In a similar way, Ito & Welsh's (1999) study presented dual effects of heparin effect in the affinity of VEGF for its receptors, observing a difference in the action according to length of the polysaccharide unit [13]. Nonetheless, this behaviour seems to be completely dependent on the angiogenic regulator's affinity and molecular requirements.

Heparin sulphate groups interaction with angiogenic regulators			
Angiogenic Regulator	**Sulphate groups**		
VEGF-A		$6\text{-}OSO_3$	
FGF2	$2\text{-}OSO_3$		NSO_3
TGF-β			NSO_3
PDGF	$2\text{-}OSO_3$	$6\text{-}OSO_3$	NSO_3
FGFR1, FGFR4		$6\text{-}OSO_3$	
Heparanase			NSO_3

Table 2.2. Specific Heparin sulphate groups interaction with angiogenic regulators. Abbreviations: **VEGF-A**: Vascular Endothelial Growth Factor A/ **FGF2**: Fibroblast Growth Factor 2/ **TGF-β**: Transforming Growth Factor Beta/ **PDGF**: Platelet Derived Growth Factor/ **FGFR1**: Fibroblast Growth Factor Receptor 1/ **FGFR4**: Fibroblast Growth Factor Receptor 4. (Adapted from: Chiodelli et al. (2015)).

Though currently heparin is mostly used to bind with growth factors and aid its release in various systems [54,66–71], its action in wound healing and angiogenesis is still explored in the field of vascular tissue engineering [72–75].

2.5.1 The use of heparin in bone healing techniques

Although the use of heparin has been mainly for releasing growth factors from functionalized matrices, in this study the use of heparin alone inducing vascularization has been studied. Yar et al (2017) has reported heparin successfully loaded onto chitosan scaffolds to improve poorly vascularised wound beds [56]. Similarly, Shahzadi et al. (2016) have bonded heparin to chitosan-PVA scaffolds to improve

neovascularization [76] and Gibliobianco et al (2015) reported layer by layer heparin coating to a PLA scaffold [77].

Regarding the use of heparin for bone tissue engineering has been previously studied. Almodovar et al. (2013) reported the use of chitosan/heparin polyelectrolyte multilayers built on modified cortical bone pieces. Their main aim was to take advantage of the antibacterial properties of chitosan in bone healing. However, they also highlight the resultant sites to bind growth factors, ensuing from the inclusion of heparin into the scaffold, this helps with their release and availability to attract mesenchymal stem cells attachment, improving bone regeneration [75].

Similarly, Yang et al. (2014) produced hydroxyapatite mineralized heparin/gelatin nanoparticles. They obtained a material enough stable to be used for growth factor release. The authors suggest their use with injectable hydrogels, so they can be delivered in situ during the bone healing [72].

Similarly, Gümüşderelioğlu & Aday (2011), functionalized freeze-dried chitosan scaffolds with heparin for bone tissue engineering. They tried two types of bonding: electrostatic interactions and covalent bonding. Their scaffold was able to release heparin for 20 days. Their findings focused mainly on bone growth, showing that covalent bonding presents better results in regards of *in vitro* osteoblast proliferation. This was explained that heparin was providing an enhancement of BMP activities. However, this team did not discuss concrete information regarding the ideal amount of heparin for promoting osteogenesis, nor effect on angiogenesis was mentioned [78].

2.6 Summary

Bone is a complex skeletal tissue, which is bioactive and is changing all the time due to the impact of loading and unloading. The challenge is to find a biomaterial that can mimic its properties. The balance between its mineral and organic matrices provides a challenge for bone tissue engineering. In addition, as our understanding of the bone improves, researchers are appreciating the importance of having a good blood supply for bone repair and regeneration. Angiogenesis, and consequently, revascularization during bone repair endows bone with the ability to maintain its nourishment and its complete functioning. However, as it is described in the following chapter, natural materials, such as, chitosan and hydroxyapatite have proven to provide positive results in bone regeneration. Similarly, the use of heparin rises the possibility of improving angiogenesis process during bone repair.

3
Materials and Methods

In this chapter, the materials used for the scaffold preparation are described in detail, including their main physicochemical characteristics and how they are expected to influence the outcome of this research project. At the end, a list of the particular materials, their sources and suppliers are provided.

The development and/or optimization of the methodology used to prepare the proposed bioactive scaffold for improving bone angiogenesis is presented in detail in chapter 5, Section I. As a result of the experiments carried out during those trials, the following protocol was obtained. Stepwise descriptions of our freeze-gelation protocol are provided. Additionally, the process of loading heparin onto the scaffolds in order to functionalize them for vascular infiltration purposes, is described.

3.1 Scaffold Materials

The following sub-sections describe in detail the materials involved in the process of preparing the scaffolds. The description includes their main physicochemical characteristics, which finally influence on the expected the outcome of the project.

3.1.1 Chitosan

There are several reviews regarding chitosan and chitosan-derivatives and their biomedical applications due to its outstanding biocompatibility and biodegradability

characteristics [79,80,89–91,81–88]. This section attempts to describe, in general terms, the most important characteristics of this material.

Chitosan is a polysaccharide derived from the deacetylation of chitin. Its chemical structure, shown in Figure 3.1, is well described by Levengood & Zhang (2014) as a linear polysaccharide consisting of glucosamine and N-acetyl glucosamine units linked by β (1-4) glycosidic bonds [79].

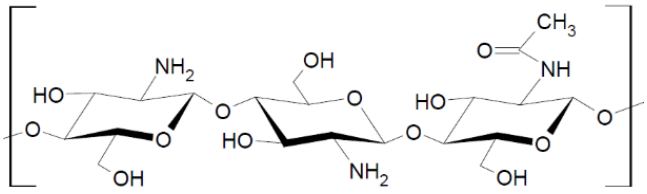

Figure 3.1 Chemical structure of chitosan. [Adapted from Mourya, V. K. et al (2008) [83]]

It is worth highlighting its naturally derived form, since chitosan is obtained from natural sources: the animal source consisting mainly in crustaceans and the vegetal source formed by certain fungi.

In arthropods, chitin is part of their protection structures (cuticle) along with proteins and calcium carbonate [90]. Being an important part of crustacean's shells, chitosan production from this source is the most common since seafood industry provides a good source from its scrap [81,90]. Croisier & Jérôme (2013) claim that chitosan obtained from vegetal sources presents a more consistent reproducibility and is favoured over crustacean chitosan for its use in healthcare [80]. Also research teams such as Kaya et al. (2015) and Mesa et al. (2015) have reported optimal biomedical-quality chitosan obtained from naturally abundant fungus [92,93]. Despite all this, the main source of the available commercial chitosan remains to be crustaceans.

3.1.1.1 Fabrication of Chitosan

The general process to obtain chitosan, whether the source is animal [90] or vegetal [93], can be summarized in the following five steps. The first step is the priming of the material, through homogenization in the case of fungi and decalcification of shells in the case of crustaceans. Secondly, a process of decomposition of proteins is followed, it is mainly performed using sodium hydroxide (NaOH) and heat. The next step is the treatment to remove the organic residues, regularly achieved through alkaline substances. However, according to Mesa et al. (2015), this is not required for fungi source. The fourth phase is pigment removal, and finally the last step is the deacetylation procedure [90,93]. The deacetylation process modifies chitosan's crystallinity, structure, and functionality endowing it the potential to be used in several applications when compared with chitin. Although chitin is naturally abundant, it is not soluble in many solvents, which complicates its handling and use.

Thus, chitosan is generally obtained by the alkali treatment of chitin, which involves the hydrolysis of the amino acetated positions on chitin backbone. This is usually achieved using NaOH and a thermal treatment ca. 80- 120 °C for approximately 5h. However, Dash et al. (2011) also refer the use of potassium hydroxide, anhydrous hydrazine, and hydrazine sulphate for this phase [81]. This process can also occur by enzymatic hydrolysis through the action of a chitin deacetylase [81]. Likewise, Yaghobi & Hormozi (2010) and Domard (2011) describe deacetylation protocols consisting in treating chitin with the alkaline substance more than once, in order to obtain a maximum level of deacetylation [86,94]. These authors also suggest that the hydroxide concentration plays a major role in this process. Most protocols show a degree of deacetylation of 70- 95%, while a 100% deacetylated chitosan can be achieved with their multistep processes [80,81,83,87].

3.1.1.2 Chemical, physical, and biological properties

Besides its natural origin, the most remarkable features of chitosan noted among all the reviews are: biocompatibility, biodegradability, antibacterial nature, low-toxicity, haemostatic behaviour, the wide variety of chemical modifications it can undergo, and its ability to promote cell attachment and proliferation [79,80,89,90,81–88], such characteristics place on chitosan high expectations to be consider in various biomedical and pharmaceutical applications.

Many authors coincide that, the degree of deacetylation (DD), the molecular weight (MW) and the number and position of amino groups present in its backbone confer to chitosan its properties and behaviour.

For instance, Alves et al. (2008), Mourya et al. (2008), Pillai et al. (2009), and Dash et al. (2011) state that the number of cationic sites formed via protonation of amino groups by acids along the chitosan chain increases its solubility, giving rise to a water-soluble polyelectrolyte. However, if the pH rises up to around 6 and 6.5, the amines lose their positive charge, becoming insoluble. Therefore, although this protonation of amino groups confers to chitosan one of its most remarkable capabilities (ionic charge) it can also limit its applications as it is only soluble in some acidic solutions [81–83,85,86]. It is important to notice that the DD determines the number of amino groups available on the chitosan structure, modifying its crystallinity, which plays a major role in the solubility of any substance.

The polycationic nature of chitosan also elucidates certain abilities that are very useful in bone tissue engineering. Chitosan is able to form stable ionic complexes with various water-soluble anionic molecules, which can improve its mechanical properties and enhance cell attachment. Park et al. (2013) and Resende et al. (2015) reported a positive

impact on chitosan flexibility and mechanical strength when combined with anionic biopolymers such as alginate or glycosaminoglycans (GAGs) [3,95]. On Kim et al. (2008) and Levengood & Zhang's (2014) reviews this last combination is especially remarked since GAGs help to regulate important processes in bone regeneration [79,89]. On the other hand, Mourya et al. (2008) and Croisier & Jérôme (2013) consider that the cell permeation improvement of chitosan can be explained by its interaction with the negative portions of the membranes, which modifies their communication channels [80,83]. Similarly, Dash et al. (2011) and Usman et al. (2016) deem that the anionic adhesion of chitosan is also reflected on its haemostatic activity, since erythrocyte membranes are negatively charged [81,84].

Biocompatibility is also affected for the DD, the aforementioned ability of chitosan to interact with cell membranes depends upon the ionic charge throughout the chitosan chain which is highly related to the DD. And as stated by Croisier & Jérôme (2013), as the number of positive charges augments, the interplay cell-chitosan increases, and this tends to enhance biocompatibility [80]. Numerous studies have analysed the influence of chitosan in cell viability, proliferation and attachment. Though these properties are highly related to the chosen system, chitosan has demonstrated to provide an adequate environment for cell adhesion and growth, especially when combined with compounds that help the system to emulate cell matrix [79–83,85–89].

Mainly, DD and MW affect the degradation rate of chitosan. Chitosan exhibits maximum levels of crystallinity when it reaches values near to 100 % of DD, this influences its biodegradation rate as low crystallinity implies a higher degradation rate and vice versa. On the other hand, MW shows the opposite effect as the higher the MW the lower degradation rate, due to the length of the chitosan chains. Biodegradation also depends upon the distribution of the acetyl residues throughout the chitosan

chain, for example, it has been found that the more alternated the position of these groups the lower the rate of enzymatic degradation [79–81,83,85]. Regarding the degradation by-products of chitosan, they are non-toxic and can be integrated into different metabolic pathways [3,79]. However, Svirshchevskaya et al. (2016) claim that a high hydrophobic substitution of chitosan can give rise to a toxicity growth [96], so attention must be paid when analysing such chitosan derivatives.

Further noteworthy characteristics of chitosan include antifungal, antimicrobial, and antioxidant activity [80,83,89,97]. Chitosan is also an FDA (*US Food and Drug Administration*) approved material for use in wound dressing and haemostasis treatments [98].

3.1.1.3 Processing of Chitosan

Chitosan can be processed to obtained a wide variety of forms such as porous scaffolds [79–81,83,85,87–89], micro/nanoparticles or micro/nanospheres [79–81,85], micro and nanofibers [79–82,87,88], hydrogels [79,80,90,81–83,85–89], films and membranes [80,81,85–89] and IPN (*interpenetrating networks*) [81]. In order to achieve these structures different methods of processing can be employed, such as, freeze-gelation [79–81,85], freeze-drying [79–81,85,87–89], gas foaming [79], emulsion droplet [81], coacervation [81], ionotropic gelation [80,81,85], spray drying [81], phase separation [79], wet-spinning [79,80,82], electrospinning [79–82,88–90], layer-by-layer deposition [80], wet casting [79,80], solution casting [79,89], chemical crosslinking [79–81,83,85,86,89], and ionic and polyelectrolyte complexes formation [80–82,85–87,89]. These are by no means an exhausted list of processing and new methods are being discovered as the understanding of the properties of chitosan is growing.

Chitosan scaffolds are most commonly obtained by freeze-drying procedure. However, alternative methods like freeze gelation are gaining recognition within the biomaterials field.

The porosity achieved with these processes confers the structure its mechanical properties, i. e. size and shape of pores, along with their distribution regulate mechanical strength of the resultant scaffold. Likewise, these characteristics dictate the scaffold behaviour associated with angiogenesis and cell ingrowth and proliferation [79,81,89]. Most of the authors generally place emphasis on the ability of chitosan of forming structures with interconnected porosity; hence, it results propitious in bone tissue engineering applications. However, it has been observed that the larger the pore diameter and interconnectivity, the more fragile the resultant scaffold would be [79,89]. None of the freeze-dried and freeze-gelled scaffolds developed to the date are suitable for load-bearing bone tissue regeneration, because the mechanical properties of these scaffolds are far from matching those of this type of bone, even though they show adequate characteristics for cell ingrowth. Ruiran et al. (2011) proposed freeze-gelled scaffolds made of chitosan and β-tricalcium phosphate (β-TCP). Likewise, Park et al. (2013) analysed freeze-dried apatite-coated scaffolds of chitosan and chondroitin 4-sulfate. In both cases, though the mechanical properties of the scaffolds improved when compared to pure chitosan, they are far from matching the values exhibited by bone and show dependence on the concentration of their components [3,99].

3.1.2 Hydroxyapatite

As mentioned in section 2.1.1.2, the major component of inorganic matrix of bone is comprised by a calcium phosphate, better known as biological apatite. This material possesses a structure and a composition very similar to hydroxyapatite. Thus, hydroxyapatite has been a widely exploited material for bone substitution and regeneration, working under the premise that this calcium phosphate is able to emulate the characteristics of bone inorganic matrix.

The following segments attempt to describe the main characteristics found in the literature related to this ceramic, as well as its significance in bone restoration applications.

3.1.2.1 Properties

Hydroxyapatite is a calcium phosphate with the main composition $Ca_{10}(PO_4)_6(OH)_2$. Its stoichiometric ratio is 1.67, which means the molecular relation between Ca and P (Ca/P) is of this value [100]. There are two main spatial distributions of hydroxyapatite identified: (1) monoclinic classified with a space group $P2_1/b$ and (2) hexagonal with a space group $P6_3/m$. However, for biological purposes, only the latter is used due to its stability [101,102]. Gruselle (2015) presents a depiction of the hydroxyapatite structure, showed in Figure 3.2. Calcium ions distribute among the phosphate groups within the structure bonding with its oxygen atoms, and the hydroxyl groups align in the c-axis of the arrangement [100].

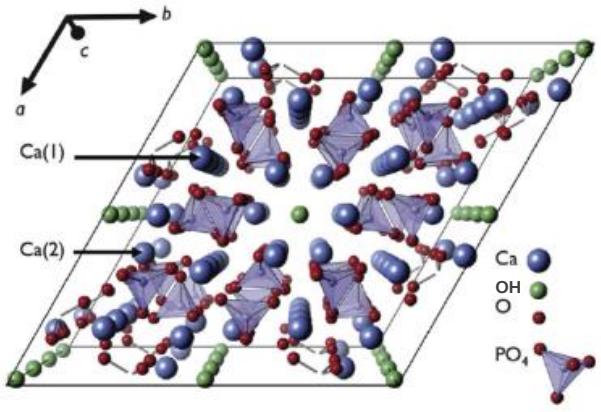

Figure 3.2 Hydroxyapatite spatial distribution. [Adapted from: Gruselle (2015)]

Gruselle (2015) also highlights the particular proneness of hydroxyapatite (and apatites in general) to establish ionic interactions, describing the main catalytic

behaviours derived from these charge exchanges. The presence of anionic groups such as OH^- or PO_4 and cationic groups like Ca^{2+} ion, within the hydroxyapatite structure allow this material to participate from a variety of surface and structural modifications, which ultimately bestow hydroxyapatite with its major qualities [100].

Bioactivity describes the interaction (chemical bonding) between a material and the tissue where is implanted [103]. This interaction would be mainly the result of a well-orchestrated ion exchange between cell-biomolecules and material surface ions [100,103]. Kokubo (1991) proposed the current standard evaluation of bioactivity in simulated body fluid (SBF) [104]. After the evaluation of biomaterials for bone applications, it was observed that if a proper correlation between the tissue and the material occurs, apatite formation would be present in the implant. This is mainly a result of the proliferation of osteoblasts around the bioactive surface [105]. Along with new apatite formation, bioactivity also implies a successful bonding between the existent biological apatite and the new apatite formed [104,105]. Hydroxyapatite has proved to induce apatite formation when implanted, and this particular quality has been widely exploited as bone implant coating [106].

Bioresorption refers to the ability of a material to dissolve within the biological environment [107]. In the same way bone is naturally resorbed by the action of the osteoclasts, it is important for a material intended for bone regeneration aid to possess the ability of being resorbable. Thus, it will provide the mechanical support needed for the tissue to develop during the healing process just long enough for the new tissue to fulfil this task by itself, as a proper regeneration works [108]. Solubility plays a major role for resorption rate of apatites and it can be modified with various ionic substitutions [101]. Among the available calcium phosphates used for bone defect treatment, hydroxyapatite possesses a low solubility in biological environment. However, several

ionic substitutions have been tested, which modify the lattice structure and ultimately, hydroxyapatite's crystallinity and solubility [5,109].

In addition, it is important to consider that once the material disintegrates, the by-products generated should not have an adverse effect in the biological environment. Hydroxyapatite is well recognized for being biocompatible, as the ions liberated during its resorption (Ca^{2+}, PO_4^- and OH^-) are not harmful for the body [101,110].

It is worth mentioning that these characteristics are mainly product of the different substitutions within the hydroxyapatite lattice structure and they may vary from one to another. Ionic substitution in hydroxyapatite will be discussed on subsequent sections.

3.1.2.2 Synthesis of Hydroxyapatite

There are several methodologies for the preparation of hydroxyapatite according to the targeted property to be modified, i.e. particle size, shape, and/or ionic substitution. For instance, some of the methods mentioned in the review by Sadat-Shojai et al. (2013) include chemical precipitation, solid-state synthesis, hydrothermal method, flow method and sol-gel method [111]. Despite of the method chosen, the ratio Ca/P of the product must preserve the value of 1.67 in order to obtain a hydroxyapatite structure [112].

After critically appraising of the literature, it became apparent that flow method and sol-gel method are preferred synthesis methods to be employed in our studies. This is because they allow control over particle size, shape, and form of the resulting hydroxyapatite.

As well described by Lakshmi et al. (1997), sol-gel synthesis implies the formation of a gel from the aggregation of suspended colloidal particles, which after heat treatment produces the entailed material [113]. This method allows the obtainment of

hydroxyapatite of more uniform structures [111,112], process settlement is simple [114], and large surface area of the crystals obtained can be achieved [111]. A range of shapes such as regular and irregular spheres, or filaments result from this process [111].

On the other hand, hydrothermal method involves the reaction of the precursors at high temperature and pressure [111]. Hydrothermal flow method consists in a system pumping the precursor solutions through separate pipes that eventually will meet in piece called "Tee" mixer. Afterwards, the blend keeps flowing through the pipe, which is now immerse in reactor with high temperature media. Ultimately, the obtained wet particles can be heat- or freeze-dried [115]. This method not only allows to synthesize hydroxyapatite in a quick process, but also to have much control of properties like size and shape of the structure [111,115].

3.1.2.3 Ionic Substitutions in Hydroxyapatite

Though commonly described as hydroxyapatite, biological apatite differs from the synthetic form of this ceramic due to the presence of various different ionic substitutions [31,102]. In their analysis of biological apatites from different sources, Liu et al. (2013) describe the most common natural substitutions found in biological apatites when compare to synthetic hydroxyapatite. Elements like Mg^{2+}, Sr^{2+}, K^{+} and Na^{+} are found in the cationic place of Ca^{2+}. Instead of P, the presence of C, As and V can be observed. And regarding the hydroxyl (OH^{-}) site, evidence of CO_3^{2-}, F^{-} and Cl^{-} are reported [31]. This explains why hydroxyapatite has been used as predecessor of several substituted-apatites, aiming to produce phosphates with a wide variety of properties and biological applications, from improving solubility [102,109] to providing antibacterial properties [116].

The most common substitution observed in biological apatite is carbonate substitution. Carbonates distribute in two different sites within hydroxyapatite structure: (1)

substituting the hydroxyl group (A-type substitution) and (2) the so-called B-type substitution, taking position of the phosphate group [101]. According to Ibrahim et al. (2010) the substitution can vary in an A/B ratio circa 0.8 [109]. This substitution influences significantly the solubility of hydroxyapatite due to lower bond energy between Ca^{2+} and the carbonate group (CO_3^{2-}) [31,101].

Hydroxyapatite chemical composition is $Ca_{10}(PO_4)_6OH$, this means that within hydroxyapatite lattice structure there are 10 atoms of Ca^{2+} for unit cell. From Figure 3.2, it is noticeable that these atoms arrange in two different sites, marked as Ca(I) and Ca(II). As explained on Šupová's (2015) and Boanini's et al. (2010) reviews, within Ca(I) sites four ions in total are harboured, aligned with c-axis of the hexagonal structure. Regarding the Ca(II) sites, six ions per unit cell are admitted in this position and they form a space known as anion channel, which can be occupied by monovalent as well as bivalent ions. Usually Ca(II) positions allocate cations bigger in size than those found in Ca(I) [101,102]. As regards to the substitution in these sites, cations such as Na^+ and Mg^{2+} have been incorporated in the lattice. Sodium has been explored to improve cell adhesion properties [101], whereas magnesium substitution is studied for cell proliferation promotion [101,117], though this latter can produce unstable hydroxyapatite [101].

3.1.3 Chitosan and Hydroxyapatite scaffolds

As mentioned in the review by Levengood & Zhang (2014), chitosan and hydroxyapatite are among the most promising materials for bone tissue engineering. A wide variety of combinations between the two materials have been studied, as they can be physically mixed or co-precipitated [79]. The reported combinations have showed favourable results in many respects: biological, mechanical, and physicochemical.

Tu et al. (2017) reported the fabrication an asymmetric nano-hydoxyapatite/chitosan composite membrane fabricated by solvent evaporating in vacuum with the ability to promote biomineralization by osteoblasts and accelerate bone regeneration [118].

Likewise, Ruixuin et al. (2017) described the formation of porous nano-hydroxyapatite/chitosan scaffolds and micro-hydroxyapatite/chitosan scaffolds prepared by compression moulding and particulate leaching method. The scaffolds exhibited remarkable porosity and pore interconnectivity which make them very suitable for guided bone regeneration. Similarly, the authors evaluated the enzymatic degradation behaviour by means of PBS (Phosphate Buffer Solution) and lysozyme, showing no noticeable degradation until week 8 of the experiment which can be translated into outstanding mechanical properties of the combination [119].

These are just some examples of the prolific use of chitosan and hydroxyapatite, and most of the reviews of both materials provide many proved cases. The success of use of both materials lies in the fact that the combination of both materials promotes cell attachment and osteoinductivity, biomineralization, osteogenic response, structural stability, and notable degradation behaviour [79].

3.1.4 Heparin

Heparin is a sulphated glycosaminoglycan (GAG) discovered in the early 1900's [120,121]. The structure of this GAG is very complex. As described by Rabenstein (2002), heparin is formed by repeating subunits of uronic acid-(1→4)-D-glucosamine. The uronic acid substitutes may be the following: α-L-iduronic (IdoA) or β-D-glucuronic acid (GlcA), which may contain sulphate moieties. The β-D-glucosamine portion can be N-acetylated or N-sulphated [120]. Figure 3.3 shows the typical structure of heparin as depicted in Linhardt's (2003) review, containing the aforementioned subunits. As observed in the first half of the repetitive structure, it can contain a highly sulphated

disaccharide. However, as shown in the other half, there is an under-sulphated part which can be substituted with X= sulphate or H, and Y=sulphate, Ac or H [121].

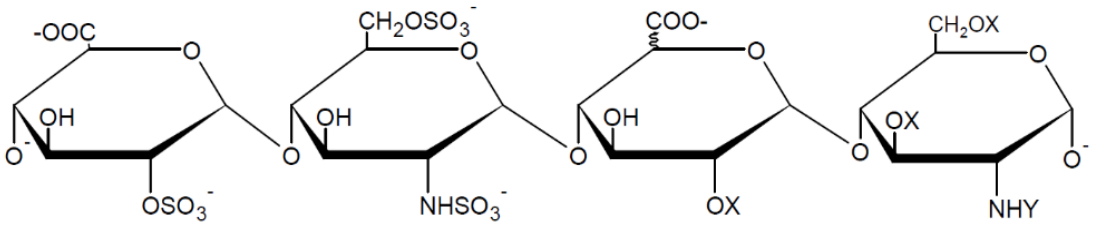

Figure 3.3. Heparin structure. [Adapted from: Linhardt (2003)]

Heparin is synthesized firstly as a proteoglycan which afterwards becomes a polydisperse blend of polysaccharides expressed and store in the mast cells (mostly in the surface) [120] with a relative molecular mass of around 5000 and 25000 [121].

3.1.4.1 Heparin sources

Normally, heparin can be found in organs such as liver, intestines and lungs [121], and it can be synthesized from different animal tissues, such as porcine and bovine [120]. This biosynthesis represents the current standard of fabrication of heparin; however, more synthesis methods are also under investigation [122]. The pharmaceutically obtained heparin can be fractionated considering its degree of sulphation and chain length. But, isolation of discrete sequences is not possible, therefore, the obtained heparin is the result of the blend of similar chains and its characterization is the representative results for these common structures [120,121]. Heparin obtained from different tissues, exhibit differences in their structures, it has been observed that porcine intestinal heparin is very similar to human heparin from mast cells [121].

Among the alternatives currently analysed to produce heparin we can find the production from Chinese hamster ovary cells, which naturally produce heparin sulphates, like heparin in structure but without the anticoagulant properties of it.

These cells have a lower production rate, which requires the use of aid substances, such as cysteine, or gene modification techniques. Though there has been a great advancement in the use of mammalian cells for production of heparin, there is still much work to be done on the field[122].

3.1.4.2 Heparin properties

Heparin is mostly recognized by its anticoagulant property [120,121], however, Chiodelli et al. (2015) also highlight mechanical functions as well as cell proliferation and differentiation influence [15]. The main reason for this variety of activities is the interaction of heparin with a wide variety of biomolecules, such as cytokines, enzymes, and growth factors.

Anticoagulant activity of heparin is elucidated mainly by its interaction with antithrombin and heparin cofactor II, serpins that regulate coagulation cascade by inhibiting thrombin and other enzymes [15,63,121]. Therefore, it has been widely exploited for the treatment of thromboembolic diseases [120].

Rabestein (2002) explains the interaction of heparin with various proteins through its anionic nature. This characteristic is mainly due to the sulphate groups allocated along its backbone [120]. The ion exchange produced through this interaction allows heparin to bind with the positive domain of several macromolecules. Linhardt (2003) remarks the following: (1) Proteins like FGF family, VEGF family, chemokines, and serpins, influencing their activity in cell recruiting, proliferation, and development during processes like inflammation, coagulation or angiogenesis [63,121]. (2) Enzymes such as prokaryotic heparin lyases (heparanase), which also influences its activity in tumour growth, tissue healing, and neovascularization [121]. And (3) viruses like Dengue, interacting with the sulphate groups of the superficial heparin in cells, consequently being important for the evolvement of the disease [121].

Functionalization of heparin, in terms of its molecular weight, has been possible due to different depolymerization and purification methods, during its preparation. According to any or both of these, we can find low molecular weight heparin (LMWH), high molecular weight heparin (HMWH) and ultra-low molecular weight heparin (ULMWH). Their coagulation properties vary according to the interaction with antithrombin, due to the differences in their sulphated groups. It has been observed a better pharmacokinetic and dosage regulation with LMWH, while ULMWH show more sites that bind with antithrombin. These modification of weight and size in heparin also influence the way it interacts with other biomolecules such as growth factors and enzymes [123].

3.1.5 List of Materials

- Chitosan molecular weight 100,000-300,000, DD ≥90%. ACROS Organics™, Lot: A0376581.
- Hydroxyapatite sintered powder. Purchased from Captal S® Batch P220S. Particle size varied from 0.5± 0.2 µm to 12 ± 1 µm.
- Heparin sodium salt, from porcine intestinal mucosa, unfractionated, IU>=100/mg. Alfa Aesar. Lot: A16198.
- Acetic acid glacial ≥99.85%. ACROS OrganicsTM. Lot: A0375749.
- Sodium hydroxide (NaOH) 98% pellets. ACROS Organics™
- Phosphate buffered Saline Tablets. Oxoid™
- Ethanol absolute. AnalR NORMAPUR
- Deionized water

3.2 Methodology for scaffold preparation

A complete description of the methodology employed to prepare the proposed bioactive scaffold for improving bone angiogenesis is presented in the subsequent sections. The development and/or optimization of this process is presented in detail in chapter 5, Section I. As a result of the experiments carried out during this part, the following protocol was obtained. Two main phases can be considered: the preparation of the scaffold via freeze-gelation and the process of loading heparin onto the scaffolds to functionalize them for vascularization infiltration purposes.

3.2.1 Freeze-gelation

As described in section 3.1.1.3 the most common method to produce chitosan scaffolds is using freeze drying techniques, however, Ho et al. (2004) hold the view that freeze-drying can be replaced by freeze-gelation due to various advantages of the latter, such as less time and energy consuming, less remaining solvent and no surface skin formation [124]. In the same way as in freeze-drying, during freeze gelation chitosan solution is frozen using a regular cooling rate to obtain the desired porosity. Pore dimension and interconnection are dependent mainly on thermal rates as well as chitosan amount; bigger pores can be obtained with lower freezing rates [79–81,125]. Once chitosan solution is frozen, it is subsequently immersed in a precooled aqueous solution to induce its gelation. Since the gelation takes place below the freezing point, the chitosan frozen solution does not dissolve again, which prevent the structure of losing its shape and porosity while drying at room temperature [79,124,126,127].

The methodology to prepare the scaffolds is based on Qasim S. B. et al (2015) [126] methodology to produce porous membranes for periodontal regeneration, with slight modifications due to the addition of heparin sodium salt, and result from the trials described in chapter 5, section I.

3.2.1.1 Optimized freeze-gelation methodology

Distilled water was warmed to 50°C in a 250 mL volumetric flask. 7.5 g of chitosan were added to this flask and the mixture was stirred for 1 hour. When this time had passed, heat was turned off and dropwise addition of glacial acetic acid began (at an approximate rate of 1mL/5min). To achieve a solution 0.3M, 4.3 mL of glacial acetic acid were used. Obtained chitosan solution was a golden colour viscous liquid. The magnet was removed, and the solution was diluted to 250 mL with deionized water while maintaining stirring for another 6 hours.

Subsequently, 7.5 g of hydroxyapatite powder were added, and the mixture was stirred overnight (approximately 13 hours).

On the following day, the solution was poured into plastic petri dishes, adding the necessary amount according to the required scaffold thickness. The containers were placed into the freezer at 4°C for 1.5 hour. After this period, the temperature was gradually decreased in -4°C per hour until a final temperature of -20°C. The frozen solution was kept at -20 °C for further 12 hours.

On the next day, the frozen discs were carefully removed from the petri dishes by pressing the edges of the mould and gently applying pressure at the bottom of the dish. A 3M NaOH/ethanol solution was poured into glass petri dishes and the frozen discs were placed into them, more NaOH solution was poured into the glass petri dish to cover completely the frozen disc. All the immersed discs were place at –20°C for 12 hours.

After 12 hours of immersion in the gelling solution, the discs were taken out and washed as follows: 15 minutes with distilled water, 5 minutes with PBS, 15 minutes in 80% ethanol solution and 15 minutes in absolute ethanol.

Finally, the obtained product was left to dry in the fume cupboard overnight (approximately 13 hours), until all moisture was removed.

3.2.2 Heparin Coating

Scaffolds were cut into cylinder shapes of approximately 5 mm of diameter using a hole puncher or a cork borer.

50 mL of different aqueous solutions of heparin with concentrations of 0.5, 1, 2 and 5 mg/mL were prepared by dissolving heparin sodium salt in the correspondent amount of deionized water (details of the amounts are presented in Table 3.1). With the purpose of all the material having undergone the same procedures, scaffolds without heparin, were put in distilled water alone, so they can be submitted to freeze-drying after heparin loading as well as the other scaffolds.

Concentration (mg/mL)	Heparin content (mg)	Distilled water (mL)
0	0	50
0.5	25	50
1	50	50
2	100	50
5	250	50

Table 3.1. Amounts of heparin according to the loading concentrations.

Subsequently, the scaffold cylinders were immersed in the heparin solution for 1.5 hours at room temperature.

After this time, the material was removed from the heparin solution and any excess of solution was blotted. Following by a removal of the moisture from the loading procedure by freeze drying the product at -25 °C, for 24 hours.

3.3 Summary

The materials chosen in this study have demonstrated good proangiogenic potential, making them excellent materials for bone repair and regeneration. Chitosan provides outstanding biodegradable and biocompatible characteristics, enable them to act as a useful organic matrix. On the other hand, hydroxyapatite has been the material of choice for years to serve as the inorganic matrix of bone in tissue engineering scaffolds due to its similar composition with the one of real bone. The combination of these two materials has been amply studied and documented with positive results.

Freeze-gelation was used to produce a good method to fabricate bioactive scaffolds for achieving the required structure characteristics, such as, interconnected porosity, pore size, bioactivity and hydroxyapatite particle distribution within the polymer matrices.

The characterisation methods are described in the following chapter.

4

Characterisation

The following sections and sub-sections describe in detail the methodology employed to characterize the chitosan/hydroxyapatite/heparin scaffolds.

The methods used for characterisation of the samples are outlined in detail. How each characterisation technique that was used as well as the procedures developed are described. Parameters that were used (finalised or altered according to requirements), such as time, settings, reagents amount, and general protocols are explained in detail, not only in this chapter but also addressed in the following chapter. Once the full chemical, biological, physical, and mechanical characterisation was achieved and the best materials identified, CAM assay was used and this has been explained fully, as this is a critical aspect of this thesis to assess angiogenesis in relation to natural materials on their own and in combination with heparin.

4.1 Structural characterisation

4.1.1 Scanning Electron Microscopy (SEM)

The morphology of the scaffolds was analysed by scanning electron microscopy (SEM). Using a Jeol JSM 7800F microscope. Another set of images were obtained with a Vega3 Tescan, under the same conditions. The cylindrical samples were observed from top, bottom, and side faces as pointed in Figure 4.1. Each sample holder was prepared with

3 samples of the same heparin concentration: one sample is placed with the top face facing up (chitosan side), another scaffold with its bottom face facing up (hydroxyapatite side) and the third scaffold was transversally cut in a half to place the edge of the scaffold facing up (4.2).

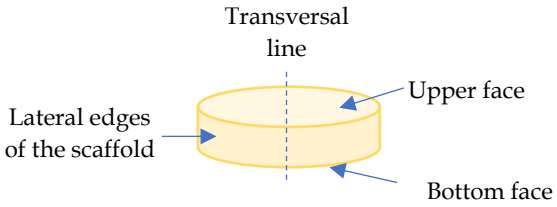

Figure 4.1 Scaffold orientation and faces.

Once placed in the holder, the scaffolds needed to be gold sputtered, with a 10 nm thickness.

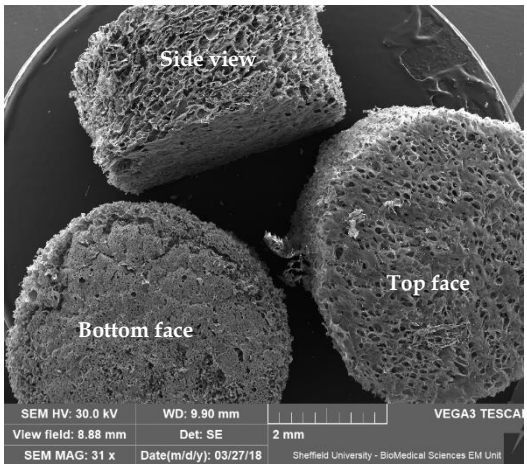

Figure 4.2 Scaffold arrangement for SEM analysis. Scale bar is 2 mm.

From the obtained images, porosity of the samples was determined by measuring the pore diameters of selected pores in the image using ImageJ®. Figure 4.3 shows an example of this process, though less pores are presented in this image with the purpose of allowing to see the measures.

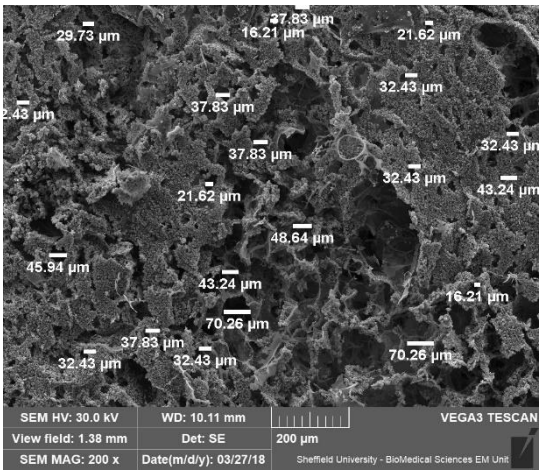

Figure 4.3 Example of representative porosity measurement using ImageJ® (less pores than usually measured are showed to provide an example). Scale bar is 200 µm.

4.1.2 EDX analysis

Additionally, Energy Dispersive X-Ray (EDX) spectroscopy was performed on the scaffolds. This technique allows the acquisition of a compositional analysis of the sample. The purpose was to verify the presence of the sulphate on the scaffold. This was performed by using a Jeol JSM 7800F microscope.

4.1.3 *In-vitro* degradation study

The procedure for the in-vitro degradation study was based on Qasim S. (2017) [128].

Four time-intervals were evaluated: 1 day (T1), 7 days (T2), 14 days (T3), and 21 days (T4).

The media solution used for this in- vitro degradation study was prepared by dissolving 500 mg of lysozyme powder (Alfa Aesar) into 500 mL of a sterile PBS solution. This solution was kept in the fridge at 10 °C.

The study consisted of 3 experiments with 3 replicates per each sample.

Every sample (and replicate) was individually weighted, and its weight was recorded as W_i. Once the samples were weighted, pictures of the first sample of each group next to a ruler were taken as a reference of their initial appearance.

Every test tube was labelled with the composition of the scaffold (indicating the heparin content), experiment number and the number of sample and/or replicate. The samples were placed individually into the test tubes followed by the addition of 3 mL of the media solution. All the tubes were placed into an oven at 37° C.

Individual set of samples was set for each designed interval, i. e. 45 samples were placed for T1 interval, 45 samples for T2 interval, etcetera.

Samples were taken out of the oven according to the designed intervals. The pH of the media for the first sample of each group was measured (while waiting for the pH measurement to take place, the samples were kept on a hot plate adjusted to 37 °C).

The rest of the samples from each group were taken out of the oven one by one and washed three times with 1 mL of deionized water each time. Next, each sample was placed on a two-layer tissue, labelled with its identification. Every sample was left on the tissue for 30 seconds for each side to remove most water from its surface.

After, every sample was transferred to an individual clean vial for a 24 hour-drying in an oven at 37 °C.

Once the samples were dried, they were taken out of the oven and individually placed on a tissue paper, applying gentle pressure 2 times on each sample to remove the surface water.

Finally, the samples were weighted, recording this data as W_f. After the weight measurements, pictures of the first sample of each group were taken for comparison.

The following equation was applied using the data from the weight measurements. This equation determines the degradation, which is expressed as % Dry weight:

$$\%\ Dry\ weight\ remaining = \left(\frac{W_f}{W_i}\right) \times 100$$

NOTES:

1) All the test tubes with samples in lysozyme media, were swirled 1 time a day manually.
2) The lysozyme solution was replaced with fresh solution **every week**.

4.2 Physicochemical characterisation

4.2.1 FTIR-ATR

FTIR characterisation was performed using a Nicolet iS50 FT-IR spectrometer, in conjunction with the Attenuated Total Reflectance (ATR) sampling accessory equipped with a diamond crystal, which allows to analyse surface of the sample. Spectra from the top and bottom surfaces of the scaffolds were obtained for comparison. Spectra were obtained at 4cm^{-1} resolution by accumulating 128 number of scans using Omnic™ 9 software.

4.2.2 Heparin determination

Toluidine Blue assay is a method based on the process developed by Smith P. K. et al (1980) [129]. The assay is based on the change from blue to purple produced when Toluidine Blue interacts with a heparin solution. A heparin-dye complex is formed which can be removed by adsorption in an immiscible organic solvent, the absorbance of the remaining dye is then read in a spectrophotometer. The purple shade and the amount of heparin-dye complex produced depend on the concentration of heparin,

thus the presence of heparin is not only visibly determined, but it also can be quantified by comparing with a calibration curve.

4.2.2.1 Calibration Curve

The calibration curve is necessary to compare the results of the absorbance of the samples against the absorbance of known concentrations.

A solution 0.05% of toluidine blue was prepared. For this purpose, 0.2 g of NaCl were dissolved in a 100 mL flask using deionized water. Once the NaCl was dissolved, 1 mL of HCl 1 N was added and let to stir for at least 10 minutes. Finally, 5 mg of toluidine blue (TB) dye were added and kept under stirring for another 15 minutes. The solution was diluted to 100 mL with deionized water.

A set of 12 concentrations of heparin solution, from 0 to 140 µg/mL, were used for the preparation of the calibration curve. To prepare these solutions, 8 mg of heparin sodium salt were dissolved in 8 mL deionized water, stirring at room temperature. To prepare 50 mL of a solution with a concentration 160 µg/mL, the 1 mg/mL heparin solution was dissolved in a 50 mL volumetric flask. Next, a series of dilutions from this solution were prepared by adding the necessary amount of the 160 mg/mL solution and deionized water, as shown in Table 4.1.

A set of clean 5 mL bijou container labelled according to the heparin concentration were prepared. 750 µL of TB solution were added to each tube. Subsequently, 250 µL of heparin solution were added to the corresponding concentration container and the mixture was swirled. These mixtures were left to rest for 30 minutes. Next, 750 µL of n-Hexane were added into each container, followed by a vigorous shake of the container for at least 30 seconds. The aqueous part of this mixture (bottom liquid) was taken out and placed it in a 96 well plate to be read. At least 2 replicates of each concentration were taken.

The absorbance of the well plate was read in a plate reader at 630 nm.

Concentration (µg/mL)	Heparin solution (mL)	Water (mL)
0	0.00	5.00
10	0.3	4.7
20	0.6	4.4
30	0.9	4.1
40	1.3	3.8
50	1.6	3.4
60	1.9	3.1
70	2.2	2.8
80	2.5	2.5
100	3.1	1.9
120	3.8	1.3
140	4.4	0.6

Table 4.1. Dilutions performed to prepare calibration curve.

The following calibration curve was obtained.

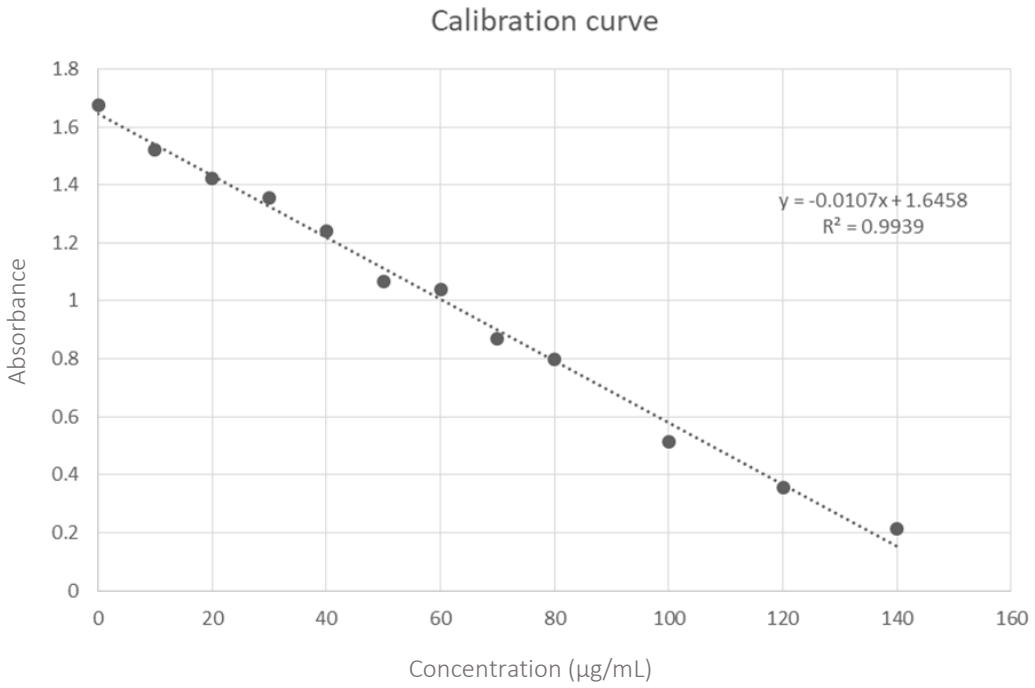

Figure 4.4 Calibration curve for heparin quantitative determination.

Along with the calibration curve, the equation for the tendency line was obtained, this equation was used to interpolate the concentration values by solving for x (Eq. 4.1):

$$x = \frac{y - 1.6458}{-0.0107} \qquad \textbf{Eq. 4.1}$$

4.2.2.2 Quantitative Heparin determination protocol

The study consisted of 3 sets of experiments with 2 replicates per each sample concentration.

For this evaluation, a 0.05% toluidine blue solution was used. This solution was prepared in 100 mL volumetric flask by dissolving 5 mg of toluidine blue dye in an aqueous solution containing 0.2 g of NaCl and 1 mL of HCl 1 N.

Seven time-intervals were tested according to the data show in Table 4.2. The same set of samples (which includes all the heparin concentrations) was evaluated on each designed interval.

Interval ID	Time
T1	30 minutes
T2	60 minutes
T3	90 minutes
T4	150 minutes
T5	210 minutes
T6	24 hours
T7	48 hours
T8	5 days

Table 4.2. Intervals for toluidine blue assay.

The cylindrical scaffolds were individually placed into test tubes adding 1 mL of deionized water into each tube, followed by incubation at 37 °C according to the test intervals mentioned before.

The samples were taken out of the oven when the first time-interval was concluded. As soon as every time interval was finished, 250 µL of the incubation water were extracted from every sample tube ** and added into correspondent tubes containing

750 µL of Toluidine Blue solution. Every tube was carefully swirled, so the incubation water is completely mixed with the Toluidine Blue solution. This process was followed by a 30-minute rest, after which 750 µL of n-Hexane were added into every tube and the mixtures were vigorously shaken for at least 30 seconds. The aqueous phase (bottom liquid) was removed and transferred into a clean 96 well plate for its reading. The absorbance of this phase was measured at 630 nm using a plate reader, the readings were compared to the results of a calibration curved previously elaborated. To obtain the correspondent amount of heparin Equation 4.1 was solved for x. The results for the scaffolds without heparin were considered as background, therefore, they were subtracted from the result.

**NOTE: Once the 250 µL of incubation water were extracted, the samples were changed to new testing tubes with clean deionized water and taken back to the oven to complete the following time interval of the experiment until it is concluded, and the process was repeated.

4.2.2.3 Qualitative Heparin determination protocol

Another set of scaffolds, two per each heparin concentration, was separately immersed in 1.5mL of the 0.05% toluidine blue solution. The scaffolds were left to rest for 5 minutes, followed by a wash with deionized water until no rests of the dye are observed in the washing water. The scaffolds were carefully dried using a tissue paper. Pictures of each scaffold were taken to verify the presence and distribution of the heparin on the scaffold by observing the purple shade.

4.2.3 pH determination

pH was measured using a Mettler Toledo GmbH, Analytical, FiveEasy Plus™ bench meter. The electrode was rinsed with distilled water, blotting the excess between every

use. Subsequently the electrode is introduced in the solution until the pH value appears on the bench meter screen.

4.3 Biological characterisation

4.3.1 Cell viability

Cell viability was evaluated through Alamar Blue assay. This method tests cell health and viability under the premise that living cells reduce the non-toxic reagent resazurin (blue and non-fluorescent) to resorufin (red and fluorescent). Therefore, an estimation of the living cells on time is performed by measuring the absorbance of their media.

The cylindrical scaffolds were disinfected using 70% ethanol and 1 hour under UV light.

Resazurin 1mM solution was prepared by dissolving 57.3 mg of Resazurin in 250 mL of sterilized PBS.

After disinfection, 30,000 cells of the line U2OS were seeded onto the scaffolds in a 24-well plate. On days 1st, 4th, 9th and 14th an Alamar blue ® assay was performed by changing the media where the scaffolds were suspended and adding the reagent (10% of the sample volume). By using a plate reader, the absorbance of each sample was obtained reading at 570 nm. Viability percentage was estimated considering the resultant absorbance for the cells growing in the well-plate without heparinized scaffold as the 100% of metabolic activity and the result for the media alone as the 0% of metabolic activity.

Once the assay was performed, the solution was removed from all the wells of the well-plate. Each scaffold was carefully washed three times with PBS to remove the colour from the Alamar Blue® assay. New cell media was added into each well and the well plate was returned to incubation.

During the test, media was weekly changed and after every cell viability evaluation, being replaced for fresh cell media.

4.3.1.1 Cell culture

The methodology to preserve the U2OS cells used for this evaluation was as described next. All these procedures must be performed inside a cell culture cabinet and using all the protective equipment, as well as performing the applicable disinfection protocols.

4.3.1.1.1 Medium preparation

For this particular methodology of cell culture, we use the DMEM (Dulbecco's Modified Eagle Medium) with 10% of additives.

50 mL of the DMEM are taken out of the bottle. Subsequently the following additives are incorporated.

- 50 mL of FCS (foetal calf serum) previously unfrozen.
- PS (penicillin-streptomycin, 5 mL vial)
- Glu (glutamine, 5 mL vial)

The media should be gently mixed and kept stored in the fridge until use.

4.3.1.1.2 Cell passage

The media was completely removed from the T75 flask containing the cells. Subsequently, the T75 flask was washed twice using 5 mL of PBS each washing.

Afterwards, Trypsin- EDTA solution was added into the flask and taken back to the incubator for 5 min. The purpose of this step is to remove the adhered cells.

The flask was taken out of the incubator and observed under the light microscope, it is possible to gently shake the flask, if necessary, to help the detachment of the cells from the flask surface.

The cell containing Trypsin-EDTA is taken out of the T75 flaks and poured into a universal tube containing 5 mL of DMEM. Then, this tube was centrifuge at 1000 rpm for 5 min. During this process, a cell pellet should be formed at the bottom of the universal tube.

The DME was carefully removed from above the cell pellet. Later, 5 mL of DMEM were added to softly resuspend the pellet, at this point, attention must be paid to avoid the creation of bubbles or foam during this process.

10 mL of DMEM were poured into a new and clean T75 flask. Put the necessary volume of cell solution (according to the cell counting). The T75 flask was incubated at 37.5 °C.

4.3.2 Angiogenic response *ex-ovo*

During *ex-ovo* CAM assay (CAM stands for chorioallantoic membrane) the scaffolds were implanted on live chicken embryo. This assay provides an overview of the performance of the material in a live environment. The followed procedure was based on Mangir et al (2019) and Eke G. et al (2017), [130,131].

Fertilized chicken eggs were carefully cleaned with 20% IMS solution prior its incubation at 37.5°C in a humidified chicken incubator. On the third day of incubation, the eggs were carefully cracked, the embryo was transferred into a sterilized petri dish containing 2mL of penicillin- streptomycin and kept in a humidified cell incubator at 37.5°C (no carbon dioxide or any other gas was used in the cell incubator).

The survival of the embryos as well as the consistency of the parameters (temperature, humidity) were daily checked and registered during the experiment.

On the 6th day, the scaffolds were sterilized using 70% ethanol and 1 h under UV light. The implantation of the sterile scaffolds within the CAM of the embryo was performed on the 7th day by taking each egg one by one out of the incubator and placing individual scaffolds on the CAM space of the embryo as mentioned by Mangir et al. (2019).

Sample pictures were obtained on the 10th day and on the sacrifice day (13th day), using an electronic PC microscope.

4.3.3 Histology

To retrieve the samples, it was necessary to carefully cut the CAM tissue surrounding the scaffold. This has to be done as fast as possible to avoid the scaffold to be bled. Immediately afterwards the chicken embryo was sacrificed.

Subsequently, the scaffolds were immersed in a bijou container with 5 mL of 3.7 % Formaldehyde solution for at least 12 hours. The fixed scaffolds were then slice-cut by using cryo-embedding technique (Leica), obtaining 10 µm slices. The slices were then stained using a regular haematoxylin & eosin protocol.

Observation under light microscope was performed to examine vascular infiltration.

4.4 Summary

All the characterisation methods are focused on highlighting and evaluating the main characteristics of our system to ensure it is a suitable structure for bone regeneration. For instance, SEM provides useful information regarding the structure of the scaffolds, such as pore size and distribution. Likewise, toluidine blue assay offers a remarkable tool to quantify the net amount of heparin loaded during the study, which represents one of the main findings of this research. Finally, CAM assay allows to test the material in a living environment, which ultimately translates to a preliminary *in vivo* performance of the scaffolds.

The next chapters contain the results obtained from these evaluations.

5

Results and Discussion

Section I:
Exploring methodologies for fabrication of hydroxyapatite/chitosan composites enabling vascular infiltration

Chitosan-hydroxyapatite composites have been reported in literature, however, to fabricate the architecture of the scaffold that would enable vascular infiltration and bone growth, it was important to test different methodologies and adapt them to satisfy our current requirements.

Detailed descriptions of the methodologies are described and alluded to as 'Trials', under the different approaches attempted. The first 5 'Trials' relate to the inclusion of carboxymethyl cellulose and the influence of pH, whilst 'Trials 6-9' describe and discuss the effect of freeze drying and freeze gelation methods and the suitability of these systems for incorporation of heparin.

The final method used to fabricate the scaffolds was selected based on the results from these different trials, and it has been fully described in Chapter 3, section 3.2.

5.1 Defining solution content: trials with carboxymethyl cellulose

The use of carboxymethyl cellulose in combination with chitosan has been previously reported with successful results [132–136]. The purpose of mixing the two polymers is mainly to improve mechanical properties of chitosan structures. Liuyun et al. (2009) reported scaffolds from nano-hydroxyapatite/chitosan/carboxymethyl cellulose for

bone tissue engineering. Their results show interconnected porosity, good mechanical strength and they allowed cell attachment and proliferation.

Additionally, Chen et al. (2015) described the preparation of a biodegradable scaffold made from bioactive glass/chitosan/carboxymethyl cellulose for bone haemostasis and bone regeneration, exhibiting successful results for reconstruction of bone defects.

For their part, Jiang et al. (2010) presented an option for preparation of a polyelectrolyte complex from chitosan/carboxymethyl cellulose/nano-hydroxyapatite for guided bone reconstruction with successful preparation results.

In the following trials the results obtained from reproducing some reported methodologies are described, in order to adapt them to the purpose of creating a good scaffold for bone regeneration and incorporation of heparin to improve angiogenic performance. It is important to highlight that, since freeze-drying and freeze-gelation methodologies were considered for the preparation of the scaffolds, the formation of a solution that was completely homogeneous in appearance was crucial in these trials. Therefore, any result that did not appear homogeneous, was immediately discarded.

5.1.1 Trial 1

Scaffold preparation based on *Liuyun, J. et al., J. Biom. Sci. (2009)* [132]

A hydroxyapatite (HA) slurry was prepared by adding 4 g of HA into 146 mL of distilled water. It was left under stirring approximately for 1 hour. Meanwhile, 3 g of chitosan and 3 g of carboxymethyl cellulose powders were weighed and mixed in a flask.

Once the powders were evenly mixed and the slurry was homogenous in appareance, the powders mixture was carefully added into the slurry keeping the stirring. A big

lump was immediately produced from the addition of the polysaccharide powders (Figure 5.1).

The mixture was kept under stirring for approximately 3 hours, until the lump was finally dissolved, and a homogeneous mixture was achieved.

Subsequently, 3 mL of glacial acetic acid were added. Formation of small lumps was instantly observed (Figure 5.2).

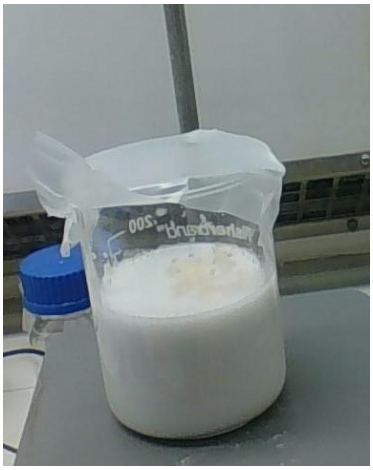

Figure 5.1. Slurry preparation of chitosan, hydroxyapatite and carboxymethyl cellulose.

Figure 5.2. Formation of small lumps within the slurry, after acetic acid addition.

5.1.2 Trial 2

The purpose of this study was to use freeze-drying or freeze-gelation methodology to prepare a porous scaffold. Therefore, a homogenous slurry is necessary to assure that the same composition can be found in any part of the scaffold. From the first trial, it was not possible to obtain a homogeneous slurry, due to the formation of lumps after the addition of acetic acid to the mixture of chitosan, hydroxyapatite and carboxymethyl cellulose. It was considered that the addition of acetic acid might have been very abrupt, therefore, for this trial this process was modified.

This trial is based on scaffold preparation following Liuyun procedure. *Liuyun, J. et al., J. Biom. Sci. (2009)* [132]

To prepare a HA slurry, 1 g of HA was slowly added into 36.5 mL of distilled water. The solution was left to stir for approximately 2.5 hours. In another beaker, 1 g of carboxymethyl cellulose was dissolved in 34.5 mL of distilled water, by the gradual addition of the polysaccharide. After the carboxymethyl cellulose was dissolved, 1 g of chitosan powder was slowly added to this solution with a spatula. Once the chitosan was completely and homogeneously distributed in the carboxymethyl cellulose solution (approximately 1 hour of stirring), this solution was carefully added into the HA slurry with the aid of a dropping funnel (Figure 5.3).

Figure 5.3. Addition of chitosan and carboxymethyl cellulose solution to the hydroxyapatite slurry.

After adding all the carboxymethyl cellulose/chitosan solution in the HA slurry, this mixture was let under stirring for approximately 1 hour, until a completely homogenous solution was obtained. Then 1 mL of glacial acetic acid was slowly added, with the aid of a burette, keeping the stirring (Figure 5.4).

Before the addition was completed lumps were formed around the stirrer (Figure 5.5).

Figure 5.4. Addition of acetic acid to the slurry.

Figure 5.5. Final slurry full of lumps.

5.1.3 Trial 3

Despite the slow addition of acetic acid, clumps were formed in trial 2. To avoid an abrupt change of pH due to the addition of glacial acetic acid, it was decided to reduce its concentration by preparing an aqueous solution. Therefore, a 2% acetic acid aqueous solution was prepared. Additionally, chitosan was previously dissolved in this 2% acetic acid aqueous solution prior its mixing with carboxymethyl cellulose.

This trial is based on Liuyun, J. et al., J Mater Sci: Mater Med (2009). [137]

Using 50 mL of an acetic acid solution 2%, 1 g of chitosan was dissolved under constant stirring. At the same time, 1 g of carboxyethyl cellulose was dissolved in 50 mL of distilled water at room temperature, by slowly adding the powder to the water.

Once the carboxymethyl cellulose was completely dissolved in the water, 1 g of HA was gradually added into this solution, keeping the stirring for approximately 1.5 hour, to obtain a homogeneous distribution of the HA.

When the HA was completely distributed in the carboxymethyl cellulose solution, the addition of the chitosan solution was started using a dropping funnel.

Once the chitosan solution became in contact with the carboxymethyl cellulose solution, beads of chitosan were formed from the drops that have fallen into the mixture (Figure 5.6)

Figure 5.6. Bead formation when chitosan solution is added to the carboxymethyl cellulose and hydroxyapatite solution.

5.1.4 Trial 4

It was observed that the interaction between the carboxymethyl cellulose was strongly abrupt, causing the formation of the beads instead of a uniform mixture. Therefore, another method, based on Jiang, H. et al., J Mater Sci: Mater Med (2011) [133], was considered.

For this, 1 g of carboxymethyl cellulose was dissolved in 100 mL of distilled water, by slow addition and constant stirring. In the meantime, 50 mL of HA slurry were prepared by pouring 2 g of HA in distilled water. Once the slurry was homogeneous, 1 g of chitosan was carefully added into it and the mixture was left under stirring for approximately 1 hour). When a homogeneous solution was obtained, the carboxymethyl cellulose solution was gradually added with the aid of a dropping funnel and was left to stir for 2.5 hours. Jiang, H. et al. stated that to prepare this solution, pH should be kept between 5 – 5.2. Therefore, with the aid of a burette, the addition of 2% acetic acid solution was carefully started, keeping this mixture under vigorous stirring and the temperature between 26 and 27 °C. The pH was constantly measured, when a pH of 5.87 was reached, a thicker mixture was observed. After 10.3 mL of the 2% acetic acid aqueous solution was added, the pH reached a value of 5.18 and the addition was stopped. The mixture was kept under stirring for 15 more minutes more until the solution was poured into a plate. The consistency of the mixture was not homogeneous in appearance and small clumps were observable (Figure 5.7).

Figure 5.7. The addition of acetic acid causes the appearance of lumps and a heterogeneous mixture when the pH reached 5.18.

5.1.5 Trial 5, the influence of pH

During trial 4 a homogenous solution was not observed. Therefore, to verify the influence of the pH on the homogeneity of the resultant mixture, different variations of the amount of acetic acid added to the solution, and consequently variations on the pH were tested.

This trial is based on Jiang, H. et al., *J Mater Sci: Mater Med* (2011). [133].

1 g of carboxymethyl cellulose was dissolved in 500 mL of distilled water by slow addition and constant stirring. In the meantime, 50 mL of HA slurry were prepared using 1 g of HA in distilled water. Once the slurry was homogeneous, 1 g of chitosan was carefully added into it. When a homogeneous solution was obtained (approximately 2 hours of stirring), the carboxymethyl cellulose solution was gradually added with the aid of a dropping funnel and was left to stir for 3 hours.

A pH value of 7.834 was measured to this slurry. Subsequently, with the aid of a burette, 2% acetic acid solution was added at a rate of 1 mL/3 min to this mixture under vigorous stirring and keeping the temperature between 27 and 28 °C.

The paper mentions that pH should be kept between 5 and 5.2, therefore acetic acid solution was added to control the pH in the slurries, until 4 different pH were observed: 5.641 (before the threshold mentioned in the paper), 4.897, 4.843 (just below the threshold) and 4.290 (more acidic media). These slurries were used to compare the results with our previous sample of this method which has a pH of 5.185 (Figure 5.8).

The most homogeneous gel was found between a pH of 5 - 4.85. Though undissolved powder remained in the solution.

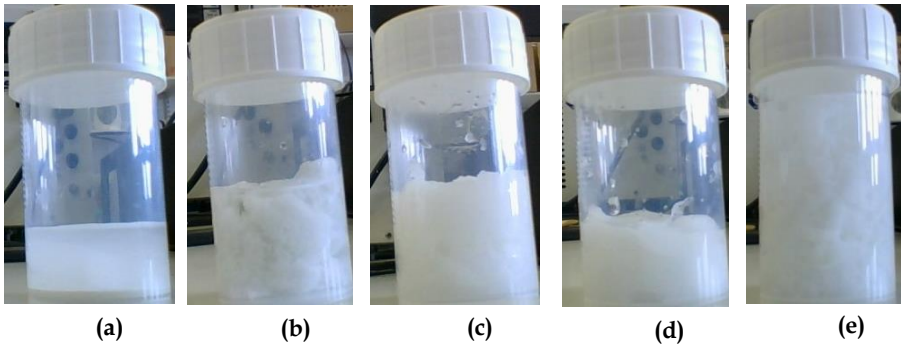

Figure 5.8. The effect of pH in forming carboxymethyl cellulose + chitosan + HA composites. 5 different pH values were tested (a) 5.641, (b) 5.185, (c) 4.897, (d) 4.843 and (e) 4.290.

5.1.6 Conclusions from the trials using carboxymethyl cellulose

After these trials it was decided to avoid the use of carboxymethyl cellulose in the fabrication of the composites. The aim of using of carboxymethyl cellulose was to improve the mechanical properties of the scaffold. However, the electrostatic interaction between chitosan and carboxymethyl cellulose is strong, producing precipitation and/or irregular mixtures. The homogeneity of the mixture was an important parameter because this mixture is going to be used with freeze-gelation and freeze-drying for scaffold formation.

In previous works, Jiang et al. (2011) compared the use of different methodologies to prepare chitosan/carboxymethyl cellulose/nano-hydroxyapatite membranes. They studied gradual electrostatic assembling (GEA), solution blending method and layered casting method. Ultimately GEA gave the most successful results, providing homogenous membranes, unlike the other two methods in which the electrostatic interactions between chitosan and carboxymethyl cellulose did not allow the formation of uniform structures [133]. Therefore, choosing the appropriate method to produce the scaffolds is crucial when working with these two polymers.

During the trials, variations of the pH provided the targeted response to eliminate precipitation formation. However, pH interval is short, and depends on several variables. Furthermore, the pH interval that provided a more homogeneous solution is a value for hydroxyapatite's dissolution in acidic media (pH <5) [138]. Therefore, if hydroxyapatite were added to the solution, it would probably become unstable, due to an excessive protonation of its lattice.

Another drawback is that precipitation and particle aggregation add one step to the process. Because, even when the lumps and clusters can be filtered and processed, it is ideal to provide a process as simple as possible (thinking about future industrialization).

Additionally, and most importantly, this strong force interaction would be a setback to add the heparin. Heparin possesses a negative charge, which, coming to this interplay of strong charge interactions, would have hindered its integration to the system. Therefore, for further protocols, carboxymethyl cellulose was not tested nor considered in this work.

5.2 The effect of chitosan: hydroxyapatite ratio in fabricating scaffolds using freeze-drying

One important aspect to consider for the fabrication of the scaffold was the ratio of chitosan and hydroxyapatite, which ultimately defines all the interactions within the composite. The following trials describe the methodologies compared to define the best chitosan: hydroxyapatite ratio to work for the bioactive scaffold's fabrication. Two main phases can be considered: the preparation of the scaffold via freeze-drying and the process of loading heparin onto the scaffolds to functionalize them for revascularization purposes.

One important factor considered during these trials was the malleability of the resultant scaffolds. This was important since the fabrication involves cutting the material into small pieces for the implantation purposes. Therefore, it was key that the obtained composite material allowed an easily cutting process.

5.2.1 Trial 6

This trial is based on methodology followed from Koç, A. et al., *J. of Biom. Appl.* (2014) [139] to prepare freeze-dried scaffolds.

50 mL of a mixture 80:20 of chitosan: hydroxyapatite was obtained by dissolving 2 g of chitosan and 0.5 g of hydroxyapatite in 47.5 mL of 2% acetic acid solution.

A second solution, with a ratio of 50:50 chitosan: hydroxyapatite, was also prepared by dissolving 1.25 g of chitosan and 1.25 g of hydroxyapatite in 47.5 mL of acetic acid solution 2%.

To prepare the previously mentioned solutions, chitosan was slowly added to the acetic acid solution 2%. Once it was completely dissolved, the solution was left to stir for approximately 2 hours. Then, the hydroxyapatite powder was slowly poured to the solution and left to stir overnight for full incorporation. Obtaining the mixtures showed in Figure 5.9.

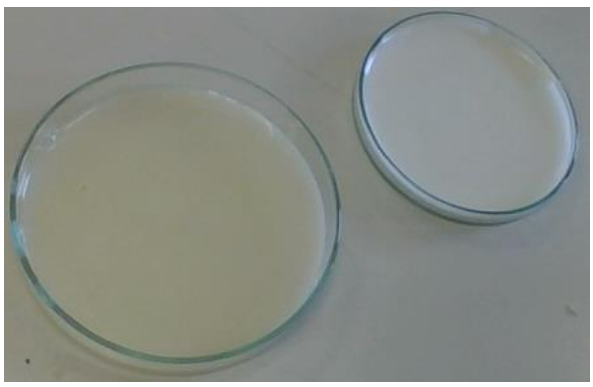

Figure 5.9. Chitosan/Hydroxyapatite solutions. Chitosan: hydroxyapatite 80:20 ratio is observed on the left, while 50:50 ratio is presented on the right. The appearance of a homogenous slurry can be observed.

Both solutions were frozen at -30° C for 12 hours. Subsequently, these solutions were freeze-dried at -15 °C with a pressure of 0.520 mbar for 29 hours. And finally, left on aeration for 40 hours.

The scaffolds shown in Figure 5.10 were obtained by this methodology. It is important to notice that the scaffold with higher hydroxyapatite content was cracked on its surface. However, both scaffolds are flexible in appearance.

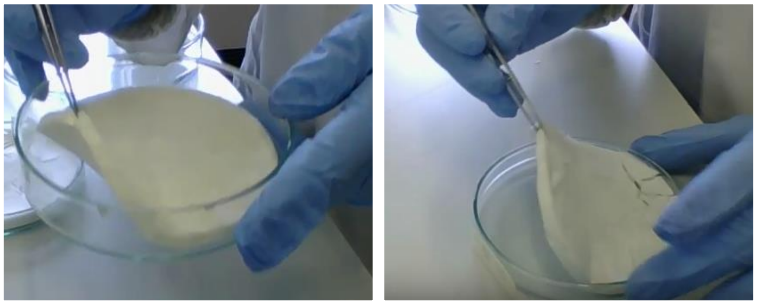

Figure 5.10. Scaffolds prepared using the methodology described in Trial 6. In the image on the right chitosan: hydroxyapatite 80:20 ratio is observed, while 50:50 ratio is presented on the right. Both scaffolds exhibited a soft foam-like appearance. Cracking can be observed on the scaffold with 50:50 ratio.

Treatment 1: Immersion in a 1M NaOH solution for 5 h

The following treatment for these materials was to immerse them into a 1M NaOH in absolute ethanol solution for 5 hours to remove acetic acid residues (Figure 5.11).

Afterwards, the scaffolds were washed with distilled water for approximately 3 minutes and underwent freeze drying again, to remove the remaining moisture.

For the moisture removing process, the scaffolds were frozen for -25 °C for 5 hours. Later, the drying began at -10 °C and a pressure of 0.520 m bar for 13 hours.

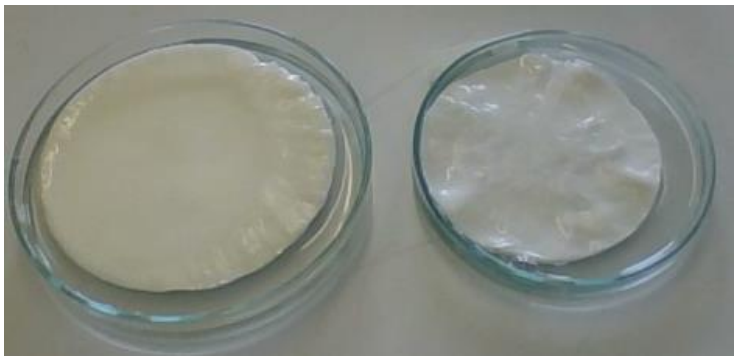

Figure 5.11. Scaffolds obtained by methodology of Trial 6 during immersion in 1M NaOH. In the image on the right chitosan: hydroxyapatite 80:20 ratio is observed, while 50:50 ratio is presented on the right.

As a result of these treatments, the scaffolds became hardened in appearance (Figure 5.12), which hinders properly cutting them into smaller scaffolds.

Figure 5.12. Appearance of the scaffolds obtained from Trial 6 methodology after following a 1M NaOH immersion treatment. Scaffolds shown on the right have a chitosan: hydroxyapatite 80:20 ratio, while 50:50 ratio is presented on the right. Image on the top present the top sides, while the bottom sides are presented in the image below.

5.2.2 Trial 7

The scaffold should have a malleable structure because they are to be cut into smaller pieces using a cork borer for the subsequent heparin loading and biological characterization. The methodology followed in Trial 6 indicated that the treatment of the freeze-gelled chitosan: hydroxyapatite scaffolds with sodium hydroxide solution affected the scaffold's structure. Hence the trial 7 experiments were aimed to determine the effect of the concentration of sodium hydroxide solution, the number of washing cycles and freeze-drying on the obtained scaffolds.

This trial is based on work reported by Koç, A. et al., *J. of Biom. Appl.* (2014) [139].
A 200 mL of 2 % acetic acid solution was prepared by drop-wise adding 4 mL of glacial acetic acid in 20 mL of distilled water. Once acetic acid was completely added, the solution was diluted with enough distilled water to make a 200 mL solution.
A solution of chitosan and hydroxyapatite, ratio 80:20, was prepared by dissolving 4 g of chitosan and 1 g of hydroxyapatite in 95 mL of the acetic acid solution 2%.

Similarly, a solution of chitosan and hydroxyapatite, ratio 50:50, was prepared by dissolving 2.5 g of chitosan and 2.5 g of hydroxyapatite in 95 mL of the acetic acid solution 2%.

For the preparation of the abovementioned mixtures, the chitosan was lowly added to the acetic acid solution. Once the powder was completely dissolved, the solution was left to stir for 3.5 hours. The resultant mixture turned into a clear-gold viscous liquid (Figure 5.13). Then, hydroxyapatite was slowly added and left to stir overnight to be fully incorporated (Figure 5.14).

Subsequently, the mixtures were poured into petri dishes (Figure 3.18) and frozen at -30 °C for approximately 12 hours.

Figure 5.13. Proper dissolution of chitosan in acetic acid solution 2% shows a clear-gold appearance.

Figure 5.14. Chitosan solution after adding the hydroxyapatite, turns into a white solution.

The freeze-drying process was started at -15 °C and 0.520 mbar for 37 hours. After the main drying process was turned off, aeration was allowed for 24 hours. The obtained sponge-like scaffolds are shown in Figure 5.16. For both chitosan: hydroxyapatite ratios, the appearance is of multiple sheets joined together to form the scaffold.

Figure 5.15. Chitosan and hydroxyapatite homogeneous solutions with ratios 80:20 (top dishes) and 50:50 (bottom dishes).

Figure 5.16. Chitosan/ hydroxyapatite sponge-like scaffolds. Ratio 80:20 is shown on the left and 50:50 on the right.

Additionally, these scaffolds were submitted for one of the following of treatments.

No treatment

One scaffold of each chitosan: hydroxyapatite (CS: HA) ratio was stored without any treatment.

Treatment 2: Washing scaffolds with distilled water

One scaffold of each ratio was washed with distilled water (running water) for around 3 minutes. It was not possible to continue washing the scaffolds longer because they started to dissolve and lost mechanical stability. pH was measured as described in section 4.2.3. pH did not change much after washing Table 5.1). The scaffolds were frozen at -20 °C for approximately 2 hours. After this time, they were freeze-dried at -25 °C for another 5 hours.

Composition (CS:HA)	Initial pH	Final pH
80:20	4.889	5.065
50:50	5.198	5.267

Table 5.1. Treatment 1, pH changes after washing the scaffolds with distilled water.

Treatment 3: Immersion in a 0.1M NaOH solution for 1.5 h

One scaffold of each CS: HA ratio were immersed (separately) in 0.1 M NaOH/ethanol solution for 1.5 hours. The pH of the NaOH/ethanol solution was 13.095. At the end of the immersion, shrinkage on the scaffolds was observed. The scaffolds were taken out of the solution and washed with distilled water until the water reaches a neutral pH (7.1< pH< 6.9).

Composition (CS:HA)	Initial pH	Final pH
80:20	13.095	6.987
50:50	13.095	7.064

Table 5.2. Treatment 3, pH changes after washing the scaffolds with distilled water.

Subsequently, the scaffolds from both treatments were frozen at -25 °C for 5 hours. Followed by the drying process at -10 °C and 0.520 mbar for 13:33 hours.

It is important to mention that all the treated scaffolds turned stiff (Figure 5.17). All sponges were oven-dried at 100 °C for 16 hours to completely remove the moisture.

Figure 5.17. Resultant scaffolds from the following treatments: (A) scaffolds washed with distilled water and (B) scaffolds immersed in a 0.1 M NaOH solution. Scaffolds of chitosan: hydroxyapatite ratio 80:20 is shown at the right, while 50:50 ratio is shown at the left of every image.

Images of the dried scaffolds were taken though a magnifying glass to observe their macroscopic structure. The images are presented in Figures 5.18 to 5.21, with view from the top (A) and a view from their lateral side (B).

Figure 5.18. Macroscopic structure of the resultant scaffolds from trial 7 after treatment 1: Immersed in NaOH 1M, for 5 hours, washed with distilled water. A sheet-like arrangement is observed on the top faces of the scaffold. Chitosan: hydroxyapatite ratio of 80:20 can be observed on the left, while the 50:50 ratio is presented on the right.

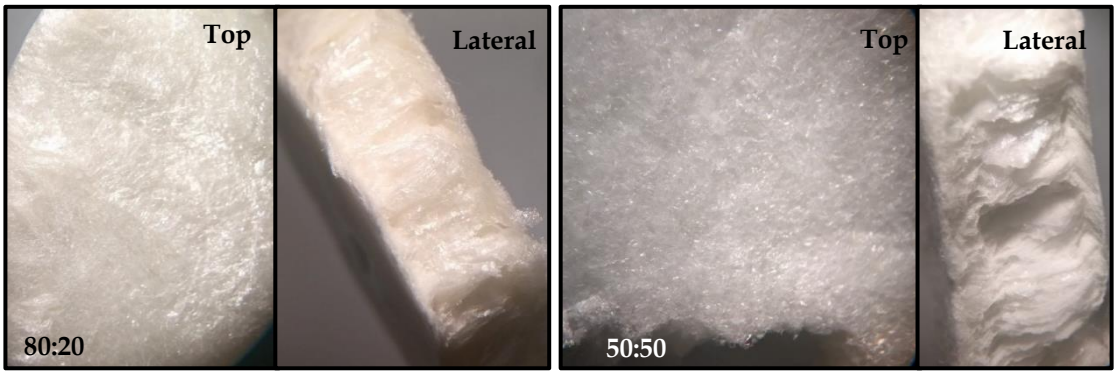

Figure 5.19. Macroscopic structure of the resultant scaffolds from trial 7 after treatment 2: Washed with distilled water for 3 minutes. It is possible to notice a sponge-like structure on the top faces of the scaffold. Chitosan: hydroxyapatite ratio of 80:20 can be observed on the left, while the 50:50 ratio is presented on the right.

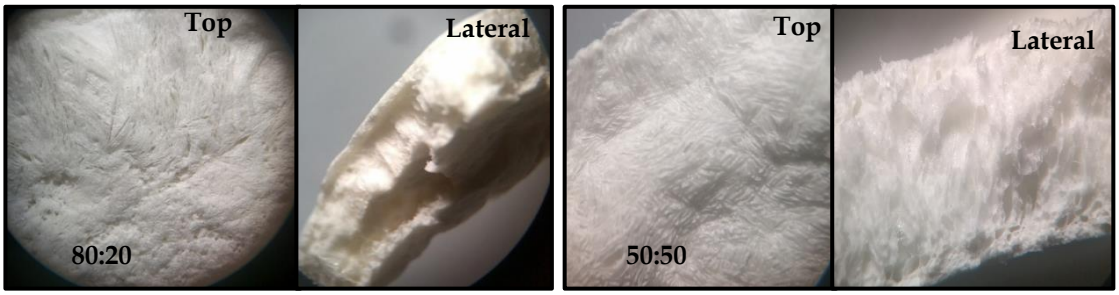

Figure 5.20. Macroscopic structure of the resultant scaffolds from trial 7 after treatment 3: Immersed in NaOH 0.1M, for 1.5 hours. Smaller ordained sheets can be seen on the top faces of the scaffolds, lateral faces present porosity. Chitosan: hydroxyapatite ratio of 80:20 can be observed on the left, while the 50:50 ratio is presented on the right.

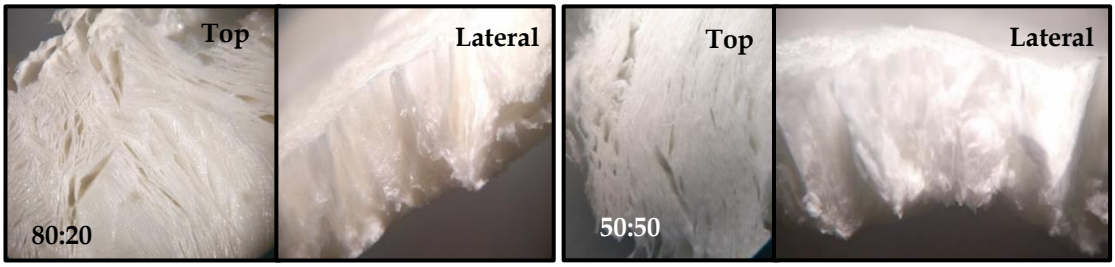

Figure 5.21. Macroscopic structure of the resultant scaffolds from trial 7 without any posterior treatment. Longer and less tighten sheets are observed from this treatment. Chitosan: hydroxyapatite ratio of 80:20 can be observed on the left, while the 50:50 ratio is presented on the right.

The appearance of stacked small sheets can be observed throughout all the images from Figures 5.18- 5.21. The rapid freezing during the beginning of the freeze-drying process causes the chitosan/hydroxyapatite solution to arrange in sheets. It is possible to observe that these sheets arrange and pack differently according to the NaOH treatment received. The purpose of the NaOH treatment is to neutralize the scaffold by deprotonating chitosan, which makes it less soluble in aqueous solutions. The presence of positive charges along the chitosan matrix, repelling each other, causes an effect on the arrangement of the chitosan/hydroxyapatite sheets. Due to this effect, a longer exposure to NaOH results in closely packed sheet, compared to those without treatment that appeared more loosely packed.

SEM images of scaffolds that were immersed in a 1M NaOH solution for 5 h and scaffolds without treatment were obtained to compare the effect of the NaOH/ethanol solution on the scaffold structure. Figure 5.22 shows a comparison of the distribution of hydroxyapatite along the chitosan matrix for the two chitosan: hydroxyapatite ratios.

NaOH did not appear to have an effect on hydroxyapatite distribution along the chitosan matrix. In general, regardless of the NaOH treatment, the appearance of the

scaffolds was as represented in Figure 5.22, i. e. the distribution of hydroxyapatite particles was similar to all the scaffolds no matter the NaOH treatment, with hydroxyapatite particles consistently distributed throughout the entire chitosan matrix. It is possible to observe a denser presence of the hydroxyapatite in the 50:50 ratio, due to the higher amount of the phosphate.

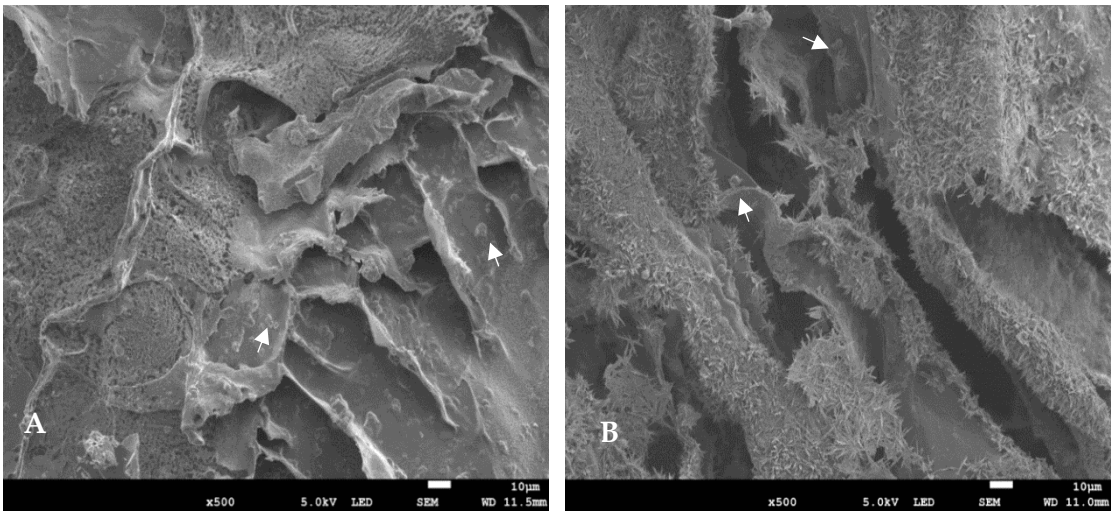

Figure 5.22. Hydroxyapatite distribution on the scaffold matrix for chitosan: hydroxyapatite ratios (A) 80:20 and (B) 50:50. Scale bars are 10 µm. Arrows point at HA particles. These two images are for the scaffolds treated with 1 M NaOH for 5 h, but are representative of the HA distribution for all the NaOH treatments. It is possible to observe the presence of hydroxyapatite particles distributed throughout the entire chitosan matrix.

Additionally, Figure 5.23 shows the impact of the NaOH/ethanol solution on the chitosan/hydroxyapatite structure, which was previously mentioned before. It is possible to observe that porosity on the laterals was conserved. However, for the scaffolds with longer exposure to NaOH, the sheet-like appearance closed down and some fibres became apparent on the structure.

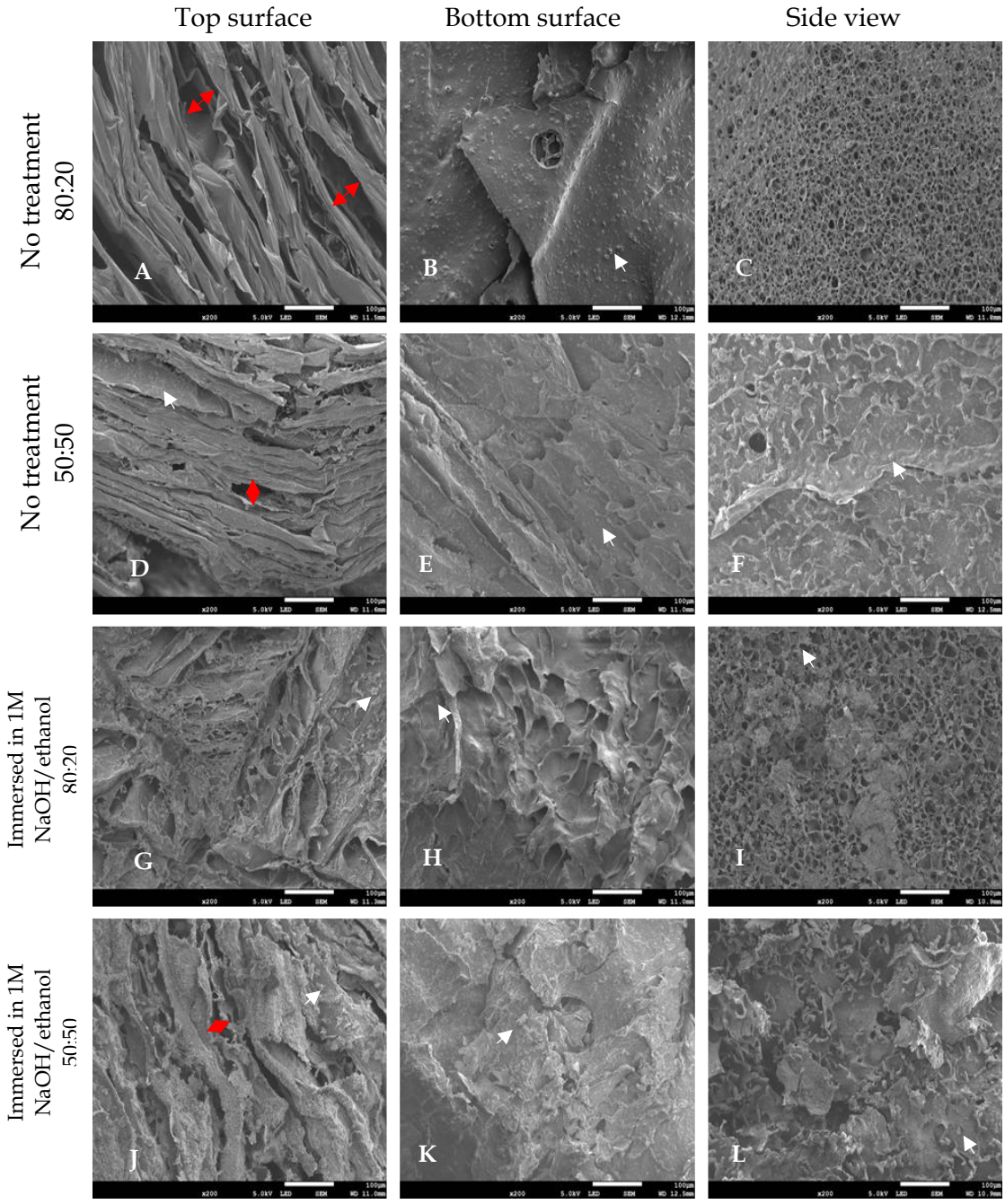

Figure 5.23. Impact of the NaOH/ethanol treatment on the scaffold's structure for both component ratios. Images of the top surfaces of the scaffold show the appearance of packed sheets, with a tighten packaging in the scaffolds with longer exposure to NaOH. The side views provide a general idea of the porosity changes with the NaOH treatment, were a closed and disorganised porosity is observed for scaffolds with longer exposure to NaOH and higher HA content. Bottom surfaces show less porosity than the rest of the scaffold surfaces. All scale bars represent 100 µm. White arrows point at HA particles. Red arrows show the space between sheets in the scaffold structure.

Following the treatments, the scaffolds were cut in small cubes of approximately 3 mm per side, to be loaded with heparin. Afterwards, two heparin solutions were prepared, one with the concentration of 1mg/mL by dissolving 120 mg of sodium heparin salt in 120 mL of distilled water and the other one with 3 mg/mL by dissolving 360 mg of sodium heparin salt in 120 mL of distilled water. The solutions were left to stir for approximately 2 hours at room temperature.

From every treatment, two groups of the cut scaffolds were separated, one was completely immersed in the heparin solutions of 1mg/mL for 1 hour and the other of 3 mg/mL for 3 hours. Once the immersion time was concluded, the solution excess was blotted, and the scaffolds were freeze-dried at -30 °C overnight.

The resultant scaffolds were analysed by FTIR- ATR to analyse the chemical composition and the presence of heparin. Since there are several combination from the scaffolds prepared, these are identified in the following table.

Chitosan: Hydroxyapatite ratio	**Treatment**	**ID**
80:20	Immersed in a 1M NaOH solution for 5 h + Immersed in heparin solution (1mg/mL)for 1 h	**CHHE11**
50:50	Immersed in a 1M NaOH solution for 5 h + Immersed in heparin solution (1mg/mL)for 1 h	**CHHE12**
80:20	Immersed in a 0.1M NaOH solution for 1.5 h + Immersed in heparin solution (1mg/mL)for 1 h	**CHHE13**
50:50	Immersed in a 0.1M NaOH solution for 1.5 h + Immersed in heparin solution (1mg/mL)for 1 h	**CHHE14**
80:20	Washed with distilled water for 3 min + Immersed in heparin solution (1mg/mL)for 1 h	**CHHE15**
50:50	Washed with distilled water for 3 min + Immersed in heparin solution (1mg/mL)for 1 h	**CHHE16**
80:20	None + Immersed in heparin solution (1mg/mL)for 1 h	**CHHE17**
50:50	None + Immersed in heparin solution (1mg/mL)for 1 h	**CHHE18**

80:20	Immersed in a 1M NaOH solution for 5 h + Immersed in heparin solution (3mg/mL)for 3 h	**CHHE31**
50:50	Immersed in a 1M NaOH solution for 5 h + Immersed in heparin solution (3mg/mL)for 3 h	**CHHE32**
80:20	Immersed in a 0.1M NaOH solution for 1.5 h + Immersed in heparin solution (3mg/mL)for 3 h	**CHHE33**
50:50	Immersed in a 0.1M NaOH solution for 1.5 h + Immersed in heparin solution (3mg/mL)for 3 h	**CHHE34**
80:20	Washed with distilled water for 3 min + Immersed in heparin solution (3mg/mL)for 3 h	**CHHE35**
50:50	Washed with distilled water for 3 min + Immersed in heparin solution (3mg/mL)for 3 h	**CHHE36**
80:20	None + Immersed in heparin solution (3mg/mL)for 3 h	**CHHE37**
50:50	None + Immersed in heparin solution (3mg/mL)for 3 h	**CHHE38**

Table 5.3. Identification of the samples according to their treatment and heparin loading concentration.

Heparin presents peaks at around 1230-1220 cm^{-1} corresponding to the asymmetric stretching of sulphate groups (SO_3- asymmetric stretching). Another characteristic sulphate peak has been reported at around 1040-1020 cm^{-1} corresponding to the symmetric stretching of sulphate groups. However, in our chitosan: hydroxyapatite scaffolds this last peak may be hindered by the presence of the phosphate υ_3 peak of hydroxyapatite, present at 1190-976 cm^{-1}.

The FTIR spectra of the scaffolds loaded with 1 mg/mL of heparin concentration are presented in figures 5.24-5.27. Each figure shows a comparison between the spectra of the two chitosan: hydroxyapatite ratios tested 80:20 and 50:50. The main peaks associated with the presence of heparin were not observed for the 1 mg/mL heparin loading concentration.

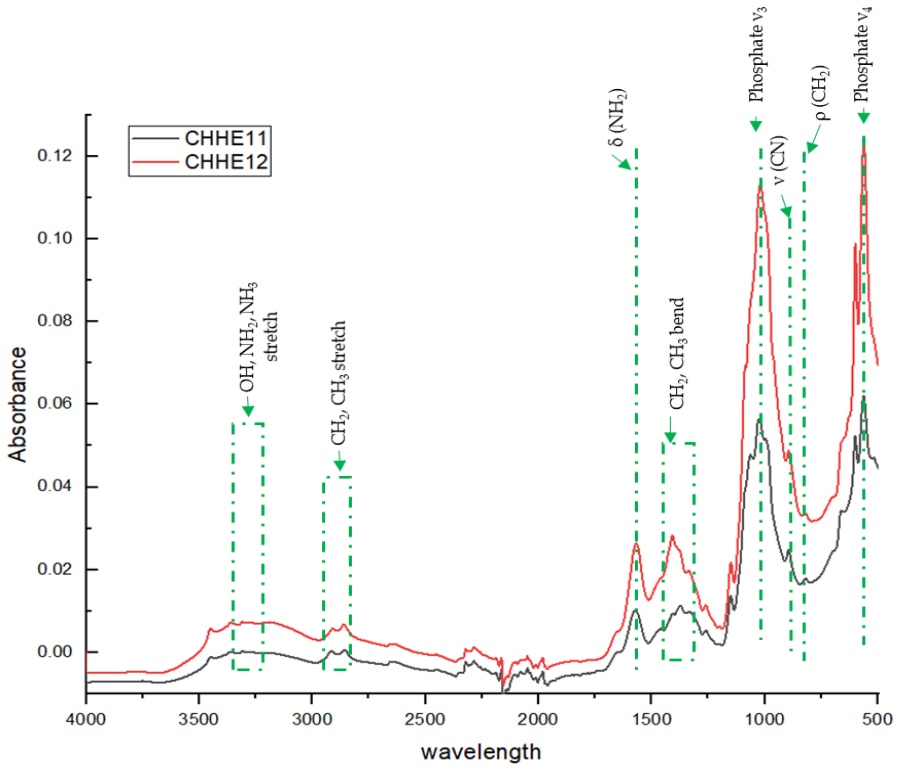

Figure 5.24. FTIR-ATR spectra of the scaffolds immersed in the NaOH 1M and loaded in the heparin sodium salt solution (1mg/mL) for 1 h. Ratios 80:20 and 50:50, respectively.

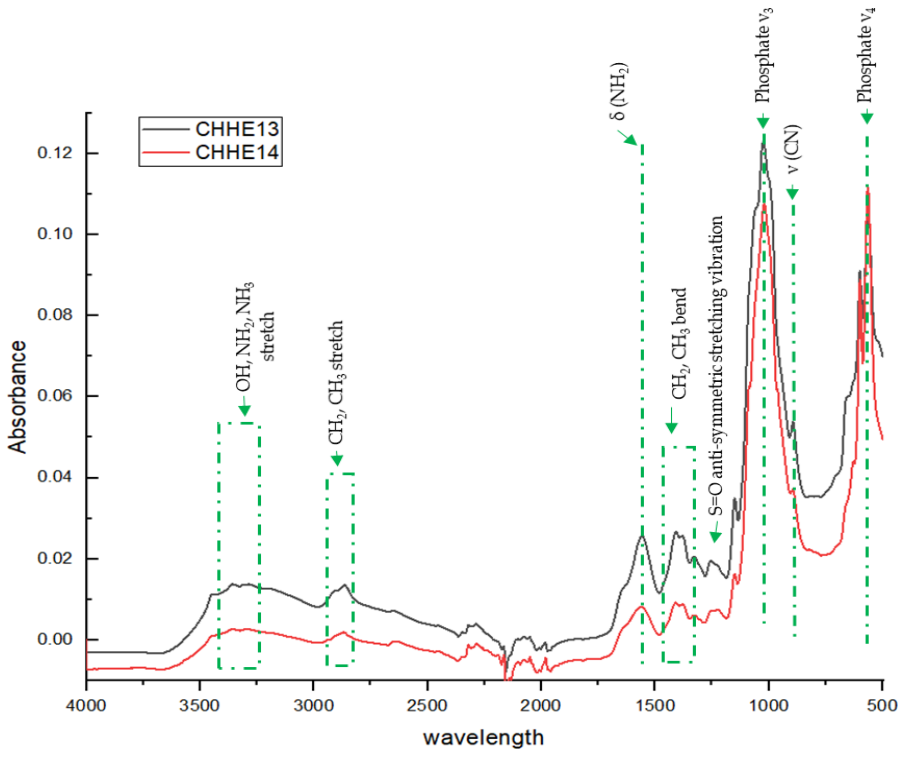

Figure 5.25 FTIR-ATR spectra of the scaffolds immersed in the NaOH 0.1M and loaded in the heparin sodium salt solution (1mg/mL) for 1 h. Ratios 80:20 and 50:50, respectively.

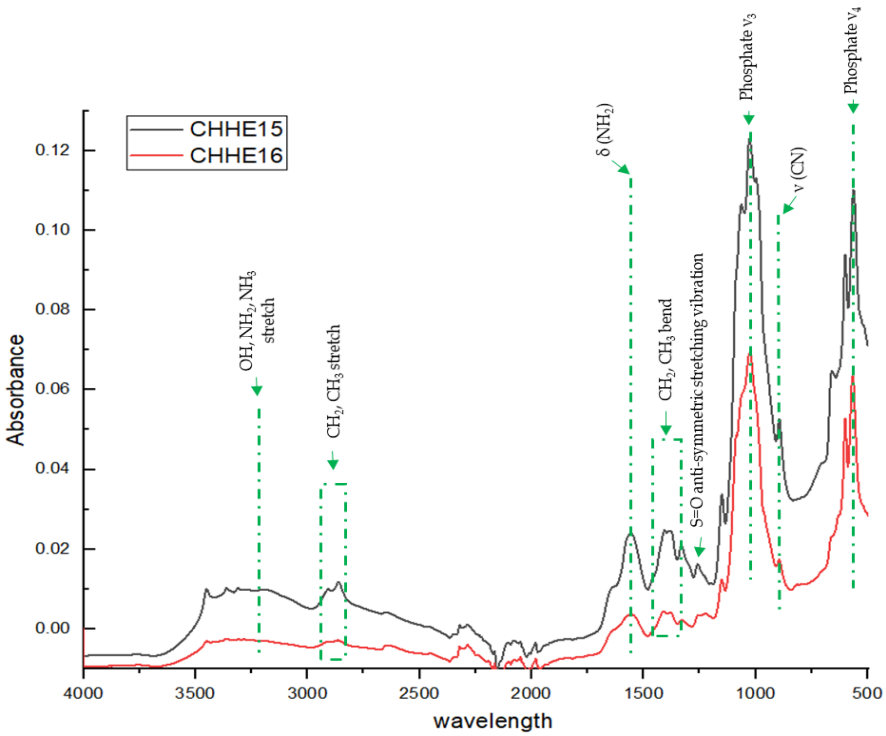

Figure 5.26 FTIR-ATR spectra of the scaffolds washed with distilled water and loaded in the heparin sodium salt solution (1mg/mL) for 1 h. Ratios 80:20 and 50:50, respectively.

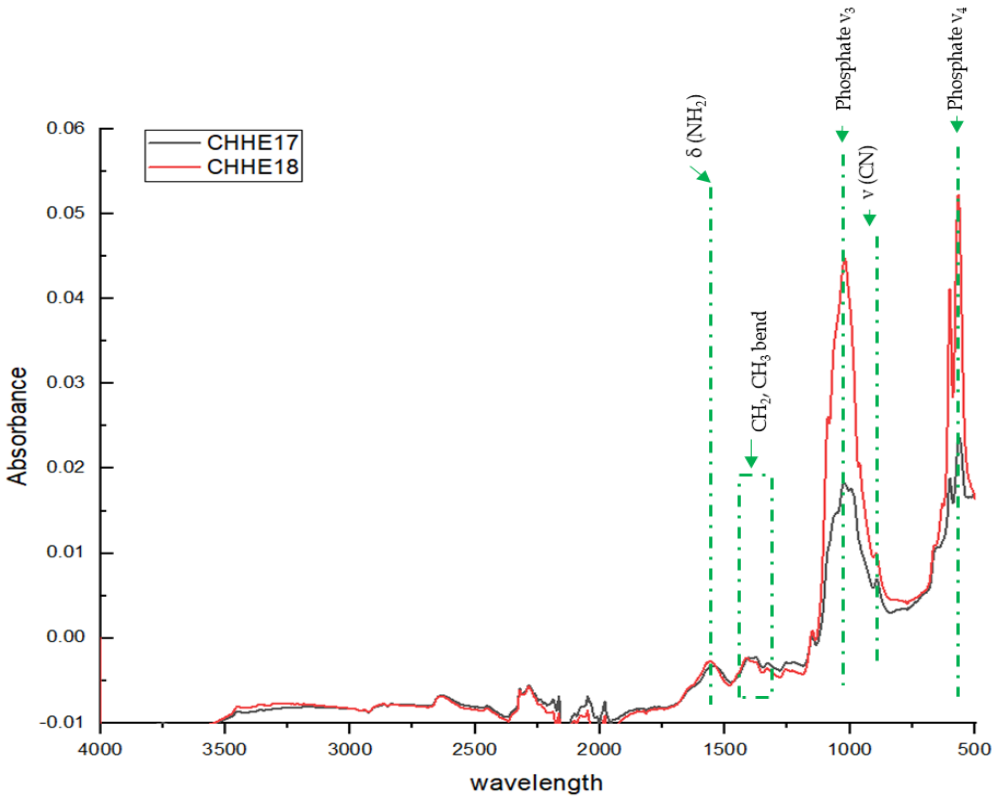

Figure 5.27 FTIR-ATR spectra of the scaffolds without a treatment and loaded in the heparin sodium salt solution (1mg/mL) for 1 h. Ratios 80:20 and 50:50, respectively.

The FTIR spectra of the scaffolds that were loaded with a higher concentration of 3mg/mL of heparin are shown in Figures 5.28-5.31. A low intensity peak was observed at 1225 cm^{-1} in these spectra, associated with the sulphate asymmetric stretching arising from heparin.

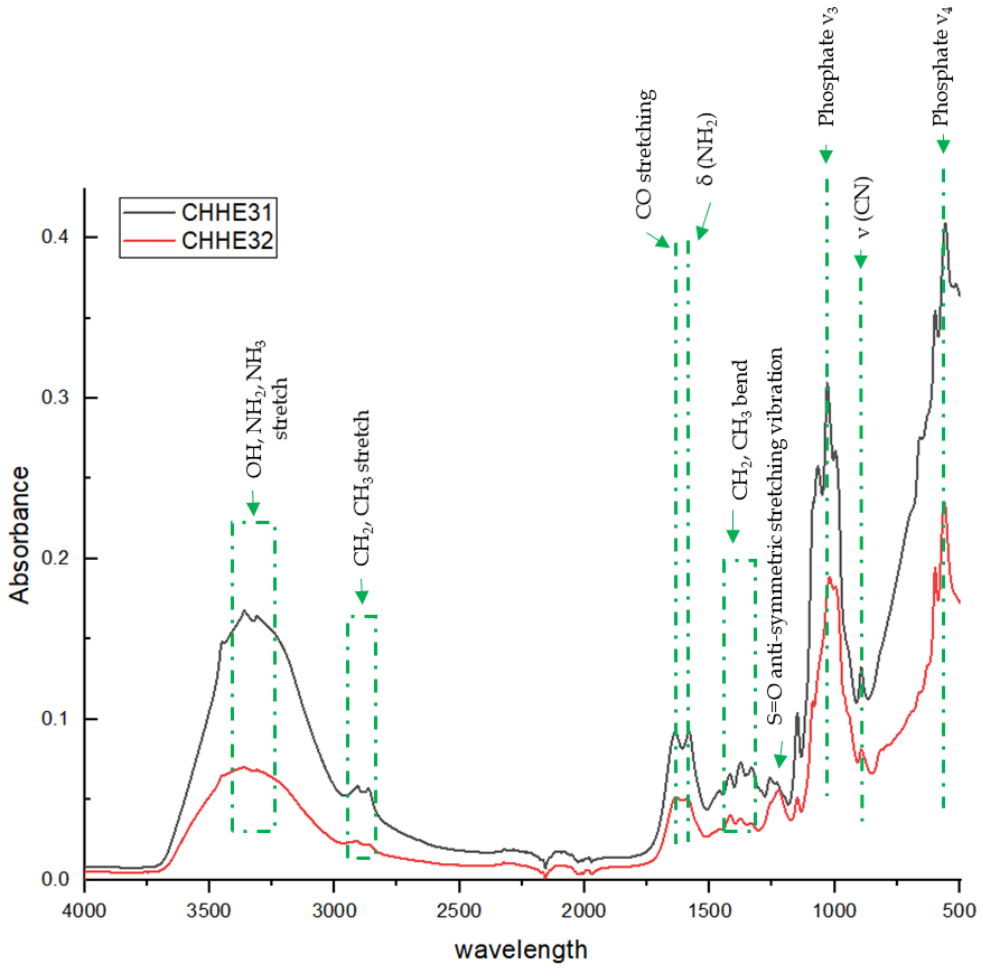

Figure 5.28. FTIR-ATR spectra of the scaffolds immersed in the NaOH 1M and loaded in the heparin sodium salt solution (3mg/mL) for 3 h. Ratios 80:20 and 50:50, respectively.

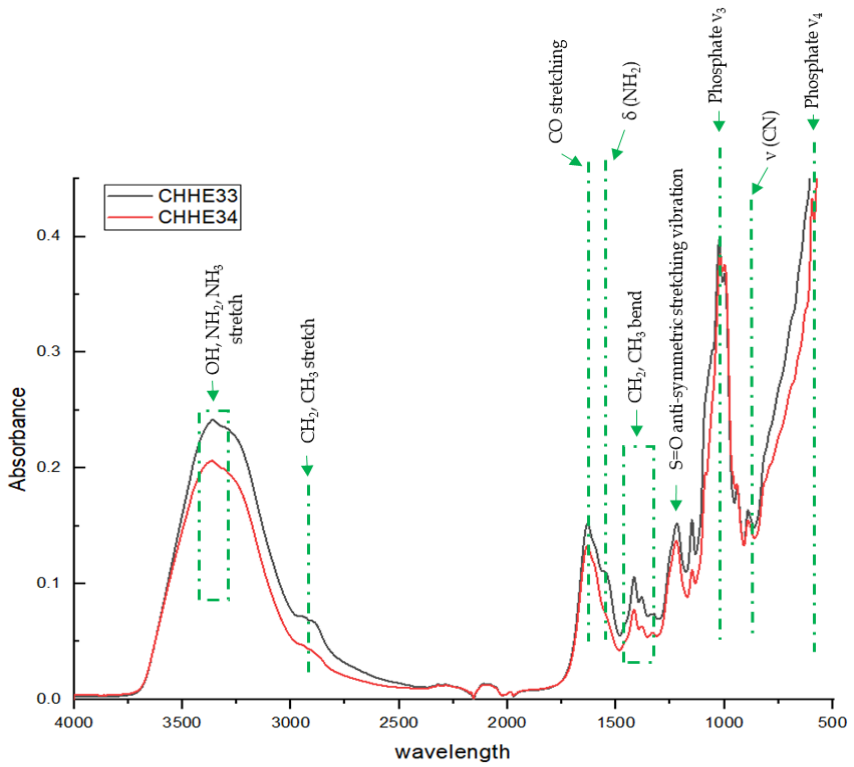

Figure 5.29. FTIR-ATR spectra of the scaffolds immersed in the NaOH 0.1M and loaded in the heparin sodium salt solution (3mg/mL) for 3 h. Ratios 80:20 and 50:50, respectively.

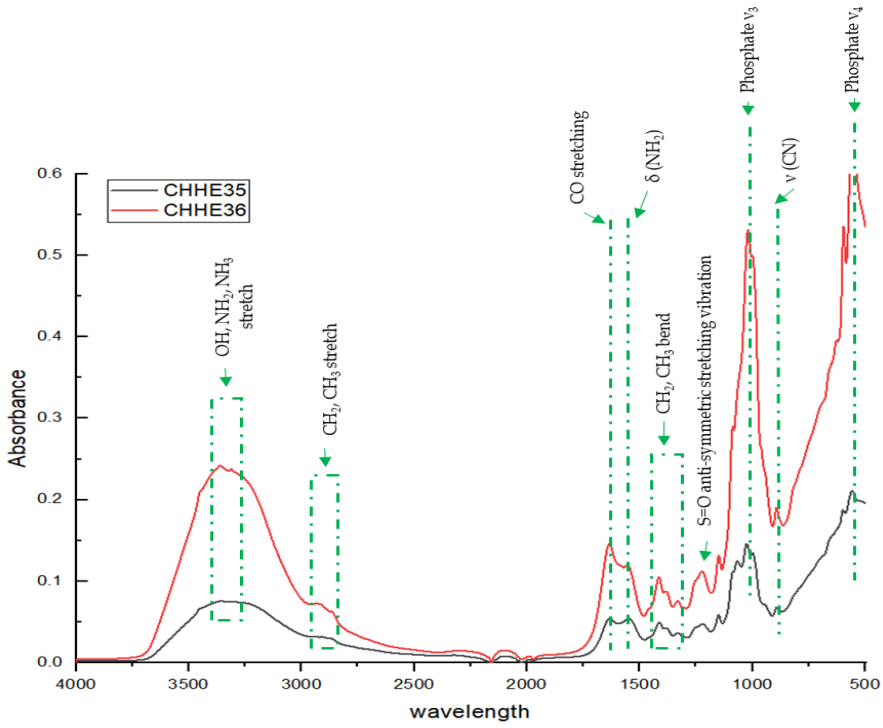

Figure 5.30. FTIR-ATR spectra of the scaffolds washed with distilled water and loaded in the heparin sodium salt solution (3mg/mL) for 3 h. Ratios 80:20 and 50:50, respectively.

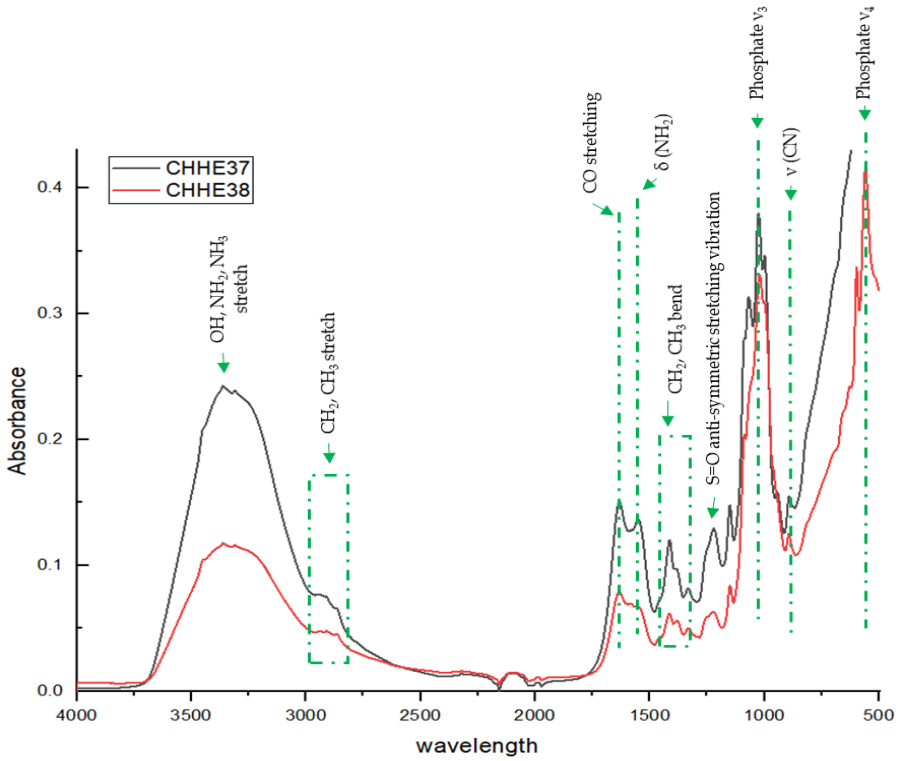

Figure 5.31. FTIR-ATR spectra of the scaffolds without treatment and loaded in the heparin sodium salt solution (3mg/mL) for 3 h. Ratios 80:20 and 50:50, respectively.

5.2.3 Conclusions from trials using different chitosan: hydroxyapatite ratio using freeze-drying methodology

Freeze-drying method is a procedure that removes moisture from a frozen solution. Sublimation of the ice crystals of the solution produces a porous solid structure.

According to Levengood & Zhang (2014) and O'Brien et al (2004), porosity during freeze-drying depends on the cooling rate used to freeze the solution. The faster the rate and the lower the temperature, the smaller the porosity achieved. This is mainly due to the nucleation and growth of the ice crystals not being uniform during quenching (fast cooling) [79,140].

Images from the macrostructure of the scaffold, Figures 5.18-5.21, show the appearance of a laminated matrix with pores in the top and lateral views of the scaffold. SEM images shown in Figure 5.23 show that for the lateral surface of freeze-dried scaffolds of 80:20 CS:HA ratio, a very small porosity was achieved, with pore size of between

9.39 and 29.21 μm, with an average of 17.55 μm. On the other hand, the sheets observed from the top surface of the scaffold presented a separation between 27.47 and 85.12 μm, with an average of 44.82 μm. This is the result of the rapid cooling rate.

Another important aspect to highlight, is the influence of hydroxyapatite in the resultant structure. Firstly, the distribution of the hydroxyapatite was not even along the chitosan matrix. As observed in Figure 5.23, the materials with 80:20 chitosan: hydroxyapatite ratio presented aggregation of hydroxyapatite in different parts of the chitosan matrix. However, the distribution of the phosphate for the 50:50 ratio was more uniform, and the phosphate was present throughout the matrix, without forming clusters. On the other hand, hydroxyapatite considerably reduced the porosity of the scaffolds. In the images showed in Figure 5.23, it is notable that for scaffolds with a CS: HA ratio of 50:50 there is an almost null porosity in the bottom surfaces, the appearance of a smooth surface is noteworthy. It is possible to observe the matrix arrangement as sheets, however the space between them is short, with a separation range of 6.48 to 37.65 μm, with an average of 16.58 μm if any space was observable.

This was mainly caused by the presence of the charge interaction: negative from hydroxyapatite and positive from chitosan, that helps to distribute the phosphate on the polymer matrix. However, increasing the amount of the hydroxyapatite creates a stronger interaction which closes down the already tight porosity from the quenching process.

Current research is still on going to look for the importance of porosity in bone tissue engineering scaffolds. The result has shown that both microporosity and macroporosity play an important role for the best performance of the scaffolds. Microporosity has been defined as the presence of pores of size <10 μm, while macroporosity includes the presence of pores >100 μm [141]. The importance of macroporosity lays on the fact that macropores provide the necessary pore size for cells

to migrate, infiltrate, organize and proliferate without space restrictions [142,143]. On the other hand, microporosity has proven to provide several factors for cell maintenance. Among them we can count the presence of different proteins that are necessary to stimulate different osteogenic functions of cells such as attachment, proliferation, and mineralization. Microporosity provides enough surface area to allow the presence of more protein adsorptions sites. However, it has been observed that an excess of micropores can have an unbeneficial effect in bone-cells development [141,144]. Therefore, a synergistic presence of both pore sizes should be present for a successful bone tissue engineering scaffold. Thus, regardless of providing good stimulation for cell maintenance, the resultant scaffolds from these procedures, may not offer an optimal structure for cell migration and development.

Furthermore, the neutralization with NaOH is usually performed to improve the degradation characteristics of the material. Neutralization process deprotonates chitosan reducing its charge and making it less prone to solubility in an aqueous media, therefore, delaying its degradation. In these trials, the treatment with NaOH affected mainly two features: porosity and heparin detection.

Firstly, from Figure 5.23 it is remarkable that the porosity from the top surfaces of the scaffolds appeared more closed after the NaOH treatment, this is also attributed to the charge interaction that occurs with NaOH, where the strong interaction of OH^- with protonated NH_3^+, closes down the porosity.

On the other hand, the treatment with NaOH defined the heparin detection with FTIR. As previously mentioned, this treatment reduces chitosan's protonation produced during its solubilization. In the FTIR spectra presented in Figures 5.24-5.30, the presence of peaks from both compounds can be observed: the phosphate groups from hydroxyapatite and the amino and alkyl groups from chitosan. However, the presence and intensity of the sulphate group was decided by the NaOH treatment.

Thus, it is possible to observe that for the scaffolds immersed for a long period in the NaOH solution with higher molarity (1 M), the peaks related to the sulphate groups have a very low intensity, if any can be observed. The very low concentration of heparin loaded onto theses scaffolds fails to show any discernible peaks. On the other hand, the scaffolds treated with the NaOH solution of lower molarity (0.1 M), exhibited sulphate peaks of the highest absorbance. This can be explained by the reduction in concentration and time of exposure to NaOH solutions reduced the deprotonation of chitosan, allowing to provide enough groups for the heparin to bind, therefore providing higher intensity peaks associated with the presence of heparin.

Regarding the scaffolds that were not neutralized with the NaOH treatment, the intensity of the sulphate peak related to heparin depended on the time of immersion in the heparin solution. For these scaffolds, it was possible to observe a relatively higher intensity in the sulphate groups for the scaffolds immersed in the 3mg/mL heparin solution for 3 hours comparing to the intensity of the peaks for the scaffolds immersed in the 1mg/mL heparin solution, which do not show any noticeable sulphate peaks.

5.3 The effect of using freeze-gelation method for fabricating chitosan/hydroxyapatite scaffolds

The following trials describe the methodologies compared to consider the use of freeze-gelation methodology to prepare the scaffolds. Two main phases can be considered: the preparation of the scaffold via freeze-gelation and the process of loading heparin onto the scaffolds to functionalize them for vascularization promotion purposes.

5.3.1 Trial 8: Preparation of chitosan/hydroxyapatite scaffolds via a known freeze-gelation methodology [126].

Previous trials explore the effects of using freeze-drying in the fabrication of the scaffolds, showing that the resultant scaffolds may provide unsuitable porosity for the purpose of this project. Therefore, it was considered that the use of freeze-gelation since, as mentioned in section 3.2.1, the porosity can be controlled during the freezing process, besides this methodology presents some advantages over freeze-drying such as energy consumption and absence of skin formation.

The following procedure was followed to prepared freeze-gelled scaffolds.

150 mL of a 1.5 % chitosan solution were prepared using 0.2 M acetic acid solution, 150 mL chitosan solution was prepared by adding the 2.25 g chitosan powder to the distilled water at 50°C. The solution was left to stir for 1 h, after which the heat was turned off. Subsequently, a 1.72 mL of acetic acid was added drop-wise to form a 0.2 M acetic acid solution. The mixture was left under stirring for approximately 20 h.

A second solution was prepared by adding the chitosan in the distilled water at 50°C. The solution was left to stir for 1 h after which the heat was turned off. Then the 1.7 mL of acetic acid was added drop-wise to form a 0.2M solution. The solution was left under stirring for 6h. After this time, 4.5 g of hydroxyapatite were added, and the new mixture was left under stirring overnight (approximately 13h).

Once both solutions were prepared, the solution of just chitosan was poured in a petri dish and left in the freezer at -4 °C for 1 h. Following this time, the temperature was decreased another 4°C (reaching a temperature of -8°C) and the solution was left in the freezer for another hour.

Subsequently, the slow addition of the solution of chitosan and hydroxyapatite was started. And both solutions were kept at -8°C for another hour (Figure 5.32). Following this time, the temperature was decreased by -4 °C each hour until a temperature of -20°C was reached. The solution was kept overnight under this conditions.

Figure 5.32. Mixture formed after the addition of the chitosan and chitosan/hydroxyapatite solutions.

The frozen solutions were removed from the plastic petri dishes by gently pressing the edges, a frozen disc was formed. Subsequently, the frozen disc was immersed in a 3 M NaOH/ethanol solution and was kept at -20°C for 12 h.

After removing the disc from the NaOH/ethanol solution, it was subjected to series of washing using the following protocol:

a) 15 minutes with distilled water.
b) 15 minutes with PBS.
c) 15 minutes with 80% ethanol solution.
d) 15 minutes with 100% ethanol.

Finally, the product was left uncovered in the hood overnight to dry.

The resultant scaffold turned mechanically stiff, i. e. not malleable to be but into smaller scaffolds.

5.3.2 Trial 9: Modification of the freeze-gelation methodology to allow heparin addition

From the previous trial, it was observed that resultant scaffolds were not easy to manipulate, as they were very stiff (as previously mentioned, stiffness is not a desirable feature for our further ends). The purpose of this trial was to observe the influence of the washings on the mechanical properties of the scaffolds, as differences were noticed during the washes with NaOH in trials 6 and 7. This trial was based on Qasim, S. B. *et al* (2015) [126], with some modification to observe the effect on the heparin loading.

A 1.5 g of chitosan was poured into distilled water warmed at 50°C and stirred during 1h, followed by the addition of 1.14 mL of acetic acid to form a solution 0.2 M (Figure 5.33 section A). The mixture was left to stir for 6 h at room temperature. After this time, 1.5 g of hydroxyapatite were added, and the solution was left under constant stirring overnight (approximately 13 h) for complete distribution of the hydroxyapatite.

On the following day, the solution was poured in plastic petri dishes. The appearance of the solution was homogeneously white (Figure 5.33 sections B and C). The solution was cooled at -4 °C for 3 h.

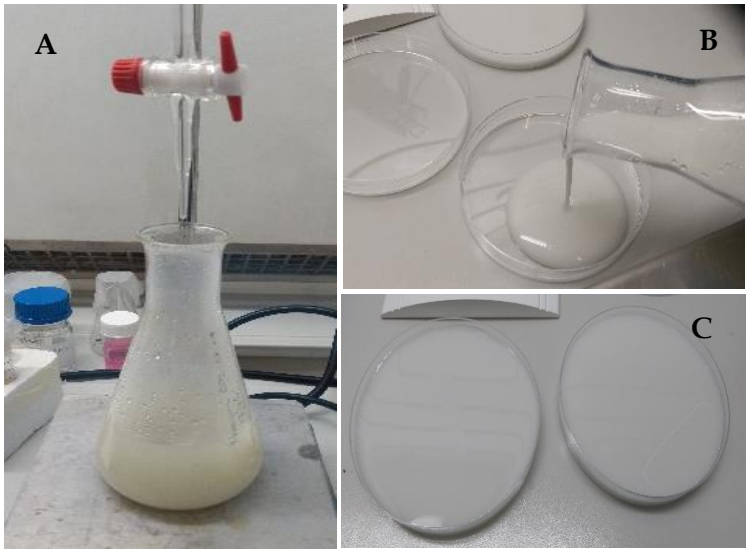

Figure 5.33. (A) Addition of acetic acid to the chitosan mixture. (B) Chitosan/hydroxyapatite slurry being poured into plastic petri dishes.

Subsequently, the temperature was decreased by 4 °C every 1.5 h until the fridge shelf reached -20°C. The solution was kept under these conditions for 25 h.

During this interval, the NaOH/ethanol 3 M solution was prepared. To prepare 500 mL of this solution, first, 60 g of NaOH were poured into 250 mL of ethanol in a beaker until saturation. Followed by the addition of 200 mL of ethanol under constant stirring. Once the remaining pearls of the NaOH were completely dissolved the solution was diluted to 500 mL with more ethanol. This solution was kept at -20°C until its use.

The frozen chitosan/hydroxyapatite solution was carefully removed from the petri dishes by gently pressing the edges of the dish. The frozen discs were transferred to a bigger glass petri dish (Figure 5.34 section A), and the precooled NaOH/ ethanol solution was slowly added until completely cover the discs (Figure 5.34 section B).

The frozen discs were removed from the NaOH/ethanol solution and two treatments were performed on the material, one to each disc:

Treatment 1 (Qasim, et al (2105) [126])	Treatment 2 (Modification)
The disc was washed with deionized water for 5 min	The disc was washed with deionized water during 20 min.
Put in PBS solution for 15 min	Put in PBS solution for 5 min
Washed several times with different concentration of ethanol (15 min per concentration wash): 70%, 80%, 90%, 95%, 100%	Washed with ethanol (15 min per concentration wash): 80% and 90%
Finally, the disc was immersed in a 1:10 glycerol solution for 15 min	

Table 5.4. Treatments performed on the resultant material.

Following the treatments, both discs were placed uncovered in the fume hood to dry at room temperature, to allow the evaporation of the solvents and washing solutions.

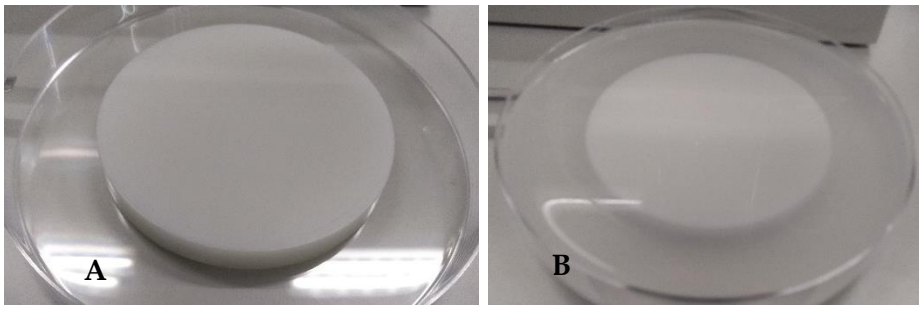

Figure 5.34. (A) The frozen discs were transferred to glass petri dishes. (B) The discs were completely covered with NaOH/ethanol solution 3M.

After 8 h of drying, the disc with treatment 1 turned hard and its edges bended upwards (Figure 5.35, left). Both discs were stored in the fridge.

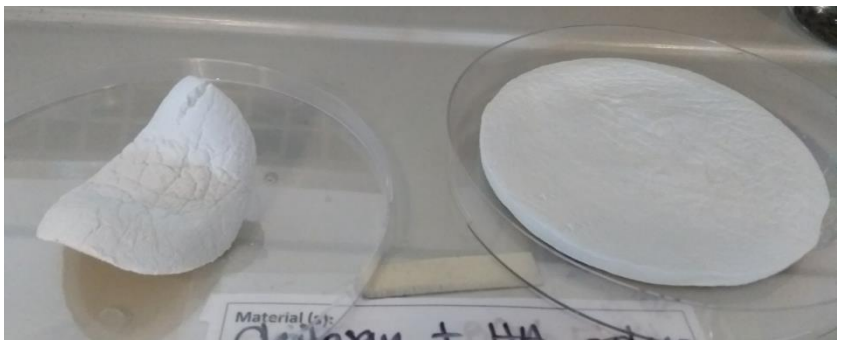

Figure 5.35. Resultant scaffolds after drying. Scaffold with treatment 1 is observed on the left of the picture, while scaffold with treatment 2 is presented on the right of the image.

Heparin loading

Two heparin solutions with concentrations of 3 mg/mL and 5 mg/mL were prepared by dissolving sodium heparin in distilled water at room temperature. Each scaffold was divided into 4 parts considering the heparin concentration was loaded onto it, according to Table 5.5. Each part of the disc was cut into cubes of approximately 3mm per side. Each correspondent quarter of the disc was fully immersed into 20 mL of the heparin solution and kept under these conditions for 24 h (Figure 5.36 section A). Precipitation was observed on disc 1 (Figure 5.36 section B).

Disc 1 Washed with deionized water, PBS (15min), 5 washes of ethanol, immersed in glycerol		Disc 2 Washed with deionized water, PBS (5min), 2 washes of ethanol	
Identification	Heparin concentration	Identification	Heparin concentration
FGAW	No heparin	**CHFG**	No heparin
FGAW3	3mg/mL	**CHFG3**	3mg/mL
FGAW5	5mg/mL	**CHFG5**	5mg/mL

Table 5.5. Heparin loading treatments performed on the obtained discs.

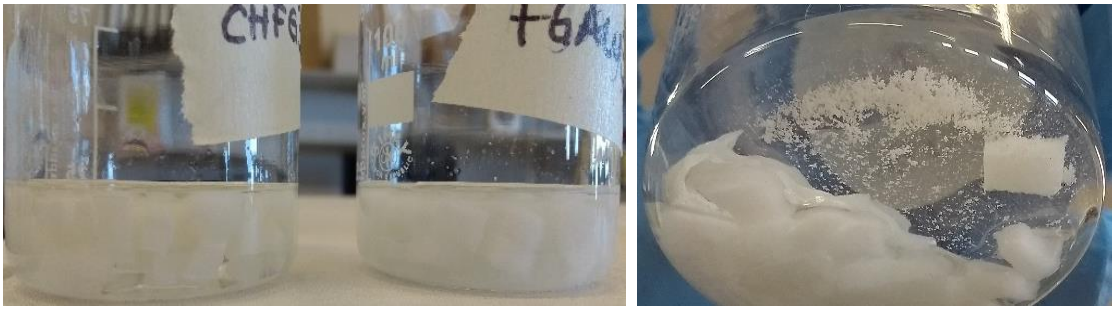

Figure 5.36. (A) Heparin loading process by immersion of the scaffolds into the heparin solution concentration 3 mg/mL, for scaffolds of both treatments. (B) Heparin precipitation was observed at the end of the loading process of scaffolds from disc 1 (FGAW, FGAW3 and FGAW5).

Finally, the scaffolds were removed from the heparin solution and placed them in open petri dishes, followed by an uncovered drying proceed at room temperature during 12h, approximately.

SEM images of the scaffolds without heparin and of the scaffolds with the highest loading concentration were obtained.

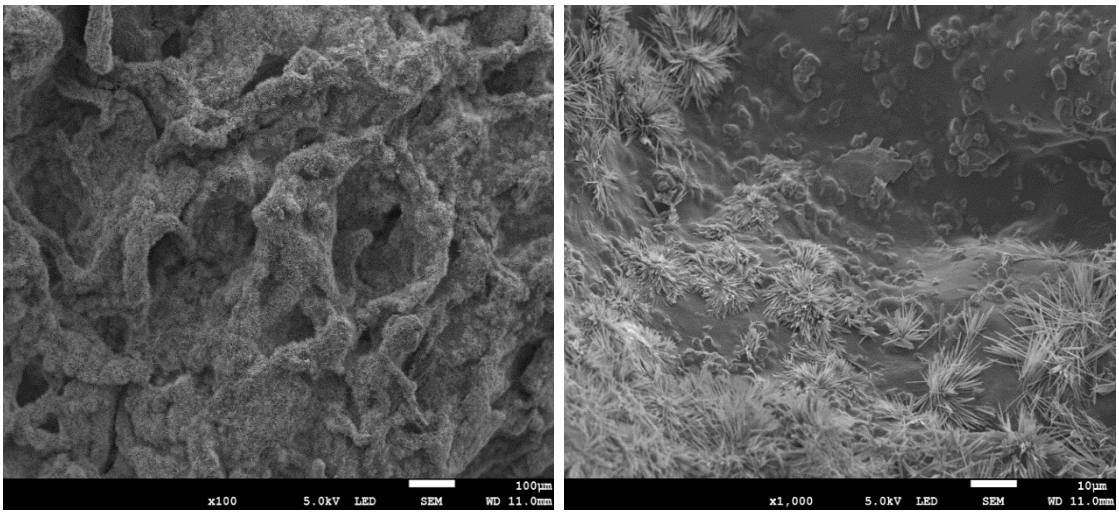

Figure 5.37. SEM images of FGAW scaffold without heparin (Scaffold washed with deionized water, PBS (15min), 5 washes of ethanol, immersed in glycerol, not loaded with heparin). Bars are 100 µm and 10 µm, respectively.

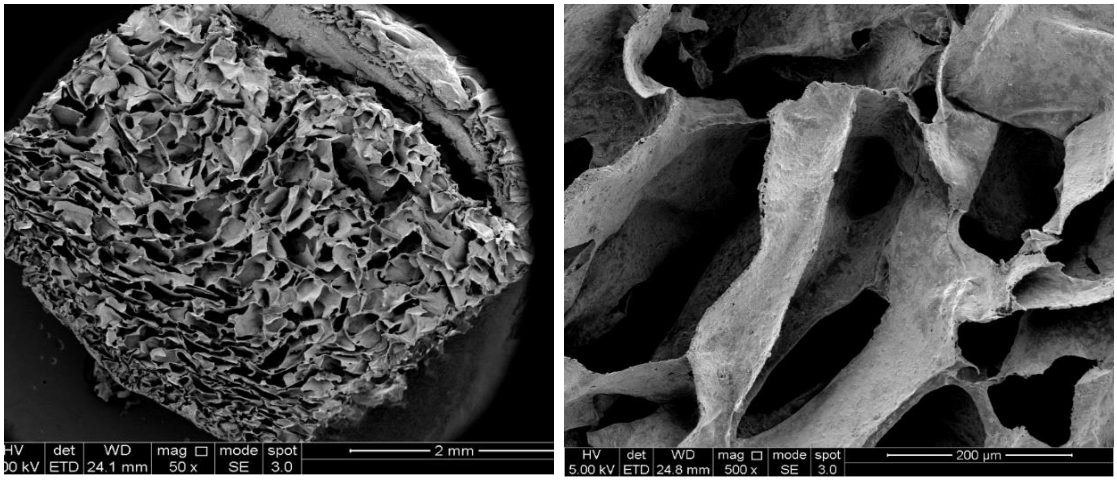

Figure 5.38. SEM images of CHFG scaffold without heparin (scaffold washed with deionized water, PBS (5min), 2 washes of ethanol, not loaded with heparin) . Bars are 2mm and 200 µm, respectively.

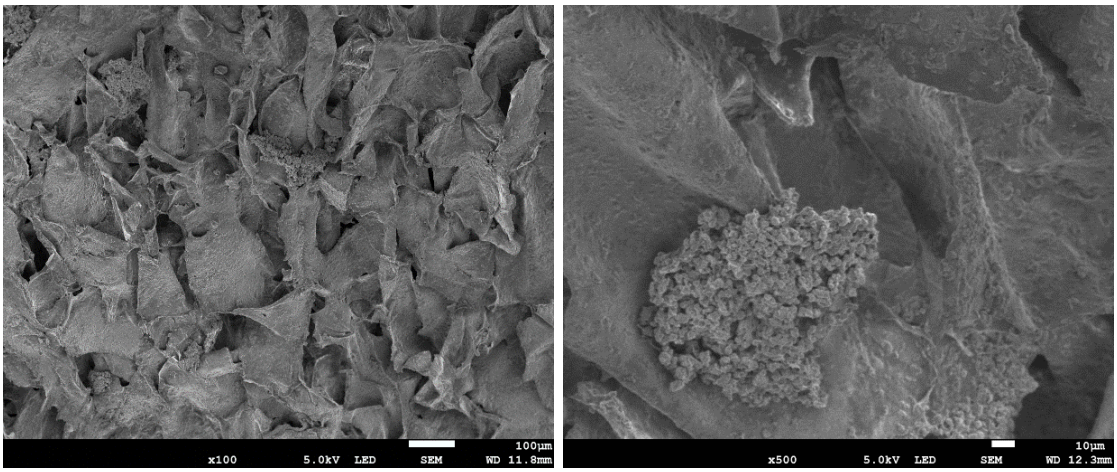

Figure 5.39. SEM images of FGAW scaffold immersed in the solution of 5 mg/mL (scaffold washed with deionized water, PBS (15min), 5 washes of ethanol, immersed in glycerol, loaded into the 5mg/mL heparin solution). Bars are 100 µm and 10 µm, respectively.

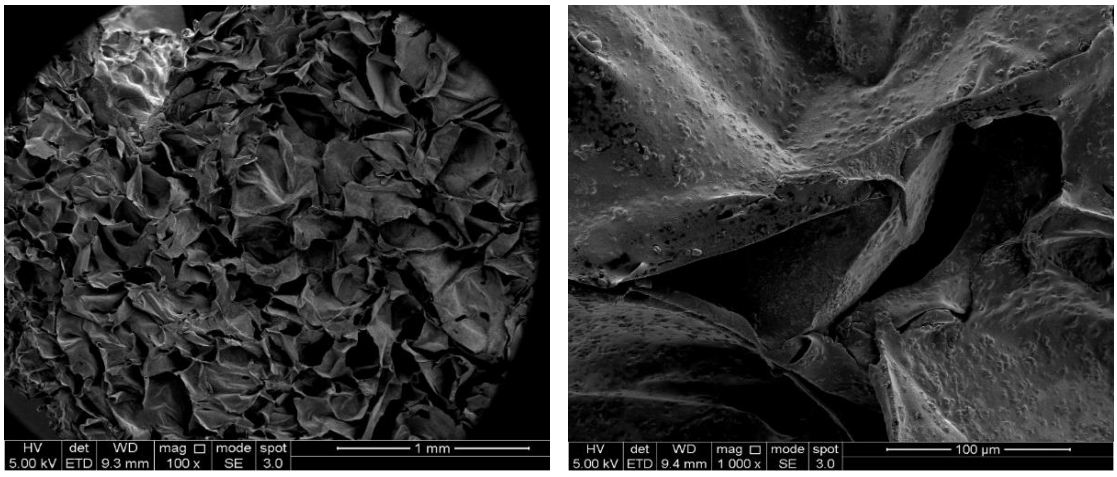

Figure 5.40. SEM images of CHFG scaffold immersed in the solution of 5 mg/mL (scaffolds washed with deionized water, PBS (5min), 2 washes of ethanol, loaded into the 5 mg/mL heparin solution). Bars are 1 mm and 100 µm, respectively.

Additionally, the FTIR-ATR spectra of the scaffolds were obtained. Results for the scaffolds with treatment 1 (FGAW) and the different heparin concentrations shall be presented.

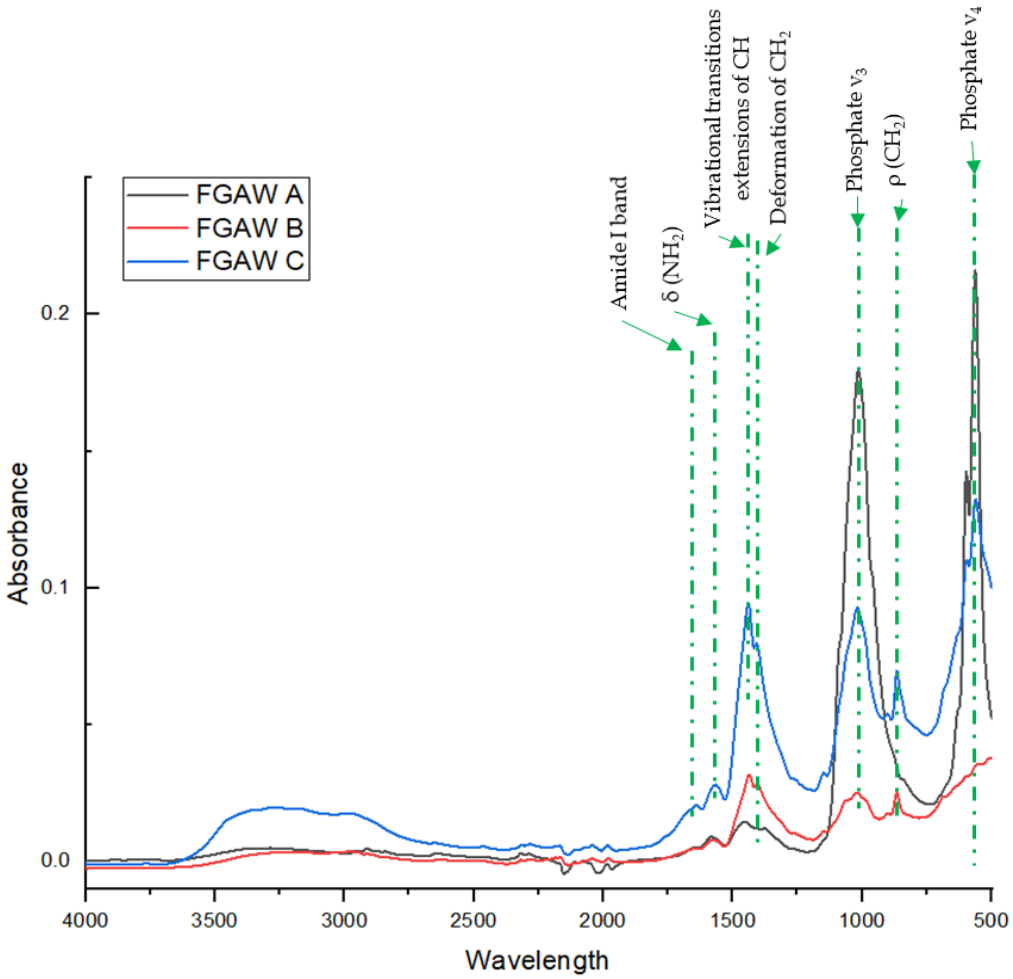

Figure 5.41. FTIR-ATR spectra of the scaffolds with all the washes (Treatment 1) and no heparin loaded (A, B and C refer to the position where the spectra were taken bottom, top or middle part, respectively).

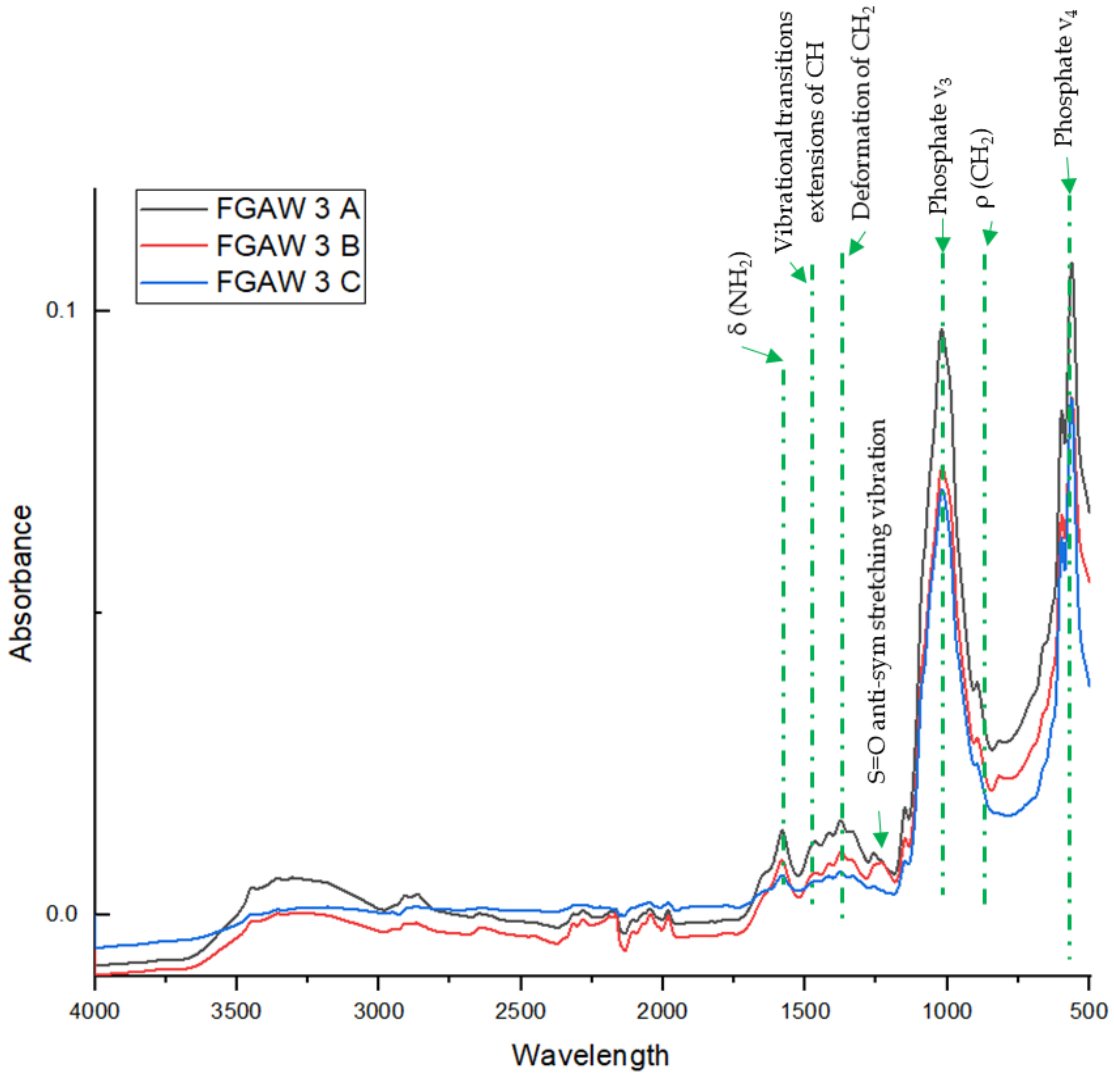

Figure 5.42. FTIR-ATR spectra of the scaffolds with all the washes (Treatment 1) and loaded in the 3mg/mL heparin solution (A, B and C refer to the position where the spectra were taken bottom, top or middle part, respectively).

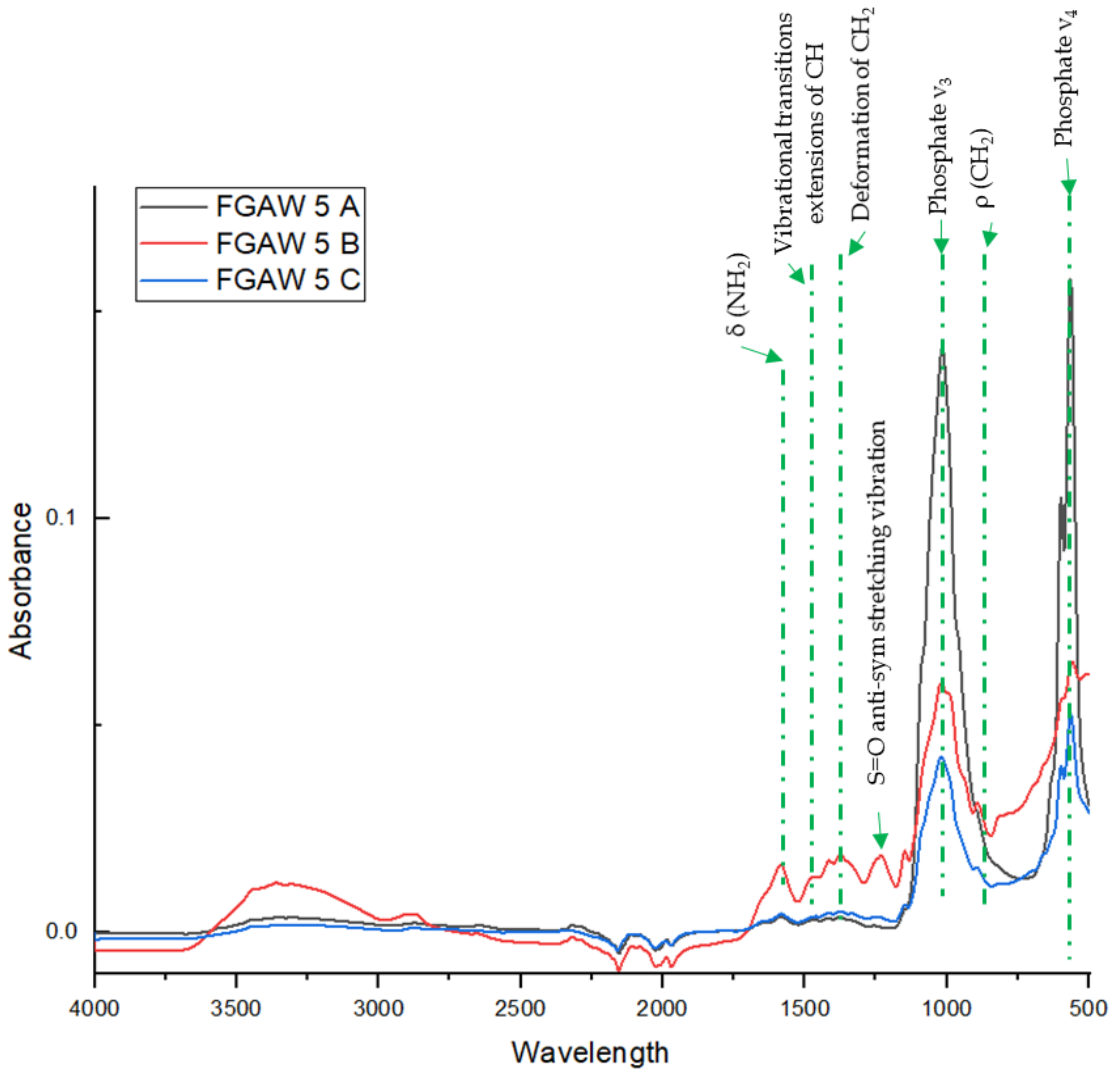

Figure 5.43. FTIR-ATR spectra of the scaffolds with all the washes (Treatment 1) and loaded in the 5mg/mL heparin solution (A, B and C refer to the position where the spectra were taken bottom, top or middle part, respectively).

Secondly the spectra of the scaffolds with treatment 2 (CHFG) and the different heparin concentrations are presented (A, B and C refer to the position where the spectrum was taken: bottom, top or middle part).

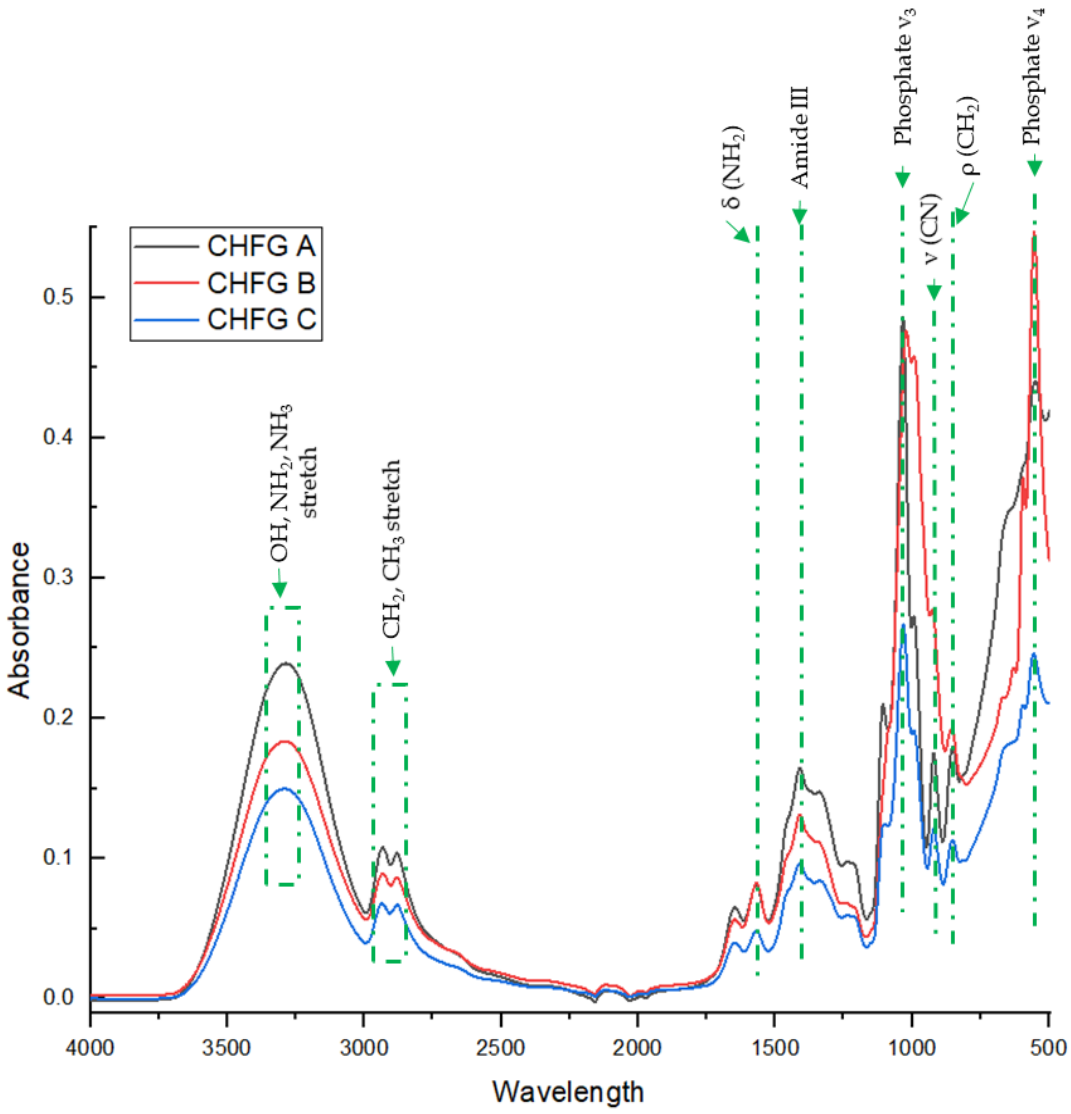

Figure 5.44. FTIR-ATR spectra of the scaffolds with the washing modification (Treatment 2) and no heparin loaded (A, B and C refer to the position where the spectrum was taken: bottom, top or middle part, respectively).

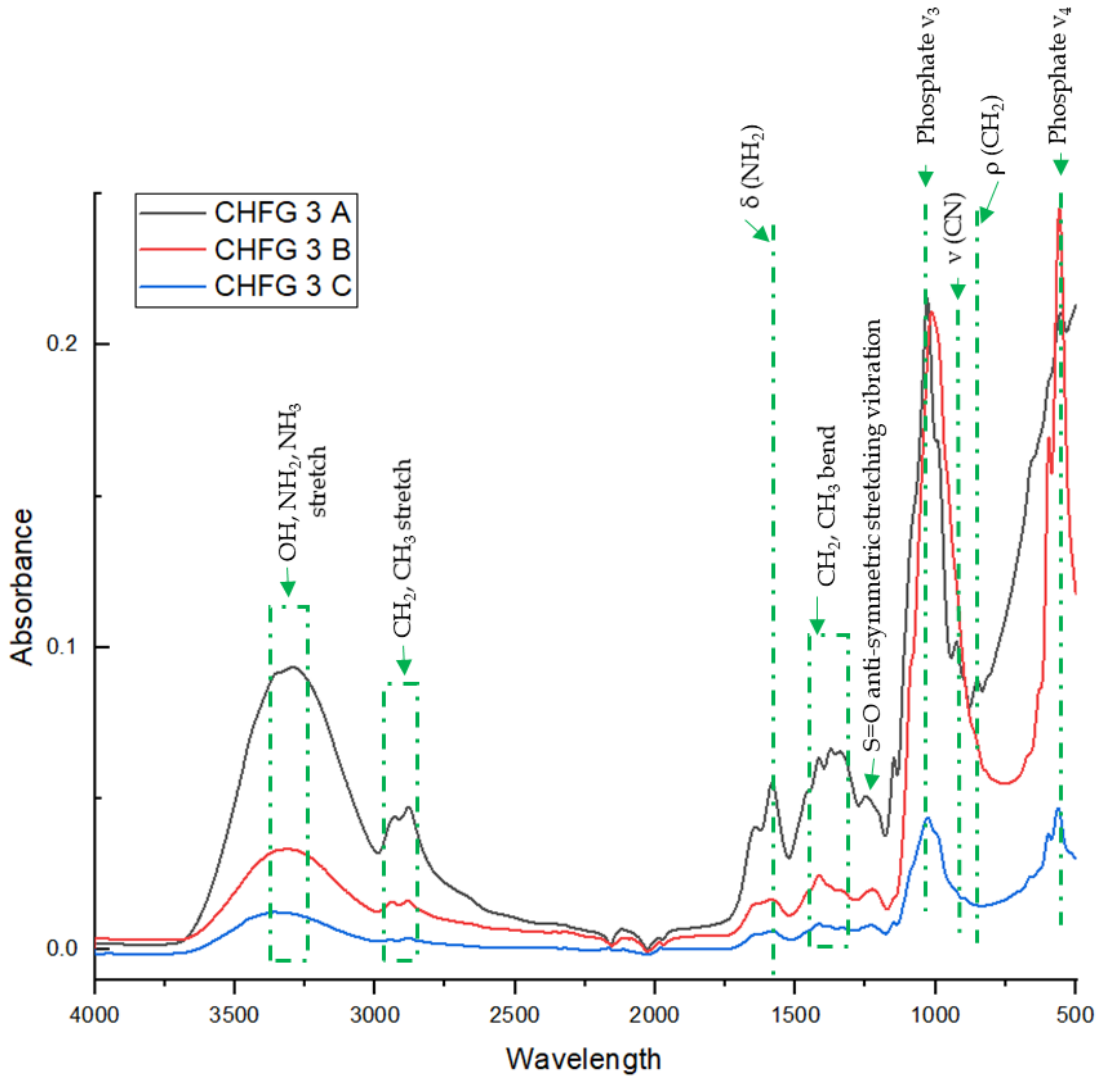

Figure 5.45. FTIR-ATR spectra of the scaffolds with the washing modification (Treatment 2) and loaded in the 3mg/mL heparin solution (A, B and C refer to the position where the spectrum was taken: bottom, top or middle part, respectively).

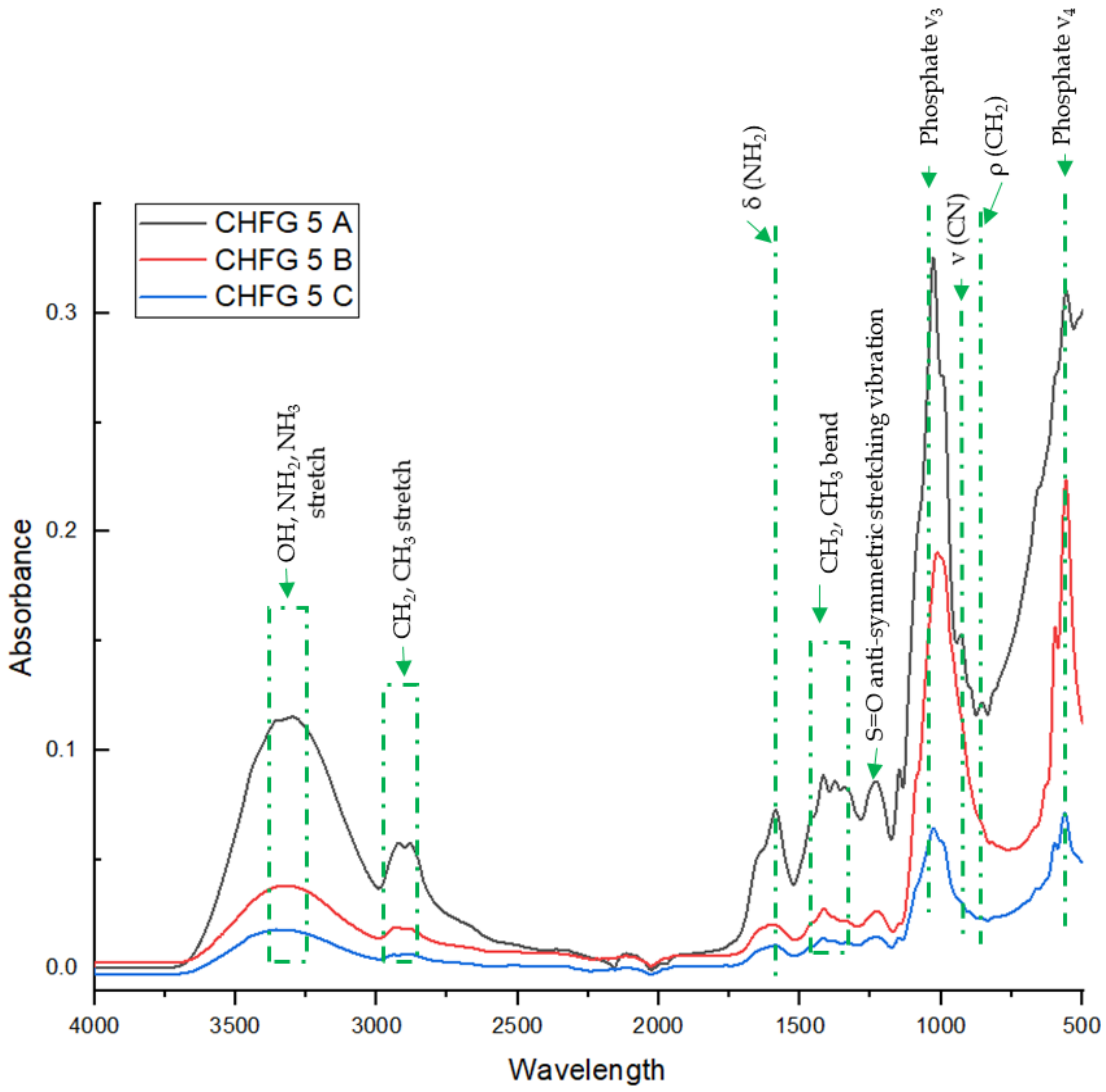

Figure 5.46. FTIR-ATR spectra of the scaffolds with the washing modification (Treatment 2) and loaded in the 5mg/mL heparin solution (A, B and C refer to the position where the spectrum was taken bottom, top or middle part, respectively).

5.3.3 Conclusions from using freeze-gelation to fabricate chitosan/ hydroxyapatite scaffolds

Freeze-gelation of chitosan is based on the fact that chitosan gels under alkaline conditions. During this process, the homogeneous polymer solution is frozen, following by an immersion in a basic-precooled coagulating solution. Therefore, the solvent is removed during the freezing stage keeping the shape and structure of the

frozen solution. The spaces left by the solvent removal, become the pores of the scaffold [124]. The freeze-gelation process upon which this work is based, followed a series of washes after the gelation process to remove the presence of NaOH and it included a washing with glycerol to improve stability of the scaffold. However, following the complete procedure resulted on obtaining rigid scaffolds, and decreasing the availability of cation sites in the scaffold structure, which is necessary for the interaction with heparin.

This is noted in the FTIR spectra of the scaffold with all the washes (FGAW) showed in Figures 5.41 to 5.44, where the low absorbance of the NH_2 peaks at 1589 cm^{-1} show the decrease of the available amino sites. Comparing the spectra of the scaffolds with the washing modification (CHFG) in Figures 5.44 to 5.46 it is notable the presence of the amino sites around 1580 cm^{-1}. These amino sites represented more available site for the heparin to bind. This is also notable for the heparin loading, since the scaffolds with the washing modification exhibited higher absorbance for sulphate peaks, around 1242 cm^{-1}. Whereas the same peak for the scaffolds with all the washings, was only observable with the higher loading concentration (5 mg/mL). Which explains the precipitation during the loading of the FGAW scaffolds since heparin could not bind properly to the scaffolds.

Regarding the scaffold structure, scaffolds with high porosity were obtained. Differences among their porosity were observed from Figures 5.37 to 5.40. Scaffolds with all the washes exhibited a pore size from 51 to 260 μm, with an average of 109.2 μm. These results were preserved regardless of the heparin loading. These scaffolds showed the presence of a spike-shaped material covering the surface, which is presumable the glycerol from the plasticizing process. The hydroxyapatite can be seen uniformly distributed throughout the chitosan matrix. On the other hand, the scaffolds with the washing modification, showed the presence of hydroxyapatite evenly

distributed on the chitosan matrix. The porosity revealed on these scaffolds goes from 120 to 460 μm, with an average size of 243 μm, regardless of the presence of heparin. The difference in porosity is also attributed to extensive washing with PBS and the plasticizing at the end, since this modifies chitosan structure and therefore, its interactions providing a tighter matrix.

5.4 The effect of the fabrication method on the bioactivity of chitosan/hydroxyapatite scaffolds

Bioactivity is defined as the ability of triggering a response or effect in the living tissue [145], in bone tissue engineering this translates to the ability to promote bone growing and the formation of a tight bond between tissue and implant, and it is very much dependent on the chemical composition of the material and the biological environment [106].

The apatite forming ability has been widely used as bioactivity evaluation. According to Kokubo & Takadama (2006) the reason is the assumption that the apatite produced by the osteoblasts should form a strong bond with the apatite layer formed on the surface of the implant, as long as its composition and structure simulates the one of bone. Hence, it is a key requirement for a material to form bonelike apatite on its surface, which can be evaluated in a solution with ion concentration similar to those in blood plasma, which they called *simulated body fluid* (SBF) [104].

The following trial compares the bioactivity results for the scaffolds prepared by freeze-drying and freeze-gelation methodologies. Additionally, the results according to the chitosan and hydroxyapatite ratio (CS: HA) are compared.

Fabrication method	Freeze Gelation		Freeze Drying	
CS:HA ratio	50:50	80:20	50:50	80:20
Short identification	FG50	FG80	FD50	FD80

Table 5.6. Identification of the chitosan: hydroxyapatite ratios tested during the bioactivity evaluation.

5.4.1 Bioactivity methodology

5.4.1.1 Solution preparation

The solution for the scaffolds was prepared as described below using the amounts shown in Table 5.7.

First, deionized water was warmed to 50 °C and chitosan was added, this mixture was left under stirring for 1h. Subsequently, heat was turned off and slow addition of acetic acid was started. Once enough amount of acetic acid to achieve 0.2 M was added, the solution was diluted to 250 mL and left under constant stirring for 6 h. Then, hydroxyapatite was slowly added, and the resultant mix was left under stirring overnight (approximately 12 h).

CS : HA	Reagent	Amount
80:20	Chitosan	12 g
	Hydroxyapatite	3 g
	Acetic acid	2.87 mL
50:50	Chitosan	7.5 g
	Hydroxyapatite	7.5 g
	Acetic acid	4.3 mL

Table 5.7. Reagent amounts to prepare 250 mL of the chitosan/hydroxyapatite solution.

To prepare 1 L of the 3M NaOH/ethanol solution, i. e. the gelation solution, 120 g of NaOH were completely diluted in 90 mL of distilled water. Next, the solution was diluted to 1L by the slow addition of ethanol. The solution was kept at -20 °C until used.

5.4.1.2 Freeze-drying protocol

The chitosan/hydroxyapatite solution was poured into glass petri dishes, adding the necessary amount according to the desired thickness of the scaffold. The solution was placed at 4 °C for 1 h, following by a decrease in the temperature by 4 °C hourly until it reached -30°C. The solution was left for freezing overnight. On the following day, the frozen solution was freeze-dried at -25 °C at 0.520 mbar for 30 hours.

5.4.1.3 Freeze-gelation protocol

The chitosan/hydroxyapatite solution was poured into plastic petri dishes, adding the necessary amount according to the thickness of the scaffold. The solution was placed at 4°C for 1 h, following by the decrease of the temperature by 4 °C hourly until it reached -20 °C. At -20 °C, the solution was left to freeze overnight. The frozen solution was removed from the petri dishes by gently pressing the edges and the frozen discs were immersed into 3M NaOH/ethanol solution (precooled at -20 °C). The frozen discs were kept in the gelation solution at -20 °C for 12 h.

Following this time, the frozen scaffolds were carefully removed from the gelation solution and the next series of washes were performed: 15 min in deionized water, 5 min in PBS, 15 min in 80% ethanol and 15 min in 100% ethanol.

The scaffolds were left uncovered in the fume hood for at least 8 h before being placed in a desiccator.

5.4.1.4 Description of bioactivity protocol

For this evaluation, the SBF composition and recipe was taken from the paper by Kokubo & Takadama (2006). A basic comparison of the nominal concentrations of Kokubo's SBF and the ones of human blood plasma is presented in Table 5.8 [104]. Excluding the values for chloride ion and carbonate, the values are very close.

The bioactivity was evaluated as part of the process of selecting the best chitosan and hydroxyapatite concentration and to define the best methodology to prepare the scaffolds: freeze-gelation or freeze-dryer (Ong B., 2017) [146].

Ion	Ion concentration (mM)	
	Blood plasma	**SBF**
Na^+	142.0	142.0
K^+	5.0	5.0
Mg^{2+}	1.5	1.5
Ca^{2+}	2.5	2.5
Cl^-	103.0	147.8
HCO_3^-	27.0	4.2
HPO_4^{2-}	1.0	1.0
SO_4^{2-}	0.5	0.5
pH	7.2 -7.4	7.4

Table 5.8. Comparison of ion concentrations of SBF and human blood plasma [104].

The scaffolds were cut into rectangles of 1.5 cm^2, weighed and this weight was registered as W_i. After preparing SBF solution following the methodology described by Kokubo & Takadama's (2006), scaffolds of each chitosan: hydroxyapatite ratio and fabrication method were individually placed into clean vials with 10 mL of SBF. The SBF solution was weekly replaced with afresh solution. The study lasted 8 weeks.

Three scaffolds of each variant were weekly retrieved from the SBF solution, carefully washed with distilled water and oven-dried at 50°C for 24 hours to remove all moisture.

The scaffolds were then weighed, registering this weight as W_f. The retrieved scaffolds were characterized using FTIR-ATR technique, SEM and EDX analysis.

For FTIR-ATR, the conditions and equipment were the ones described in chapter 4, section 4.2.1.

For SEM observation a Hitachi TM3030Plus was used, while the EDX analysis was performed by a Quantax 70 EDS accessory for this SEM equipment. For this equipment, no coating was required, and the samples were simply adhered to a specimen holder.

5.4.2 Conclusions on the study of the effect of the fabrication method on the bioactivity of chitosan/hydroxyapatite scaffolds

The resultant chitosan/hydroxyapatite scaffolds prepared by freeze- drying method are shown on the left in Figure 5.47, while the scaffolds prepared via freeze- gelation are shown on the right in Figure 5.47. The formation of surface skin (circled in red) on the surface of the scaffolds prepared by freeze-drying method was observed. Scaffolds prepared by freeze-gelation method, did not present surface skin.

As discussed by Levengood & Zhang (2014), the presence of surface skin is not desirable when fabricating tissue engineering scaffolds: Since surface skin is not porous, it may impede the ingress of nutrients and oxygen to the scaffold structure, also hindering the egress of wastes from it [79], which would lead to scaffold malfunction and failure.

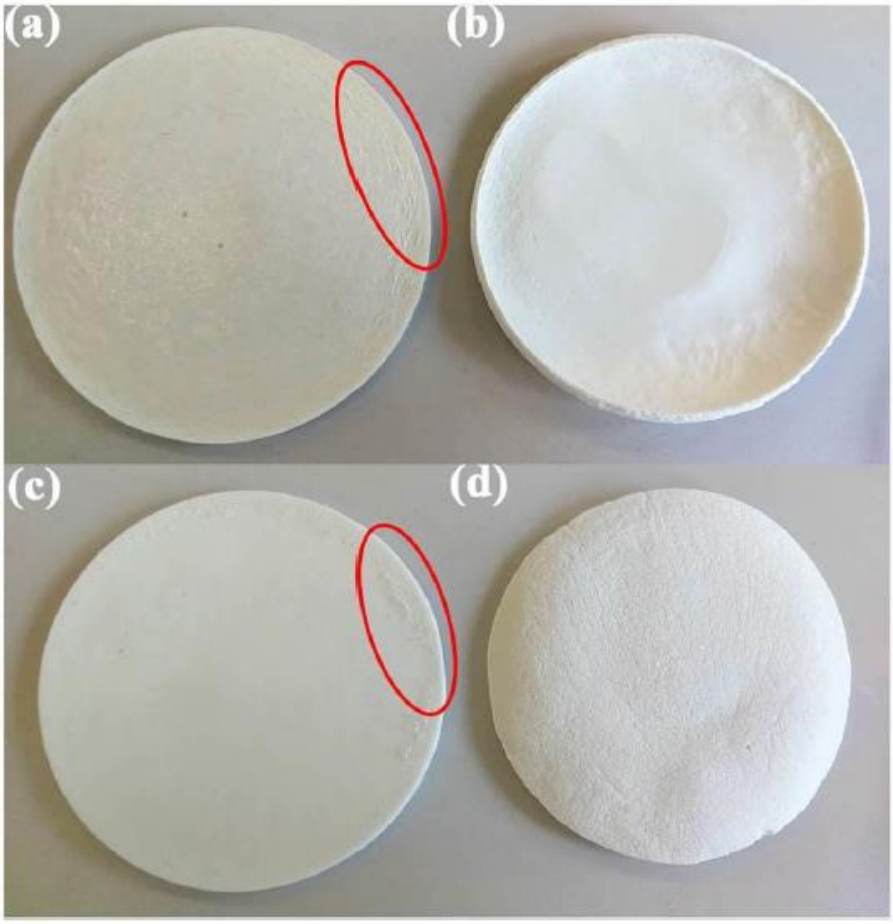

Figure 5.47. (a) and (c) Scaffold prepared by freeze-drying method, top and bottom surfaces, respectively. (b) and (d) Scaffold prepared by freeze-gelation method, top and bottom surfaces, respectively.

The scaffolds prepared by freeze drying exhibited a tight porosity, more on the top surface of the scaffold. The top surface had the appearance of a structure formed by stacked sheets. Table 5.9 presents the pore size (in μm) according to the fabrication method and the chitosan: hydroxyapatite ratio. As described in section 4.1.1, from the obtained SEM images, porosity of the samples was determined by measuring every pore diameter in the image using ImageJ®.

Scaffold	FD50 Bottom	FD50 Top	FD80 Bottom	FD80 Top	FG50 Bottom	FG50 Top	FG80 Bottom	FG80 Top
Average	39.20	33.53	47.74	71.20	15.56	72.98	28.22	127.58
Minimum	21.05	20.12	16.72	30.68	10.09	24.30	16.67	77.19
Maximum	55.95	47.23	100.29	127.93	29.16	118.38	52.63	177.05

Table 5.9. Pore size according to the fabrication method (on week 0). **All measurements are given in μm**. **FD50** and **FD80** are the scaffolds prepared by freeze-drying with chitosan: hydroxyapatite ratio of 50:50 and 80:20 respectively. **FG50** and **FG80** are the scaffolds prepared by freeze-gelation with chitosan: hydroxyapatite ratio of 50:50 and 80:20 respectively.

SEM images of the scaffolds showing the effect of SBF on the scaffolds structure with time can be observed in Figures 5.47 (top surfaces) and 5.48 (bottom surfaces).

Firstly, the differences from the fabrication methods, are shown on the images of week 0, i. e. before undergoing any treatment.

It is possible to observe that, with a longer exposure to the SBF, pore size and shape changes. For scaffolds prepared by freeze-drying, the pores are completely covered by week 8, presumably with the apatite layer. On the other hand, for the scaffolds prepared via freeze-gelation it is possible to observe a reduction on the pore size as well as a higher presence of apatite on the surface.

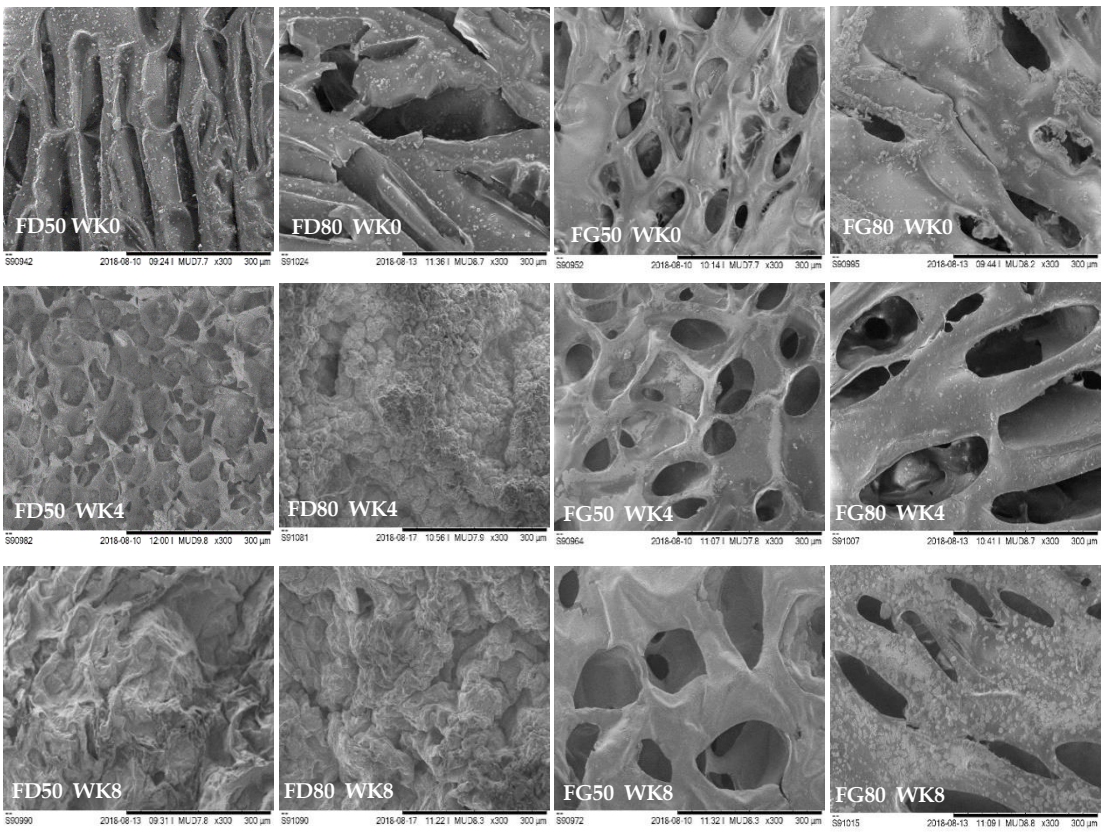

Figure 5.48. Comparison on the effect of SBF on the scaffold structure. Top surfaces of the scaffolds. **FD50** and **FD80** are the scaffolds prepared by freeze-drying with chitosan: hydroxyapatite ratio of 50:50 and 80:20 respectively. **FG50** and **FG80** are the scaffolds prepared by freeze-gelation with chitosan: hydroxyapatite ratio of 50:50 and 80:20 respectively. WK0= week 0, WK4= week 4, and WK8= week 8 of exposure to SBF. Images are 300X, all bars represent 300 µm.

The same effect is observed for the bottom surface of the scaffolds in Figure 5.49. This surface is already apatite rich due to the preparation methodology, however, a higher accumulation of apatite and a reduction of the pore size, is also observable.

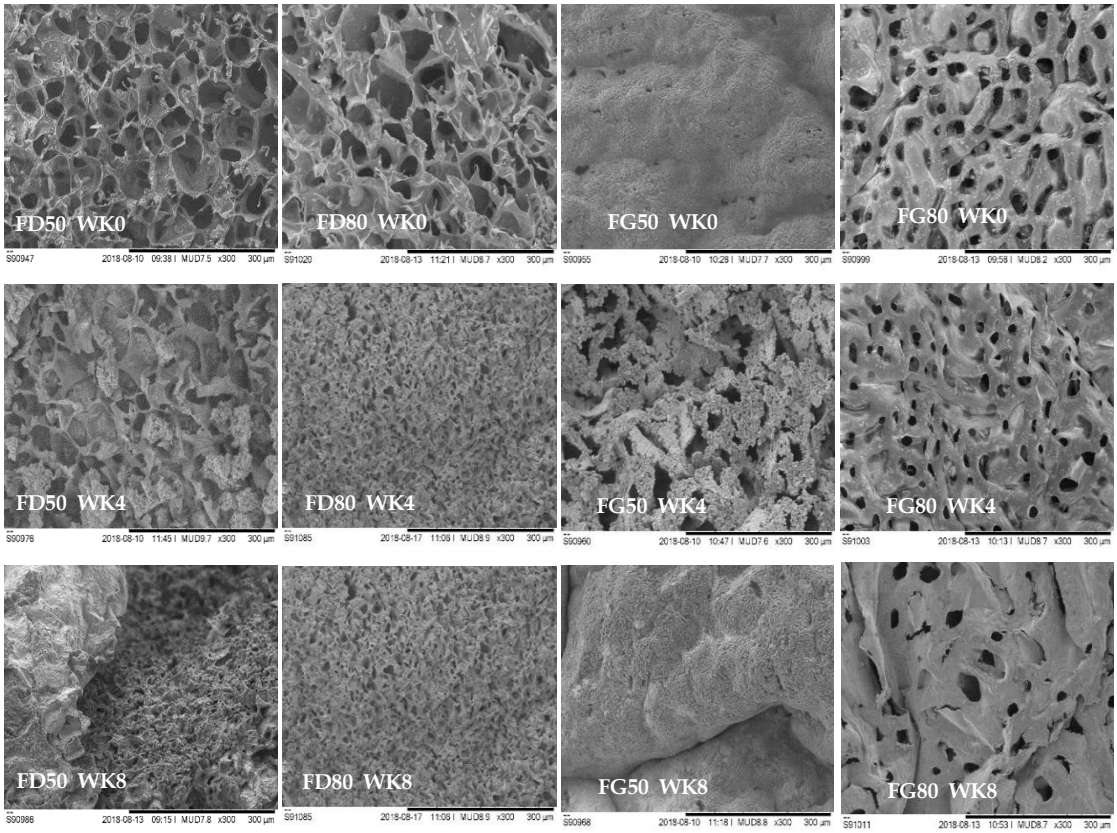

Figure 5.49. Comparison on the effect of SBF on the scaffold structure. Bottom surfaces of the scaffolds. **FD50** and **FD80** are the scaffolds prepared by freeze-drying with chitosan: hydroxyapatite ratio of 50:50 and 80:20 respectively. **FG50** and **FG80** are the scaffolds prepared by freeze-gelation with chitosan: hydroxyapatite ratio of 50:50 and 80:20 respectively. WK0= week 0, WK4= week 4, and WK8= week 8 of exposure to SBF. All scale bars represent 300 µm.

It is possible to observe from Table 5.9, that the presence of hydroxyapatite tightens the porosity, since the pore size is lower for the scaffold of 50:50 ratio. This is mainly due to the interaction among hydroxyapatite lattice ions, i.e. Ca^{2+}, OH^- and PO_4^{3-}, and the positively charged amino groups from of chitosan. This interaction diminishes with a lower amount of hydroxyapatite, causing that the 80:20 ratio exhibited a more relaxed structure.

In previous trials, showed in section 5.2, freeze-drying also exhibited very small pore size due to the quenching. However, for this study the solution preparation, as well as the freezing rate was the same for both processes, showing that the phase separation

also plays an important part on the pore formation. Most of the articles suggest that freezing rate and temperature, and solution concentration are the defining parameters in pore size definition. During this trial, the only change is the process for the removal of the solvent: sublimation in freeze-drying and gelation of a homogeneous solution during freeze-gelation. The most important parameters during freeze-drying are temperature and pressure. Transforming ice into vapor requires energy since the product needs to be heated to facilitate the removal of water. However, if during this warming process the temperature goes higher that the eutectic point, changes in the structure of the frozen solution can occur [147]. The eutectic point for a 60% acetic acid/water solution is -26.5 °C [148]. The freeze-drying process was conducted at -25°C which probably allowed changes on the frozen solution that lead to a reduced porosity. Regarding the effect of SBF on the structure of the scaffolds, changes on the pore size are notable regardless of the fabrication method. For freeze dried scaffolds it is possible to observe that during the bioactivity test the entire surface appears with a decreased porosity and cover with phosphate. On the other hand, for freeze gelation, though it is possible to observe formation of an apatite layer in the SEM images, the structure yielded in time, with a wider averaged porosity.

Figures 5.50 to 5.57 show the FTIR spectra of the scaffolds throughout the bioactivity study. The spectra show characteristic peaks from both chitosan and hydroxyapatite, demonstrating the phosphate dispersed through the polymer matrix.

The high absorbance for phosphate groups and carbonate peaks can be highlighted. There has been an increase in the intensity of hydroxyl peaks at around 3340cm^{-1} over 8 weeks in each sample spectrum, except for 80FG. This can be attributed to the water present in the structure with the increased amount of time immersed in the SBF. It is also highly likely due to the presence of calcium phosphate.

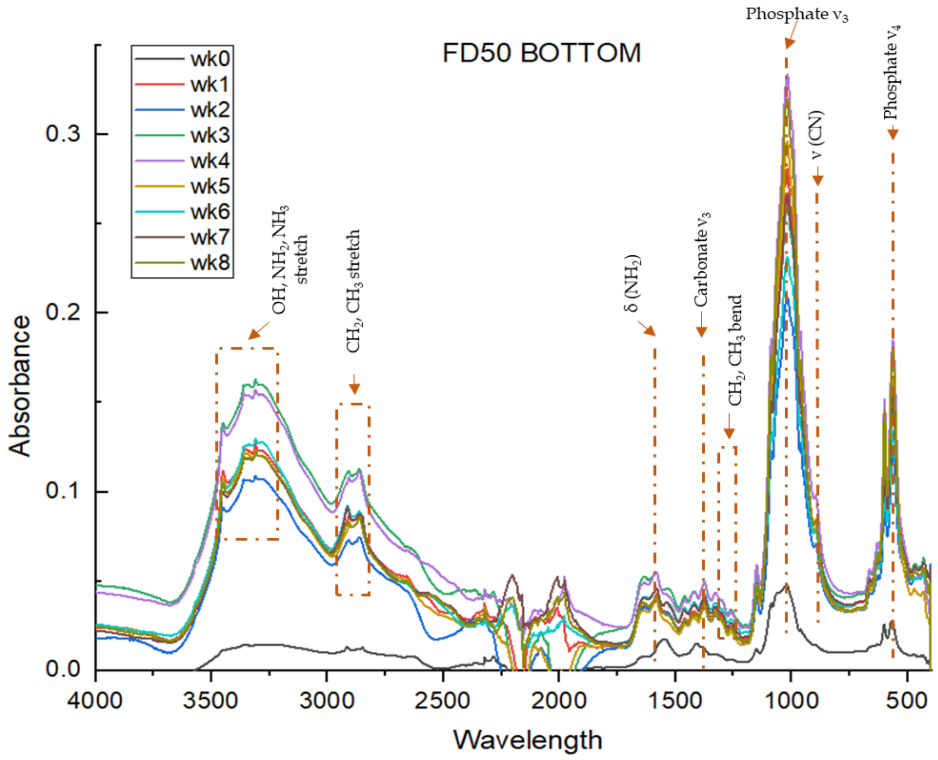

Figure 5.50. Comparison on the effect of SBF on the chemical structure through the 8 weeks of study. FD50 Bottom surfaces.

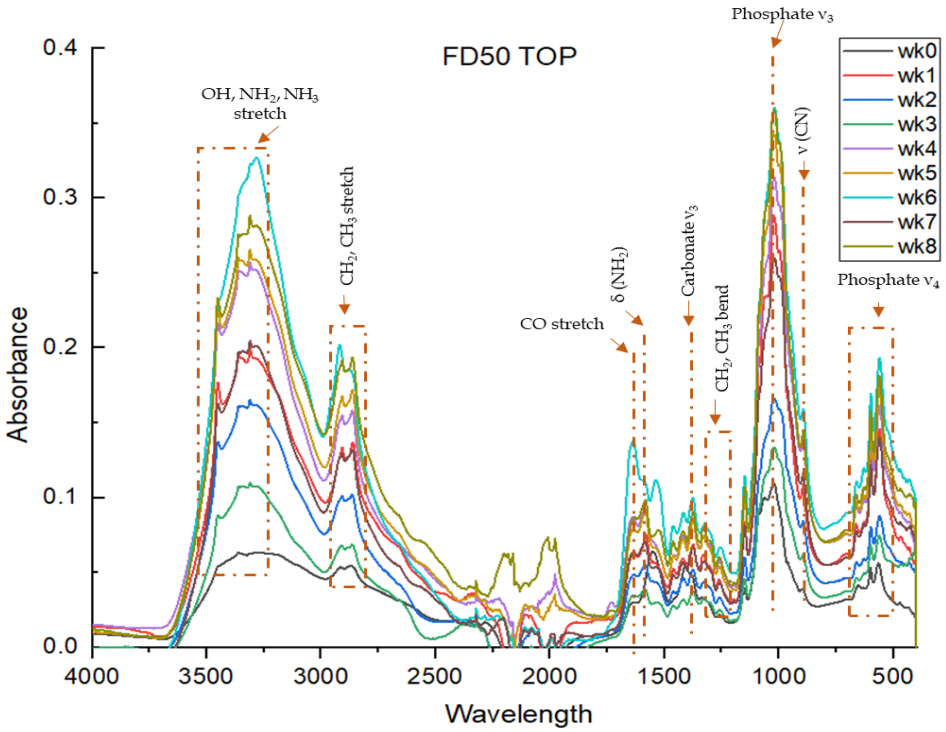

Figure 5.51. Comparison on the effect of SBF on the chemical structure through the 8 weeks of study. FD50 Top surfaces.

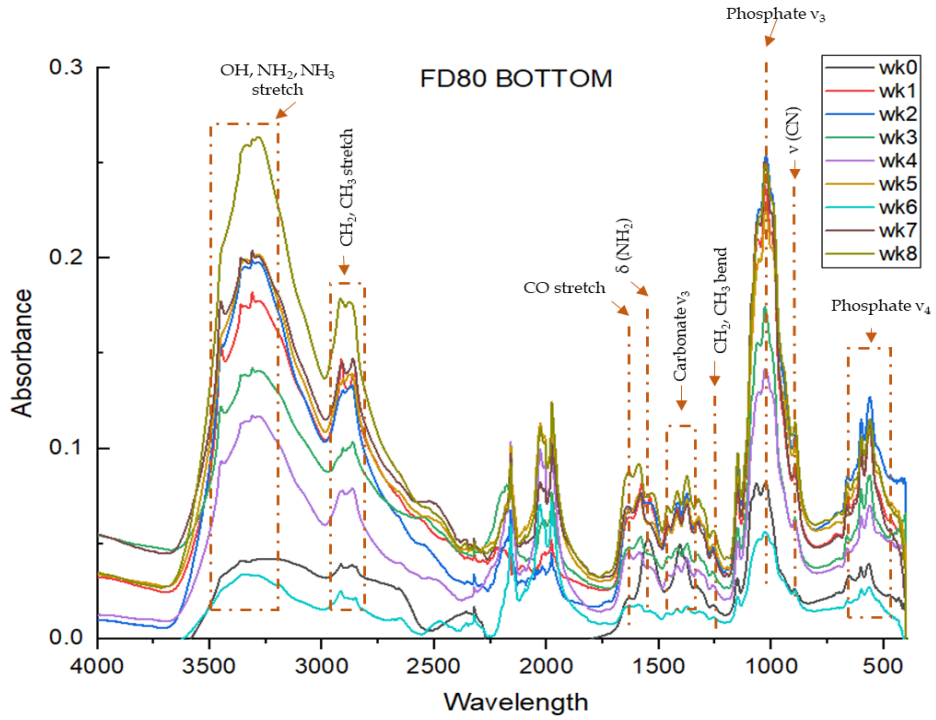

Figure 5.52. Comparison on the effect of SBF on the chemical structure through the 8 weeks of study. FD80 Bottom surfaces.

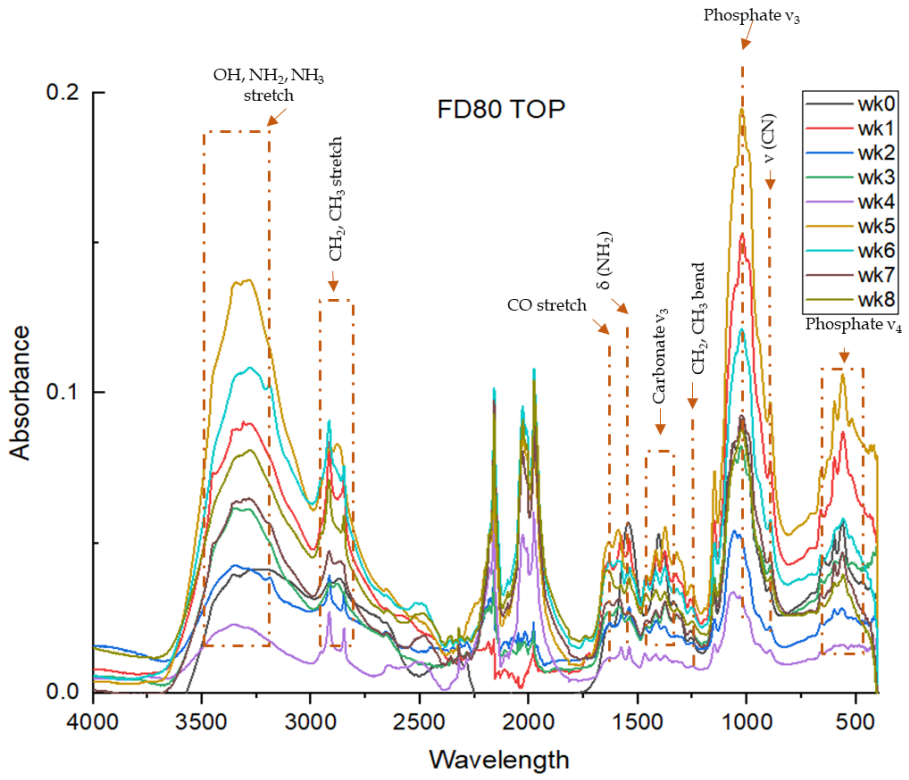

Figure 5.53. Comparison on the effect of SBF on the chemical structure through the 8 weeks of study. FD80 Top surfaces.

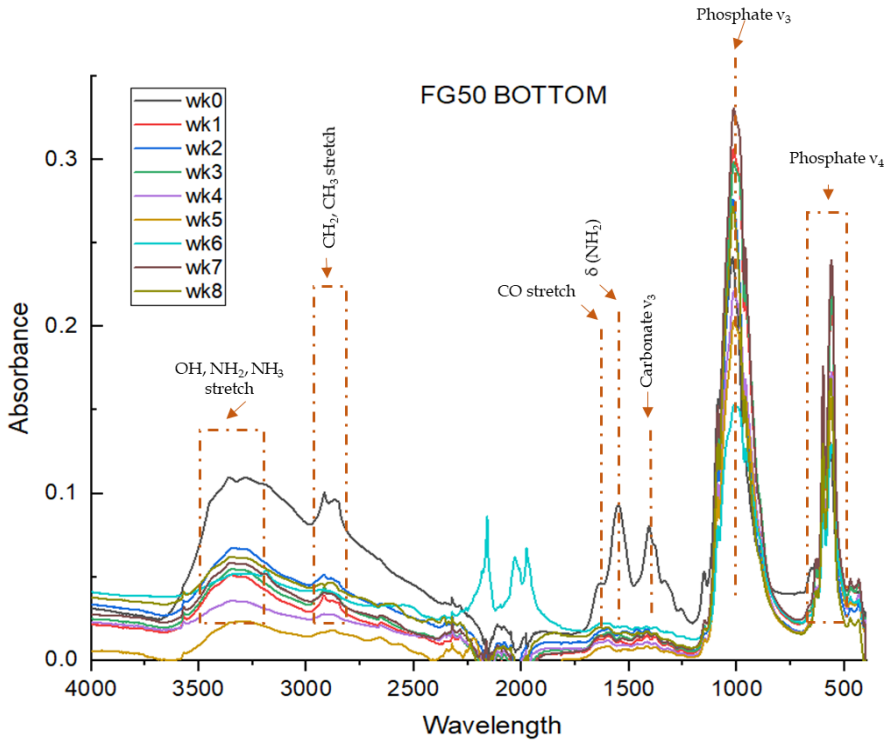

Figure 5.54. Comparison on the effect of SBF on the chemical structure through the 8 weeks of study. FG50 Bottom surfaces.

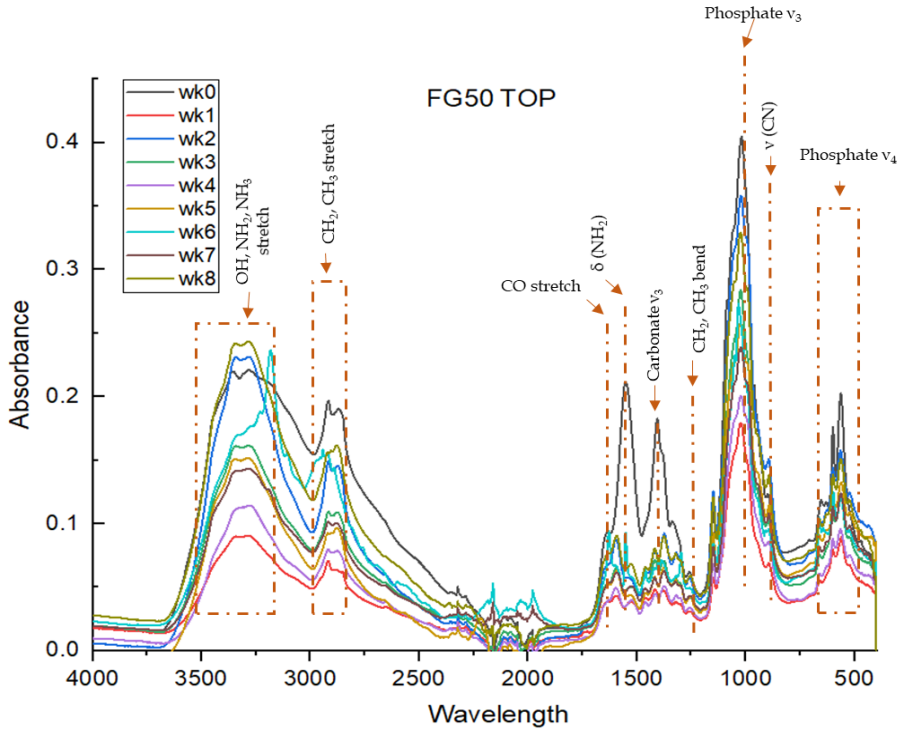

Figure 5.55. Comparison on the effect of SBF on the chemical structure through the 8 weeks of study. FG50 Top surfaces.

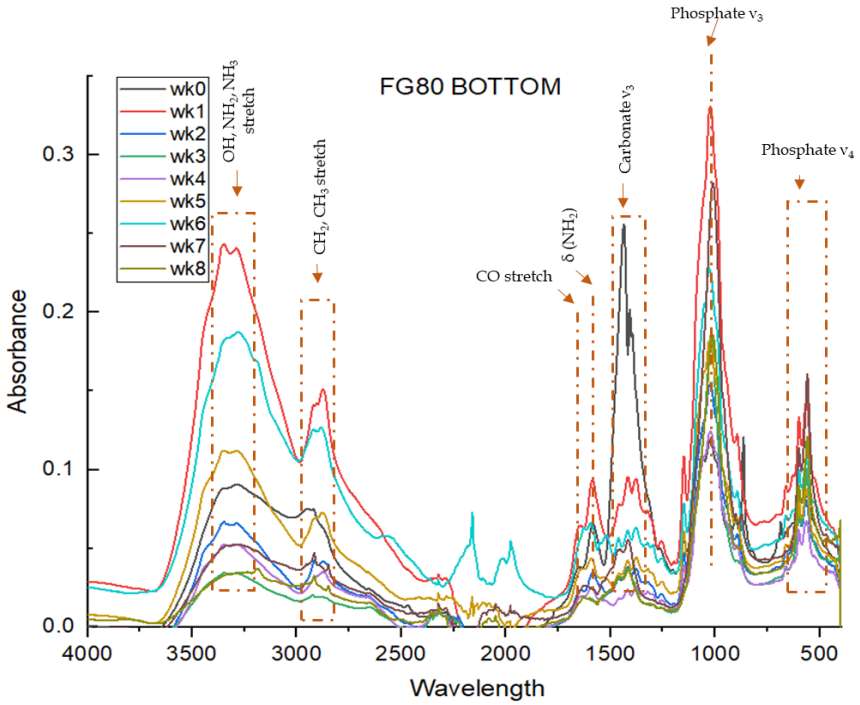

Figure 5.56. Comparison on the effect of SBF on the chemical structure through the 8 weeks of study. FG80 Bottom surfaces.

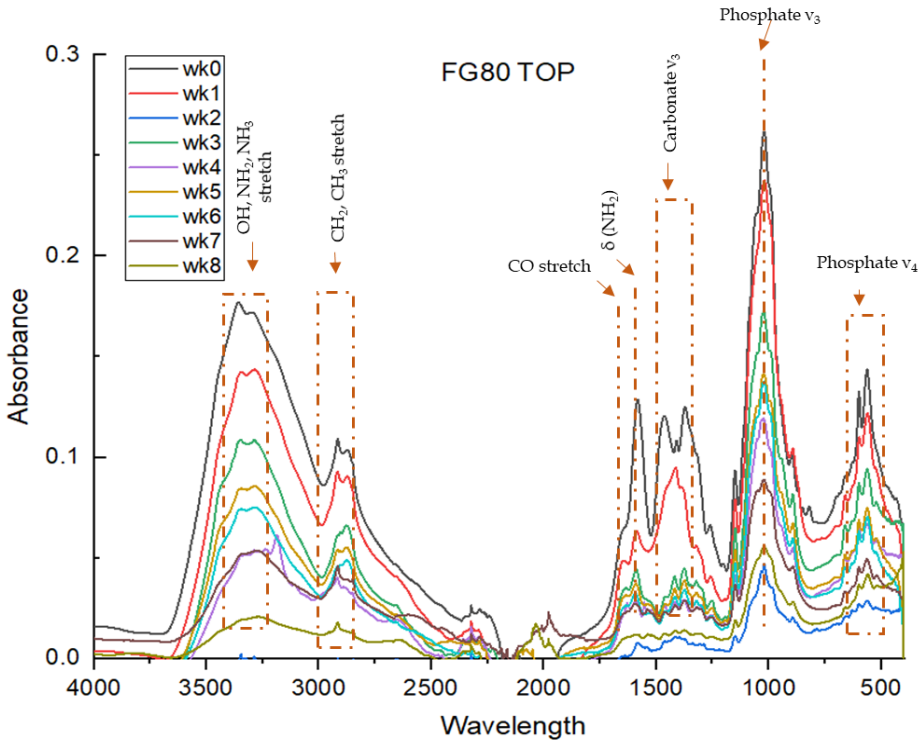

Figure 5.57. Comparison on the effect of SBF on the chemical structure through the 8 weeks of study. FG80 Top surfaces

The increase in the hydroxyl peak is mostly attributed to the formation of calcium phosphate that relies on the concentration of HA present in the scaffold. This can be confirmed by the gradual increase in phosphate peaks too. Which indicates that a layer of calcium phosphate apatite has been formed.

From the EDS analysis, Ca/P ratio was calculated. The resultant Ca/P ratios for the scaffolds before and after bioactivity study are presented in Table 5.10.

(A) FD50		
Element	Wk0	Wk8
	[norm. at.%]	
Carbon	46.02	62.22
Oxygen	41.29	28.91
Calcium	8.52	2.86
Phosphorus	4.18	1.46
Chlorine	-	4.56
Ca/P ratio	2.04	1.96

(B) FG50		
Element	Wk0	Wk8
	[norm. at.%]	
Carbon	29.46	28.86
Oxygen	55.35	52.90
Calcium	10.33	11.77
Phosphorus	4.87	6.47
Chlorine	-	-
Ca/P ratio	2.12	1.82

(C) FD80		
Element	Wk0	Wk8
	[norm. at.%]	
Carbon	53.63	51.93
Oxygen	43.23	36.48
Calcium	2.13	2.21
Phosphorus	1.01	1.80
Chlorine	-	4.23
Sodium	-	3.35
Ca/P ratio	2.11	1.23

(D) FG80		
Element	Wk0	Wk8
	[norm. at.%]	
Carbon	40.13	51.66
Oxygen	50.42	38.73
Calcium	0.97	3.27
Phosphorus	0.62	1.53
Chlorine	-	2.60
Sodium	7.87	2.20
Ca/P ratio	1.56	2.13

Table 5.10. Results from EDX analysis for each scaffold in the beginning and at the end of the bioactivity study.

For scaffolds with 80:20 ratio, the presence of sodium and chloride on the surface of the sample can be observed. As SBF has very high content of these two elements present, it is very likely that formation of NaCl crystals occurred. This is most likely caused by insufficient washing of the samples which was carried out to remove the minerals present on the surface [149]. It can be seen that all fabricated samples, except 80FG scaffold, have a Ca/P ratio higher than the stoichiometric ratio of hydroxyapatite. Additionally, that the Ca/P ratio has decreased after 8 weeks of immersion in SBF. This suggests that calcium phosphate apatite layer has been formed which causes the percentage of phosphate ions (PO_4^{3-}) present in 50FG, 50FD and 80FD to increase. On the other hand, from the Ca/P ratio of 80FG, it is suggested that there is decrease in the percentage of PO_4^{3-} . However, the Ca/P ratio is not an accurate representation of the nature of the calcium phosphate phase, as the bone apatite is usually nonstoichiometric. The formation of bone apatite implies the electrostatic interaction of the positive Ca^{+} ions and the negative charged ions available in the surface and the microenvironment. Furthermore, the process of apatite formation is a slow one [150], which explains the differences in the Ca/P ratios among the tested scaffolds.

Finally, even when SBF immersion provides an insight of the way the scaffold can chemically interact with the surroundings, it has been suggested by Drouet (2013) that this process should not be taken as a conclusive proof of the bioactive properties of a material. This is mainly due to fact that SBF immersion only considers the interaction of the scaffold with a mineral rich environment, it is necessary to contemplate the cellular behaviour as well [149].

5.5 Final conclusions from exploring methodologies for fabrication of hydroxyapatite/chitosan composites enabling vascular infiltration

After finalizing the trials to study various protocols to develop our material we can conclude as follows:

- Composites elaborated with carboxymethyl cellulose require careful treatment, since the interaction with chitosan is very strong it produces non-homogenous solutions.
- Chitosan: hydroxyapatite ratio plays a major role in the final behaviour of the produced scaffolds. All electrostatic interactions depend on the presence of the phosphate. Therefore, characteristics such as the porosity and the heparin attraction will be defined by the phosphate distribution throughout the matrix.
- Freeze-drying methodology provides a simple process to obtain porous scaffolds. However, attention must be paid in the cooling rates in order to achieve a desired or required porosity.
- Freeze-gelation provides a simple, yet efficient procedure to produce porous scaffolds. The characteristics achieved with the chitosan/hydroxyapatite mixture offer a possibility to explore further to produce bone tissue engineering scaffolds.
- Bioactivity is an important characteristic of tissue engineering scaffolds. Scaffolds prepared with chitosan/hydroxyapatite mixture, preliminarily

proved to be bioactive since formation of apatite layer was observed on their surface, regardless of the fabrication method or the phosphate concentration.

5.6 Summary

The complete development of the process for fabrication of a hybrid bioactive scaffold to promote bone angiogenesis was presented in this chapter. Firstly, the content was defined, always aiming to allow the addition of heparin, since our hypothesis is that the presence of heparin will induce and promote bone angiogenesis. Therefore, different compositions and protocols were tested in order to obtain the best option that allows us to test our hypothesis.

Finally, the best option to continue the study of heparin influence in bone angiogenesis is the scaffold produced with freeze-gelation with a chitosan: hydroxyapatite ratio of 50:50. Since it is endowed with the required characteristics in terms of porosity, chemical characteristics, and bioactivity performance, providing a suitable scaffold for bone tissue engineering purposes.

The following chapter contains the results of the characterisation of the scaffolds obtained by this selected protocol.

6

Results and Discussion

Section II.
Optimized freeze-gelled heparinized chitosan/ hydroxyapatite scaffolds

The previous section explored two methodologies for chitosan/hydroxyapatite scaffold preparation. Two CS:HA ratios were studied, as well as different modifications in the freeze-gelation methodology, analysing the impact of these variations on the scaffold's structure, bioactivity, and heparin interaction in general. Therefore, as mentioned in the conclusions from the previous section, based on the results from these trials an optimized freeze-gelation methodology was developed, since it is expected they will provide an appropriate structure for vascular infiltration. The optimized freeze-gelation methodology has been described in detail in chapter 3, section 3.2.

Hence, the present chapter describes and reports all the results obtained from characterising the scaffolds prepared with the optimized freeze-gelation methodology, working only with a 50:50 chitosan/hydroxyapatite ratio. The characterisation methods employed to analyse these scaffolds have been described in chapter 4. These results are discussed in detail in this chapter to provide a comprehensive conclusion form this study.

6.1 Structural characterization

The scaffolds obtained by freeze-gelation method had a sponge-like appearance. They looked white in colour due to the presence of hydroxyapatite. After cutting them with the cork borer they were shaped into cylindrical scaffolds of cylindrical of 5mm of diameter and approximately 2.5 mm of thickness. Their average weight is 6.47 ± 0.076 mg (SD=1.014).

Figure 6.1 Appearance of the produced scaffolds. Scale bars are 2.5 mm.

The following table shows the abbreviations used to name the samples obtained, according to the concentration of heparin loading solution they were immersed in during their fabrication.

Sample Name	Scaffold matrix	Heparin loading concentration (mg/mL)
MMW	Scaffold prepared of pure chitosan medium molecular weight for comparison purposes	
M0	Chitosan + hydroxyapatite 50:50 ratio	0
M0.5		0.5
M1		1
M2		2
M5		5

Table 6.1. Abbreviatory names for the scaffolds, according to their composition and heparin loading concentration.

6.1.1 Scanning Electron Microscopy (SEM)

The morphology of the freeze-gelled scaffolds was analysed using SEM. As shown in Figure 6.2, embedded hydroxyapatite crystals can be observed completely distributed throughout the polymer matrix.

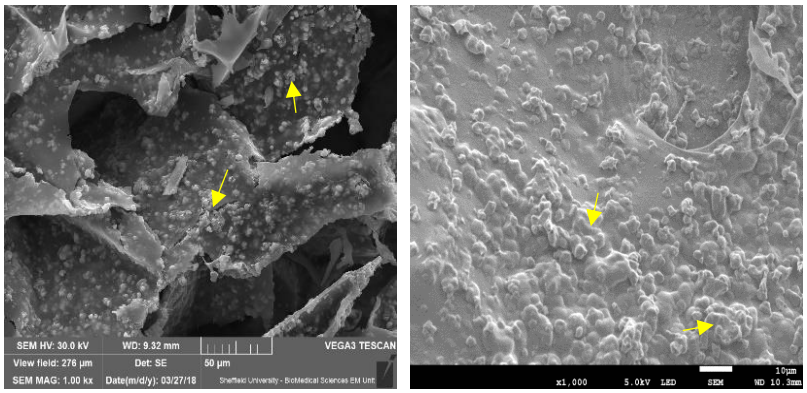

Figure 6.2. Structure of chitosan/hydroxyapatite scaffolds without heparin. The presence of embedded hydroxyapatite crystals can be observed throughout the chitosan matrix (yellow arrows). Dispersion of hydroxyapatite was similar in all the scaffolds regardless of the heparin loading concentration, therefore only this concentration was shown as representative. Scale bars are 50µm and 10µm, respectively.

One significant difference that can be spotted on the porosity and hydroxyapatite distribution according to the side of the cylinder-shaped scaffold. A chitosan-rich side was found on the top face of the scaffold. A surface with scattered hydroxyapatite particles and irregular porosity can be seen in Figure 6.3 (A). Lateral views of the scaffold, Figure 6.3 (B), show consistent porosity and hydroxyapatite is evenly embedded throughout the chitosan matrix on this side. The bottom face of the scaffold exhibited the hydroxyapatite-rich side, Figure 6.3 (C), where a surface rough in appearance and with little or no porosity can be observed.

Figures 6.4 to 6.6 show a more detailed view of the structure of the scaffold according to its different faces (top face, bottom face, edges). These images show that heparin loading did not affect pore distribution on the scaffolds, as mentioned before, since porosity was similar in size and distribution among the different concentrations. To

compare the effect of adding hydroxyapatite on the chitosan matrix we have included the scaffold prepared with chitosan MMW, i. e. without hydroxyapatite.

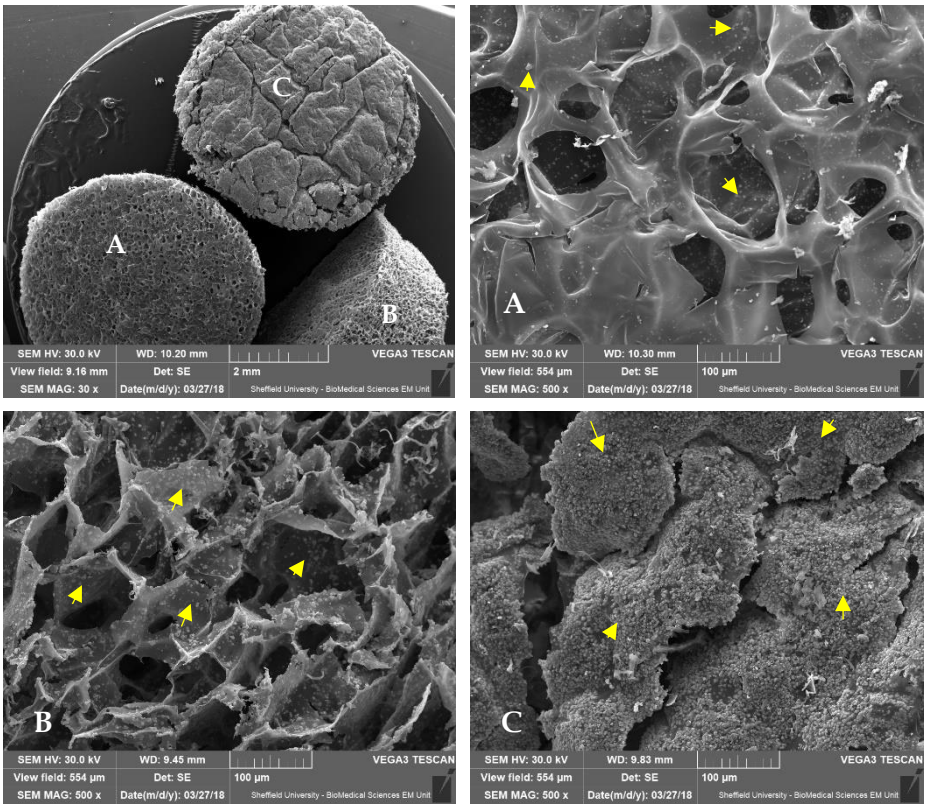

Figure 6.3. Differences in porosity and hydroxyapatite distribution according to scaffold's view. The scaffold presented in these image as a representation of the hydroxyapatite distribution is the scaffold M0.5 (immersed in a 0.5 mg/mL heparin solution), however the same phosphate distribution was observed in all of the scaffold prepared. HA particles shown with yellow arrows. (A) correspond to the top face of the scaffold where random porosity can be seen, less hydroxyapatite crystals are observed. (B) are the side views of the scaffold, bigger interconnected pores can be found. (C) correspond to the bottom face of the scaffold. A dense concentration of hydroxyapatite particles is seen, causing the reduction of porosity observed, instead, a lot of cracks can be notices. Scales bars are 2mm, 100 µm, 100 µm, and 100 µm, respectively.

Figure 6.4 shows in detail the top surface of the scaffolds. In this image all the heparin concentration are compared. Pore distribution on this face was between 42.59 µm and 264.52 µm, with and average pore size of 118.29 µm as showed in Histogram 6.1. Pore size was determined as described in section 4.1.1.

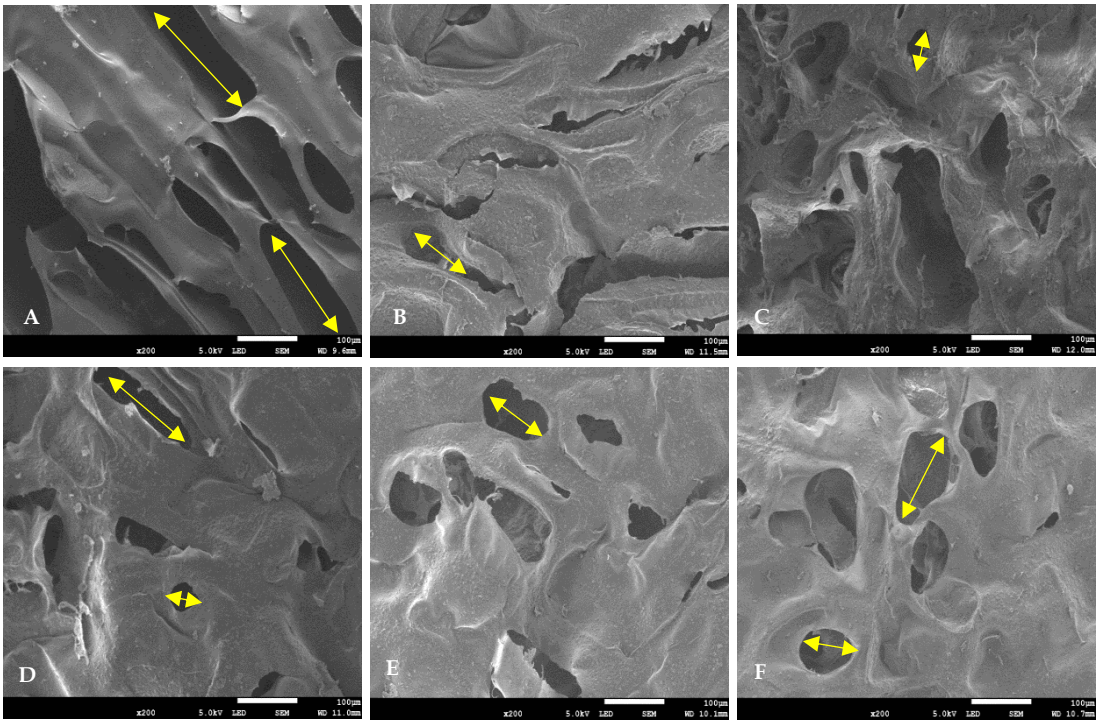

Figure 6.4. Top surface of the scaffolds. Elongated pores can be observed in the scaffold without HA and/or heparin, though this length and consequently the pore size is slightly reduced in most of the pores with the addition of HA (yellow arrows). Pore size distribution is ample, finding pores from around 40 µm to 200 µm. Heparin content did appear to have any visible effect in the porosity of the scaffolds, since pore size distribution was similar in all the samples, regardless of the heparin concentration. (A) chitosan MMW without hydroxyapatite. (B) M0 scaffold without heparin. (C) M0.5 scaffold loaded in the 0.5 mg/mL heparin solution. (D) M1 scaffold loaded in the 1 mg/mL heparin solution. (E) M2 scaffold loaded in the 2 mg/mL heparin solution. (F) M5 scaffold loaded in the 5 mg/mL heparin solution. Scale bars are 100 µm for all images.

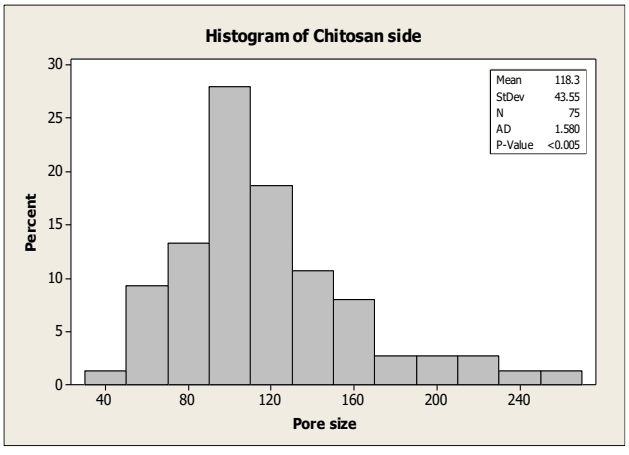

Histogram 6.1. Distribution of pore sizes in the top surface of the scaffold, also called chitosan-side. The majority of the pores have sizes between 100-130 µm.

As observed in Figure 6.4 the porosity in the top face varies in size. It is also notable that the pore size and shape changed in the chitosan matrix with the addition of

hydroxyapatite. Since pores in the image of the scaffold made of only chitosan (i.e without any hydroxyapatite or heparin), present long pores. Even, when this pore shape was observed in the rest of the samples, the length of the pores was shorter in the presence of hydroxyapatite.

Figure 6.5 shows the side views of the cylindrical scaffolds. This side of the scaffolds exhibited the bigger pore size, with a wide size distribution from 53.56 μm to 392.63 μm, and an average of 153.93 μm (see Histogram 6.2).

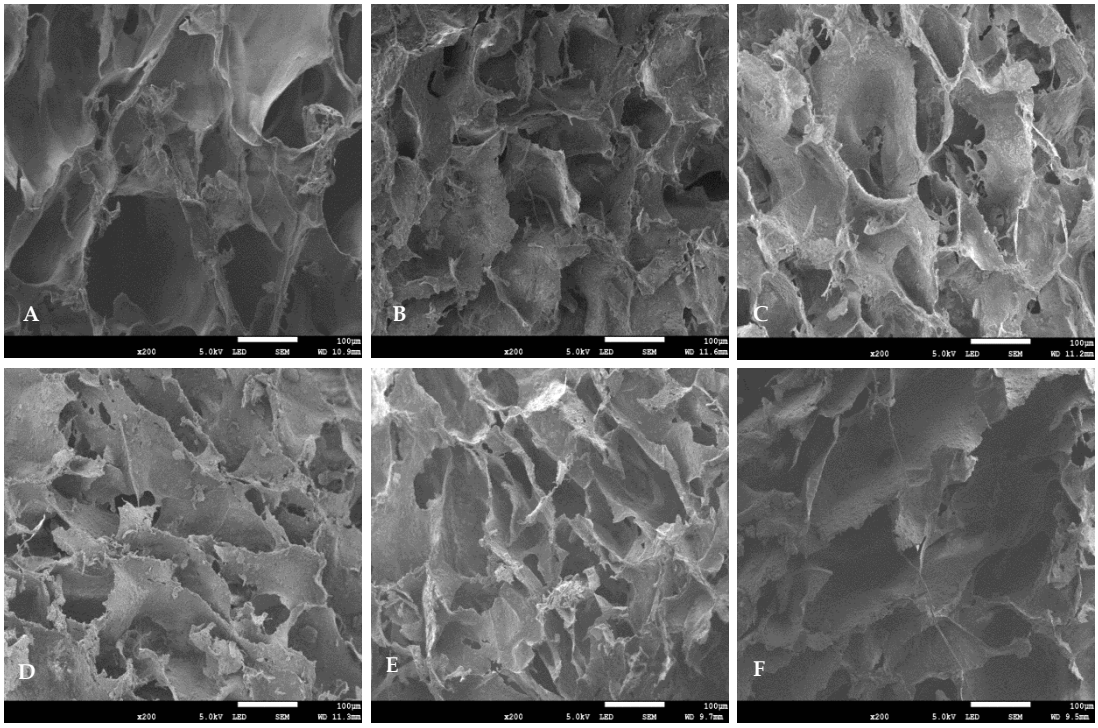

Figure 6.5. Side views of the scaffolds. Higher porosity and bigger pores can be observed on this face of the scaffold. The pore size and distribution are similar in all the scaffolds including the scaffold without HA and/or heparin. Pore size distribution is ample too , finding pores from around 50 μm to nearly 300 μm. Heparin content did appear to have any visible effect in the porosity of the scaffolds, since pore size distribution was similar in all the samples, regardless of the heparin concentration. (A) chitosan MMW without hydroxyapatite. (B) M0 scaffold without heparin. (C) M0.5 scaffold loaded in the 0.5 mg/mL heparin solution. (D) M1 scaffold loaded in the 1 mg/mL heparin solution. (E) M2 scaffold loaded in the 2 mg/mL heparin solution. (F) M5 scaffold loaded in the 5 mg/mL heparin solution. Scale bars are 100 μm for all images.

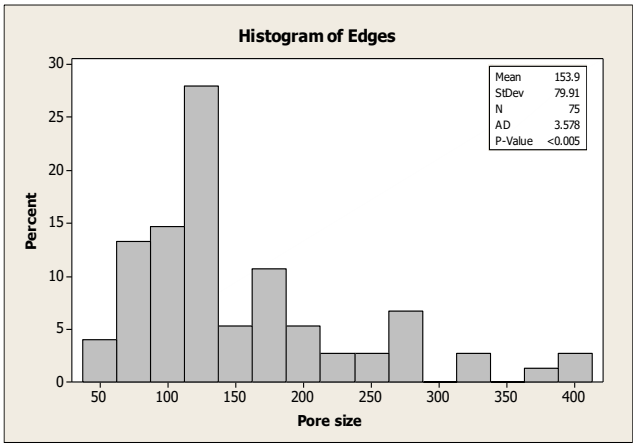

Histogram 6.2. Distribution of pore sizes in the lateral surface of the scaffold, also called edges. The majority of the pores have sizes between 120-150 µm.

As observed in Figure 6.5 the porosity in the side views of the scaffolds also varies in size. In this parts of the scaffolds the pore size and shape did not appear to be changed with the addition of hydroxyapatite to the chitosan matrix, since pores in the images of the scaffold made of only chitosan (i.e without any hydroxyapatite or heparin), present similar size and shape to those of the rest of the samples.

Lastly, Figure 6.6 presents the bottom side of the scaffolds. This side was found to be characterized for a porosity ranging from 16.21 µm to 168.19 µm, with an average of 60.23 µm (see Histogram 6.3). The entire surface of the polymer matrix appears to be covered by the hydroxyapatite particles, which gives it the appearance of a very rough surface when compared to the surface of the scaffold made of only chitosan (i.e without any hydroxyapatite or heparin). Though some porosity can be observed in this side, the presence of cracks along these surfaces was characteristic, revealing inner porosity in the interior of the scaffold (interconnectivity) (red arrows).

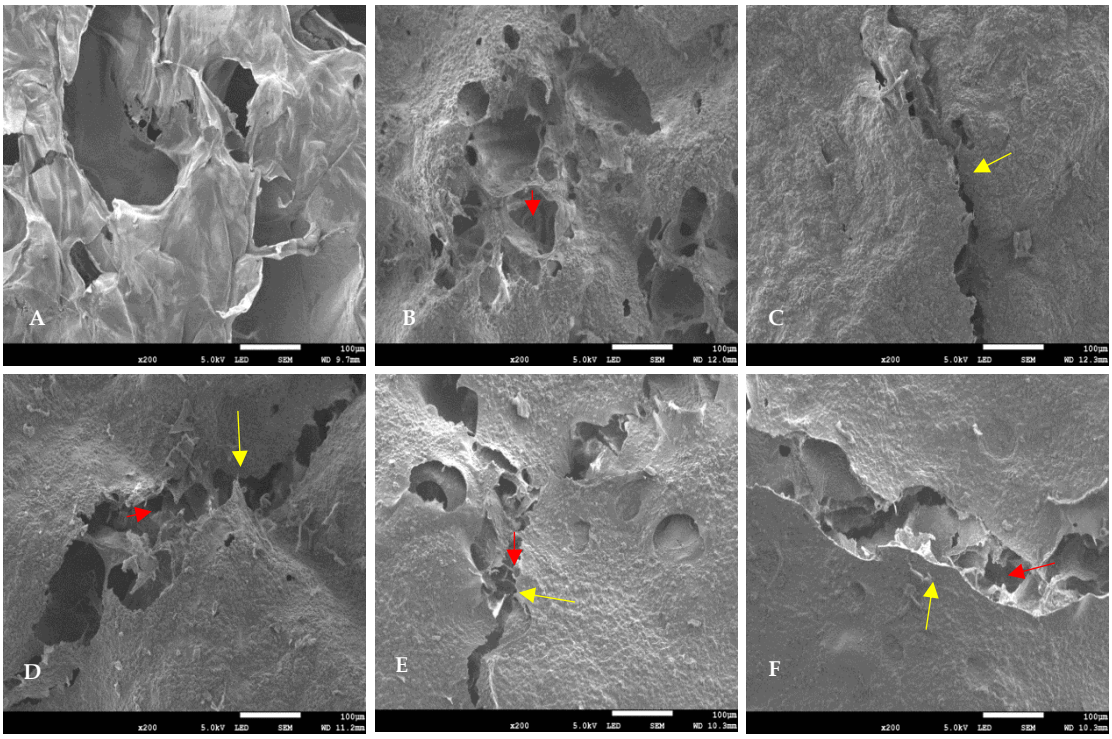

Figure 6.6. Bottom surface of the scaffolds. Lower porosity and smaller pores can be observed on this face of the scaffold. The presence of cracks is noticeable (yellow arrows). The pore size and distribution are similar in all the scaffolds with HA, appearing denser than the scaffold without HA and/or heparin. Inner porosity is shown with red arrows. Pore size distribution goes from around 16 µm to nearly 160 µm. Heparin content did appear to have any visible effect in the porosity of the scaffolds, since pore size distribution was similar in all the samples, regardless of the heparin concentration. (A) chitosan MMW without hydroxyapatite. (B) M0 scaffold without heparin. (C) M0.5 scaffold loaded in the 0.5 mg/mL heparin solution. (D) M1 scaffold loaded in the 1 mg/mL heparin solution. (E) M2 scaffold loaded in the 2 mg/mL heparin solution. (F) M5 scaffold loaded in the 5 mg/mL heparin solution. Scale bars are 100 µm for all images.

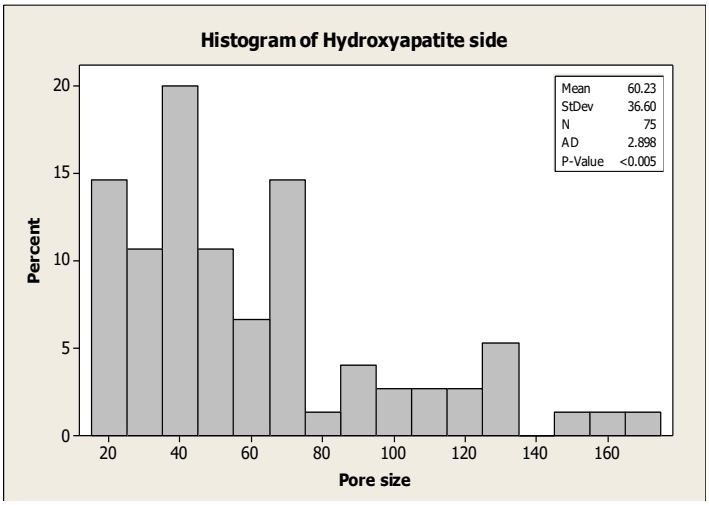

Histogram 6.3. Distribution of pore sizes in the bottom surface of the scaffold, also called hydroxyapatite-side. The majority of the pores have sizes between 40-70 µm.

6.1.1.1 EDX analysis

Energy Dispersive X-Ray Spectroscopy (EDX) is a characterization method based on the discrimination of the X-Ray energies by a detector, knowing that each energy is characteristic of the orbital transition of some electrons in each element, during the X-Ray interaction with the sample. Therefore, this technique allows the acquisition of a compositional analysis of the sample.

The results from EDX analysis allowed to detect the sulphate on the sample. The sulphate confirms the presence of the heparin on the scaffold. There is a low presence of sulphate, around 0.7 to 1.3 Wt%.

The elements detected on the samples are shown in Table 6.2. Figures 6.7 to 6.11 show the EDX spectra for each sample.

Element	**Wt %**				
	M0	**M0.5**	**M1**	**M2**	**M5**
C	36.9	30.4	49.9	34.3	46.0
O	25.5	17.8	12.6	12.6	10.7
Ca	6.4	2.1	0.5	8.4	4.4
P	4.6	1.0	-	2.8	1.2
N	6.8	3.7	-	3.2	8.2
S	**-**	**1.0**	**0.7**	**1.3**	**1.0**
Na	2.0	7.4	7.1	4.1	3.2
Cl	0.2	0.4	0.8	1.0	0.6
Mg	0.2	0.1	0.4	0.2	0.2
Au	*17.5*	*36.0*	*27.9*	*32.1*	*24.6*

Table 6.2. EDX results for all the samples.

The presence of Na is explained due to the addition of the sodium heparin.

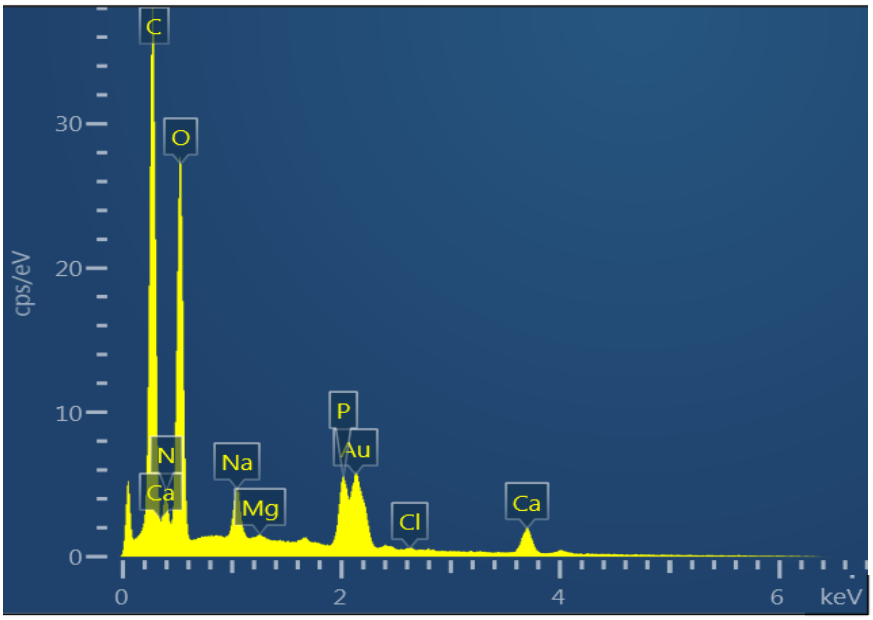

Figure 6.7. EDX spectrum for M0 (scaffold without heparin).

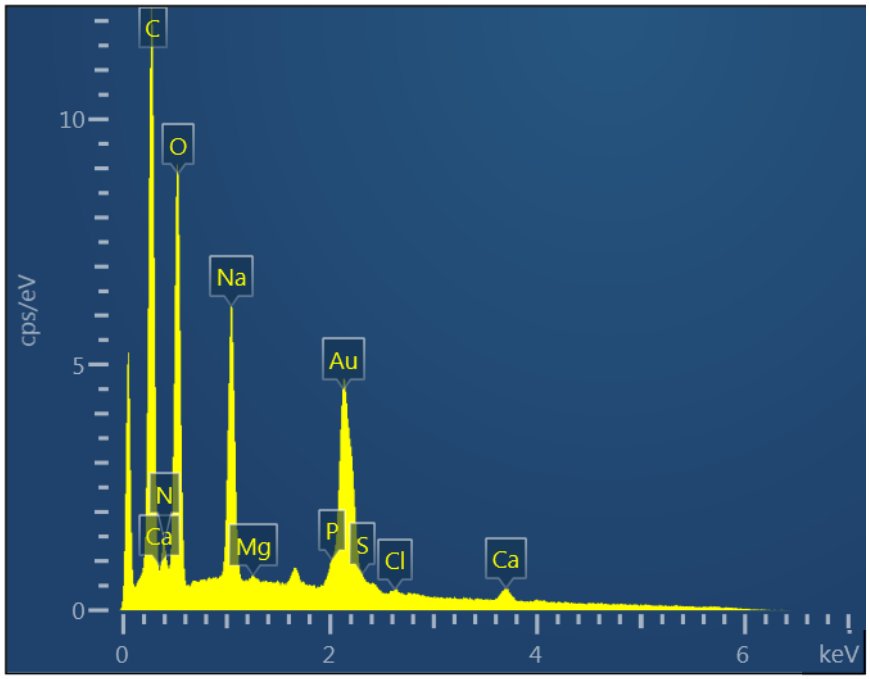

Figure 6.8. EDX spectrum for M0.5 (scaffold loaded in the 0.5 mg/mL heparin solution).

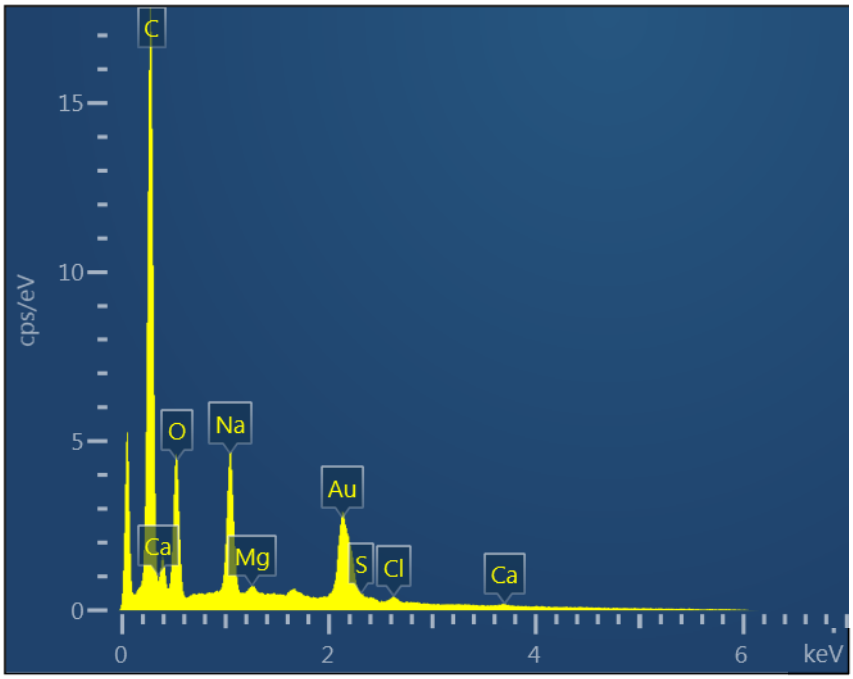

Figure 6.9. EDX spectrum for M1 (scaffold loaded in the 1 mg/mL heparin solution).

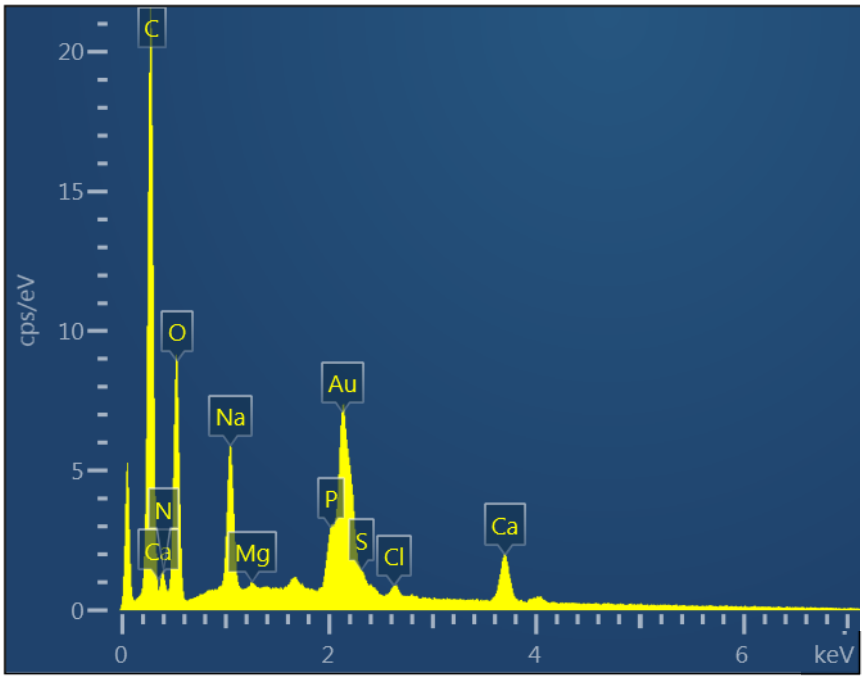

Figure 6.10. EDX spectrum for M2 (scaffold loaded in the 2 mg/mL heparin solution).

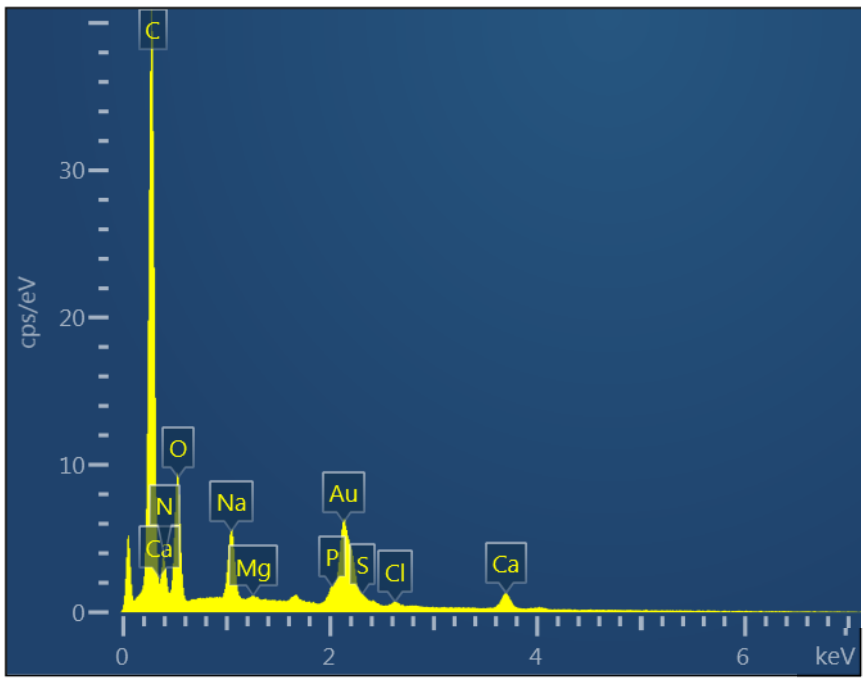

Figure 6.11. EDX spectrum for M5 (scaffold loaded in the 5 mg/mL heparin solution).

6.1.1.2 Discussion of SEM results

Images of the scaffold show that a scaffold with interconnected porosity was obtained (Figures 6.2 – 6.6).

The addition of heparin onto the scaffold by immersion in aqueous solution, did not affect the structure scaffolds regardless of the heparin concentration. The addition of hydroxyapatite, however, did change the porosity when comparing to scaffolds without hydroxyapatite, since the porosity appear to be closed in those with the phosphate.

According to Hsieh et al. (2007) porosity in chitosan scaffolds prepared *via* freeze-gelation depends mainly on two factors: a) freezing rate and temperature and b) acetic acid concentration.

During the freezing stage of the freeze-gelation process, the lower the temperatures and the faster freezing rates, the smaller pores were obtained. This is because these two variables control the ice crystals sizes and their formation process.

The acetic acid concentration influences the heat release during neutralization with the 3M sodium hydroxide solution of the gelation phase. In this part of the process, some of the frozen chitosan solution slightly melt, creating zones of different concentration. From Hsieh et al. (2007) it can be concluded that a more acidic the solution, produces a higher exothermic rate of the neutralization process, leading to an excessive remelting of the frozen solution, forming denser and more compact zones [151].

Moreover, hydroxyapatite surface charge usually is slightly negative, according to the concentration of the ions present on the lattice surface, being in decreasing order Ca^{2+} (4.5 ions /nm^2), PO^{3-}_4 (3.02 ions/nm^2) and OH^- (2.57 ions/nm^2) [138]. Therefore, the presence of hydroxide and phosphate groups on its lattice surface determine the nature of its charge. However, this charge can change with pH[152]. When hydroxyapatite becomes in contact with an acidic solution, there is a change on its surface charge due to the adsorption of H^+ onto the hydroxide ions and the protonation of the phosphate groups of the surface [138]. This protonation is what ultimately leads to hydroxyapatite dissolution in acidic media (pH <5). Even when chitosan was dissolved in a solution of acetic acid for the freeze-gelation process, the solution is not strong enough to dissolve hydroxyapatite and despite this change on its surface charge, it is still attracted to chitosan positive charges sufficiently to not precipitate and keep mostly dispersed into the matrix chitosan provides. Therefore, this chitosan solution was used to form a matrix in which the phosphate would be suspended.

The dispersion of hydroxyapatite along the chitosan matrix ultimately affects it density, and its concentration produces differences on the frozen zones, affecting the porosity size and distribution.

Figures 6.3 to 6.6 also present a difference between the surfaces of the scaffold. This gradient of hydroxyapatite from top to bottom was originated during freezing part of the freeze-gelation process. During the process of freeze-gelation, the porous are formed by removing the solvent while the frozen shape is retained. As mentioned before, the freezing rate is decisive for pore size determination. The freezing rate used during this process was at a relatively slow rate to carefully form the crystals which formed the pores in the chitosan matrix. Therefore, during this process, an amount of the suspended hydroxyapatite settled at the bottom of the container. However, majority of the hydroxyapatite was kept in suspension due to the surface charge interplay mentioned above and it could be observed homogeneously dispersed in the rest of the scaffold, as shown in Figure 6.3. Having a hydroxyapatite-rich side of the scaffold will allow to provide better bioactive properties to our scaffold. Since hydroxyapatite is often used as coating to induce bioactivity on orthopaedic implants, mainly because of the interaction of the osteoblasts around the bioactive surface, which promotes the formation of new mineralised bone matrix.

Lastly, the pore size represents a very important parameter for designing any scaffold in tissue engineering. It influences the cellular activity in terms of attachment, matrix deposition and differentiation. It seems to exist a general agreement within the field of bone tissue engineering to consider that the optimal pore size for bone tissue scaffolds is between 100 and 500 μm, to have good cell adhesion and proliferation, and vascular ingrowth [50,142]. Therefore, considering the porosity of the scaffolds as shown in histograms 6.1- 6.3, they are able provide an optimum environment for new bone growth and support for micro-vascularity to distribute blood across the entire scaffold.

6.1.2 In-vitro degradation study

A study of the in-vitro degradation of the prepared scaffolds was performed using a solution containing chicken egg white lysozyme.

Firstly, the results showing the changes on the scaffold structure are shown. The following figures present the SEM images obtained over time from the different faces of the cylindrical scaffolds. For comparative purposes only images of the scaffold without hydroxyapatite (MMW), the scaffold without heparin (M0), and the scaffold with highest concentration of heparin, i. e. 5 mg/mL (M5) were taken.

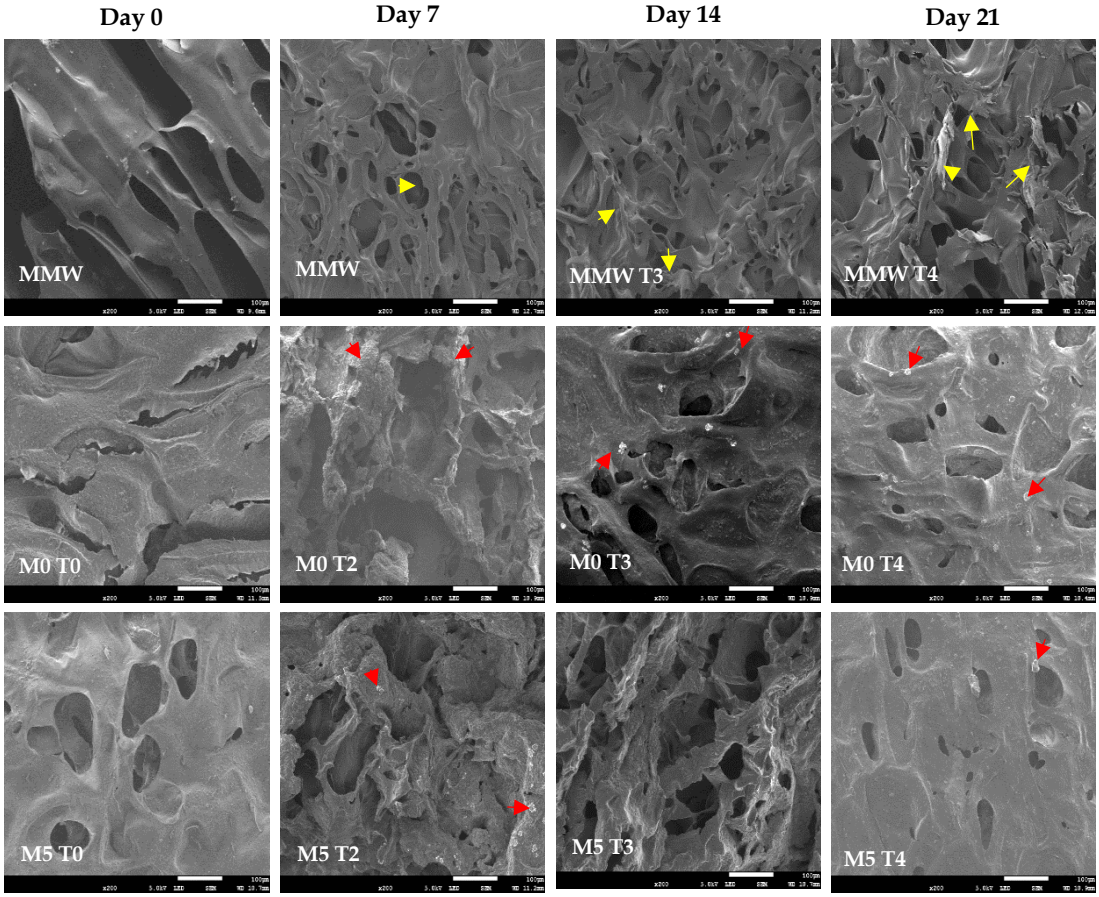

Figure 6.12. SEM images (200X) of the top surfaces of the scaffolds over time immersed in PBS and lysozyme. A ripped surface is observable for MMW sample, showing signs of degradation (yellow arrows). Mineral precipitation on the scaffolds with HA is pointed with red arrows. MMW: scaffold without hydroxyapatite. M0: scaffold without heparin. M5: scaffold loaded in the 5 mg/mL heparin solution. All scale bars are 100 µm.

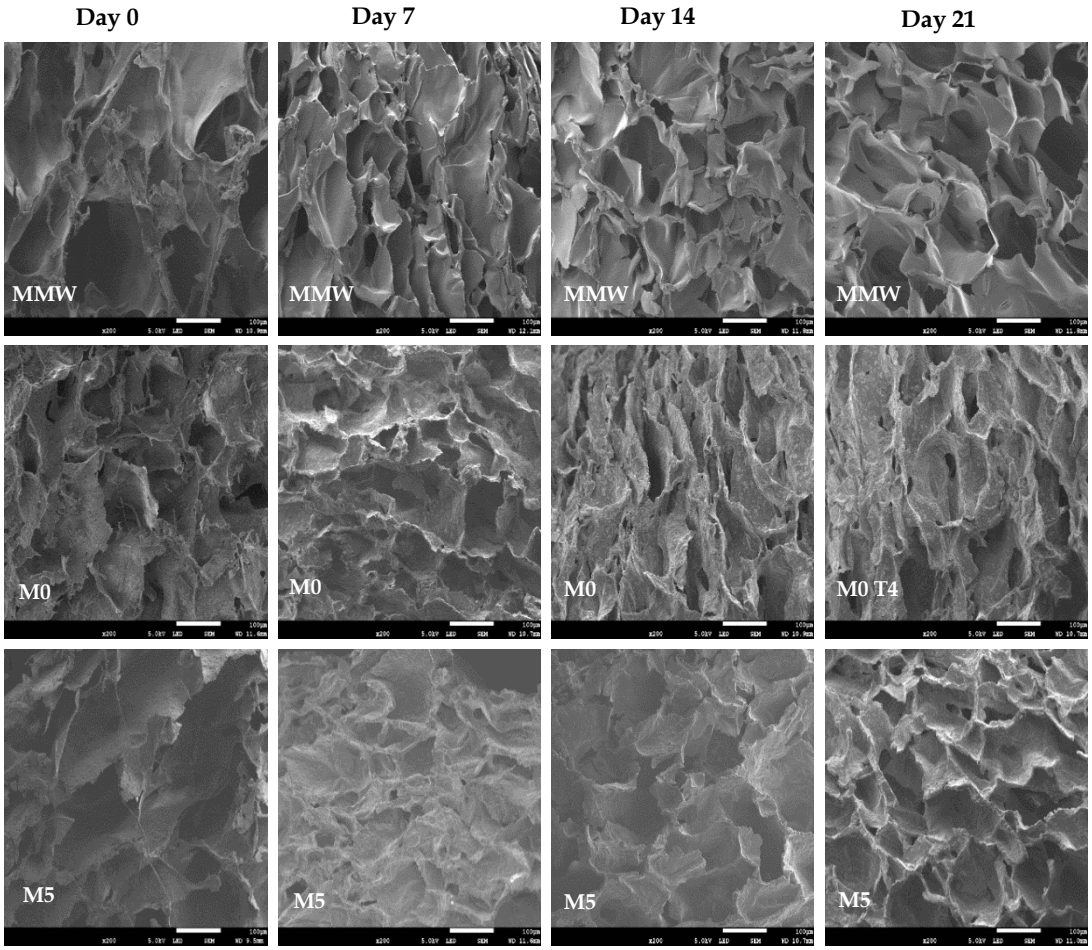

Figure 6.13. . SEM images (200X) of the side views of the scaffolds over time immersed in PBS and lysozyme. No visible changes were observed in this side on the scaffold. MMW: scaffold without hydroxyapatite. M0: scaffold without heparin. M5: scaffold loaded in the 5 mg/mL heparin solution. All scale bars are 100 μm.

From Figures 6.12 it is possible to observe that the structure of the scaffolds was less affected by the exposure to the lysozyme solution for the scaffolds with hydroxyapatite content. On the contrary, the scaffold without hydroxyapatite (MMW), showed signs of degradation of its walls all throughout the experiment. Formation of mineral deposits precipitation of salts on the scaffold surface is observable in the top surface. The SEM images indicates that by day 14 and 21, the structure of the scaffold prepared only with chitosan (MMW) is highly decayed, with walls that appeared to be ripped, moreover on the top surface (Figure 6.12, MMW, Day 21).

In Figure 6.13, the side views of the scaffolds are presented. There were no visible changes on the structure on the lateral sides of the scaffolds. Showing similar porosity and pore size, throughout the study. A similar case can be observed in Figure 6.14, where the bottom surfaces of the scaffold are presented. In this figure, however, the scaffold prepared of only chitosan (i. e. without hydroxyapatite or heparin), exhibited a loss of porosity throughout the experiment (yellow arrows), with a loss of stability of the structure too (red arrows).

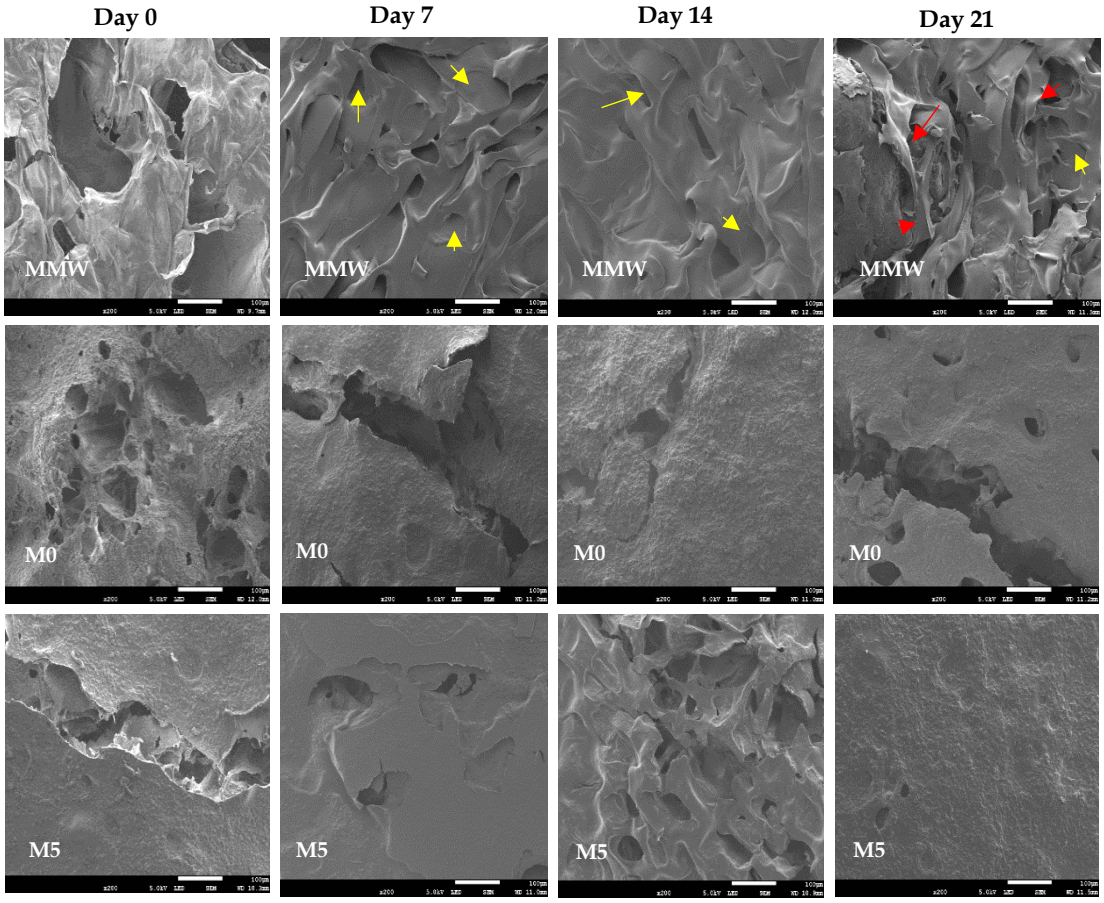

Figure 6.14. SEM images (200X) of the bottom surfaces of the scaffolds over time immersed in PBS and lysozyme. No visible changes were observed in this side on the scaffold for the scaffold with HA content. For the scaffolds without HA and/or heparin a reduction on porosity (yellow arrows) and a structure decay (red arrows) are observed. MMW: scaffold without hydroxyapatite. M0: scaffold without heparin. M5: scaffold loaded in the 5 mg/mL heparin solution. All scale bars are 100 µm.

Figure 6.15 shows the variations of the scaffolds weight percentage over time. It is possible to note that the scaffold prepared with pure chitosan (MMW) lost nearly 7% of its weight by day one of exposure to the PBS/lysozyme solution and on the last day of the experiment, day 21, it had lost at least 16% of its weight.

The behaviour for the scaffolds with hydroxyapatite is, however, the opposite. They gained closely between 5 – 8% of weight on the first day. Nonetheless, on the following days, these scaffolds started to lose this weight, ending up the experiment with approximately the 99% of their weight remaining. The complete description of the *in-vitro* degradation study, including how these weights were determined is included in Chapter 4, part 4.1.3.

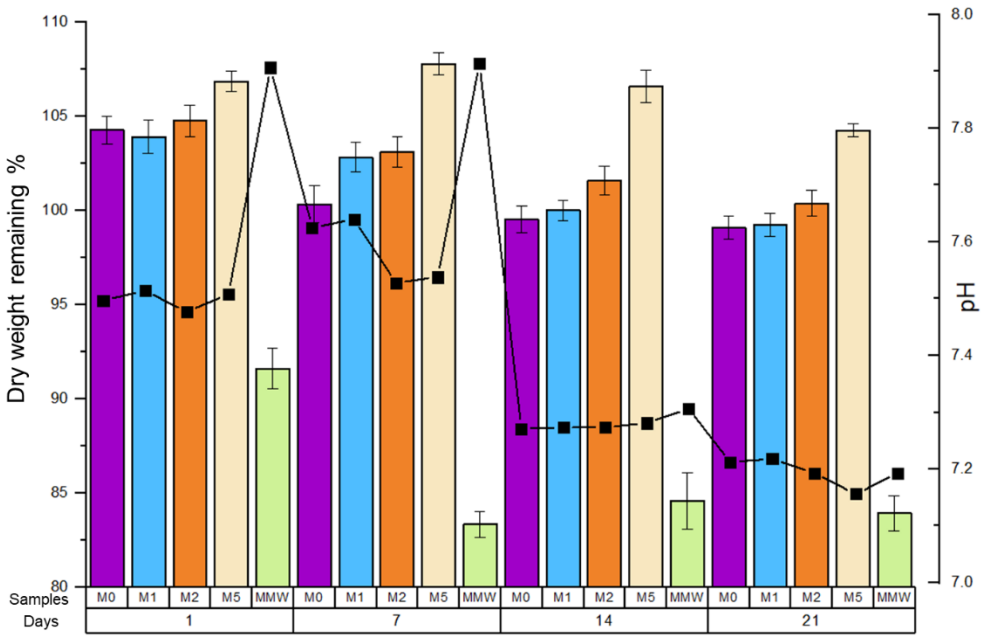

Figure 6.15. Dry weight remaining ratio (%) and pH change from scaffolds exposed to PBS and lysozyme over time.

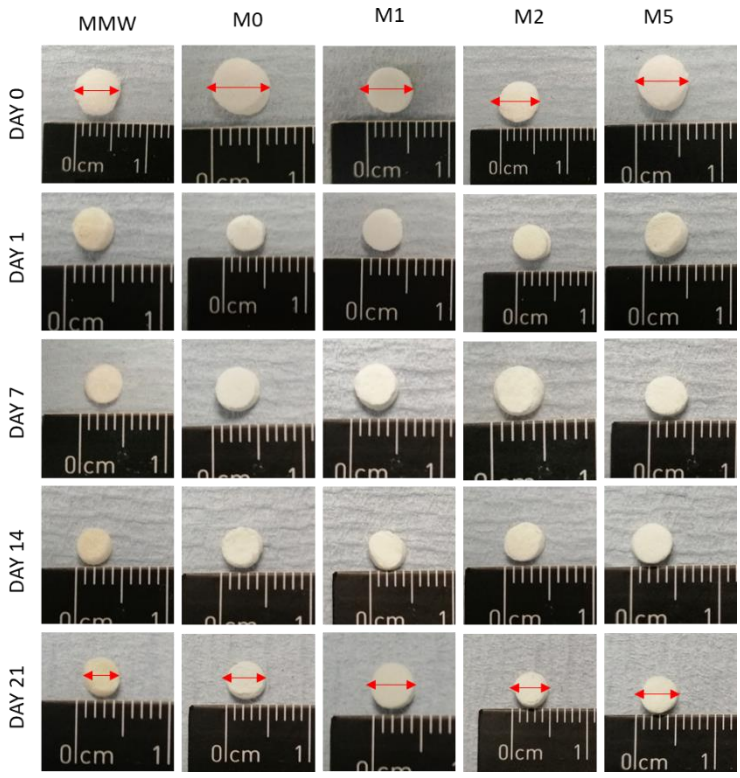

Figure 6.16. Changes in the appearance of the scaffolds exposed to PBS and lysozyme solution.

It was notable from Figure 6.15 that the higher the heparin concentration, the more gain weight for the scaffold during the first week of the study. By day 14th, as stated before, these scaffolds started to lose weight. Behaviour of the pH was consistent with these trends. For the MMW scaffold there was an increment of the pH up to 7.9 on the first two weeks of the study, following by a descend of the pH value to 7.2 on the last week of the experiment. Scaffolds with hydroxyapatite and heparin followed the same trend, with pH up to 7.6 on the first two weeks and finalizing the experiment with a pH of 7.2.

In addition, Figure 6.16 shows the changes in the appearance and size of the scaffolds during the exposure to PBS and lysozyme solution. It is possible to observe that the most significant changes in the diameter of the scaffolds, from 1 to 2 mm smaller, are seen on the last day of the experiment due to the degradation of the scaffold.

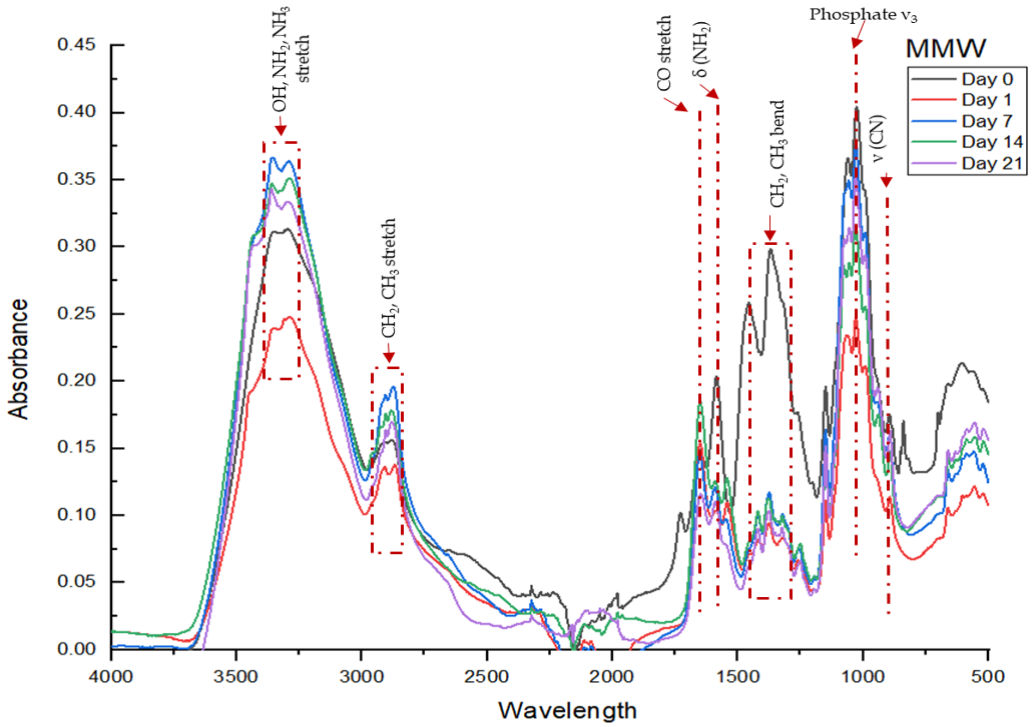

Figure 6.17. FTIR-ATR spectra from MMW (scaffold of just chitosan, i.e. without HA and/or heparin) exposed to PBS and lysozyme over time.

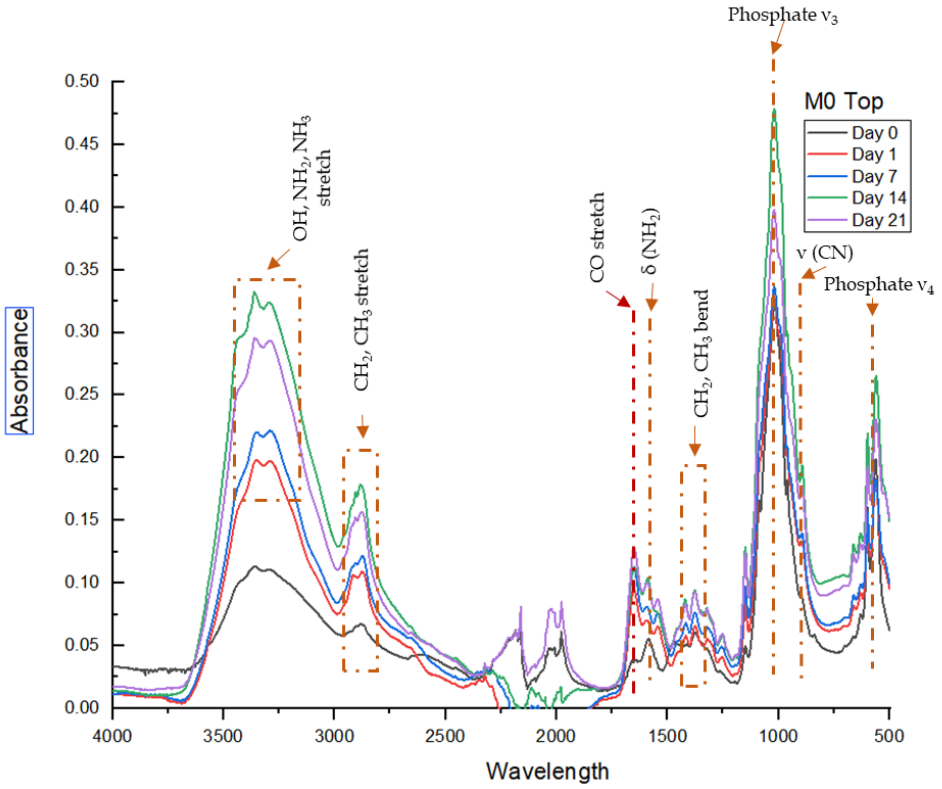

Figure 6.18. FTIR-ATR spectra from the Top Face of M0 (scaffold without heparin) exposed to PBS and lysozyme over time.

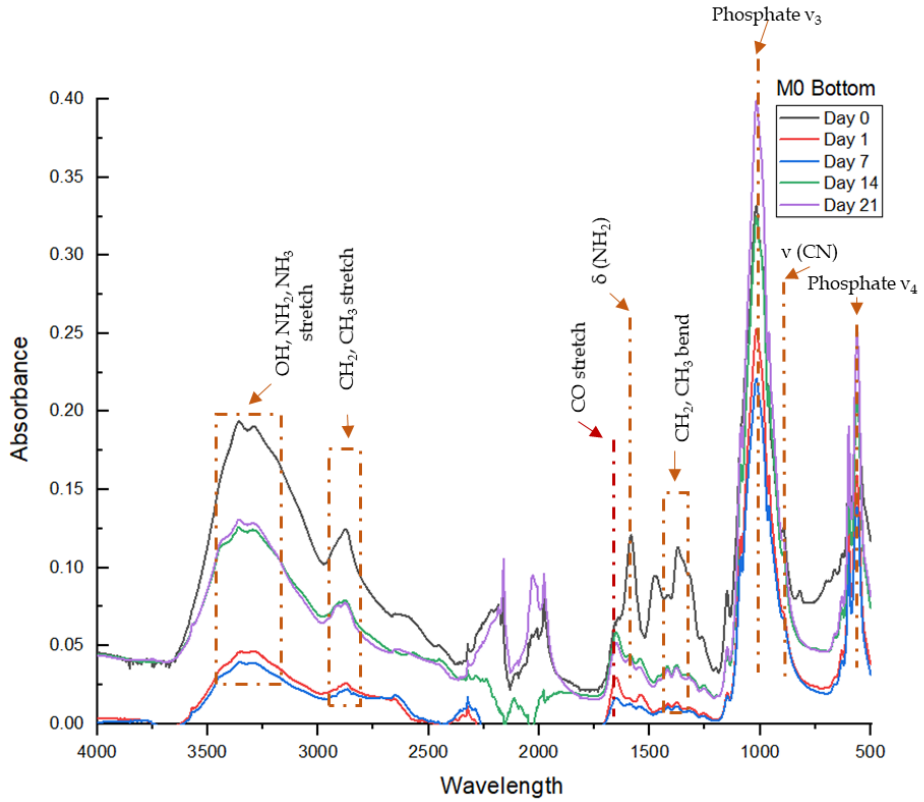

Figure 6.19. FTIR-ATR spectra from the Bottom Face of M0 (scaffold without heparin)exposed to PBS and lysozyme over time.

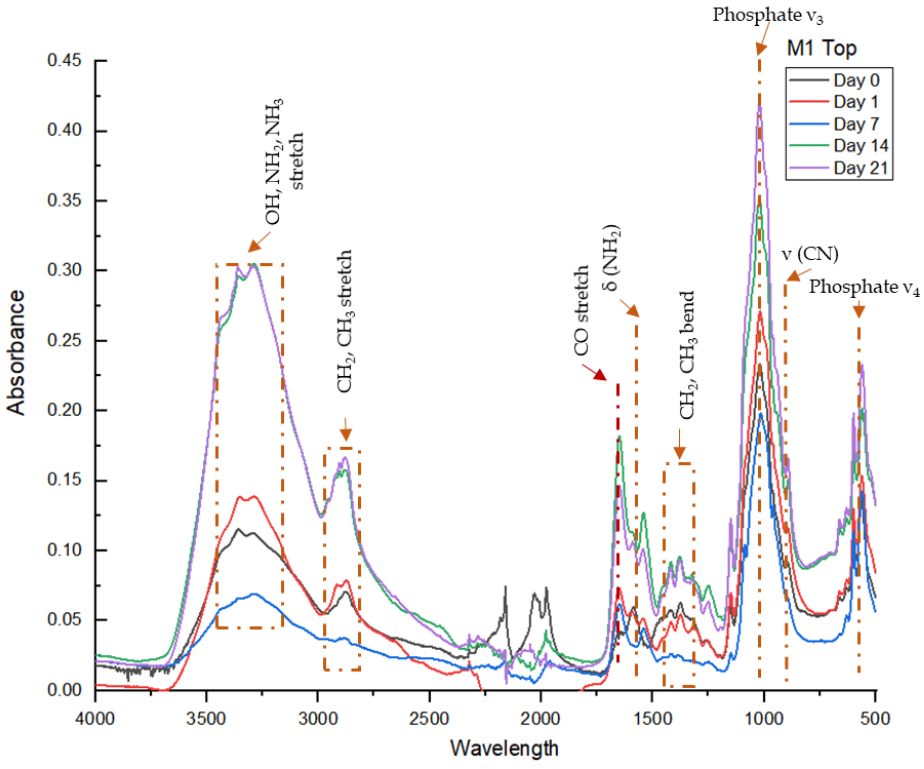

Figure 6.20. FTIR-ATR spectra from the Top Face of M1 (scaffold loaded in a 1mg/mL heparin solution) exposed to PBS and lysozyme over time.

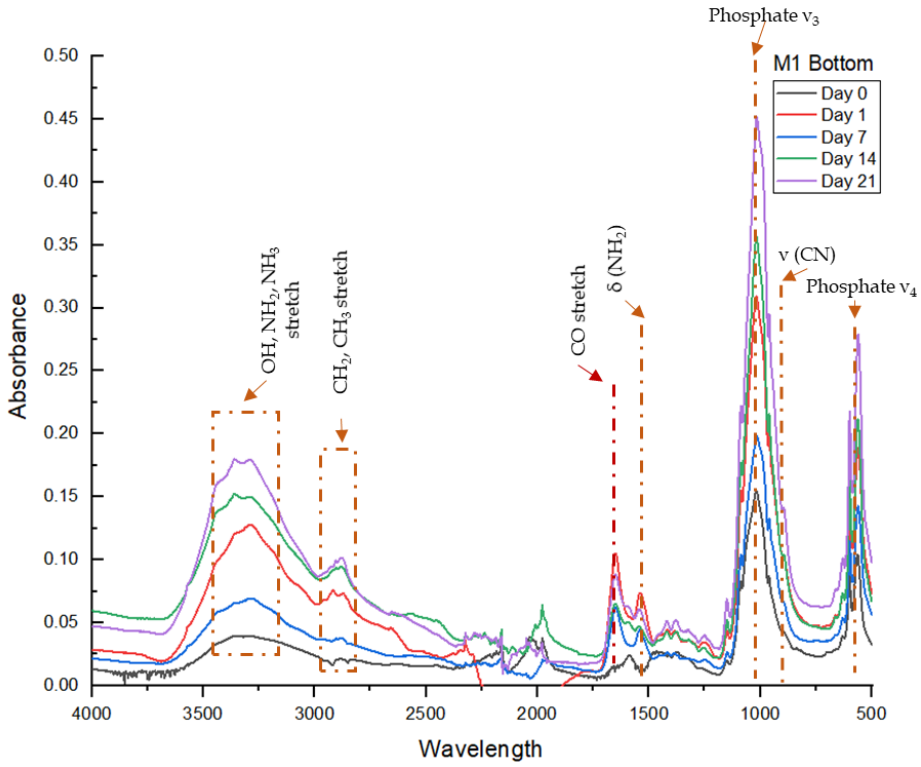

Figure 6.21. FTIR-ATR spectra from the Bottom Face of M1 (scaffold loaded in a 1mg/mL heparin solution) exposed to PBS and lysozyme over time.

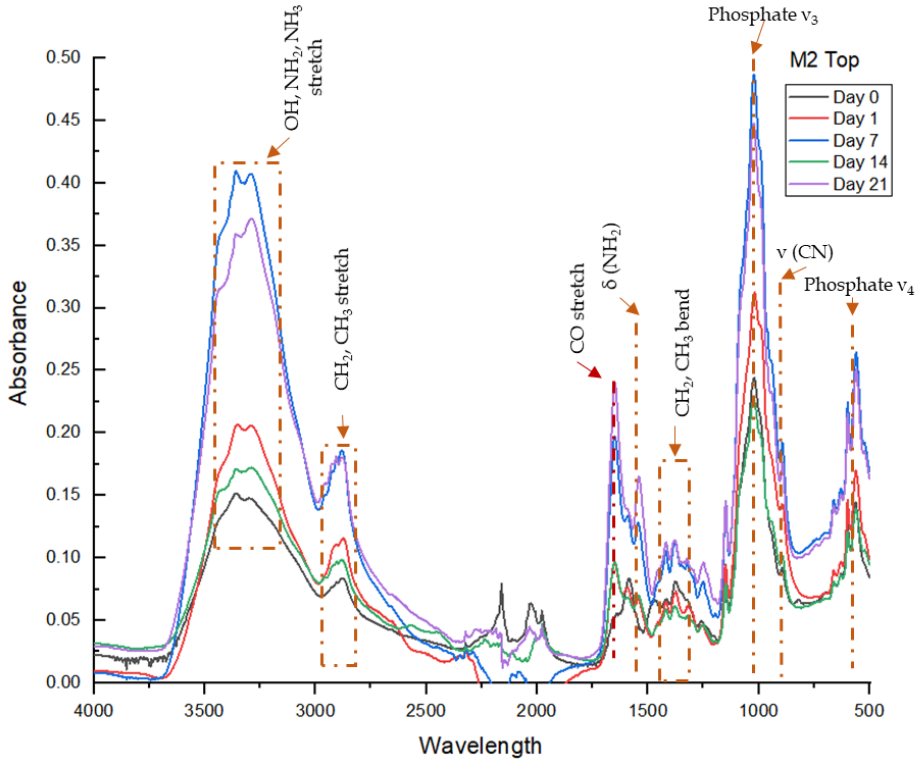

Figure 6.22. FTIR-ATR spectra from the Top Face of M2 (scaffold loaded in a 2mg/mL heparin solution) exposed to PBS and lysozyme over time.

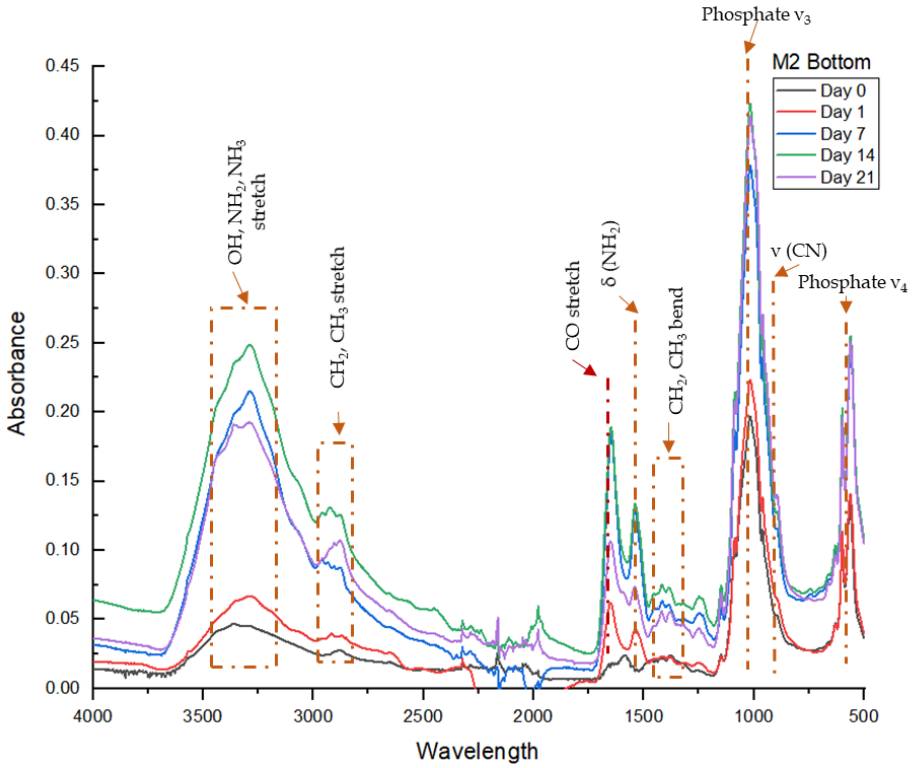

Figure 6.23. FTIR-ATR spectra from the Bottom Face of M2 (scaffold loaded in a 2mg/mL heparin solution) exposed to PBS and lysozyme over time

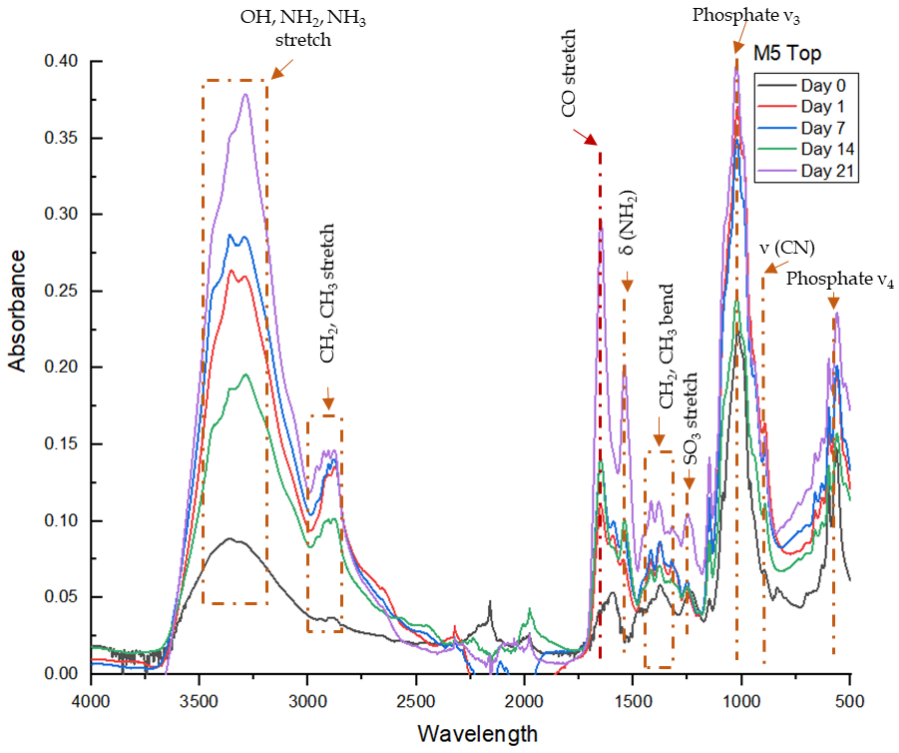

Figure 6.24. FTIR-ATR spectra from the Top Face of M5 (scaffold loaded in a 1mg/mL heparin solution) exposed to PBS and lysozyme over time.

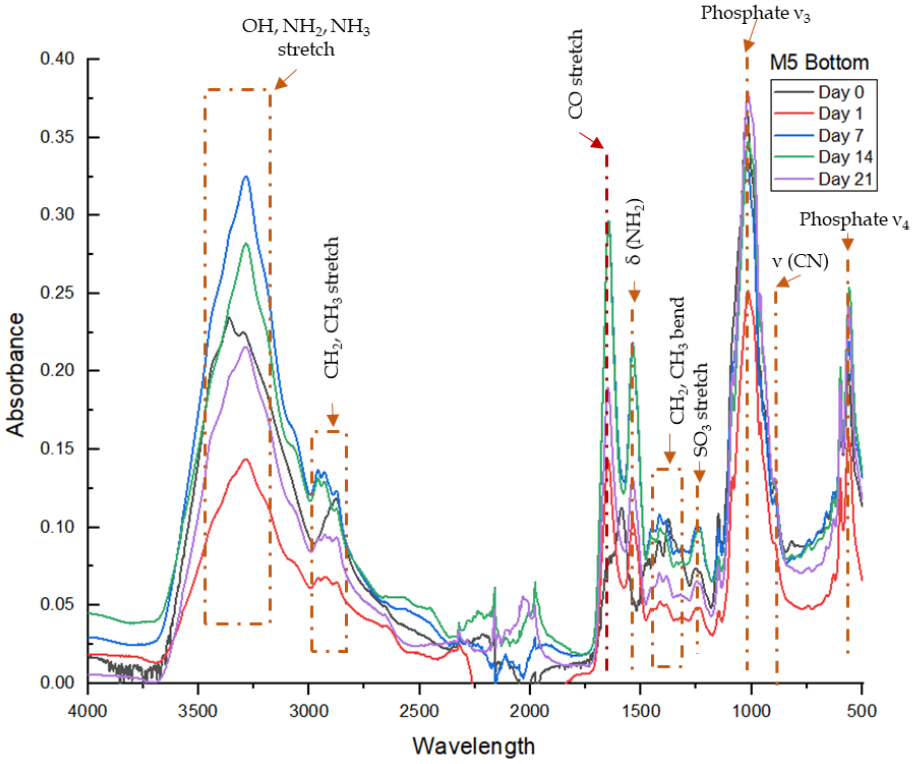

Figure 6.25. FTIR-ATR spectra from the Bottom Face of M5 (scaffold loaded in a 1mg/mL heparin solution) exposed to PBS and lysozyme over time.

Regarding the macrostructure of the scaffolds (Figure 6.16), MMW exhibits the major changes on its size over time losing over 2mm in diameter. However, the rest of the scaffolds reduced their diameter only by 1 mm at the end of the experiment.

FTIR spectra show consistent results for all the scaffolds. The following Table 6.3 lists the peaks that show a sharper figure and higher absorbance over time. It is possible to observe that consistently for all the scaffolds with hydroxyapatite, the phosphate peaks as well as the NH_2 bending and stretching bands sharpened over time. Finally, the peaks of the OH band separated during the in vitro degradation study, clearly showing OH stretching for chitosan and for hydroxyapatite.

Peak Assignment	Scaffold over time/ Wavelength								
	MMW	M0 T	M0 B	M1 T	M1 B	M2 T	M2 B	M5 T	M5 B
Phosphate υ_4	-	567	562	562	562	562	562	562	562
Phosphate υ_4	-	600	600	600	600	600	600	600	600
Phosphate υ_3	-	1017	1017	1021	1017	1021	1022	1026	1017
SO_3 stretching	-	-	-	-	-	-	-	1242	1242
CH_2 bending	1366	-	1371	1376	-	1380	-	1380	-
CH bending	1457	-	1471	1424	-	1419	-	1419	-
NH_2 bending From chitosan and lysozyme	1586	1539	1582	1551	-	1534	1539	1538	1538
CO stretching From sulphate and lysozyme	1648	1645	-	1649	-	1649	1654	1649	1649
CH_2 stretching	2880	2882	2876	2875	2872	2890	2876	2880	2880
CH_3 stretching	2904	-	-	-	2910	-	2919	2923	2909
NH_2 bending	-	3284	3292	3287	3288	3292	3288	3287	3288
OH stretching chitosan	3350	3366	3350	3359	3356	3354	3360	3359	-
OH stretching hydroxyapatite	-	-	3441	3435	3442	3435	3441	3426	-

Table 6.3. FTIR peak assignment for the changes on the chemical structure of the scaffold over time in the in-vitro degradation study. NOTES: Peaks in red decreased their absorbance. T: Before biodegradation study. B: At the end of degradation study. Phosphate appear in MMW due to PBS exposure.

6.1.2.1 Discussion of *in-vitro* degradation study results

The purpose of exposing the material to the action of an enzyme was to mimic the degradation it undergoes during implantation, since lysozyme is present in various human fluids in varied concentrations [153]. For comparison purposes, scaffolds of just chitosan medium molecular weight (MMW) were prepared via freeze- gelation methodology, to observe the effect of adding hydroxyapatite into the chitosan matrix. Figures 6.12 – 6.14 showed the variations of the scaffolds structure over time under the immersion in the PBS + Lysozyme. The SEM images only compare the effect of the degradation media on the structure of the scaffold of pure chitosan (MMW), scaffolds of chitosan and hydroxyapatite without heparin (M0) and scaffolds made of chitosan/hydroxyapatite/heparin in the highest loading concentration (M5). It is

possible to observe that for day 7 there is precipitation of salts all over the scaffolds with hydroxyapatite, particularly for the scaffold with heparin (Figure 6.12). By day 14 and 21 we can observe a similar trend with all the scaffolds, salts precipitation on hydroxyapatite/scaffolds-surface, but all of them present slightly opening porosity, due to the degradation of chitosan matrix (Figure 6.12). This can also be confirmed with graph presented in Figure 6.15, which shows the percentage of dry weigh remaining after degradation protocol and Figure 6.16, which shows the changes in the size of the scaffolds overtime.

Commonly, immediately after immersion in liquids, chitosan hydrogels tend to swell and retain water, which can explain little or non-existent weight loss on the first day of immersion [153]. However, as time goes by the swelled structure provides a higher porosity and surface area that favours lysozyme degradation of the structure and loss of the weight and integrity of the scaffold. This is notable for scaffold MMW, the weight loss was immediate since lysozyme degrades chitosan by hydrolysing its glucosamine bonds. This also shows that chitosan degradation is dependent on the degree of deacetylation (DD). As mentioned before, lysozyme degrades chitosan by acting on the NH_2 groups, the availability of these groups increases, of course, with the DD. For the scaffold's matrix, chitosan with a DD ≥90% was used, providing an ample source of NH_2 groups for lysozyme to hydrolyse during its interaction with the scaffold.

For the scaffolds with phosphate, however, matrix degradation is affected by the presence of hydroxyapatite, which hampers lysozyme interaction with chitosan. Lysozyme is able to be adsorbed onto hydroxyapatite surfaces, favoured by the interactions of lysozyme functional groups and hydroxyapatite phosphate groups [154]. This is also reflected on the FTIR spectra (Figures 6.17 -6.25) with the phosphate, NH_2 and CO peaks being sharper and with an increased absorbance. Furthermore, chitosan

matrix degradation depends on pH, and the presence of heparin decreases protonation of chitosan amino groups due to its complexation with the negative charged heparin-functional groups, neutralizing pH with time [155], as observed in Figure 6.15.

The degradation behaviour of the scaffolds is mainly a result of the deposition of lysozyme on hydroxyapatite and the presence of heparin holding up chitosan degradation. However, pore size and distribution, and interconnectivity of the matrix provided enough surface for the interaction of all the components, being determining factors for the degradation process. As a result, it is notable the degradation process from surface to bulk of the scaffold by the light beginning of weight loss and a slight yielding of chitosan structure by the 21 day of exposure.

6.2 Physicochemical characterization

6.2.1 FTIR-ATR

Top and bottom surfaces of the cylinder-shaped scaffolds were analysed by ATR-FTIR spectroscopy.

Figure 6.26 shows the resulting spectra comparing top and bottom surfaces of the scaffold M0 and the precursors used for its fabrication (chitosan and hydroxyapatite). FTIR spectra confirmed the composition of the scaffold and, in accordance with the SEM results, they show the clear difference between the two surfaces. For comparison purposes hydroxyapatite spectrum (C) was placed right below the bottom surface spectrum (D), the same case with chitosan (A) and the top surface (B).

Regarding the presence of heparin, Figures 6.27 and 6.28 show the scaffolds top and bottom surface spectra. Besides sharing the matrix characteristic peaks, indicated in Figure 4.26, it is notable the band at 1230 cm^{-1} corresponding to the SO_3 asymmetric stretching.

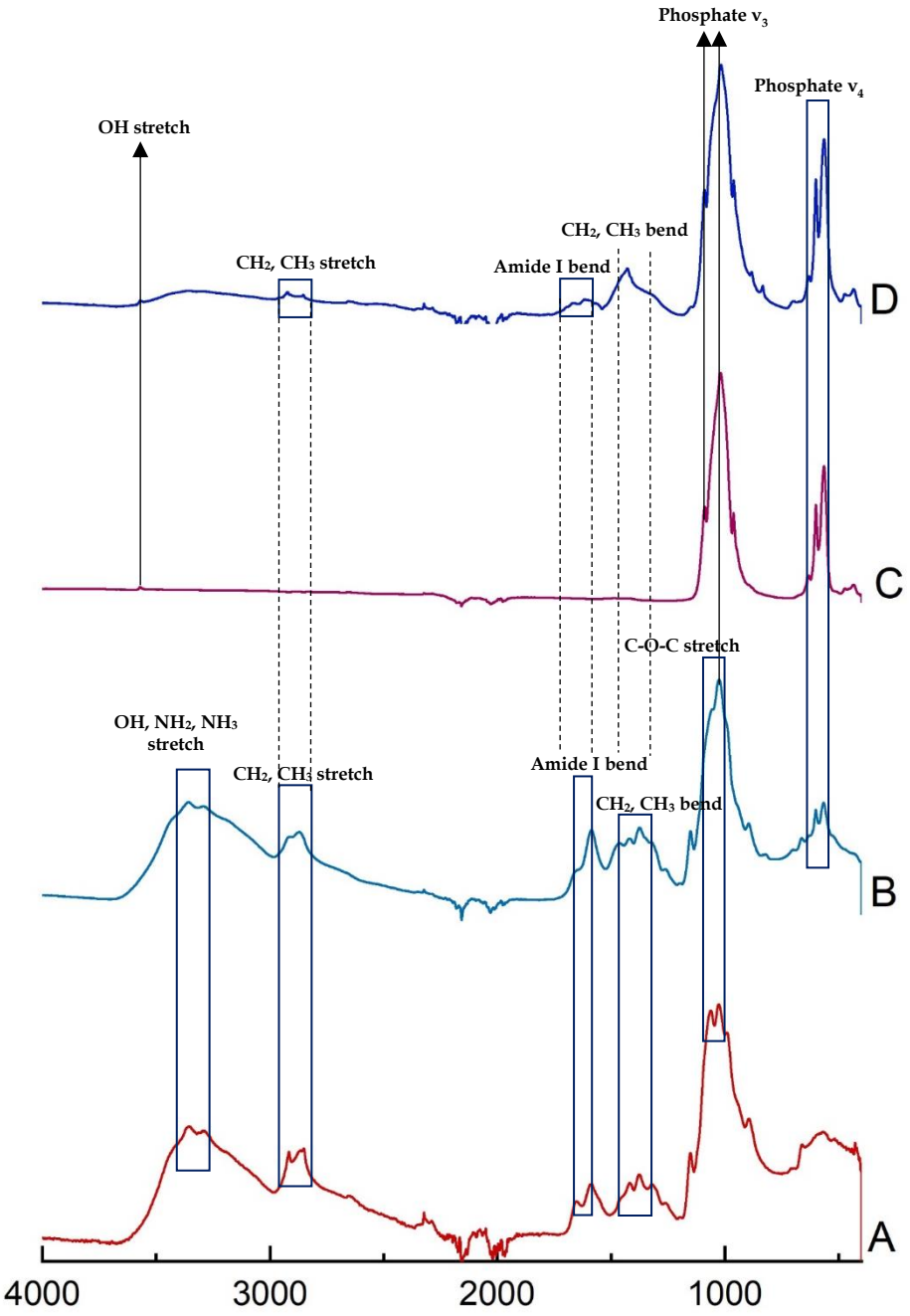

Figure 6.26. FTIR results in the spectral region 4000-400 cm^{-1} for (A) Chitosan, (B) Top surface of scaffold M0, (C) Hydroxyapatite, (D) Bottom surface of scaffold M0.

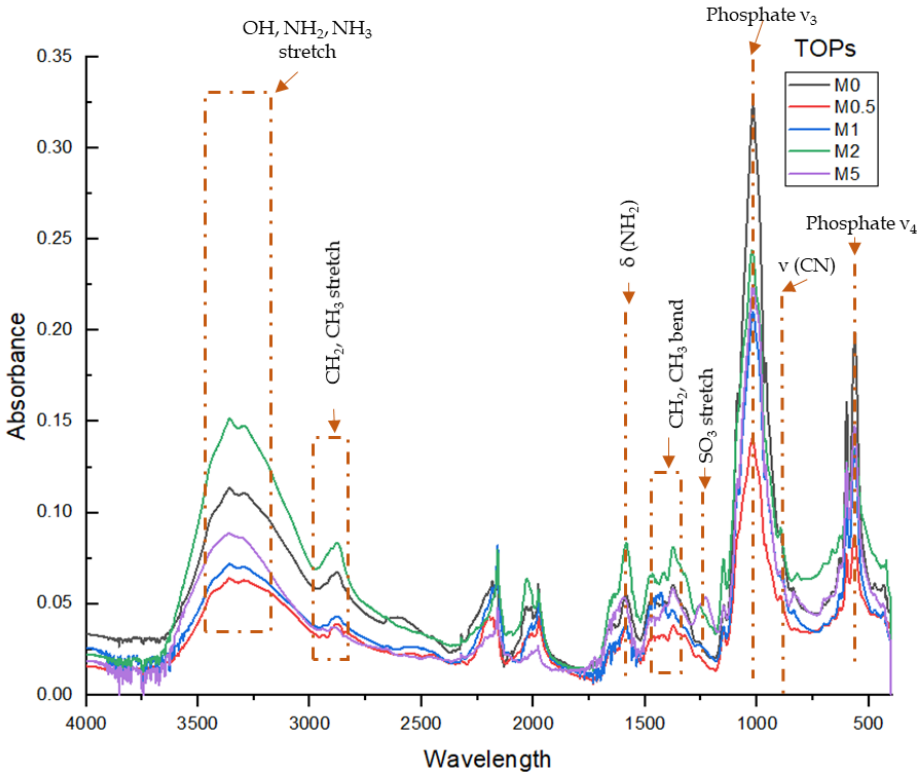

Figure 6.27. FTIR results in the spectral region 4000-400 cm^{-1} for top surfaces of the scaffolds M0, M0.5, M1, M2 and M5.

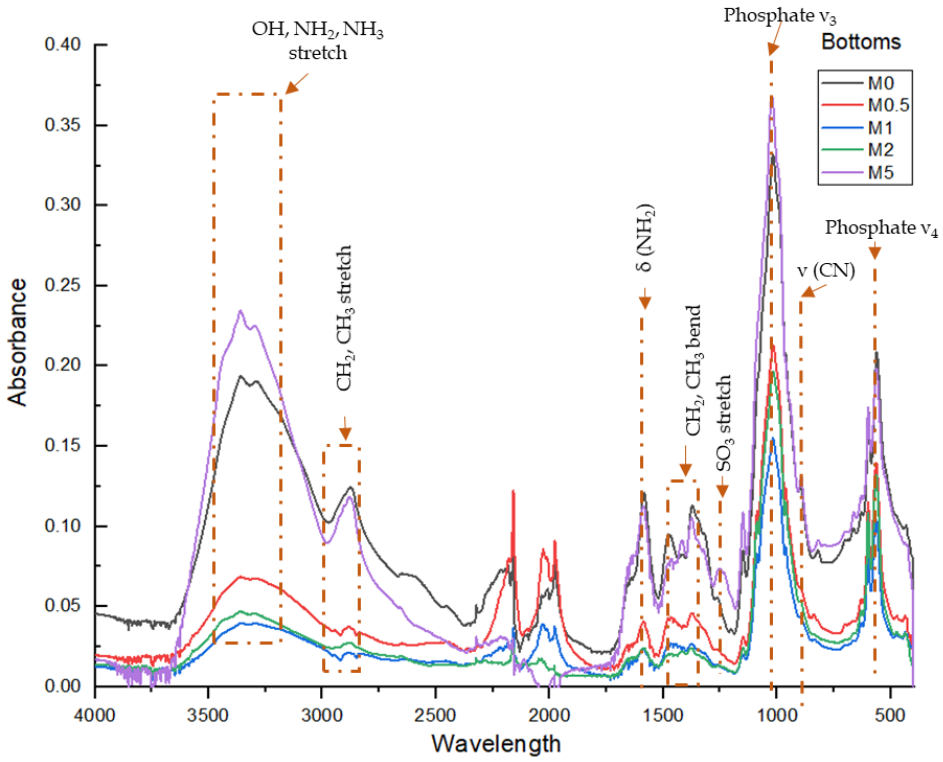

Figure 6.28. FTIR results in the spectral region 4000-400 cm^{-1} for bottom surfaces of the scaffolds M0, M0.5, M1, M2 and M5.

Peak assignment is shown in Table 6.3, for the scaffolds T, which represents the results before undergoing biodegradation.

6.2.1.1 Discussion of FTIR results

Chemical interaction between the components of the matrices (M0 scaffold) was characterised by ATR-FTIR spectroscopy. From the spectra of Figure 6.26 it is possible to observe that a functionalized scaffold was achieved, with a chitosan-rich surface and a hydroxyapatite-rich surface, as explained in section 6.1.1.1.

Spectra from hydroxyapatite and the bottom surface showed well-defined phosphate (PO_4) peaks at 564 cm^{-1} and 1018 cm^{-1}, corresponding to PO_4 ν_4 and PO_4 ν_3 stretching modes, respectively. Likewise, hydroxyl (OH) stretch peak was observed at 3571cm^{-1} for both spectra [156].

Regarding chitosan and the top surface, their spectra showed a band for alkyl (CH_2, CH_3) bending at 1375-1415 cm^{-1}, a small hump between 1586 and 1650 cm^{-1} corresponds to the CO stretching from Amide I, and, the peaks of CH_2, CH_3 stretch near 2850-2915 cm^{-1} [157,158]. These spectra also show a band assigned to C-O-C stretching between 1025-1060 cm^{-1} and a broad peak of OH and NH_2, NH_3 stretching vibrations at 3555 cm^{-1} [157,158].

On the other hand, the presence of the heparin was not evident for the lower concentration loads, due to the small amount present on the scaffold. However, for M2 and M5 we can observe the presence of a band between 1230 – 1258 cm^{-1} which can be attributable to the SO_3 asymmetrical stretching according to Kim & Urban (1998). A broaden around the 1020-1040 cm^{-1} band can also be due to the presence of the SO_3 symmetrical stretching of the heparin. It also remarkable that the presence of these heparin peaks is higher in the chitosan-rich side than in the hydroxyapatite side, where the heparin peaks are only notable for the M5 scaffold. This is mainly due the fact that

chitosan, a polycation, attracts a higher amount of the negatively charged heparin compared to hydroxyapatite (being slightly negative on its surface as described in section 6.1.1.1).

6.2.2 Heparin determination

6.2.2.1 Qualitative determination of heparin

The objective of the qualitative determination of heparin onto the scaffolds, performed with a 0.05% Toluidine Blue solution, was to observe the presence and distribution of heparin on the scaffold. The solution changed from blue to purple almost immediately after the immersion of the scaffolds in the Toluidine Blue solution. As showed in Figure 6.29, the purple shade is also an indication of the amount of heparin present in the scaffold, the tube on the right (corresponding to M5) has a more intense purple shade.

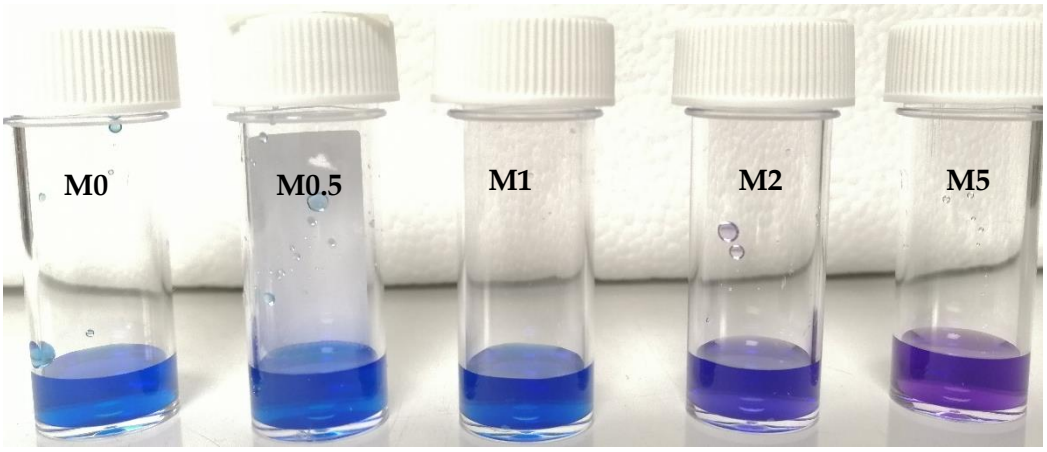

Figure 6.29. Toluidine Blue solutions after the immersion of the scaffolds.

The purple shade also helped to observe of the distribution of heparin throughout the scaffold. Figure 6.30-A presents samples of M5 scaffold, showing its top and bottom surface, and its core obtained with a transversal cut of the scaffold body. It is possible to observe the presence of heparin even within the scaffold. Figure 6.30-B shows one

part the well-plate used for the qualitative heparin determination. The scaffolds within the wells confirm the presence of heparin due to the visible purple shade.

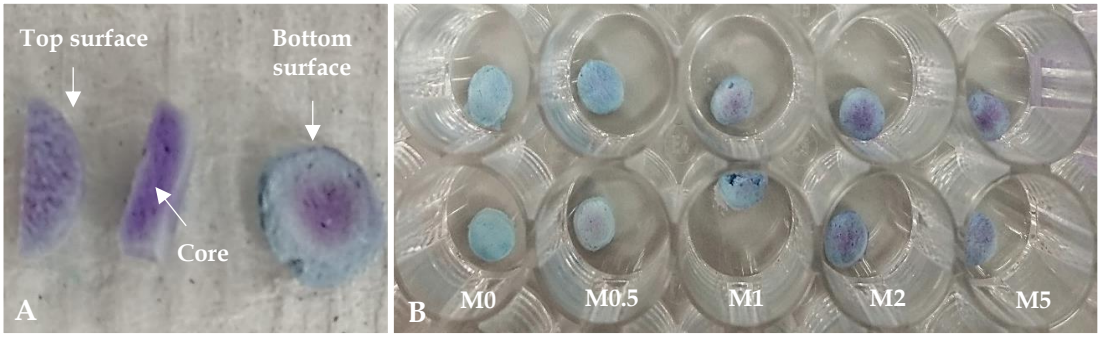

Figure 6.30. Scaffolds tainted with Toluidine Blue. The change from blue to purple denotes the presence and distribution of heparin.

Closer images of the scaffolds (20X) were taken on the purple shade zone on every scaffold to observe if the shade could give an indication of the amount of heparin present in each concentration. From Figure 6.31 (A to E), it is possible to notice the difference between the sample without heparin which exhibits a completely blue surface, and the rest of the samples with heparin, which can be seen as purple surfaces with some scattered blue spots.

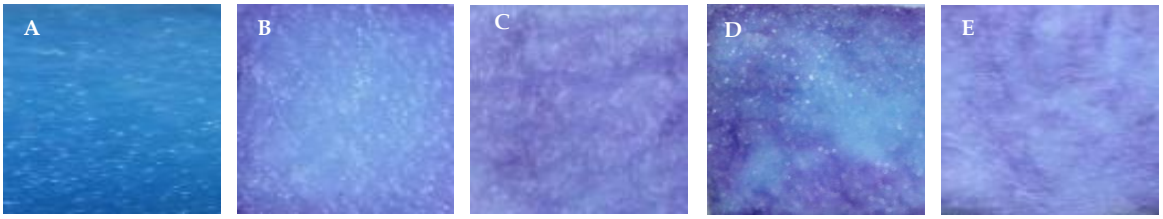

Figure 6.31. Scaffolds stained with Toluidine blue (20X); it is possible to observe the change from blue to purple in the presence of heparin. Loading concentrations: (A) M0, (B) M0.5, (C) M1, (D) M2, (E) M5.

6.2.2.2 Quantitative determination of heparin

At the end of the Toluidine Blue assay for heparin quantification it was observable that total amount of heparin detected on every scaffold, varied according to the loading concentration where they were immersed. Figure 6.32 shows an image of the vials at

the end of the Toluidine Blue assay. It is notable how, after the n-hexane extracts the heparin-Toluidine Blue complex (purple liquid), the rests of the dye in aqueous phase are significantly lower when the heparin concentration is higher (blue liquid). This allowed to visually determine which scaffolds present more heparin amount.

By using the data of the amount of heparin the scaffolds release over time, the total sum of all the results was obtained, providing an estimated total concentration of heparin per scaffold, showed in Table 6.4. Average concentrations go from 28.14 µg to 315.89 µg per scaffold. Considering that the scaffolds weighed an average of 6.47 ± 0.076 mg, the percentage heparin from of the scaffold's weight was also estimated.

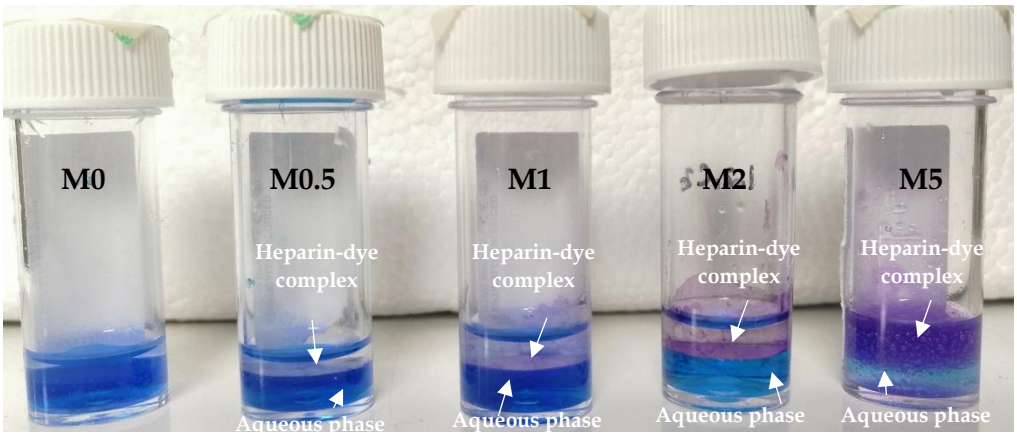

Figure 6.32. Vials during Toluidine Blue assay, showing how higher heparin concentrations create a thicker Toluidine Blue-Heparin complex after n-Hexane extraction.

Loading Concentration mg/ mL	Approximate Content µg /scaffold	% of total scaffold weight	% release within the first 1.5 h
0.5	28.14	0.435	44.68
1	50.14	0.775	57.06
2	138.85	2.146	82
5	315.89	4.882	90.38

Table 6.4. Average total content of heparin, according to the loading concentration used.

Regarding the quantification of the heparin, Figure 6.33 presents a graph showing the percentage of heparin released throughout the different time intervals.

It is interesting to highlight that higher loading concentrations (M2 and M5) showed a faster heparin release, losing more than 80% of the heparin content within the first 1.5 hours of the experiment.

The lower loading concentrations (M0.5 and M1), however, kept a steady release over time exhibiting a release close to 13% still on the 5th day of the experiment.

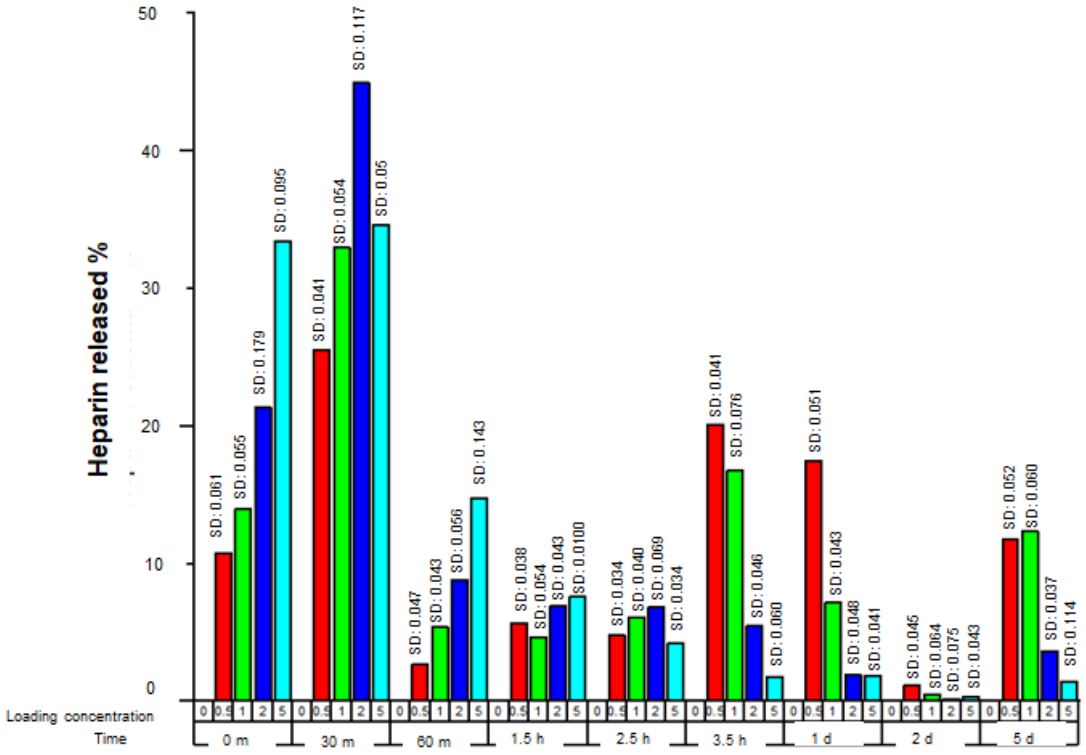

Figure 6.33. Percentage of heparin released from the scaffolds over time.

6.2.2.3 Discussion of heparin determination

Toluidine Blue assay allowed the quantitative determination of the heparin content as well as its qualitative distribution on the scaffold.

The distribution of heparin throughout the scaffold was confirmed by showing the change of colour from blue to purple along the chitosan matrix, and even within the scaffold, due to the interconnected porosity which allowed the penetration of the heparin solution even to the core of the scaffold (Figure 6.30-A). The change of colour in the Toluidine Blue solution was immediate after the immersion of the scaffolds, with gradual differences in the shades of blue and purple according to the heparin concentration (Figure 6.29). In Figure 6.31 (A to E), it is possible to spot the difference among the sample without heparin which presents a completely blue surface, and the rest of the samples with heparin, which show purple surfaces with some scattered blue spots. However, the purple shade in the heparinized scaffolds did not give much information about the concentration of each sample, as no apparent difference among scaffolds was notable, regardless of the concentration.

The loading of heparin onto chitosan is caused by the presence of positive charge (amine groups) in the polymer matrix and anionic charge (sulphate and carboxyl groups) of heparin. Therefore, the DD of the chitosan plays an important role on heparin loading, as mentioned before the scaffold matrix was prepared with a chitosan with DD ≥ 90%, thus, presenting enough amino groups for the heparin interaction. However, it is important to highlight that during this study most of the heparin was released within the first 1.5 hours of immersion in water as shown in Figure 6.33. The higher the loading concentration of the scaffold the higher the percentage of heparin content released within the first 1.5 hours, with the maximum concentration losing the 90% of the heparin content within this time. Gümüşderelioğlu & Aday (2011) reported a fast release with their functionalized chitosan scaffold where heparin had been bonded electrostatically [78]. These authors, however, report a release of at least 50% within the first 10 days of exposure to cell culture process. This means that the addition of hydroxyapatite, causes the electrostatic interaction between chitosan and heparin to

be weaker, since the distribution of hydroxyapatite throughout all chitosan matrix hinders their interaction. Additionally, as explained in section 6.1.1.1 how hydroxyapatite exhibits a slightly negative charge due the presence of phosphate and hydroxyl groups. This negative charge causes a repulsion of between these two components during their interaction in the matrix. This explains the faster release when more heparin is presented. This is also why the top surface presented in Figure 6.30-A presented a deeper purple shade spread all over the surface rather than only in one spot of it like in the bottom surface. Covalent bonding of heparin would represent an option worth to explore, as well as the response of this bonding and the addition of hydroxyapatite.

Nonetheless, heparin was successfully loaded onto the matrices, creating a functionalized scaffold for heparin liberation. Furthermore, a steady release was achieved by those scaffolds with less than 1% wt of heparin, giving an important indication of the loading limits of a chitosan/hydroxyapatite matrix.

6.3 Biological characterization

6.3.1 Cell viability determination using Alamar blue assay

Alamar Blue assay was performed to assess cell viability, this characteristic defines the ability of the material to maintain the cells alive within the scaffold during a certain period. This is achieved by the qualitative measurement of the metabolic activity of the cells. While performing metabolism, the organisms decompose different molecules to obtain energy and at the same time they produce several nutrients to satisfy their needs. Therefore, during Alamar Blue assay the living cells reduce the non-toxic reagent resazurin (blue and non-fluorescent) to resorufin (red and fluorescent). It was

possible to observe the colour change of this process when the dye goes from blue to pink. The lighter the colour obtained, the higher the metabolic activity indicating that the cells are able to survive and proliferate in the media they are kept. Figure 6.34 shows the colour change during the experiment, showing the comparison with the dye with no cells, the dye with just cells and where the cells were implanted in a scaffold.

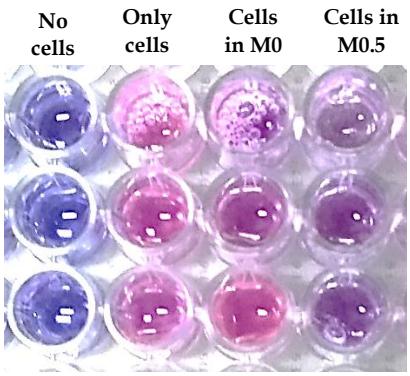

Figure 6.34. Part of a well-plate after Alamar Blue assay on day 9th. Showing the differences in the shades obtained after resazurin reduction. The lighter the colour the higher the metabolic activity.

The metabolic activity of U2OS cells on the scaffolds is presented in Figure 6.35. The cells were evaluated for 14 days, with readings taken on the 1st, 4th, 9th and 14th day. It can be observed that for the scaffolds without heparin, the proliferation of cells was greater over time (higher metabolic activity) when compared to the behaviour observed in the scaffolds with different heparin concentrations.

For the scaffolds with different heparin content, according to these results, cell activity remains constant throughout the entire evaluation regardless of the heparin content.

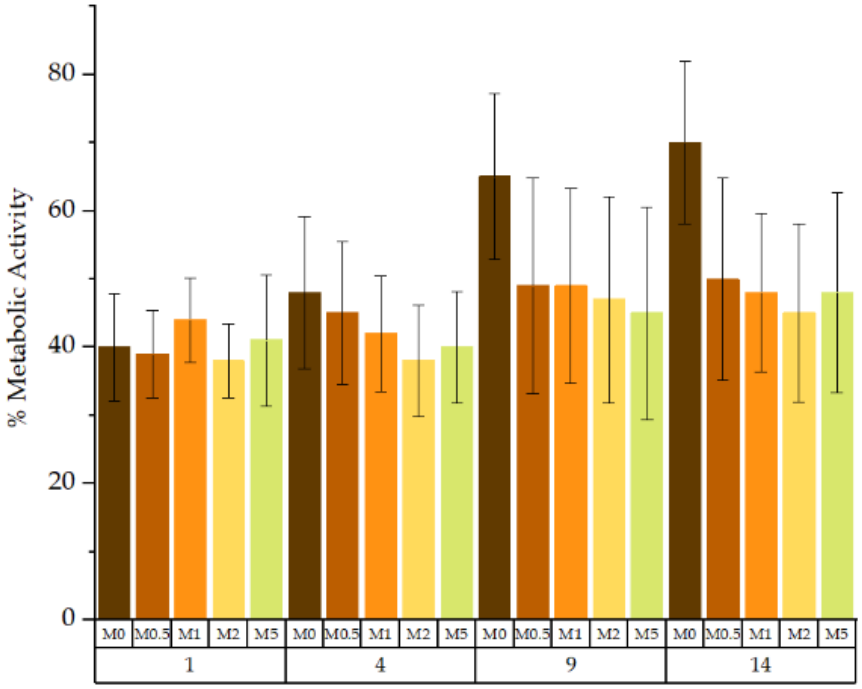

Figure 6.35. Metabolic activity of the U2OS cells on the heparinized scaffolds for 14 days. p <0.005

6.3.1.1 Discussion of cell viability results

The scaffold should provide a suitable environment in terms of attachment and space for cell migration. Chitosan and hydroxyapatite scaffolds are already known to offer the appropriate biocompatible characteristics for cell survival [155]. The evaluation of cell viability with of an Alamar Blue assay qualitatively determines the metabolic activity of the cells.

The metabolic activity of U2OS cells on the scaffolds is presented in Figure 6.35. U2OS is an osteosarcoma cell line, a well-characterized model frequently used in biomedical evaluations due to their fast growth and sharing features with osteoblast and fibroblast cells [159,160]. The cells were evaluated for 14 days, with readings taken on the 1st, 4th, 9th and 14th day. According to these results, regardless of the heparin content, cell activity remains constant throughout the entire evaluation. Proving cell attachment, during the first day, and cell survival, until the last day of the assay.

Furthermore, it can be observed that for the scaffolds without heparin, the proliferation of cells was greater in time (higher metabolic activity) when compared to the behaviour observed in the scaffolds with different concentrations of heparin. This is mainly because the heparin concentration hinders cells proliferation: the scaffolds present a fast desorption of heparin, as mentioned previous sections, which does not allow heparin to interact with fibronectin and other attachment factors [78], causing the low proliferation profile in these results. Additionally, heparin binds biomolecules such as FGF which plays an important role on cell processes such as proliferation and differentiation[121]. Likewise, it has been recently suggested that sulphate groups mediate heparin's interaction with selectins, and they can potentiate their inhibitory effect causing the restraint of cell adhesion and migration [122]. Similar results are presented by Gümüşderelioğlu & Aday (2011), scaffolds with electrostatically loaded heparin reported no particular proliferation during their study [78].

6.3.2 Angiogenic response *ex-ovo*

CAM assay allowed to analyse the preliminary performance of the heparin-loaded scaffolds. Micrographs of the samples were taken on the third and the sixth day after the implantation of the scaffold in the CAM. The following figures show these images to assess the changes in the vascularity surrounding the scaffold. These changes can help to estimate of the influence of the scaffold in the microvascularity of the CAM.

The main idea is that if an implant is not angiogenic, there will not be a visible vascular response in the surrounding of the sample, i. e. blood vessels will not grow towards or into the sample, rather they will not grow at all or they will continue their normal growth despite the sample presence. During the experiment, a filter paper was used as a negative control sample, assuming vascularization will not grow towards this material. Figure 6.36 shows the results for the control sample. It can be observed that

by day 6, the microvessels continue to grow below the scaffold regardless of the presence of the filter paper, forming a continuity of the vascularization under the control sample.

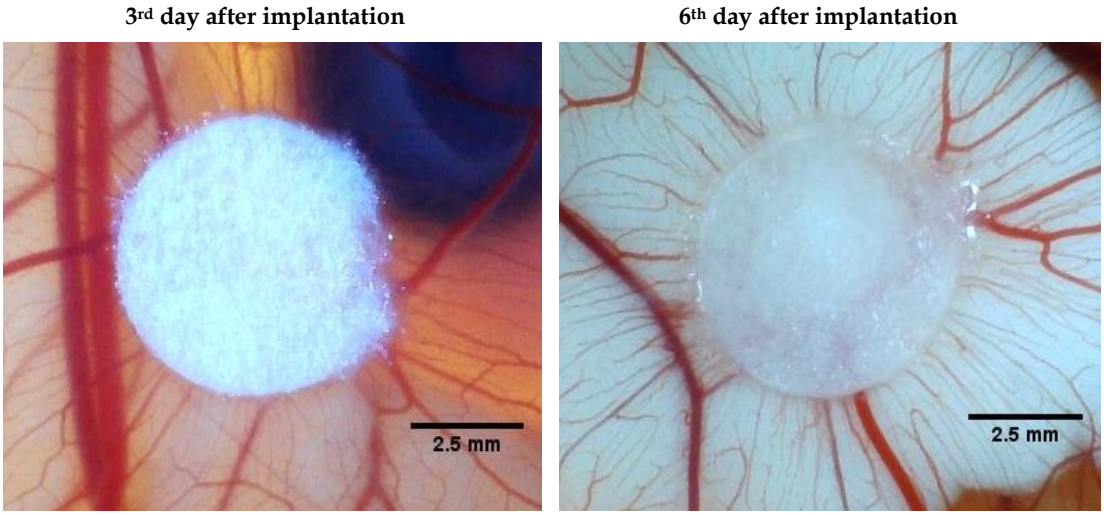

Figure 6.36. Micrograph of filter paper sample implanted on the CAM at the 3rd and the 6th day of implantation.

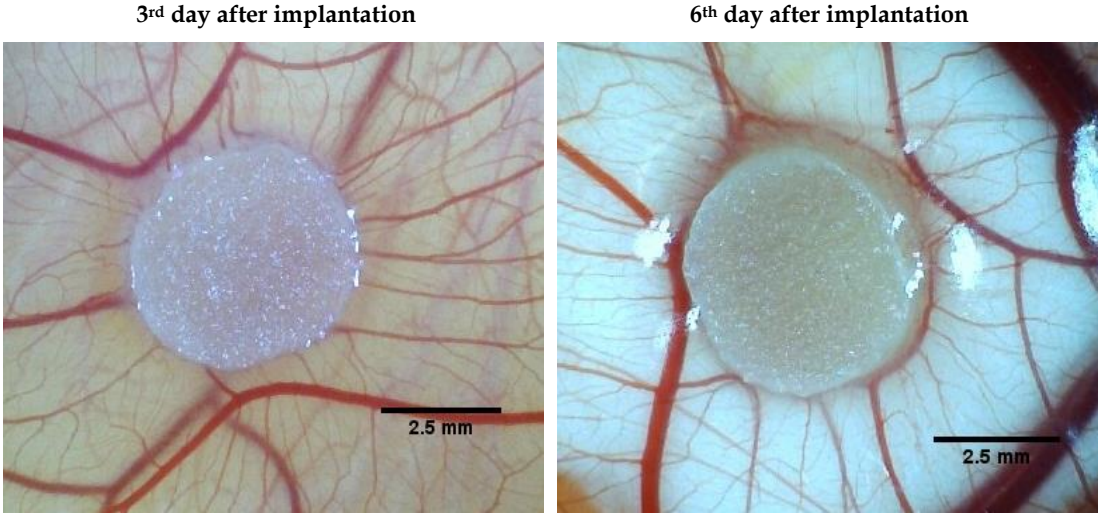

Figure 6.37. Micrograph of MMW sample (scaffold of just chitosan, i.e. without hydroxyapatite or heparin content) implanted on the CAM at the 3rd and the 6th day of implantation.

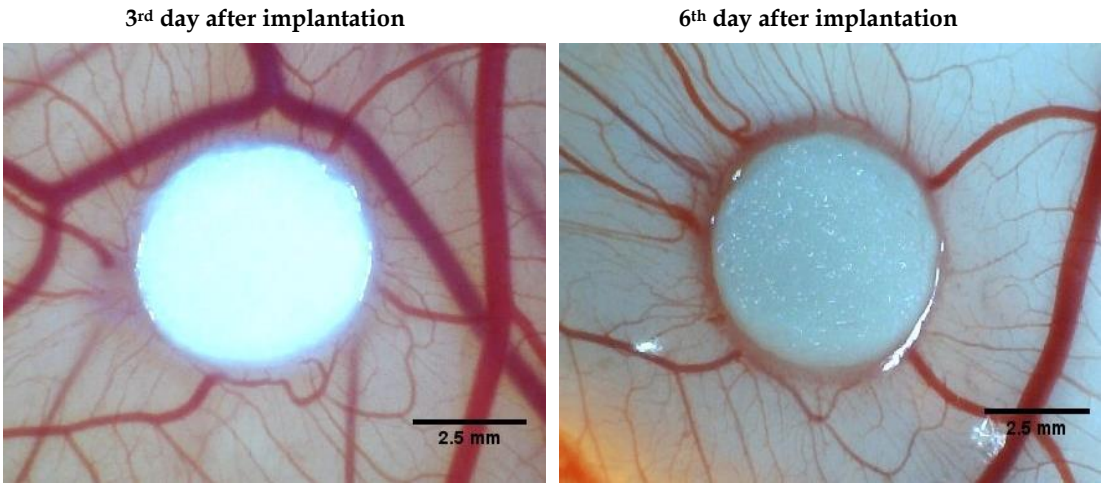

Figure 6.38. Micrograph of M0 sample (scaffold without heparin) implanted on the CAM at the 3rd and the 6th day of implantation.

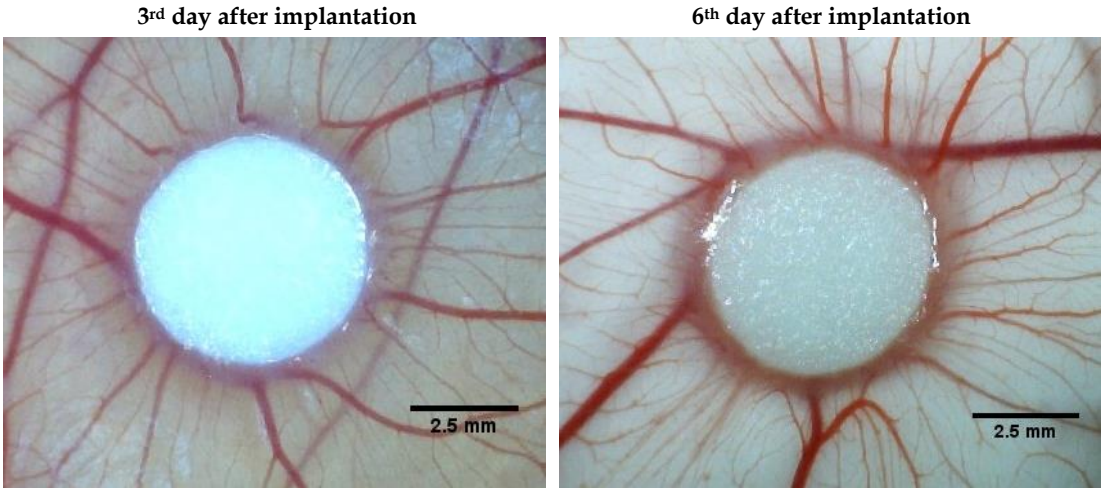

Figure 6.39. Micrograph of M0.5 sample (scaffold loaded in the 0.5 mg/mL heparin solution) implanted on the CAM at the 3rd and the 6th day of implantation.

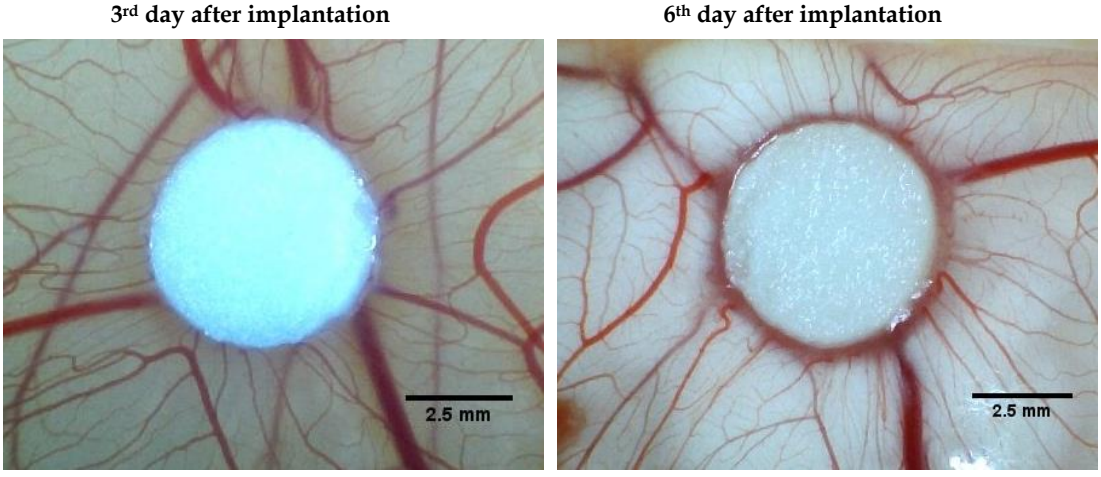

Figure 6.40. Micrograph of M1 sample (scaffold loaded in the 1 mg/mL heparin solution) implanted on the CAM at the 3rd and the 6th day of implantation.

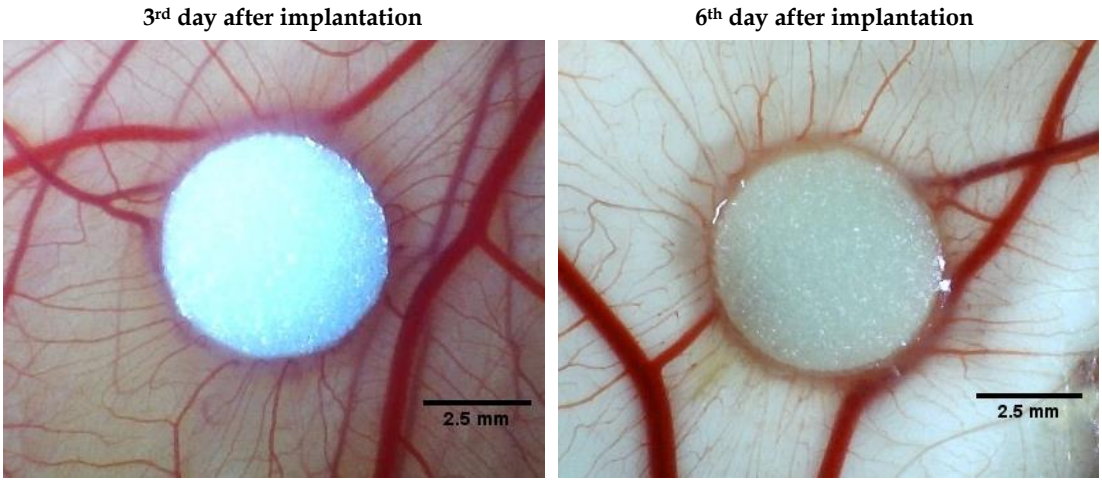

Figure 6.41. Micrograph of M2 sample (scaffold loaded in the 2 mg/mL heparin solution) implanted on the CAM at the 3rd and the 6th day of implantation.

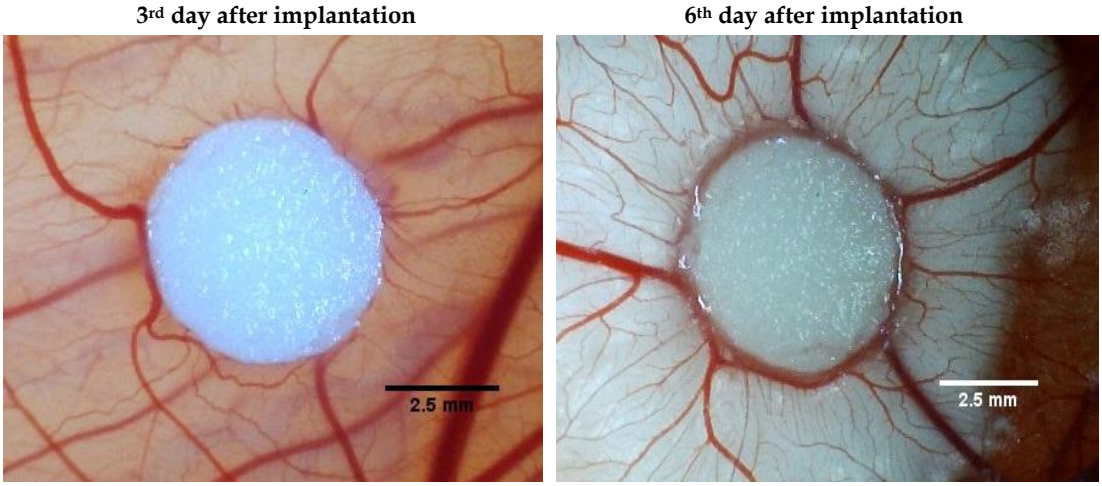

Figure 6.42. Micrograph of M5 sample (scaffold loaded in the 5 mg/mL heparin solution) implanted on the CAM at the 3rd and the 6th day of implantation.

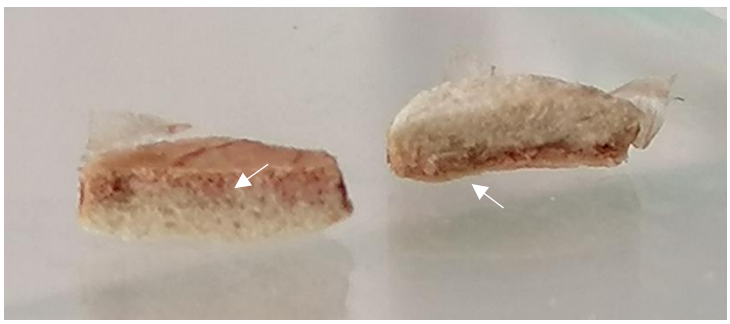

Figure 6.43. Transversal cut of a M1 sample (scaffold loaded in the 1 mg/mL heparin solution), exhibiting vascular ingrowth in the lower part (white arrows).

Figures 6.37 - 6.42 present the changes observed in the CAM tissue surrounding the implanted scaffold. Samples M0, M0.5, M1 and M2 exhibit the growth of ordered microvascularization towards the sample, unlike the highest concentration M5, which shows less vascular ingrowth towards the sample and the vessels have a disorganized appearance. It is also possible to observe how sample MMW presents a lower angiogenic response compared to the scaffold with hydroxyapatite.

On the other hand, Figure 6.38 presents an image of a transversal cut of a M1 scaffold (fixed and dried after retrieval). It is possible to observe the presence of vessel inside the lower part of the sample, proving the vascular infiltration to the scaffolds.

The images from Figures 6.36 – 6.42 were used to count the blood vessel growing towards the scaffolds, using the method described by Barnhill et al. (1983) for the calculation of the vasculogenic index (VIx). The vasculogenic index represents the number of blood vessels attached to the scaffold creating a steering wheel pattern [161]. Figure 6.44-A shows the methodology used for VIx calculation based on Barnhill et al (1983), section B of this figure presents an example of VIx calculation in a real image taken during CAM assay.

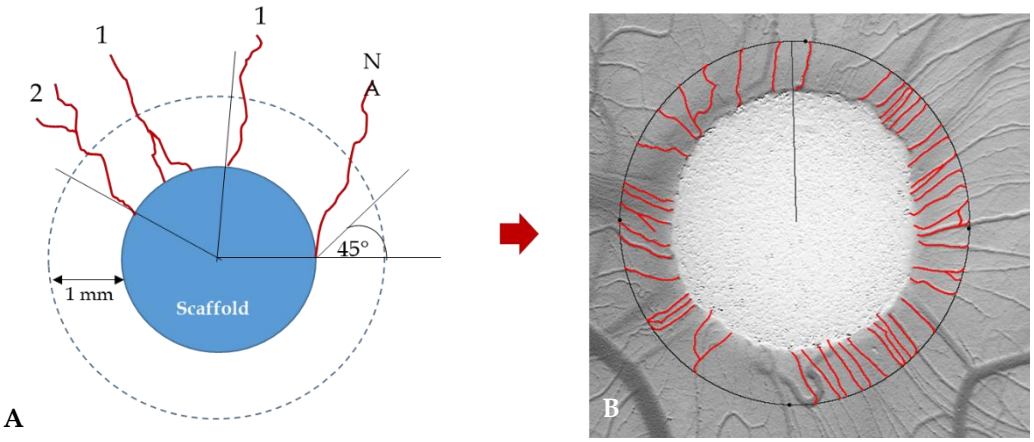

Figure 6.44. (A) Pictorial representation of the methodology used for VIx calculation. For this drawing, VIx= 4. (B) Determination of VIx based on the methodology represented on the right. For this scaffold, VIx = 41.

Vasculogenic indexes were determined on the 6th day after scaffold implantation on the CAM. Table 4.5 shows a comparison of the average VIx for the different loading concentrations of the heparinized scaffold.

Sample	VIx
MMW	16.33 ± 1.45
M0	33.5 ± 2.34
M0.5	36.8 ± 2.33
M1	32 ± 2.07
M2	33 ± 3.60
M5	28.5 ± 1.06

Table 6.5. Vascular index results of the scaffolds with increasing heparin content designated by: MMW (scaffold of just chitosan, i.e. without hydroxyapatite or heparin content), M0, (scaffold without heparin), M0.5 (scaffold of chitosan: hydroxyapatite 50:50 loaded in the 0.5 mg/mL heparin solution), M1 (scaffold of chitosan: hydroxyapatite 50:50 loaded in the 1 mg/mL heparin solution), M2 (scaffold of chitosan: hydroxyapatite 50:50 loaded in the 2mg/mL heparin solution) and M5 (scaffold of chitosan: hydroxyapatite 50:50 loaded in the 5 mg/mL heparin solution).

From the vasculogenic indexes calculation it was observed that for most of the concentrations, the results were very close regardless of the amount of loaded heparin, with a slightly better performance from the scaffold loaded in the 0.5 mg/mL solution. However, visually this is not completely notable, as observed in Figures 6.37 – 6.42.

It is important to mention that for the highest heparin loading concentration, most of the embryos died, (survival rate of 20%). Many of them showed bleeding vessels surrounding the scaffold as showed in Figure 4.45. Bleeding in a system is an indication of heparin overdose [162].

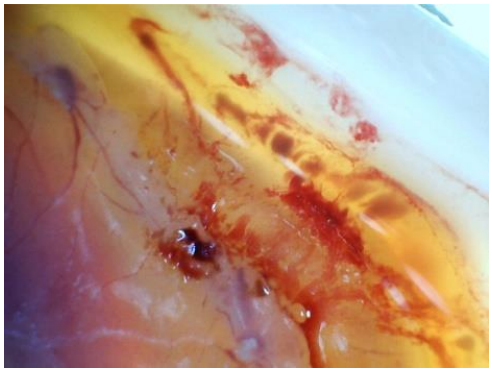

Figure 6.45. Spontaneous bleeding of an embryo implanted with the scaffolds with the highest heparin dose (M5 (scaffold of chitosan: hydroxyapatite 50:50 loaded in the 5 mg/mL heparin solution)).

6.3.2.1 Histology

Figure 6.46 shows the results from the H&E staining after the retrieval of the samples of the CAM assay.

From Figure 6.46 it can be noticed that there is a well define area where CAM's connective tissue can be observed integrating with the scaffold. It is also possible to see the appearance of secondary vessels surrounding the CAM tissue (white arrows). No anomalies or appearance of inflammatory cells was detectable.

It is important to highlight cellular infiltration into the scaffolds. It may also be stated that for the scaffolds with higher loading concentrations, the integration is not well defined, and the presence of blood vessels appear to be messy.

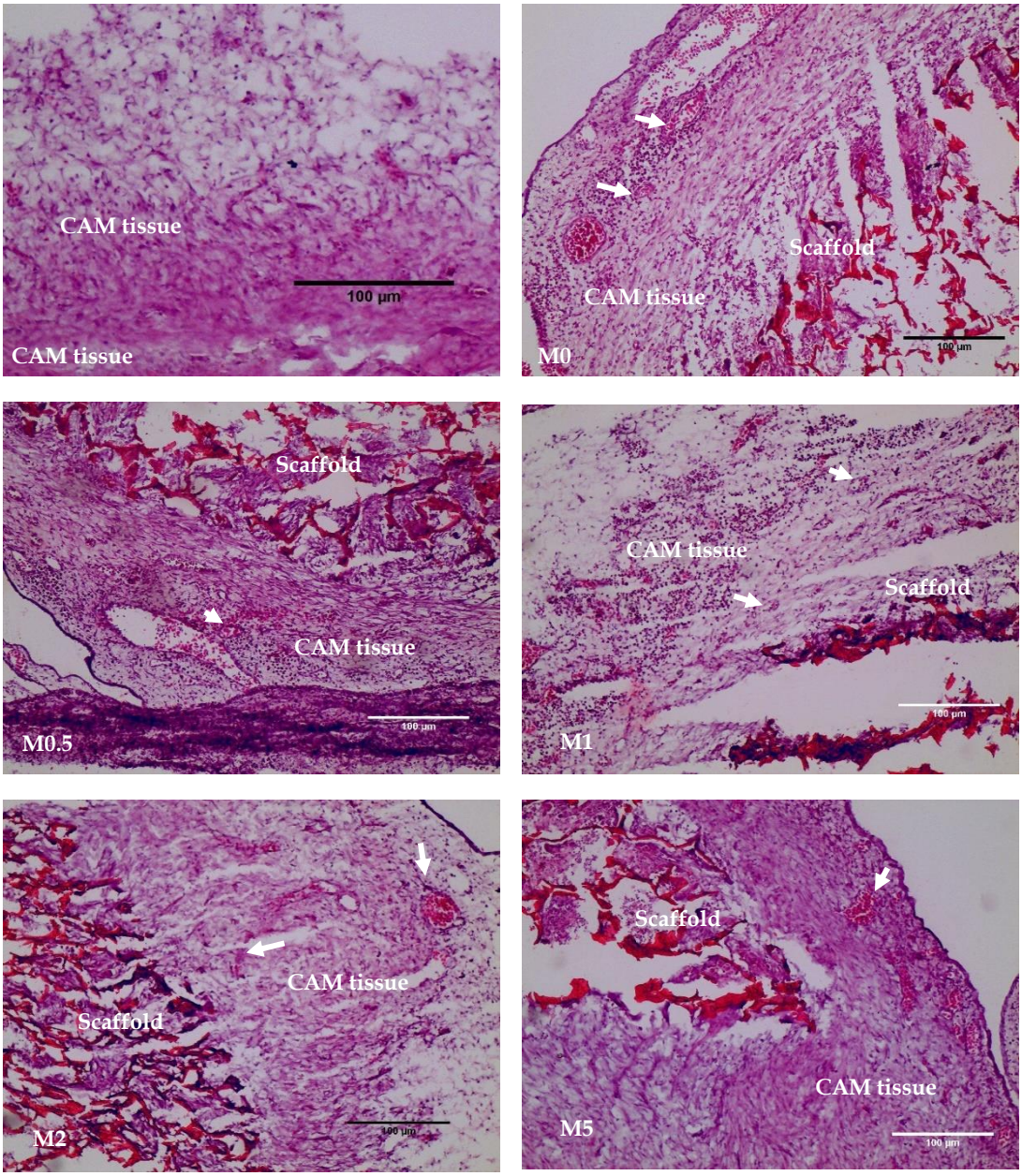

Figure 6.46. Comparison of the H&E staining of the samples for the different heparin concentrations and regular CAM tissue. Arrows point to the appearance of secondary blood vessels. All scale bars are 100 µm.

6.3.2.2 Discussion of angiogenic response

The chorioallantoic membrane, CAM, functions as a gas exchanger, and a disposer for the chick embryo's waste. It also plays part in the mineral transport for the bone development of the embryo. These activities are mainly due to its location and its

highly vascularized nature [163]. Ribatti (2017) describes CAM assay as an outstanding model to assess angiogenic performance of materials and drugs [164], and Mangir et al. (2019) and Eke et al. (2017) highlighted the use of the *in-ovo* technique to improve the visual analysis, monitoring, and comparison of the materials under evaluation [130,131].

CAM assay presents preliminary data regarding the effect of the heparin-loaded scaffolds in a living model. Chick embryo's health and survival, as well as changes in the vascularization surrounding or attaching the scaffolds, provide useful information on the angiogenic activity of the scaffolds produced in this study.

The micrographs of the scaffolds taken on the third and the sixth day after the implantation were used for the calculation of the vasculogenic index. From these results, it was observed that the angiogenic behaviour in all the samples was very similar despite the heparin content of the scaffold. There was a slightly better performance from the scaffold loaded in the 0.5 mg/mL solution indicating that this loading concentration provided better angiogenic response. Comparable results were observed from a parallel project within our research group with injectable heparinized-chitosan hydrogels. From the histology results, it is also notable that the scaffolds did not trigger an inflammatory response and they integrated uniformly with the CAM tissue (Figure 6.46).

Angiogenesis is an activity that depends on the constant stimulus to the microvascular endothelial cells. As mentioned in section 1.2 hypoxia can prompt the angiogenic growth factors (AGF) to trigger angiogenesis (and osteogenesis). To start the angiogenic process, tipping cells break down the extracellular matrix, opening the path that the capillary sprout should follow. These cells possess several AGF receptors, detecting its variations along the surface. The tipping cells align and adjust towards the AGF stimulus, followed by the recently proliferated endothelial cells that were behind them (Figure 1.1). This creates the elongation of the capillary sprout. With time,

the leading cells will join together, creating a continuous tubular structure that will allow blood to flow through it. With the oxygen levels returning to normal due to the re-established blood flow the AGF levels decrease to their usual values, and the angiogenic stimulus disappears. Therefore, it is important to provide an AGF stimulus to induce an angiogenic response.

Heparin binds with angiogenic growth factors such as VEGF and FGF, by an electrostatic interaction of the cationic domains of these proteins with the highly negatively charged heparin. The heparin release process for lower loading concentrations (M0.5 and M1) offered a constant and sustained heparin release, providing heparin availability longer than the rest of the concentrations and without 'overdosing' the implanted area and the subject. A longer availability provides enough time for heparin to bind with surrounding angiogenic factors, creating a gradient that will stimulate an angiogenic response.

According to the study by Ito & Claesson-Welsh (1999), heparin contributes to present VEGF and FGF to their receptors in the cells. Likewise, they concluded that this effect can be dependent on the heparin dose, since a reduction of the growth factor affinity can be caused by exogenous heparin competing with endogenous heparan sulphates for binding VEGF [13]. This explains the results for M5 sample, since the high amount of heparin being rapidly released caused a decrease on the angiogenesis process, along with the overdose of the specimens.

Visually, however, the slight better angiogenic response of M0.5 was not easily spotted, as observed in Figures 6.37 – 6.41. The scaffold without heparin (M0) also presented an angiogenic response and vascular ingrowth, suggesting that the material *per se* also generates an angiogenic response in the implanted area. This is also observable in Figure 4.45, where scaffolds M0 show a good integration with CAM tissue as well as the presence of secondary blood vessels towards the scaffold. Even when chitosan

provides an extracellular-matrix-like structure, with interconnected porosity, to provide vascular ingrowth and infiltration, this does not seem to be the determining factor for our results. In Figure 6.37, though MMW scaffolds induced vascular attachment, this is very low as compared with the rest of the samples. As mentioned earlier M0 samples reported similar results to the heparinized scaffolds. This is mainly due to the presence of hydroxyapatite.

Meagher M. et al. (2016) report a similar behaviour with scaffolds made from collagen/hydroxyapatite combinations. They observe a better angiogenic response from scaffolds with hydroxyapatite compared to scaffolds of just collagen. Furthermore, this angiogenic behaviour improves with the amount of hydroxyapatite added to the scaffolds.

As mentioned earlier, hydroxyapatite enhances bioactive properties. Bioactivity describes the effect a material will have on an organism. The presence of Ca^{2+}, PO^{3-}_4 and OH^- ions on hydroxyapatite's surface provides the ability to interact with several molecules from the microvascular cells and their surface, improving and promoting their migration and attachment. More studies are required to confirm this interesting finding.

6.4 Summary

The primary aim of the study was to identify suitable materials(s) that promote angiogenesis. For this purpose, the material should comply a number of characteristics that allow this process to take place such as adequate pore size and pore interconnectivity, good bioactive properties, and it also should provide angiogenic stimuli.

Within this research, using the freeze-gelation technique, it was possible to obtained porous scaffolds able to promote cell infiltration and proliferation. Additionally, these scaffolds proved to be bioactive by the apatite layer formed onto them during the bioactivity study. It was also possible to confirm that heparin (alone) produces a positive angiogenic effect on CAM assay when loaded on to chitosan/hydroxyapatite scaffolds. This ability is dependent on the concentration of the glycosaminoglycan; therefore, the importance of this study lies on the fact that it defines a starting point of the angiogenic effect as well as a point where antiangiogenic results were observed.

Further conclusions are presented in the next sect

7

Conclusions and Future Work

7.1 Conclusions

The aim of this study was to produce a scaffold able to promote and improve angiogenesis during bone regeneration. This study focused on the fabrication of a scaffold from materials that have proven to promote osteogenesis, adding heparin that binds with angiogenic growth factors with the hypothesis that this mixture will produce a composite able to promote angiogenesis.

During the development process, the main goal was to obtain a scaffold with a homogeneous composition, this would provide a constant availability of amino groups for heparin to interact and bond with the matrix. At the same time, obtaining a porous structure that would provide sufficient surface for bone tissue to grow and develop. Stable chitosan/hydroxyapatite scaffolds with controlled porosity were prepared by employing freeze-gelation methodology. It was observed that freeze-drying yielded porous scaffolds; however, the resultant characteristics of surface skin, closed porosity and lack of availability of amino groups were not satisfactory for heparin loading purposes. Freeze-gelation, on the other hand, provided a structure with pore size able to induce cell growth and proliferation, besides, the interconnectivity of its pores offers an ideal surface for vascularization to proliferate. Through SEM characterization it was confirmed that the produced scaffolds were bestowed with the necessary organization and porosity to enable and promote osteogenesis. Additionally, with FTIR analysis it was proven that hydroxyapatite was distributed throughout the chitosan matrix, even

creating a hydroxyapatite-rich side, which will provide a highly bioactive surface for bone tissue engineering purposes.

Likewise, this study has demonstrated that 50:50 chitosan: hydroxyapatite ratio and freeze-gelation process provide the best combination to produce a porous scaffold for the purpose of promoting osteogenesis and angiogenesis. Preliminary *in-vitro* bioactivity performance showed that the scaffolds provide a surface capable to promote apatite layer formation, which holds promises for a positive *in-vivo* performance, where osteoblasts can bond with this apatite layer to induce osteogenesis.

Vascularization plays a crucial role in bone development and maintenance as it helps to deliver a variety of nutrients, as well as transport a variety of molecules that ultimately control its microenvironment. The process of angiogenesis aids to uphold vascularization in any tissue. This process depends on the interaction of the tip endothelial cells of the blood vessels with the angiogenic growth factors that will stimulate the proliferation of more endothelial cell so the vessel can sprout and join to form new capillaries. Therefore, maintaining a proper availability of these angiogenic factors is critical for the angiogenesis to occur.

Heparin binds with several angiogenic factors; thus, it can define their availability or functionalization. In this study, heparin was successfully loaded to the porous scaffolds. The final amount of heparin loaded to the scaffold was defined by the electrostatic interaction between the heparin and the chitosan matrix. Scaffolds loaded with higher concentrations of heparin resulted on weak interactions providing a fast desorption of the heparin. Nonetheless, low concentrations offered a slow release, providing a sustained availability of the heparin in the implantation site assuring its interaction with the local angiogenic factors.

Furthermore, in-vitro degradation study showed that the presence of hydroxyapatite and heparin in the scaffold play a major role on its degradation profile. The modification of surface charge of the scaffolds resulted in a delay of the chitosan matrix degradation due to the interaction of hydroxyapatite and heparin with lysozyme. This translates on the scaffold providing a stable framework for bone to regenerate.

It is important to highlight the biological response to the produced scaffold material, since the porous chitosan/hydroxyapatite scaffolds did not exhibit cytotoxic effects. The cytotoxicity was evaluated with U2OS osteosarcoma cells, which are widely used to evaluate osteoblast-like features. Therefore, their proliferation and survival during the evaluation provides a preliminary approach on the expected behaviour of the scaffolds when interacting with osteoblasts.

Additionally, the angiogenic response was evaluated by CAM assay. This methodology provides a closer view to the expected performance *in-vivo*, the angiogenic response, i. e. the promotion and attachment of blood vessels to the scaffold, was analysed. It was observed that after six day of implantation, the scaffolds are able to trigger an angiogenic response without the presence of heparin, providing a plus-feature to the material. However, low heparin concentrations exhibited the best angiogenic performance during the study, with a higher vasculogenic index (number of blood vessels attached to the scaffold), providing an efficiency reference of heparin addition. It was also noted that high concentrations of heparin resulted in a non-angiogenic behaviour, therefore, this research provides information regarding the amount of heparin necessary to promote angiogenesis, beyond which a toxic effect can be observed.

In conclusion, this study demonstrated the feasibility of using heparin alone to promote angiogenesis in an *in-vivo* microenvironment. Other approaches have shown it is possible to use heparin to promote bone angiogenesis, however all of them use external growth factors or bone proteins. Additionally, the heparin loading procedure used during this research is relatively simple and inexpensive technology, which adds to the potential of the scaffold for clinical applications. Furthermore, this research has also demonstrated that there is a threshold amount for heparin to induce a positive angiogenic effect and it is possible to provide bioactive features to the composite by including hydroxyapatite.

7.2 Further Work

During this research, an unprecedented pandemic event took place which hindered the possibility of complementing some of the results presented in this thesis, since there is the possibility of evaluating the interaction of the scaffolds with VEGF. Based on the work performed by Gigliobianco et al. (2015), one approach is to directly immerse the scaffolds in a VEGF solution, and subsequently determine the amount of VEGF loaded onto the scaffolds by an ELISA assay. Another option consists of submerging the scaffolds into VEGF or human blood plasma, after this process the scaffolds can be functionalised with fluorescent antibodies and be observed under the fluorescence microscope [77]. This analysis would help to analyse the distribution of VEGF over the scaffold surface. Both experiments provide an overview of the interaction of heparinized scaffolds with this crucial angiogenic growth factor.

Another approach would have been to compare the action of the scaffolds loaded with VEGF and the produced heparinized scaffolds; this would provide a useful

comparison on the angiogenic action of the heparin alone with the angiogenic effect of the growth factor.

It would have been also interesting to address better and improved loading of heparin by exploring the creation of covalent bonding between heparin and the chitosan. The process for bonding heparin covalently with chitosan involves a process of incubating of the chitosan/hydroxyapatite scaffolds in a solution containing heparin, MES (2-(N-morpholino) ethanesulfonic acid), EDAC (1-Ethyl-3-(3-dimethylaminopropyl) carbodiimide) and NHS (N-hydroxysuccinimide), followed by extensive washings with ultrapure water[165], according to Gümüşderelioğlu & Aday (2011) this process functionalises the amino groups from chitosan and the carboxyl group from heparin. This characterization would show the interaction among the three components, providing another insight into the release effect of the heparin from the chitosan/hydroxyapatite matrix. Moreover, it offers the possibility of analysing different release mechanisms, according to the concentrations of heparin, providing more information regarding the effect of heparin in a long-term release.

Further studies can be focused on the effects of different hydroxyapatite ratios in the angiogenic response. Since it was found that the produced scaffolds trigger angiogenesis even without the presence of heparin, exploring the effect of hydroxyapatite in the angiogenic response would provide deeper understanding on the effects of hydroxyapatite and its use in bone tissue engineering constructs. During the developing process it was observed that the addition of hydroxyapatite tightened the porosity of the scaffold. In additional investigation the amount of hydroxyapatite can be decreased to improve porosity and elasticity, hence, the wider interconnected porosity would provide a more accessible path for vascular infiltration and retaining bioactivity. Likewise, the amount of hydroxyapatite can be increased to compare its

effect on the bioactive properties of the composite, as well as to observe differences in the porosity and vascular access to the scaffold.

Similarly, to broaden the scope of the previous suggestion, it is worth exploring the effects of different hydroxyapatite substitutions and their effect on the angiogenic response. Ionic substitutions may not only have an effect on the osteogenic response, but on the angiogenic effect of hydroxyapatite as well, improving its' bioactivity and may enhance biocompatibility as well. For example, incorporation of silica has been reported to have positive effects on both osteogenesis and angiogenesis processes [166,167]. Silica can substitute phosphate groups in hydroxyapatite during hydrothermal synthesis[168], providing a source to potentiate the pro-angiogenic effect of the system proposed in this work.

There is a latent need for materials to be able to promote and enhance bone regeneration. Revascularisation plays an important role in this process, therefore, the need to improve this process is extensive. Despite the complementary work that can be conducted, this research provides baseline information regarding the angiogenic effect of heparin in an *in-vivo* model and the necessary amount to trigger a pro-angiogenic response.

8

References

1. Bueno, E. M. & Glowacki, J. *Biologic Foundations for Skeletal Tissue Engineering*. *Synthesis Lectures on Tissue Engineering* **3**, (2011).
2. Doblaré, M., García, J. M. & Gómez, M. J. Modelling bone tissue fracture and healing: A review. *Eng. Fract. Mech.* **71**, 1809–1840 (2004).
3. Park, H. *et al.* Anionic carbohydrate-containing chitosan scaffolds for bone regeneration. *Carbohydr. Polym.* **97**, 587–596 (2013).
4. Sanjeev, K. & Einhorn, T. A. Tissue Engineering of Bone. in *Bone Tissue Engineering* (eds. Hollinger, J. O., Einhorn, T. A., Doll, B. A. & Sfeir, C.) 277–302 (CRC Press, 2005).
5. Dorozhkin, S. Calcium Orthophosphate-Containing Biocomposites and Hybrid Biomaterials for Biomedical Applications. *J. Funct. Biomater.* **6**, 708–832 (2015).
6. Prendergast, P. J. & van der Meulen, M. C. H. Mechanics of Bone Regeneration. in *Bone Mechanics Handbook* (ed. Cowin, S. C.) 32-1-32–13 (CRC Press, 2001).
7. Hollister, S. J., Gabriel, T.-M., Halloran, J. W. & Feinberg, S. E. Design and Manufacture of Bone Replacement Scaffolds. in *Bone Mechanics Handbook* (ed. Cowin, S. C.) 1–14 (CRC Press, 2001).
8. Pneumaticos, S. G., Triantafyllopoulos, G. K., Basdra, E. K. & Papavassiliou, A. G. Segmental bone defects: From cellular and molecular pathways to the development of novel biological treatments. *J. Cell. Mol. Med.* **14**, 2561–2569 (2010).
9. Hankenson, K. D., Dishowitz, M., Gray, C. & Schenker, M. Angiogenesis in bone regeneration. *Injury* **42**, 556–561 (2011).
10. Saran, U., Gemini Piperni, S. & Chatterjee, S. Role of angiogenesis in bone repair. *Arch. Biochem. Biophys.* **561**, 109–117 (2014).
11. Loi, F. *et al.* Inflammation, fracture and bone repair. *Bone* **86**, 119–130 (2016).
12. Bayer, E. A., Gottardi, R., Fedorchak, M. V. & Little, S. R. The scope and sequence of growth factor delivery for vascularized bone tissue regeneration. *J. Control. Release* **219**, 129–140 (2015).

13. Ito, N. & Claesson-Welsh, L. Dual effects of heparin on VEGF binding to VEGF receptor-1 and transduction of biological responses. *Angiogenesis* **3**, 159–166 (1999).
14. Rema, R. B., Rajendran, K. & Ragunathan, M. Angiogenic efficacy of Heparin on chick chorioallantoic membrane. *Vasc. Cell* **4**, 1–7 (2012).
15. Chiodelli, P., Bugatti, A., Urbinati, C. & Rusnati, M. Heparin/heparan sulfate proteoglycans glycomic interactome in angiogenesis: Biological implications and therapeutical use. *Molecules* **20**, 6342–6388 (2015).
16. Mescher, A. L. *Junqueira's basic histology: text and atlas*. (McGraw-Hill Education Medical, 2013).
17. Lowe, J. S. & Anderson, P. G. *Steven's & Lowe's Human Histology*. (Elsevier Mosby, 2015).
18. Bartl, R. & Frisch, B. Biology of Bone. in *Osteoporosis. Diagnosis, Prevention, Therapy* 7–28 (Springer Berlin Heidelberg, 2009).
19. Boskey, A. L. The Organic and Inorganic Matrices. in *Bone Tissue Engineering* (eds. Hollinger, J. O., Einhorn, T. A., Doll, B. A. & Sfeir, C.) 91–123 (CRC Press, 2005).
20. Webster, S. S. J. Integrated Bone Tissue Phisiology: Anatomy and Phisiology. in *Bone Mechanics Handbook* (ed. Cowin, S.) 1-1-1–68 (CRC Press, 2001).
21. Whiting, W. C. & Zernicke, R. F. Concepts of Injury and Healing. in *Biomechanics of Musculoskeletal Injury* 124–151 (Human Kinetics, 2008).
22. Liu, Y., Luo, D. & Wang, T. Hierarchical Structures of Bone and Bioinspired Bone Tissue Engineering. *Small* **12**, 4611–4632 (2016).
23. Schenk, R. K., Hofstetter, W. & Felix, R. Morphology and Chemical Composition of Connective Tissue: Bone. in *Connective tissue and its heritable disorders: molecular, genetic and medical aspects* (eds. Royce, P. M. & Steinmann, B.) 67–120 (Wiley-Liss, 2002).
24. Zanchetta, J. R. & Talbot, J. R. *Osteoporosis: Fisiología, diagnóstico, prevención y tratamiento*. (Editorial Médica Panamericana, 2001).
25. Kini, U. & Nandeesh, B. N. Physiology of Bone Formation, Remodeling and Metabolism. in *Radionuclide and Hybrid Bone Imaging* (eds. Fogelman, I., Gnanasegaran, G. & Van der Wall, H.) 29–57 (Springer Berlin Heidelberg, 2012).
26. Gelse, K., Pöschl, E. & Aigner, T. Collagens - Structure, function, and biosynthesis. *Adv. Drug Deliv. Rev.* **55**, 1531–1546 (2003).

27. Ferreira, A. M., Gentile, P., Chiono, V. & Ciardelli, G. Collagen for bone tissue regeneration. *Acta Biomater.* **8**, 3191–3200 (2012).
28. Olszta, M. J. *et al.* Bone structure and formation: A new perspective. *Mater. Sci. Eng. R Reports* **58**, 77–116 (2007).
29. Garnero, P. The Role of Collagen Organization on the Properties of Bone. *Calcif. Tissue Int.* **97**, 229–240 (2015).
30. Buck, D. & Dumanian, G. Bone Biology and Physiology: Part II. Clinical Correlates. *Plast Reconstr Surg* **129**, 950e-956e (2012).
31. Liu, Q., Huang, S., Matinlinna, J. P., Chen, Z. & Pan, H. Insight into biological apatite: Physiochemical properties and preparation approaches. *Biomed Res. Int.* **2013**, (2013).
32. Liu, Q., Pan, H., Chen, Z. & Matinlinna, J. P. Insight into bone-derived biological apatite: Ultrastructure and effect of thermal treatment. *Biomed Res. Int.* **2015**, (2015).
33. Palmer, L. C., Newcomb, C. J., Kaltz, S. R., Spoerke, E. D. & Stupp, S. I. Biomimetic systems for hydroxyapatite mineralization inspired by bone and enamel. *Chem. Rev.* **108**, 4754–4783 (2008).
34. Burr, D. B. The contribution of the organic matrix to bone's material properties. *Bone* **31**, 8–11 (2002).
35. Fernandez-Tresguerres Hernandez-Gil, I., Alobera Gracia, M. A., Del Canto Pingarrin, M. & Blanco Jerez, L. Bases fisiologicas de la regeneración osea I. Histologia y fisiologia del tejido oseo. *Med. Oral Patol. Oral Cir. Bucal* **11**, 32–36 (2006).
36. Rucci, N. & Teti, A. The 'love-hate' relationship between osteoclasts and bone matrix. *Matrix Biol.* **52–54**, 176–190 (2016).
37. Florencio-Silva, R., Sasso, G. R. D. S., Sasso-Cerri, E., Simões, M. J. & Cerri, P. S. Biology of Bone Tissue: Structure, Function, and Factors That Influence Bone Cells. *Biomed Res. Int.* **2015**, (2015).
38. Ural, A. & Vashishth, D. Hierarchical perspective of bone toughness – from molecules to fracture. *Int. Mater. Rev.* **59**, 245–263 (2014).
39. Rho, J. Y., Kuhn-Spearing, L. & Zioupos, P. Mechanical properties and the hierarchical structure of bone. *Med. Eng. Phys.* **20**, 92–102 (1998).
40. Weinkamer, R. & Fratzl, P. Mechanical adaptation of biological materials - The examples of bone and wood. *Mater. Sci. Eng. C* **31**, 1164–1173 (2011).

41. Guo, X. E. Mechanical Properties of Cortical Bone and Cancellous Bone Tissue. in *Bone Mechanics Handbook* (ed. Cowin, S. C.) 10-1-10–23 (CRC Press, 2001).
42. Gupta, H. S. & Zioupos, P. Fracture of bone tissue: The 'hows' and the 'whys'. *Med. Eng. Phys.* **30**, 1209–1226 (2008).
43. Jepsen, K. J., Davy, D. T. & Akkus, O. Observations of Damage in Bone. in *Bone Mechanics Handbook* (ed. Cowin, S. C.) 17-1-17–18 (CRC Press, 2001).
44. Maes, C. & Clemens, T. L. Angiogenic–osteogenic coupling: the endothelial perspective. *Bonekey Rep.* **3**, 1–4 (2014).
45. Marsell, R. & Einhorn, T. A. The biology of fracture healing. *Injury* **42**, 551–555 (2011).
46. Hu, K. & Olsen, B. R. The roles of vascular endothelial growth factor in bone repair and regeneration. *Bone* **91**, 30–38 (2016).
47. Adair, T. H. & Montani, J.-P. *Angiogenesis*. (Morgan & Claypool Life Sciences, 2011).
48. Kusumbe, A. P., Ramasamy, S. K. & Adams, R. H. Coupling of angiogenesis and osteogenesis by a specific vessel subtype in bone. *Nature* **507**, 323–328 (2014).
49. Lafage-Proust, M. H., Prisby, R., Roche, B. & Vico, L. Bone vascularization and remodeling. *Jt. Bone Spine* **77**, 521–524 (2010).
50. Roseti, L. *et al.* Scaffolds for Bone Tissue Engineering: State of the art and new perspectives. *Mater. Sci. Eng. C* **78**, 1246–1262 (2017).
51. Yu, X., Suárez-González, D., Khalil, A. S. & Murphy, W. L. How does the pathophysiological context influence delivery of bone growth factors? *Adv. Drug Deliv. Rev.* **84**, 68–84 (2015).
52. Stegen, S., van Gastel, N. & Carmeliet, G. Bringing new life to damaged bone: The importance of angiogenesis in bone repair and regeneration. *Bone* **70**, 19–27 (2015).
53. Geris, L., Gerisch, A., Sloten, J. Vander, Weiner, R. & Oosterwyck, H. Van. Angiogenesis in bone fracture healing: A bioregulatory model. *J. Theor. Biol.* **251**, 137–158 (2008).
54. Pike, D. B. *et al.* Heparin-regulated release of growth factors in vitro and angiogenic response in vivo to implanted hyaluronan hydrogels containing VEGF and bFGF. *Biomaterials* **27**, 5242–5251 (2006).
55. Yar, M. *et al.* Production of chitosan PVA PCL hydrogels to bind heparin and induce angiogenesis. *Int. J. Polym. Mater. Polym. Biomater.* **65**, 466–476 (2016).

56. Yar, M. *et al.* Heparin binding chitosan derivatives for production of pro-angiogenic hydrogels for promoting tissue healing. *Mater. Sci. Eng. C* **74**, 347–356 (2017).
57. García, J. R. & García, A. J. Biomaterial-mediated strategies targeting vascularization for bone repair. *Drug Deliv. Transl. Res.* **6**, 77–95 (2016).
58. Blinder, Y. J., Mooney, D. J. & Levenberg, S. Engineering approaches for inducing blood vessel formation. *Curr. Opin. Chem. Eng.* **3**, 56–61 (2014).
59. Sharma, S. *et al.* Delivery of VEGFA in bone marrow stromal cells seeded in copolymer scaffold enhances angiogenesis, but is inadequate for osteogenesis as compared with the dual delivery of VEGFA and BMP2 in a subcutaneous mouse model. *Stem Cell Res. Ther.* **9**, 1–13 (2018).
60. Koob, S. *et al.* Bone Formation and Neovascularization Mediated by Mesenchymal Stem Cells and Endothelial Cells in Critical-Sized Calvarial Defects. *Tissue Eng. Part A* **17**, 311–321 (2010).
61. Hankenson, K. D., Dishowitz, M., Gray, C. & Schenker, M. Angiogenesis in bone regeneration. *Injury* **42**, 556–561 (2011).
62. Vo, T. N., Kasper, F. K. & Mikos, A. G. Strategies for controlled delivery of growth factors and cells for bone regeneration. *Adv. Drug Deliv. Rev.* **64**, 1292–1309 (2012).
63. Bhakuni, T. *et al.* Role of heparin and non heparin binding serpins in coagulation and angiogenesis: A complex interplay. *Arch. Biochem. Biophys.* **604**, 128–142 (2016).
64. Rema, R. B., Rajendran, K. & Ragunathan, M. Angiogenic efficacy of Heparin on chick chorioallantoic membrane. *Vasc Cell* **4**, 8 (2012).
65. Collen, A. *et al.* Unfractionated and Low Molecular Weight Heparin Affect Fibrin Structure and Angiogenesis in Vitro Unfractionated and Low Molecular Weight Heparin Affect Fibrin Structure and Angiogenesis in vitro. *Cancer Res.* **300**, 6196–6200 (2000).
66. Lee, K. W. *et al.* Sustained release of vascular endothelial growth factor from calcium-induced alginate hydrogels reinforced by heparin and chitosan. *Transplant. Proc.* **36**, 2464–2465 (2004).
67. Wu, Q. *et al.* The effect of heparinized decellularized scaffolds on angiogenic capability. *J. Biomed. Mater. Res. - Part A* **104**, 3021–3030 (2016).
68. Teixeira, S., Yang, L., Dijkstra, P. J., Ferraz, M. P. & Monteiro, F. J. Heparinized

hydroxyapatite/collagen three-dimensional scaffolds for tissue engineering. *J. Mater. Sci. Mater. Med.* **21**, 2385–2392 (2010).

69. Freudenberg, U. *et al.* Heparin desulfation modulates VEGF release and angiogenesis in diabetic wounds. *J. Control. Release* **220**, 79–88 (2015).
70. Chung, Y. Il *et al.* Efficient revascularization by VEGF administration via heparin-functionalized nanoparticle-fibrin complex. *J. Control. Release* **143**, 282–289 (2010).
71. Tan, Q. *et al.* Controlled release of chitosan/heparin nanoparticle-delivered VEGF enhances regeneration of decellularized tissue-engineered scaffolds. *Int. J. Nanomedicine* **6**, 929–942 (2011).
72. Yang, Y. *et al.* Novel mineralized heparin-gelatin nanoparticles for potential application in tissue engineering of bone. *J. Mater. Sci. Mater. Med.* **25**, 669–680 (2014).
73. Yar, M. *et al.* Production of chitosan PVA PCL hydrogels to bind heparin and induce angiogenesis. *Int. J. Polym. Mater. Polym. Biomater.* **65**, 466–476 (2016).
74. Wang, J., Wan, Y. & Huang, Y. Immobilisation of heparin on bacterial cellulose-chitosan nano-fibres surfaces via the cross-linking technique. *IET Nanobiotechnology* **6**, 52 (2012).
75. Almodóvar, J. *et al.* Chitosan-heparin polyelectrolyte multilayers on cortical bone: Periosteum-mimetic, cytophilic, antibacterial coatings. *Biotechnol. Bioeng.* **110**, 609–618 (2013).
76. Shahzadi, L. *et al.* Triethyl orthoformate covalently cross-linked chitosan-(poly vinyl) alcohol based biodegradable scaffolds with heparin-binding ability for promoting neovascularisation. *J. Biomater. Appl.* **31**, 582–593 (2016).
77. Gigliobianco, G., Chong, C. K. & MacNeil, S. Simple surface coating of electrospun poly-L-lactic acid scaffolds to induce angiogenesis. *J. Biomater. Appl.* **30**, 50–60 (2015).
78. Gümüdereliolu, M. & Aday, S. Heparin-functionalized chitosan scaffolds for bone tissue engineering. *Carbohydr. Res.* **346**, 606–613 (2011).
79. Levengood, S. K. L. *et al.* Chitosan-based scaffolds for bone tissue engineering. *J. Mater. Chem. B* **2**, 3161 (2014).
80. Croisier, F. & Jérôme, C. Chitosan-based biomaterials for tissue engineering. *Eur. Polym. J.* **49**, 780–792 (2013).
81. Dash, M., Chiellini, F., Ottenbrite, R. M. & Chiellini, E. Chitosan - A versatile

semi-synthetic polymer in biomedical applications. *Prog. Polym. Sci.* **36**, 981–1014 (2011).

82. Pillai, C. K. S., Paul, W. & Sharma, C. P. Chitin and chitosan polymers: Chemistry, solubility and fiber formation. *Prog. Polym. Sci.* **34**, 641–678 (2009).
83. Mourya, V. K. & Inamdar, N. N. Chitosan-modifications and applications: Opportunities galore. *React. Funct. Polym.* **68**, 1013–1051 (2008).
84. Usman, A. *et al.* Chitin and chitosan based polyurethanes: A review of recent advances and prospective biomedical applications. *Int. J. Biol. Macromol.* **86**, 630–645 (2016).
85. Alves, N. M. & Mano, J. F. Chitosan derivatives obtained by chemical modifications for biomedical and environmental applications. *Int. J. Biol. Macromol.* **43**, 401–414 (2008).
86. Domard, A. A perspective on 30 years research on chitin and chitosan. *Carbohydr. Polym.* **84**, 696–703 (2011).
87. Rinaudo, M. Chitin and chitosan: Properties and applications. *Prog. Polym. Sci.* **31**, 603–632 (2006).
88. Muzzarelli, R. A. A. Chitins and chitosans for the repair of wounded skin, nerve, cartilage and bone. *Carbohydr. Polym.* **76**, 167–182 (2009).
89. Kim, I.-Y. *et al.* Chitosan and its derivatives for tissue engineering applications. *Biotechnol. Adv.* **26**, 1–21 (2008).
90. Kurita, K. Chitin and chitosan: Functional biopolymers from marine crustaceans. *Mar. Biotechnol.* **8**, 203–226 (2006).
91. Upadhyaya, L., Singh, J., Agarwal, V. & Tewari, R. P. Biomedical applications of carboxymethyl chitosans. *Carbohydr. Polym.* **91**, 452–466 (2013).
92. Kaya, M., Akata, I., Baran, T. & Menteş, A. Physicochemical Properties of Chitin and Chitosan Produced from Medicinal Fungus (Fomitopsis pinicola). *Food Biophys.* **10**, 162–168 (2015).
93. Mesa Ospina, N. *et al.* Isolation of chitosan from Ganoderma lucidum mushroom for biomedical applications. *J. Mater. Sci. Mater. Med.* **26**, 1–9 (2015).
94. Yaghobi, N. & Hormozi, F. Multistage deacetylation of chitin: Kinetics study. *Carbohydr. Polym.* **81**, 892–896 (2010).
95. Pires, A. L. R. & Moraes, Â. M. Improvement of the mechanical properties of chitosan-alginate wound dressings containing silver through the addition of a biocompatible silicone rubber. *J. Appl. Polym. Sci.* **132**, 1–9 (2015).

96. Svirshchevskaya, E. V. *et al.* Analysis of toxicity and biocompatibility of chitosan derivatives with different physico-chemical properties. *Appl. Biochem. Microbiol.* **52**, 483–490 (2016).
97. Moreno-Vásquez, M. J. *et al.* Functionalization of chitosan by a free radical reaction: Characterization, antioxidant and antibacterial potential. *Carbohydr. Polym.* **155**, 117–127 (2017).
98. Ratner, B. D. *Biomaterials Science. an Introduction to Materials in Medicine*. (Academic Press, 2013).
99. Hao, R., Wang, D., Yao, A. & Huang, W. Preparation and characterization of ??-TCP/CS scaffolds by freeze-extraction and freeze-gelation. *J. Wuhan Univ. Technol. Mater. Sci. Ed.* **26**, 371–375 (2011).
100. Gruselle, M. Apatites: A new family of catalysts in organic synthesis. *J. Organomet. Chem.* **793**, 93–101 (2015).
101. Šupová, M. Substituted hydroxyapatites for biomedical applications: A review. *Ceram. Int.* **41**, 9203–9231 (2015).
102. Boanini, E., Gazzano, M. & Bigi, A. Ionic substitutions in calcium phosphates synthesized at low temperature. *Acta Biomater.* **6**, 1882–1894 (2010).
103. Rezwan, K., Chen, Q. Z., Blaker, J. J. & Boccaccini, A. R. Biodegradable and bioactive porous polymer/inorganic composite scaffolds for bone tissue engineering. *Biomaterials* **27**, 3413–3431 (2006).
104. Kokubo, T. & Takadama, H. How useful is SBF in predicting in vivo bone bioactivity? *Biomaterials* **27**, 2907–2915 (2006).
105. Kokubo, T. Bioactive glass ceramics: properties and applications. *Biomaterials* **12**, 155–163 (1991).
106. Wang, M. Developing bioactive composite materials for tissue replacement. *Biomaterials* **24**, 2133–2151 (2003).
107. Cairns, M. L. *et al.* Through-thickness control of polymer bioresorption via electron beam irradiation. *Acta Biomater.* **7**, 548–557 (2011).
108. Tsai, C. H., Lin, R. M., Ju, C. P. & Chern Lin, J. H. Bioresorption behavior of tetracalcium phosphate-derived calcium phosphate cement implanted in femur of rabbits. *Biomaterials* **29**, 984–993 (2008).
109. Ibrahim, D. *et al.* Chemical characterization of some substituted hydroxyapatites. *Chem. Cent. J.* **5**, 74 (2011).
110. Roberto J., H. & Committee, P. D. Hydroxyapatite. Safety and Efficacy Report.

Plast. Resconstructive Surg. **110**, 1176–1179 (2002).

111. Sadat-Shojai, M., Khorasani, M. T., Dinpanah-Khoshdargi, E. & Jamshidi, A. Synthesis methods for nanosized hydroxyapatite with diverse structures. *Acta Biomater.* **9**, 7591–7621 (2013).
112. Liu, D. M., Troczynski, T. & Tseng, W. J. Water-based sol-gel synthesis of hydroxyapatite: Process development. *Biomaterials* **22**, 1721–1730 (2001).
113. Lakshmi, B. B., Dorhout, P. K. & Martin, C. R. Sol−Gel Template Synthesis of Semiconductor Nanostructures. *Chem. Mater.* **9**, 857–862 (1997).
114. Chen, J. *et al.* A simple sol-gel technique for synthesis of nanostructured hydroxyapatite, tricalcium phosphate and biphasic powders. *Mater. Lett.* **65**, 1923–1926 (2011).
115. Chaudhry, A. A. *et al.* Instant nano-hydroxyapatite: A continuous and rapid hydrothermal synthesis. *Chem. Commun.* 2286–2288 (2006). doi:10.1039/b518102j
116. Kolmas, J., Groszyk, E. & Kwiatkowska-Rózycka, D. Substituted hydroxyapatites with antibacterial properties. *Biomed Res. Int.* **2014**, (2014).
117. Lala, S. *et al.* Magnesium substitution in carbonated hydroxyapatite: Structural and microstructural characterization by Rietveld's refinement. *Mater. Chem. Phys.* **170**, 319–329 (2016).
118. Tu, Y. *et al.* Fabrication of nano-hydroxyapatite/chitosan membrane with asymmetric structure and its applications in guided bone regeneration. *Biomed. Mater. Eng.* **28**, 223–233 (2017).
119. Ruixin, L. *et al.* Degradation behavior and compatibility of micro, nanoHA/chitosan scaffolds with interconnected spherical macropores. *Int. J. Biol. Macromol.* **103**, 385–394 (2017).
120. Rabenstein, D. L. Heparin and heparan sulfate: Structure and function. *Nat. Prod. Rep.* **19**, 312–331 (2002).
121. Linhardt, R. J. 2003 Claude S. Hudson award address in carbohydrate chemistry. Heparin: Structure and activity. *J. Med. Chem.* **46**, 2551–2564 (2003).
122. Oduah, E. I., Linhardt, R. J. & Sharfstein, S. T. Heparin: Past, present, and future. *Pharmaceuticals* **9**, 1–12 (2016).
123. Casu, B., Naggi, A. & Torri, G. Re-visiting the structure of heparin. *Carbohydr. Res.* **403**, 60–68 (2015).
124. Ho, M. H. *et al.* Preparation of porous scaffolds by using freeze-extraction and

freeze-gelation methods. *Biomaterials* **25**, 129–138 (2004).

125. Sawyer, L. C. *Polymer Microscopy*. (Springer Science & Business Media, 2012).
126. Qasim, S. B., Delaine-Smith, R. M., Fey, T., Rawlinson, A. & Rehman, I. U. Freeze gelated porous membranes for periodontal tissue regeneration. *Acta Biomater.* **23**, 317–328 (2015).
127. Reis, R. L. *et al. Natural-Based Polymers for Biomedical Applications*. (Elsevier Science, 2008).
128. Qasim, S. B. *et al.* In-vitro and in-vivo degradation studies of freeze gelated porous chitosan composite scaffolds for tissue engineering applications. *Polym. Degrad. Stab.* **136**, 31–38 (2017).
129. Smith, P. K. & Mallia, a K. Colorimetric Method for the Assay of Heparin Immobilized Heparin Preparations Content in. *Anal. Biochem.* **473**, 466–473 (1980).
130. Eke, G., Mangir, N., Hasirci, N., MacNeil, S. & Hasirci, V. Development of a UV crosslinked biodegradable hydrogel containing adipose derived stem cells to promote vascularization for skin wounds and tissue engineering. *Biomaterials* **129**, 188–198 (2017).
131. Mangir, N., Dikici, S., Claeyssens, F. & Macneil, S. Using ex Ovo Chick Chorioallantoic Membrane (CAM) Assay to Evaluate the Biocompatibility and Angiogenic Response to Biomaterials. *ACS Biomater. Sci. Eng.* **5**, 3190–3200 (2019).
132. Liuyun, J., Yubao, L. & Chengdong, X. Preparation and biological properties of a novel composite scaffold of nano-hydroxyapatite/chitosan/carboxymethyl cellulose for bone tissue engineering. *J. Biomed. Sci.* **16**, 1–10 (2009).
133. Jiang, H. *et al.* A homogenous CS/NaCMC/n-HA polyelectrolyte complex membrane prepared by gradual electrostatic assembling. *J. Mater. Sci. Mater. Med.* **22**, 289–297 (2011).
134. Rosca, C., Popa, M. I., Lisa, G. & Chitanu, G. C. Interaction of chitosan with natural or synthetic anionic polyelectrolytes. 1. The chitosan-carboxymethylcellulose complex. *Carbohydr. Polym.* **62**, 35–41 (2005).
135. Chen, C. *et al.* Biodegradable composite scaffolds of bioactive glass/chitosan/carboxymethyl cellulose for hemostatic and bone regeneration. *Biotechnol. Lett.* **37**, 457–465 (2014).
136. Il'ina, A. V. & Varlamov, V. P. Chitosan-based polyelectrolyte complexes: A

review. *Appl. Biochem. Microbiol.* **41**, 5–11 (2005).

137. Liuyun, J., Yubao, L. & Chengdong, X. A novel composite membrane of chitosan-carboxymethyl cellulose polyelectrolyte complex membrane filled with nano-hydroxyapatite I. Preparation and properties. *J. Mater. Sci. Mater. Med.* **20**, 1645–1652 (2009).
138. Dorozhkin, S. V. Dissolution mechanism of calcium apatites in acids: A review of literature. *World J. Methodol.* **2**, 1 (2012).
139. Koç, A., Finkenzeller, G., Elçin, A. E., Stark, G. B. & Elçin, Y. M. Evaluation of adenoviral vascular endothelial growth factor-activated chitosan/hydroxyapatite scaffold for engineering vascularized bone tissue using human osteoblasts: In vitro and in vivo studies. *J. Biomater. Appl.* **29**, 748–760 (2014).
140. Harley, B. A. & Gibson, L. J. freeze-dried collagen-GAG scaffolds . **25**, (2004).
141. Zhang, K., Fan, Y., Dunne, N. & Li, X. Effect of microporosity on scaffolds for bone tissue engineering. *Regen. Biomater.* **5**, 115–124 (2018).
142. Guda, T. *et al.* Hydroxyapatite scaffold pore architecture effects in large bone defects in vivo. *J. Biomater. Appl.* **28**, 1016–1027 (2014).
143. Rosa, A. L., de Oliveira, P. T. & Beloti, M. M. Macroporous scaffolds associated with cells to construct a hybrid biomaterial for bone tissue engineering. *Expert Rev. Med. Devices* **5**, 719–728 (2008).
144. Salerno, A., Guarnieri, D., Iannone, M., Zeppetelli, S. & Netti, P. A. Effect of micro-and macroporosity of bone tissue three-dimensional- poly(ε-caprolactone) scaffold on human mesenchymal stem cells invasion, proliferation, and differentiation in vitro. *Tissue Eng. - Part A* **16**, 2661–2673 (2010).
145. Guaadaoui, A., Benaicha, S., Elmajdoub, N., Bellaoui, M. & Hamal, A. What is a bioactive compound? A combined definition for a preliminary consensus. *Int. J. Food Sci. Nutr.* **3**, 17–179 (2014).
146. Ong Yu Min, B. A study on the bioactivity and biodegradation of chitosan / hydroxyapatite scaffolds in stimulated body fluid. (University of Sheffield, 2017).
147. Pereiro, R. Book review: Acceleration and automation of solid sample treatment. *Anal. Bioanal. Chem.* **377**, 1089–1090 (2003).
148. Choi, W. S. & Kim, K. J. Separation of Acetic Acid from Acetic Acid-Water

Mixture by Crystallization. *Sep. Sci. Technol.* **48**, 1056–1061 (2013).

149. Christophe Drouet. Apatite formation: why it may not work as planned, and how to conclusively identify apatite compounds. *Biomed Res. Int.* **2013**, Article ID 490946 (2013).
150. Sukhorukova, I. V., Sheveyko, A. N., Kiryukhantsev-Korneev, P. V., Levashov, E. A. & Shtansky, D. V. In vitro bioactivity study of TiCaPCO(N) and Ag-doped TiCaPCO(N) films in simulated body fluid. *J. Biomed. Mater. Res. - Part B Appl. Biomater.* **105**, 193–203 (2017).
151. Hsieh, C. Y. *et al.* Analysis of freeze-gelation and cross-linking processes for preparing porous chitosan scaffolds. *Carbohydr. Polym.* **67**, 124–132 (2007).
152. Harding, I. S., Rashid, N. & Hing, K. A. Surface charge and the effect of excess calcium ions on the hydroxyapatite surface. *Biomaterials* **26**, 6818–6826 (2005).
153. Online, F. A. & Rogina, A. Journal of Tissue Repair and Regeneration. 23–27 (1840). doi:10.14302/issn.2640
154. Lee, W. H., Loo, C. Y., Van, K. L., Zavgorodniy, A. V. & Rohanizadeh, R. Modulating protein adsorption onto hydroxyapatite particles using different amino acid treatments. *J. R. Soc. Interface* **9**, 918–927 (2012).
155. Levengood, S. K. L. & Zhang, M. Chitosan-based scaffolds for bone tissue engineering. *J. Mater. Chem. B* **2**, 3161–3184 (2014).
156. Rehman, I. & Bonfield, W. Characterization of hydroxyapatite and carbonated apatite by photo acoustic FTIR spectroscopy. *J. Mater. Sci. Mater. Med.* **8**, 1–4 (1997).
157. Zając, A., Hanuza, J., Wandas, M. & Dymińska, L. Determination of N-acetylation degree in chitosan using Raman spectroscopy. *Spectrochim. Acta - Part A Mol. Biomol. Spectrosc.* **134**, 114–120 (2015).
158. Shahzadi, L. *et al.* Triethyl orthoformate covalently cross-linked chitosan-(poly vinyl) alcohol based biodegradable scaffolds with heparin-binding ability for promoting neovascularisation. *J. Biomater. Appl.* **0**, 1–12 (2016).
159. Burmester, A., Luthringer, B., Willumeit, R. & Feyerabend, F. Comparison of the reaction of bone-derived cells to enhanced MgCl2-salt concentrations. *Biomatter* **4**, e967616 (2014).
160. Pautke, C. *et al.* Characterization of osteosarcoma cell lines MG-63, Saos-2 and U-2 OS in comparison to human osteoblasts. *Anticancer Res.* **24**, 3743–3748 (2004).

161. Barnhill, R. L. & Ryan, T. J. Biochemical modulation of angiogenesis in the chorioallantoic membrane of the chick embryo. *J. Invest. Dermatol.* **81**, 485–488 (1983).
162. Monagle, P., Studdert, D. M. & Newall, F. Infant deaths due to heparin overdose: Time for a concerted action on prevention. *J. Paediatr. Child Health* **48**, 380–381 (2012).
163. Ribatti, D. The chick embryo chorioallantoic membrane (CAM). A multifaceted experimental model. *Mech. Dev.* **141**, 70–77 (2016).
164. Ribatti, D. The chick embryo chorioallantoic membrane (CAM) assay. *Reprod. Toxicol.* **70**, 97–101 (2017).
165. Gümüdereliolu, M. & Aday, S. Heparin-functionalized chitosan scaffolds for bone tissue engineering. *Carbohydr. Res.* **346**, 606–613 (2011).
166. Götz, W., Tobiasch, E., Witzleben, S. & Schulze, M. Effects of silicon compounds on biomineralization, osteogenesis, and hard tissue formation. *Pharmaceutics* **11**, 1–27 (2019).
167. Dashnyam, K. *et al.* A mini review focused on the proangiogenic role of silicate ions released from silicon-containing biomaterials. *J. Tissue Eng.* **8**, (2017).
168. Aminian, A. *et al.* Synthesis of silicon-substituted hydroxyapatite by a hydrothermal method with two different phosphorous sources. *Ceram. Int.* **37**, 1219–1229 (2011).